

MECHANICAL AND MICROSTRUCTURE ANALYSIS OF  
COPPER TO COPPER FOAM BRAZING USING COPPER-  
TIN-NICKEL-PHOSPHORUS AMORPHOUS FILLER  
ALLOYS

NUR AMIRAH BINTI MOHD ZAHRI

FACULTY OF ENGINEERING  
UNIVERSITY OF MALAYA  
KUALA LUMPUR

2021

MECHANICAL AND MICROSTRUCTURE ANALYSIS OF  
COPPER TO COPPER FOAM BRAZING USING COPPER-  
TIN-NICKEL-PHOSPHORUS AMORPHOUS FILLER  
ALLOYS

NUR AMIRAH BINTI MOHD ZAHRI

THESIS SUBMITTED IN FULFILMENT OF THE  
REQUIREMENTS FOR THE DEGREE OF DOCTOR OF  
PHILOSOPHY

FACULTY OF ENGINEERING  
UNIVERSITY OF MALAYA  
KUALA LUMPUR

2021

**UNIVERSITI MALAYA  
ORIGINAL LITERARY WORK DECLARATION**

Name of Candidate: Nur Amirah Bt. Mohd Zahri

Registration/Matric No: 17035473/1 (KHA160020)

Name of Degree: Doctor of Philosophy

Title of Project Paper/Research Report/Dissertation/Thesis (“this Work”): Mechanical and Microstructure Analysis of Copper to Copper Foam Brazing using Copper-Tin-Nickel-Phosphorus Amorphous Filler Alloys.

Field of Study: Materials Engineering

I do solemnly and sincerely declare that:

- (1) I am the sole author / write of this Work;
- (2) This Work is original;
- (3) Any use of any work in which copyright exist was done by way of fair dealing and for permitted purposes and any excerpt or extract from, or reference to or reproduction of any copyright work has been disclosed expressly and sufficiently and the title of the Work and its authorship have been acknowledged in this Work;
- (4) I do not have any actual knowledge nor do I ought reasonably to know that the making of this work constitutes an infringement of any copyright work;
- (5) I hereby assign all and every rights in the copyright to this Work to the University of Malaya (“UM”), who henceforth shall be owner of all the copyright in this Work and that any reproduction or use in any form or by any means whatsoever is prohibited without the written consent of UM having been first had and obtained;
- (6) I am fully aware that if in the course of making this Work I have infringed any copyright whether intentionally or otherwise, I may be subject to legal action or any other action as may be determined by UM.

Candidate’s Signature

Date

Subscribed and solemnly declared before,

Witness’s signature

Date

Name:

Designation:

# **MECHANICAL AND MICROSTRUCTURE ANALYSIS OF COPPER TO COPPER FOAM BRAZING USING COPPER-TIN-NICKEL-PHOSPHORUS AMORPHOUS FILLER ALLOYS**

## **ABSTRACT**

Heat exchangers made with metal foams elements have great potential in thermal applications as they have high heat flux cooling due to their large surface to volume ratio. However, finding an effective joining method to incorporate metal foams into heat exchanger designs is very challenging and has become a topic of interest in brazing technology. In this study, the brazing of copper foam to solid copper using different copper-tin-nickel-phosphorus (Cu-Sn-Ni-P) amorphous filler alloys was investigated. The parameters evaluated included the pore densities of Cu foams (pore per inch- PPI), the fillers metal and the brazing temperatures. The resultant joints were evaluated for compressive and shear strengths to determine their mechanical reliabilities. Microstructural evaluations were conducted on the brazed interface using Scanning electron microscope (SEM), X-ray diffraction (XRD) and Energy-dispersive X-ray spectroscopy (EDX) (point, line and area mapping). Finally, the corrosion behaviours of crystalline filler alloys and Cu/Cu foam/Cu brazed joints were analysed using electrochemical potentiodynamic polarisation and immersion tests, respectively. It was found that the compressive strengths of brazed Cu/Cu foam/Cu increase with increasing foam pore density. The highest compressive strength of 14.4 MPa was obtained for 50 PPI Cu foam brazed sample followed 25 PPI and 15 PPI Cu foams. This increase in compressive strength was due to the dense interconnected branches in 50 PPI Cu foam. In contrast, the highest shear strength of 3.7 MPa was obtained for brazed joint sample of 15 PPI Cu foam as compared to 25 PPI (3.3 MPa) and 50 PPI (2.8 MPa) Cu foams. This was due to the larger area of interconnected branches in 15 PPI Cu foam. SEM images revealed increases in cavities formation in the joint interface with increasing Cu foam

pore density which correspond with the decrease in brazing joint strengths. EDX and XRD analysis have shown the concentrations of Cu, Cu<sub>6</sub>Sn<sub>5</sub>, Cu<sub>3</sub>P and Ni<sub>3</sub>P in the joint. EDX line scanning has verified the diffusion of P element into the Cu foam, which would have strengthened the Cu foam branches and contribute to its high compressive strength properties. The electrochemical potentiodynamic polarisation tests have shown that the Cu-9.7Sn-5.7Ni-7.0P filler has less noble corrosion potential ( $E_{\text{corr}}$ ) which make it prone to corrosion attack. However, Cu-9.7Sn-5.7Ni-7.0P filler has a more negative of corrosion current density ( $I_{\text{corr}}$ ), indicating low corrosion rate and high corrosion resistance. This observation agrees with the immersion test of Cu/Cu foam/Cu using Cu-9.7Sn-5.7Ni-7.0P filler, which resulted in the thickest patina layer formation (initially formed by an aggressive corrosion) protecting the interface from further corrosion attack (high corrosion resistant). By considering the aspect of manufacturing, Cu foam strength, brazed joint strength, microstructure and corrosion performance, it is proposed that Cu/Cu foam /Cu with 15 PPI Cu foam using Cu-9.7Sn-5.7Ni-7.0P filler at brazing temperature of 680 °C would be the most suitable configuration for use in heat exchanger applications.

**Keywords:** metal foam; amorphous filler; brazing; diffusion; electrochemical

# **ANALISA MEKANIKAL DAN MIKROSTRUKTUR PADA PENYAMBUNGAN PATERI KERAS KUPRUM KEPADA KUPRUM BERPORI DENGAN MENGGUNAKAN PANCALOGAM PENGISI TIDAK BERHABLUR KUPRUM-TIN-NIKEL-FOSFORUS**

## **ABSTRAK**

Pembuatan penukar haba menggunakan logam berpori berpotensi besar bagi aplikasi haba kerana mempunyai penyejukan fluks haba yang tinggi disebabkan oleh nisbah permukaan yang luas terhadap isi padu. Walaubagaimanapun, teknik penyambungan logam berpori yang efektif menjadi cabaran dan mulai mendapat perhatian dalam beberapa penyelidikan teknologi pateri keras. Kajian ini menjalankan penyambungan kuprum/kuprum berpori/kuprum (Cu/Cu berpori/Cu) dengan menggunakan pancalogam pengisi tidak berhablur (amorfus) kuprum-tin-nikel-fosforus (Cu-Sn-Ni-P) melalui kaedah pateri keras. Parameter-parameter yang diuji ialah ketumpatan pori logam berpori (pori per inci-PPI), pancalogam pengisi dan suhu pateri keras. Sambungan Cu/Cu berpori/Cu telah menjalani kekuatan mampatan dan kekuatan ricih bagi kebolehpercayaan mekanikal. Mikroskop pemindai elektron (SEM), Pembelauan sinar-X (XRD) dan Tenaga serakan sinar-X (EDX) spektroskopi (titik, garisan dan pemetaan) telah digunakan untuk menganalisa mikrostruktur pada sambungan pateri keras Cu/Cu berpori/Cu. Akhir sekali, kakisan mengenai amorfus dan sambungan pateri keras Cu/Cu berpori/Cu, masing-masing dilakukan dengan menggunakan polarisasi potensiodinamik elektrokimia dan ujian rendaman. Kekuatan mampatan pateri keras Cu/Cu berpori/Cu menunjukkan peningkatan dengan meningkatnya ketumpatan pori bagi kuprum berpori. Kuprum berpori 50 PPI mendapat kekuatan mampatan paling tinggi sebanyak 14.4 MPa, diikuti oleh kuprum berpori 25 PPI dan 15 PPI. Peningkatan ini disebabkan bentuk rangka struktur sambungan kuprum berpori 50 PPI yang lebih mampat. Berbeza dengan kekuatan ricih, sambungan pateri keras Cu/Cu berpori menunjukkan kuprum berpori 15 PPI mempunyai kekuatan ricih yang tinggi sebanyak 3.7 MPa berbanding kuprum berpori 25

PPI (3.3 MPa) dan 50 PPI (2.8 MPa). Hal ini kerana kuprum berpori 15 PPI mempunyai kawasan rangka sambungan yang lebih luas. SEM menunjukkan peningkatan pembentukan liang kosong dengan meningkatnya ketumpatan pori kuprum berpori (dari pori 15 PPI ke pori 25 PPI dan pori 50 PPI) yang mana memberi kesan penurunan kekuatan pateri keras. EDX dan XRD menemui Cu, Cu<sub>6</sub>Sn<sub>5</sub>, Cu<sub>3</sub>P dan Ni<sub>3</sub>P di kawasan sambungan. Pengimbasan garisan EDX membuktikan bahawa P berjaya mengukuhkan rangka struktur kuprum berpori, dibuktikan dengan keputusan mampatan yang tinggi bagi Cu/Cu berpori/Cu yang telah dipateri keras. Polarisasi potensiodinamik menunjukkan pengisi Cu-9.7Sn-5.7Ni-7.0P menghadapi serangan potensi kakisan ( $E_{corr}$ ) yang tinggi dari pengisi yang lain. Namun, keputusan ketumpatan arus kakisan ( $I_{corr}$ ) yang rendah mempamerkan pengisi ini mempunyai kadar kakisan yang rendah dan dapat menghasilkan rintangan kakisan yang tinggi. Keadaan ini dipersetujui melalui ujian rendaman dengan pembentukan lapisan patina yang paling tebal pada Cu/Cu berpori/Cu menggunakan pengisi Cu-9.7Sn-5.7Ni-7.0P yang mana dapat menghalang kakisan seterusnya. Keputusan mencadangkan Cu/Cu berpori/Cu bersama kuprum berpori 15 PPI dengan menggunakan pengisi Cu-9.7Sn-5.7Ni-7.0P pada suhu pateri keras 680 °C adalah yang paling sesuai untuk diaplikasikan dalam penukar haba. Faktor yang menyokong keputusan ini adalah dari segi pembuatan yang menggunakan teknik pateri keras, kekuatan Cu berpori, kekuatan sambungan, mikrostruktur dan prestasi kakisan.

**Kata kunci:** logam berpori; pancalogam pengisi tidak berhablur; pateri keras; penyerapan; elektrokimia

## ACKNOWLEDGEMENTS

In the name of Allah, the Most Gracious and the Most Merciful

Alhamdulillah, all praises to Allah SWT for the strengths and blessings given to me in completing this research work. I wish to express my utmost gratitude to my supervisors, Dr. Nazatul Liana Sukiman, Assoc. Prof. Dr Farazila Yusof and Professor Dr. A.S.M.A. Haseeb for their constant support and guidance throughout my academic journey in University of Malaya. Special thanks to Professor Dr. Yukio Miyashita in providing the laboratory facilities in Nagaoka University of Technology (NUT), Japan, Professor Emeritus Dr. Tadashi Ariga (Tokai University, Japan) and Professor Dr. Luqman Chuah Abdullah (UPM, Malaysia) for their expert advice and opinions. Their constructive comments and suggestions have contributed greatly to the success of this research work.

Appreciations and thanks to Mrs Hartini, Mr Nasrul, & Mr Khairil and the administrative staffs in Faculty of Engineering, University of Malaya for their assistance. Sincerest thanks to all my colleagues in University of Malaya especially to Wahida, Shira, Kanesh (Dr.) and Maisarah; in NUT, Japan, namely Yumi, Fida, Onodzuka, Sarita, and Aisah, their willingness in assisting me in both inside and outside of the laboratory and all those who contributed directly and indirectly in this research journey. I would like to acknowledge the financial support provided by the Ministry of Education, Malaysia via the MyPhD scholarship programme.

To my family, I wish to express my gratitude firstly to my beloved parents; Zahri and Norzani, whom have given unconditional love, supports, prayers, and times with the boys. I hope that my achievements have made both of you proud. To my siblings (Dila-Qaiyum, Dijah, Sya, Enel and Fattah) and aunt Yati, thank you for the understanding, encouragements and assistance with the boys. I appreciate all my boys, Samran, Sarhan, Shazan, and my little girl Annasya, for their patience and endurance with me; all of you have made me stronger and better and more fulfilled. Finally, a very special thanks to my husband, Sam, a lot of loving thanks for the love, care and understanding throughout this journey.

## TABLE OF CONTENTS

ORIGINAL LITERARY WORK DECLARATION	ii
ABSTRACT	iii
ABSTRAK	v
ACKNOWLEDGEMENTS	vii
TABLE OF CONTENTS	viii
LIST OF FIGURES	x
LIST OF TABLES	xiv
LIST OF SYMBOLS AND ABBREVIATIONS	xv
LIST OF APPENDICES	xvi
<b>CHAPTER 1 : INTRODUCTION</b>	<b>1</b>
1.1 Introduction	1
1.2 Problem Statement	3
1.3 Objectives of the Study	6
1.4 Scope of the Study	6
1.5 Thesis Layout	7
<b>CHAPTER 2 : LITERATURE REVIEW</b>	<b>8</b>
2.1 Introduction	8
2.2 Heat Exchanger	8
2.2.1 Plate Heat Exchanger	10
2.2.2 Materials and Structure of Plate-fin Heat Exchanger	12
2.2.3 Fabrication of Plate Heat Exchanger	17
2.3 Metal Foam	20
2.4 Brazing Metal Foam as Joining Method	24
2.4.1 Brazing Filler Alloys	27
2.4.2 Mechanism of Brazing	33
2.5 Current Research on Foam Brazing	37
2.6 Corrosion Behaviour of Brazing Joints	40
2.6.1 Electrochemical Potentiodynamic Polarisation	41
2.6.2 Corrosion of Copper	42
2.7 Summary	44
<b>CHAPTER 3 : METHODOLOGY</b>	<b>45</b>
3.1 Introduction	45
3.2 Materials	48
3.3 Copper Foam	49
3.4 Brazing Process	50
3.5 Mechanical Testing	53
3.5.1 Shear test of Cu/Cu foam/Cu Brazed Joint Interface	53
3.5.2 Compression Test of Cu/Cu foam/Cu	54
3.5.3 Vickers Microhardness Test	55
3.6 Material Characterisation	56
3.6.1 Microscopic Evaluation	54
3.6.2 Scanning Electron Microscopy (SEM) and Energy-Dispersive X-ray Spectroscopy (EDX)	56
3.6.3 X-ray Diffraction (XRD)	57
3.7 Corrosion	58
3.7.1 Electrochemical Potentiodynamic Polarisation	58
	viii

3.7.2	Immersion Test	58
<b>CHAPTER 4 : RESULTS AND DISCUSSION</b>		<b>60</b>
4.1	Introduction	60
4.2	Characterisation of Copper Foam	61
4.3	Characterisation of Cu-Sn-Ni-P Amorphous Filler Alloys	62
4.4	Preliminary Investigation on Brazing Holding Time	63
4.5	Mechanical Evaluation of Brazed Cu/Cu foam/Cu using different Cu-Sn-Ni-P Amorphous Filler Alloys at 5 min brazing holding time	65
4.5.1	Effect of Brazing Temperature, Amorphous Filler alloys and Cu Foam Pore Density on Compressive Strength of Cu/Cu foam/Cu	65
4.5.2	Effect of Brazing Temperature, Amorphous Filler alloys and Cu Foam Pore Density on Shear Strength of Cu/Cu foam/Cu	76
4.5.3	Comparison on Compressive and Shear Strength of Brazed Cu/Cu foam/Cu	84
4.5.4	Microhardness of Cu/Cu foam Brazed Joint Interface	85
4.6	Microstructure of Brazed Cu/Cu foam/Cu using Cu-Sn-Ni-P Amorphous Filler Alloys	91
4.6.1	Shear-Fracture of Brazed Cu/Cu foam	91
4.6.2	Brazed Joint Interface of Cu/Cu foam	99
4.6.3	Surface Diffusion of Filler across the Brazed Cu/Cu foam/Cu	115
4.6.3.1	Microstructure of Cross-Section Brazed Cu/Cu foam/Cu using different Amorphous Fillers alloys with Foam A	115
4.6.3.2	Brazed Cu/Cu foam/Cu using different fillers with different Cu Foams	121
4.7	Diffusion Mechanism of Cu-Sn-Ni-P Filler into Cu Foam	124
4.8	Corrosion Behaviour on Cu-Sn-Ni-P Filler and Cu/Cu foam/Cu Brazed Joint Interface using different Filler with Foam A	126
4.8.1	Crystalline Cu-Sn-Ni-P Filler	127
4.8.2	Electrochemical Characteristics of Crystalline Cu-Sn-Ni-P Filler	131
4.8.2.1	Open Circuit Potential	131
4.8.2.2	Potentiodynamic Polarisation	132
4.8.3	Corrosion Behaviour of Cu/Cu foam A/Cu Brazed Joint Interface	137
4.8.3.1	Microstructure of Cu/Cu foam A Brazed Joint Interface (Pre-Immersed)	137
4.8.3.2	Corrosion Product of Post-Immersed for Uncleaned Cu/Cu foam A Brazed Joint Interface	139
4.8.3.3	Microstructure characterisation of post-immersed for cleaned Cu/Cu foam A brazed joint interface	143
<b>CHAPTER 5 : CONCLUSION</b>		<b>146</b>
5.1	Introduction	146
5.2	Conclusion	146
5.3	Recommendations	148
REFERENCES		150
LIST OF PUBLICATIONS/CONFERENCES		165
APPENDICES		166

## LIST OF FIGURES

<b>Figure 1.1</b>	: Heat exchanger (a) Non-compact (Shell-and-tube) (b) Compact	2
<b>Figure 2.1</b>	: Extended surface of fin geometries for plate heat exchangers (a) plain (triangular) (b) (rectangular) (c) wavy (d) offset strip (e) multilouver (f) perforated (Shah & Sekulic, 2003)	11
<b>Figure 2.2</b>	: Type of heat-exchanger (a) louver fin (b) porous fin (Jacobi et al., 2008) and inset is porous metal foam (Zhao, 2012)	15
<b>Figure 2.3</b>	: Automotive cooling system (Shah & Sekulic, 2003)	17
<b>Figure 2.4</b>	: Component of a plate-fin heat exchanger (Shah & Sekulic, 2003)	18
<b>Figure 2.5</b>	: (a) Closed-cell (El-Hadek & Kaytbay, 2008) (b) Open-cell of metal foam	22
<b>Figure 2.6</b>	: Polyhedron cell model and cross-section shape of metal foam branch based on foam porosity	23
<b>Figure 2.7</b>	: Cu foam at different pore density (a) 15 PPI (b) 25 PPI (c) 50 PPI	23
<b>Figure 2.8</b>	: The microstructure of amorphous (Cu-8.27Sn-5.74Ni -7.35P) and crystalline (Cu-8.99Sn-6.63Ni -7.57P) filler alloys (Xu et al., 2019).	30
<b>Figure 2.9</b>	: Illustration of diffusion brazing (Jacobson & Humpston, 2005)	34
<b>Figure 3.1</b>	: Summary of overall work	47
<b>Figure 3.2</b>	: Schematic diagram of specimen arrangement	50
<b>Figure 3.3</b>	: Summary of Cu/Cu foam/Cu brazing process	51
<b>Figure 3.4</b>	: Brazing cycle of Cu/Cu foam/Cu	52
<b>Figure 3.5</b>	: Schematic diagram of shear test for Cu/Cu foam/Cu	53
<b>Figure 3.6</b>	: Schematic diagram of compression test for Cu/Cu foam/Cu	55
<b>Figure 3.7</b>	: Cu/Cu foam/Cu brazed joint interface	55
<b>Figure 3.8</b>	: Schematic diagram of Cu substrate surface from the shear test of brazed Cu/Cu foam/Cu	57
<b>Figure 3.9</b>	: Schematic diagram of electrochemical set-up	58
<b>Figure 3.10</b>	: Schematic diagram of immersion test (Initial: 0 day)	59

<b>Figure 4.1</b>	: Digital microscope image of Cu foam and cross-sectional view of Cu foam interconnected branch (a & a-i) Foam A (b & b-i) Foam B (c & c-i) Foam C	61
<b>Figure 4.2</b>	: XRD pattern of Cu-Sn-Ni-P amorphous filler alloys	63
<b>Figure 4.3</b>	: Shear strength of brazed Cu/Cu foam using filler B at different holding time	64
<b>Figure 4.4</b>	: Compressive strength ( $\sigma_{comp}$ ) of Cu/Cu foam/Cu using (a) filler A (b) filler B (c) filler C with different Cu foam at different brazing temperature	66
<b>Figure 4.5</b>	: Compressive load exerted on Cu/Cu foam/Cu with (a) foam A (b) foam B and (c) foam C	68
<b>Figure 4.6</b>	: Compressive stress-strain curve of nonbrazed Cu/Cu foam/Cu and the inset shows an elastic curve at strain range of 0 - 0.14 $\epsilon$	70
<b>Figure 4.7</b>	: Compressive stress-strain curve of brazed Cu/Cu foam/Cu using filler A at 680 °C with different foam and inset shows an elastic curve at strain range of 0 - 0.14 $\epsilon$	73
<b>Figure 4.8</b>	: Compressive stress-strain curve of brazed Cu/Cu foam/Cu using filler B at 720 °C with different foam and inset shows an elastic curve at strain range of 0 - 0.14 $\epsilon$	74
<b>Figure 4.9</b>	: Compressive stress-strain curve of brazed Cu/Cu foam/Cu using filler C at 700 °C with different foam and inset shows an elastic curve strain range of 0 - 0.14 $\epsilon$	75
<b>Figure 4.10</b>	: Shear strength of Cu/Cu foam using (a) filler A (b) filler B (c) filler C	77
<b>Figure 4.11</b>	: Shear stress-strain curve of brazed Cu/Cu foam/Cu using filler A at 660 °C with different foam	81
<b>Figure 4.12</b>	: Shear stress-strain curve of brazed Cu/Cu foam/Cu using filler B at 680 °C with different foam	82
<b>Figure 4.13</b>	: Shear stress-strain curve of brazed Cu/Cu foam/Cu using filler C at 660 °C with different foam	83
<b>Figure 4.14</b>	: Micro-hardness test for Cu/Cu foam brazed interface joint using filler A with (a) foam A (b) foam B and (c) foam C at $T_{br}$ of 660 °C	86
<b>Figure 4.15</b>	: Microhardness test for Cu/Cu foam brazed interface joint using filler B with (a) foam A (b) foam B and (c) foam C at $T_{br}$ of 680 °C	87

<b>Figure 4.16</b>	: Microhardness test for Cu/Cu foam brazed interface joint using filler C with (a) foam A (b) foam B and (c) foam C at $T_{br}$ of 660 °C	88
<b>Figure 4.17</b>	: Hardness value (HV) of Cu/Cu foam brazed joint interface based on indentation position in Figure 4.14 to Figure 4.16	90
<b>Figure 4.18</b>	: Top view of Cu substrate surface from shear test of brazed Cu/Cu foam using filler A with (a) foam A (b) foam B and (c) foam C at $T_{br}$ of 660 °C	93
<b>Figure 4.19</b>	: Top view of Cu substrate surface from shear test of brazed Cu/Cu foam using filler B (a) foam A (b) foam B and (c) foam C at $T_{br}$ of 680 °C	94
<b>Figure 4.20</b>	: Top view of Cu substrate surface from shear test of brazed Cu/Cu foam using filler C with (a) foam A (b) foam B and (c) foam C at $T_{br}$ of 660 °C	95
<b>Figure 4.21</b>	: Side view of Cu substrate surface from shear test of brazed Cu/Cu foam using filler C with (a) foam A (b) foam B and (c) foam C at $T_{br}$ of 660 °C	97
<b>Figure 4.22</b>	: Top view mapping analysis of Cu substrate surface from shear test of brazed Cu/Cu foam using filler C with (a) foam A (b) foam B and (c) foam C at $T_{br}$ of 660 °C	98
<b>Figure 4.23</b>	: Brazed joint interface of Cu/Cu foam	99
<b>Figure 4.24</b>	: Microstructure of Cu/Cu brazed joint interface using (a) filler A (b) filler B and (c) filler C	101
<b>Figure 4.25</b>	: Microstructure of Cu/Cu foam brazed joint interface using filler A with (a) foam A (b) foam B and (c) foam C	103
<b>Figure 4.26</b>	: Microstructure of Cu/Cu foam brazed joint interface using filler B with (a) foam A (b) foam B and (c) foam C	104
<b>Figure 4.27</b>	: Microstructure of Cu/Cu foam brazed joint interface using filler C with (a) foam A (b) foam B and (c) foam C	105
<b>Figure 4.28</b>	: X-ray diffraction (XRD) pattern of Cu substrate surface from shear test of brazed Cu/Cu foam using (a) filler A (b) filler B and (c) filler C	107
<b>Figure 4.29</b>	: Elemental composition and mapping analysis on Cu/Cu foam brazed joint interface using filler A with (a) foam A (b) foam B and (c) foam C	109
<b>Figure 4.30</b>	: Elemental composition and mapping analysis on Cu/Cu foam brazed joint interface using filler B with (a) foam A (b) foam B and (c) foam C	110

<b>Figure 4.31</b>	: Elemental composition and mapping analysis on Cu/Cu foam brazed joint interface for filler C with (a) foam A (b) foam B and (c) foam C	111
<b>Figure 4.32</b>	: EDX line scanning analysis at selected area across brazed Cu/Cu foam A/Cu using filler A	116
<b>Figure 4.33</b>	: EDX line scanning analysis at selected area across brazed Cu/Cu foam A/Cu using filler B	117
<b>Figure 4.34</b>	: EDX line scanning analysis at selected area across brazed Cu/Cu foam A/Cu using filler C	118
<b>Figure 4.35</b>	: Illustration of filler before brazing (a to c) and molten filler during brazing (a-i to c-i)	124
<b>Figure 4.36</b>	: Proposed diffusion mechanism of Cu-Sn-Ni-P amorphous filler alloys	125
<b>Figure 4.37</b>	: Microstructure of crystalline (a) filler A (b) filler B (c) filler C with inset of EDX point analysis for elemental composition in Table 4.10 at 2000 magnification	129
<b>Figure 4.38</b>	: Mapping analysis and area elemental composition (wt.%) analysis for crystalline (a) filler A (b) filler B (c) filler C	130
<b>Figure 4.39</b>	: Open circuit potential for crystalline Cu-Sn-Ni-P filler	132
<b>Figure 4.40</b>	: Anodic and cathodic polarisation curve of crystalline Cu-Sn-P-Ni filler	134
<b>Figure 4.41</b>	: Polarisation parameters of (a) $E_{\text{corr}}$ and (b) $I_{\text{corr}}$ by Tafel fit for filler A, filler B and filler C	135
<b>Figure 4.42</b>	: Cyclic polarisation curve of crystalline Cu-Sn-Ni-P fillers	137
<b>Figure 4.43</b>	: Pre-immersed microstructure of Cu/Cu foam A brazed joint interface (pre-immersed) using (a) filler A (b) filler B and (c) filler C	138
<b>Figure 4.44</b>	: Post-immersed optical images of uncleaned Cu/Cu foam A using (a) filler A (b) filler B and (c) filler C	141
<b>Figure 4.45</b>	: Post-immersed microstructure of uncleaned Cu/Cu foam A using (a) filler A (b) filler B and (c) filler C	142
<b>Figure 4.46</b>	: Post-immersed microstructure of cleaned Cu/Cu foam A brazed joint interface using (a) filler A (b) filler B and (c) filler C	145

## LIST OF TABLES

<b>Table 2.1</b>	: Summary of metal foam heat exchanger studies	13
<b>Table 2.2</b>	: Summary of brazing studies on various material	26
<b>Table 2.3</b>	: Summary of filler foil from previous studies	31
<b>Table 2.4</b>	: Summary of parameter studies for metal foam	37
<b>Table 3.1</b>	: Materials for the current research work	48
<b>Table 4.1</b>	: Characterisation of Cu foam	61
<b>Table 4.2</b>	: Highest compressive strength and highest shear strength of brazed Cu/Cu foam/Cu	85
<b>Table 4.3</b>	: Summary of elemental composition at Cu/Cu foam brazed joint interface using different fillers and foams based on points in Figure 4.29, 4.30 and 4.31	114
<b>Table 4.4</b>	: Elemental composition across brazed Cu/Cu foam A/Cu using filler A based on points label in Figure 4.32	116
<b>Table 4.5</b>	: Elemental composition across brazed Cu/Cu foam A/Cu using filler B based on points label in Figure 4.33	117
<b>Table 4.6</b>	: Elemental composition across brazed Cu/Cu foam A/Cu using filler C based on points label in Figure 4.34	118
<b>Table 4.7</b>	: Summary of elemental composition across brazed Cu/Cu foam A/Cu using different fillers based on points in Figures 4.32, 4.33 and 4.34	119
<b>Table 4.8</b>	: Points label across brazed Cu/Cu foam/Cu using different fillers with different Cu foam pore density	122
<b>Table 4.9</b>	: Summary of elemental composition across brazed Cu/Cu foam/Cu using different fillers with different Cu foam pore density as label in Table 4.8	123
<b>Table 4.10</b>	: EDX point analysis for elemental composition (at.%) of crystalline filler A, crystalline filler B and crystalline filler C based on Figure 4.39	128
<b>Table 4.11</b>	: EDX point analysis for elemental composition of post-immersed uncleaned Cu/Cu foam A brazed joint interface in Figure 4.45	140
<b>Table 4.12</b>	: EDX point analysis for elemental composition of pre-immersed Cu/Cu foam A (Figure 4.43) and post-immersed for cleaned Cu/Cu foam A brazed joint interface (Figure 4.46)	143

## LIST OF SYMBOLS AND ABBREVIATIONS

$\gamma$	Gamma-phase
$\epsilon$	Strain
$\sigma$	Compressive stress
$\sigma_{\text{comp}}$	Compressive strength
$\tau$	Shear stress
$\tau_{\text{shear}}$	Shear strength
Cr	Chromium
Cu	Copper
EDX	Energy-dispersive X-ray spectroscopy
G	Graphene
HV	Hardness value
ICSD	Inorganic crystal structure database
IMC	Intermetallic compound
Mg	Magnesium
Ni	Nickel
O	Oxygen
OFAT	One-factor-at-a-time
OCP	Open current potential
P	Phosphorus
PPI	Pore per inch
SEM	Scanning electron microscopy
Si	Silicon
SiC	Silica carbide
Sn	Tin
SS	Stainless steel
$T_{\text{br}}$	Brazing temperature
Ti	Titanium
$T_{\text{L}}$	Liquidus temperature
$T_{\text{S}}$	Solidus temperature
V	Vanadium
wt.%	Weight in percentage
XRD	X-ray diffraction
Zn	Zinc

## LIST OF APPENDICES

<b>Appendix A</b>	: Supplementary Materials and Data	166
<b>Appendix A.1</b>	: Classification of Heat Exchangers	166
<b>Appendix A.2</b>	: Purity of Copper Substrate	167
<b>Appendix A.3</b>	: Inorganic Crystal Structure Database (ICSD)	168
<b>Appendix B</b>	: Materials and Data Measurement	179
<b>Appendix B.1</b>	: Pore Diameter, Cell Wall Diameter and Branch Diameter of Cu Foam	179
<b>Appendix B.2</b>	: Percentage of Cu Foam Porosity	181
<b>Appendix B.3</b>	: Extrapolation of Linear Tafel Plot	182
<b>Appendix C</b>	: Supplementary Figure	185

## CHAPTER 1 : INTRODUCTION

### 1.1 Introduction

Heat exchangers are used to transfer heat between two or more fluids (liquids, vapors and gases) at different temperatures (Ohadi, 2000). The heat exchange mechanism results in an increase in temperature on the cooler side and a decrease in temperature on the hotter side. Usually, there are no external thermal and work interactions involved in heat exchanger operations (Vohra, Aijaj & Saxena, 2013). However, internal thermal generation can be present such as those in nuclear fuel and electric heater elements. Similarly, chemical reaction and combustion may occur within the heat exchanger such as in boilers, fire heaters and fluidized-bed exchangers.

Heat exchangers are widely utilized for industrial and engineering applications as heating or cooling devices. They are used in manufacturing, power plants, petroleum, automotive, space, conditioning, heat recovery, refrigeration, and cryogenic (low temperature applications). In typical applications, heat exchangers are vital components in operations such as in heaters, coolers, boilers, evaporators or condenser systems. Others application may use heat exchangers to recover or reject heat, sterilize, pasteurize, fractionate, distill, concentrate, crystallize, or control process fluids (Rai & Dubey, 2017)

Due to global concern in environmental protection and energy saving, there is increasing pressure for the industry to recover process energy and reduce carbon dioxide emissions. Industrial developments also include improvements in heat exchanger performance and efficiency, which can maximize financial returns while at the same time comply with governmental requirements of environmental protections.

Heat exchangers can be classified based on the transfer process, fluids number, surface compactness, construction, flow arrangements and heat transfer. A summary of

heat exchanger classification is listed in **Appendix A.1**. Most heat exchanger applications are direct-transfer type (recuperator) or indirect-contact heat exchangers, where the heat is exchanged continuously with the cold fluid through a separating wall. Common direct-transfer heat exchangers are tubular, plate-type, and extended surface exchangers.

Compact heat exchangers have a high surface area density as compared to non-compact exchangers (e.g. tubular heat exchanger). This can result in increased heat transfer surface area per the heat exchanger volume. The compact design reduces space, weight, energy, cost, and is enclosed in a supported structure.

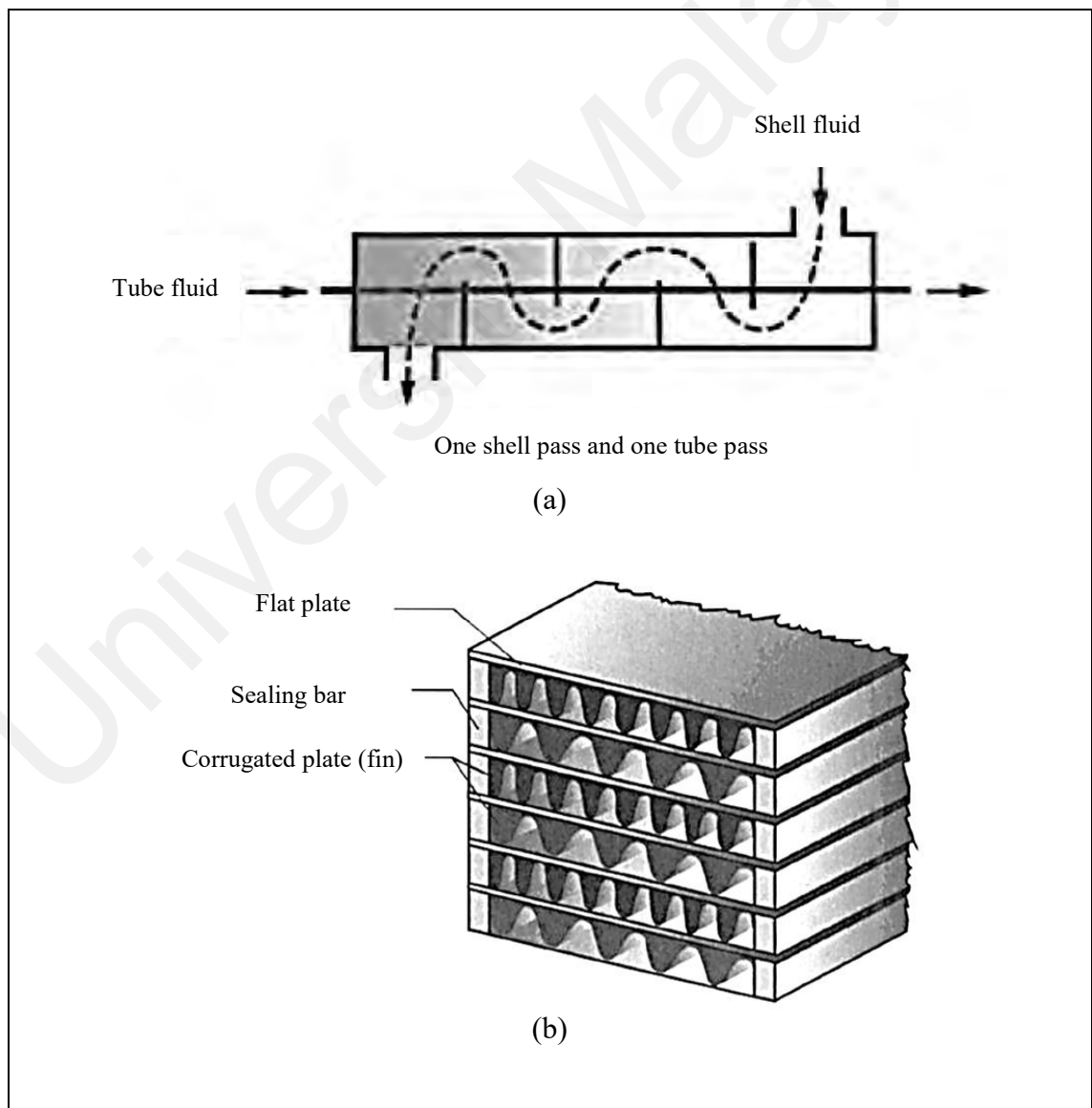


**Figure 1.1:** Heat exchanger (a) Non-compact (Shell-and-tube) (b) Compact

The heat exchange effectiveness also depends on the type of flow of the fluid streams. Flow arrangements in a heat exchanger can be divided into counter-flow (both fluids flow in the opposite sides of the exchanger), parallel-flow (fluids flow in the same side of exchanger, parallel to each other from one end and flows out to the other side of exchanger), and cross-flow (fluids flow in a perpendicular direction). Lastly, the mechanism of heat transfer consists of single phase-convection, two-phase convection, and combined convection and radiation heat transfer. (Ohadi, 2000; Shah, 1981)

## **1.2 Problem Statement**

This work focuses on the analysis of brazed Cu/Cu foam/Cu joint using amorphous filler alloys. The output of this research work would be beneficial for other researchers and engineers as a guideline in joining metal foams for heat exchanger designs and applications.

Heat exchangers are used in many parts of the automobile, such as the radiator, heater, condenser, evaporator, oil cooler and charge air cooler. The automobile heat exchanger radiators were introduced 1910 (Shah & Sekulić, 2003) to withdraw the heat generated from the combustion process away from the engine. Excessive engine temperatures may degrade performance and seize the operation of the engine (Dubey, 2015). The heat exchanger is a solution to dissipate the heat produced and controls the engine system from overheat. The development of radiators are continuously being improve in term of design, analysis and manufacturing. Improvements include more compact designs, higher efficiency, increased durable and reduced production costs (Jacobi et al., 2008). The challenge to remove heat in this thermal application is to utilise a material that has a high surface area with a small volume.

Compact heat exchangers have large area densities which consist of many corrugated plates arranged in a small volume. A common compact heat exchanger in automotive and aircraft is a plate heat exchanger with a louver fin structure. The structure is very complicated and costly to manufacture (Zhao, 2012). The fabrication of compact and complicated heat exchanger configuration involves many internal joints (Hartmann & Nuetzel, 2010). Failure in heat exchanger is usually caused by internal or external leakages. These failures are caused by mechanical stresses, chemically induced corrosion, scale (mud, algae etc. fouling) and a combination of mechanical and chemically induced corrosion (Schwartz, 1982).

The brazing technique is often used as the joining technology for heat exchanger fabrication. During the brazing process, incomplete gaps filling may occur due to poor wetting of filler metals and local contaminations. Flaws in brazing joint are due to cavities and geometrical misalignments in brazed structure. Entrapped gases may increase the formation of voids and pores, which lead to imperfect brazed joint (Luo et al., 2017). A low strength joint causes a high thermal resistance at the brazed joint interface which reduces the thermal conduction significantly between the metals due to lower brazed contact interface (Jaeger et al., 2012). Furthermore, imperfect brazing could reduce the performance of the heat transfer and shorten the life service of the heat exchanger (Boomsma, Poulidakos & Zwick 2003; Nawaz, Bock & Jacobi, 2012). Indirectly, the heat transfer coefficients would decrease and cause further performance problems in heat exchanger design and operation (Jingxin et al., 2015). During heat exchanger operations, the rapidly moving large mass flow of fluid requires a strong brazed joint between the metals (Heo, Kim, Yeon, Moon & Chun, 2019). The heat exchanger is well known to be able to continuously operate at high temperatures for a long duration of service. The joined metal plate pair would be heated up more than adjacent metals, leading to possible expansion of metal plate pair. This metal expansion induces shear stresses on the joined

metal plate, which may damage the plate joints (Santos, Morgado, Martinho, Pereira & Moita, 2017). This condition may induce creep failures. Thus, the presence of brazed joint defects or flaws will contribute to the creep failure initiation in the heat exchanger. (Ghovanlou, Jahed & Khajepour, 2013; Shi et al., 2012).

The operation of heat exchangers is exposed to various extreme conditions making them the heat susceptible to the corrosion. There is a high tendency of corrosion reaction to occur on the materials in the presence of liquid (aqueous solution, molten salts, molten metals), air (oxygen or any gaseous at ambient or elevated temperature) (American Welding Society C3 committee (AWS), 2011), moisture and particular volatile compounds (Peltola & Lindgren, 2015). The heat exchangers could be exposed to chemical products cleaning, environment pollutants compound (exhaust gas, brake dust, SO<sub>x</sub> and NO<sub>x</sub>), and de-icing salts for seasonal countries (Renault et al., 2018). The cleaning process of heat exchanger parts includes degreasing and pickling operations using a corrosive organic acid such as chlorinated organic solvents and synthetic lubricant oils, which could initiate corrosion activities (Peltola & Lindgren, 2015). Leaks in heat exchanger structure can form if corrosion goes unnoticed. Leakages would cause reduction on pressure and heat coefficient. The worst case is formation of a hole in the heat exchanger that would result in fluid cross-contamination (Ghayad, Hamid & Gomaa, 2015).

New plate heat exchanger designs have utilized foam-based structures to increase the surface area within a small volume. This design is an improvement of louver fin structures. However, the joining of porous structures onto solid metal is challenging and studies on the mechanical and corrosion performance of these joint configuration are still scarce. Thus, this study proposes the utilization of amorphous filler alloys for the brazing of Cu/Cu foam/Cu joint, which can be utilized for heat exchanger designs. This study

would also evaluate the influence of pore density of Cu foam on the joinability, which may have an influence on heat transfer efficiencies.

### **1.3 Objectives of the Study**

The following objectives are outlined for this study:

1. To fabricate Cu/Cu foam/Cu joint via brazing using Cu-Sn-Ni-P (Sn: tin, Ni: nickel, P: phosphorus) amorphous filler alloys.
2. To investigate the effect of brazing temperatures, Cu foam pore density and Cu-Sn-Ni-P amorphous filler alloys on the mechanical properties of Cu/Cu foam/Cu brazed joint.
3. To determine the effect of Cu foam pore densities and Cu-Sn-Ni-P amorphous filler alloys on the microstructure of Cu/Cu foam/Cu brazed joints.
4. To evaluate the corrosion behaviour of Cu-Sn-Ni-P filler and Cu/ foam Cu/Cu brazed joints.

### **1.4 Scope of the study**

Metallic foam materials, such as Cu foams, are potential components in high performance heat exchanger applications. The reliability and performance of the heat exchangers would depend on the strength and quality of the joint components, as the system would be exposed to high pressure and temperature fluid flows. Furthermore, the components would be immersed in aggressive fluid environments that is prone to corrosion. Thus, studies on the joining of porous metals have been the topic of interest of many researchers, although the area is yet to be explored in detail. In this study, the joining of Cu/Cu foam/Cu by brazing technique using Cu-Sn-Ni-P amorphous filler alloys was investigated. The Cu/Cu foam/Cu was brazed with different Cu foam pore densities (pore

per inch- PPI) which are 15 PPI, 25 PPI and 50 PPI using different Cu-Sn-Ni-P amorphous filler alloys Cu-4.0Sn-9.9Ni-7.8P, Cu-9.7Sn-5.7Ni-7.0P and Cu-9.0Sn-7.0Ni-6.0P at different brazing temperatures (660 °C, 680 °C, 700 °C and 720 °C). The microstructure analysis was carried out to evaluate shear-fracture, micro-hardness, brazed joint interface and diffusion of filler across the Cu/Cu foam/Cu. Corrosion analysis was also conducted to reflect the durability of the Cu/Cu foam/Cu in the aggressive environment of heat exchanger applications.

### **1.5 Thesis layout**

This thesis consisting of 5 chapters are outlined as follows:

Chapter 1: Introduction section containing a brief review on the background of study, the problem statement, objectives and scope of the study.

Chapter 2: Literature review on the research subject, including a detailed assessment related to heat exchangers, Cu foams, amorphous filler alloys, brazing process and corrosion.

Chapter 3: A section on material and methods which explains the method for Cu/Cu foam/Cu brazing. The methods for analysis and characterisation are also included.

Chapter 4: Result and discussion are presented on the mechanical properties, microstructure, and corrosion behaviour of Cu/Cu foam/Cu brazed joint interface with lists of data, analysis and detailed discussions.

Chapter 5: Conclusion section to recap the major findings of the current work to reflect the research objectives. Suggestions for future studies are also proposed.

## CHAPTER 2 : LITERATURE REVIEW

### 2.1 Introduction

This chapter presents a literature review on heat exchanger, metal foam, brazing method, current research on foam brazing and corrosion behaviour on the Cu/Cu foam brazed joints.

### 2.2 Heat Exchanger

Heat exchangers can be classified into many categories depending on their construction, flow arrangement, transfer process, number of fluids, and heat transfer mechanisms. Such classification of heat exchanger is needed due to the different requirements of equipment types, applications areas, and design techniques. For most heat exchanger system designs, heat exchanger construction is divided into tubular exchangers and compact heat exchangers. Subsequent consideration, such as flow arrangements, can then be taken into account in designing heat exchanger systems.

Common design of tubular heat exchanger is the shell-and-tube heat exchanger type. In this design, many tubes are mounted parallel in a shell, where one fluid flows inside the tubes while the other fluid flows through the shell. The heat is transferred from the fluid inside the tube side to the fluid in the shell or vice versa, depending on the temperatures of each fluids. A vast heat transfer area can be obtained by utilizing extended surface and large number of tubes to achieve high heat transfer efficiency (Santos et al., 2017). This design can be customized based on capacity, working fluid type, operating pressure, and temperature. The shell-and-tube heat exchanger has been utilised in power industries (for steam generators, condensers, evaporators, feed water heaters and oil coolers) and chemical industries (process heat exchangers).

Compact heat exchanger is characterized by having a large surface area density. The large surface area density is the ratio of heat transfer surface area to the heat exchanger volume. The heat transfer efficiency increases with large surface area density of compact heat exchanger, achieving comparable performance to shell-and-tube heat exchanger in a smaller volume. In fact, the reduction in size of exchanger enhances the heat transfer surface and has become a motivation in designing increasingly compact heat exchangers (Rai & Dubey, 2017). Shah (1981) defined a compact heat exchanger as having an area density  $>700 \text{ m}^2/\text{m}^3$  with a hydraulic diameter  $\leq 6 \text{ mm}$ , while a shell-and-tube heat exchanger has an area density  $\leq 100 \text{ m}^2/\text{m}^3$  (Shah, 2003). The large area density of compact heat exchanger is created through the close arrangement of corrugated plates in the structure. The corrugated plates would be in contact with the fluid and create a highly turbulent fluid flow, yielding a high heat transfer coefficient. Compact heat exchangers generally have good thermal performances and are widely used in high operating temperature applications such as in aerospace, power plants and automobiles (Li, Flamant, Yuan, Neveu & Luo, 2011).

Thus, compact heat exchangers are competitive alternatives and offer great advantages over shell-and-tube heat exchangers. They are space saving and lightweight, due to the less use of material, and are less costly to install as compared to the multi-shell arrangement design of shell-and-tube exchanger. The maintenance costs are low as fouling occurrence is minimized and the cleaning process is simple and fast by using high-pressure water jet to clean the panels. However, compact heat exchangers require a stronger pumping mechanism as the turbulent flow results in high pressure drops. Nevertheless, it has been reported by Gunnarsson, Sinclair and Alanis (2009) that the pumping costs for compact heat exchangers are normally low as compared to multi-shell installation in shell-and-tube exchanger. Compact heat exchanger may not be suitable for all thermal applications and some engineers may favour the familiarity of conventional

shell-and-tube exchangers. With the advancement of heat exchanger design and technologies, compact heat exchangers have become a competitive alternative over conventional shell-and-tube designs and should therefore not be overlooked.

### **2.2.1 Plate Heat Exchanger**

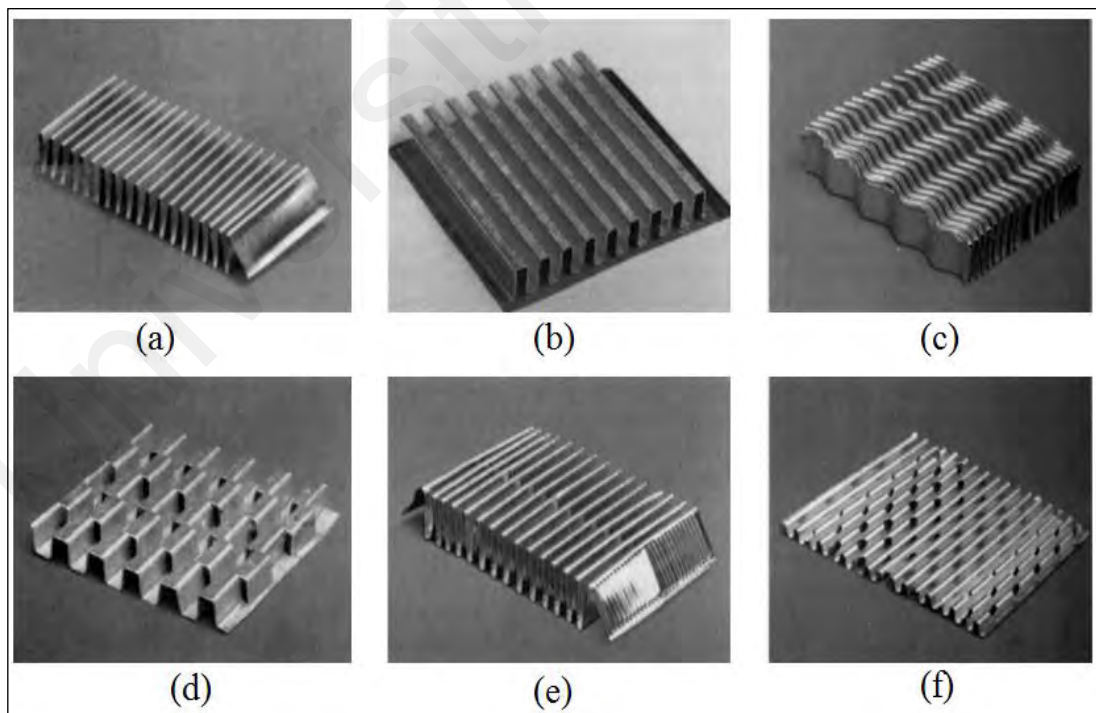
Compact heat exchangers come in several designs such as the plate heat exchangers (Reay, 1994), printed circuit heat exchangers (Li et al., 2011; Reay, 1994), spiral heat exchangers, and ceramic heat exchangers (Li et al., 2011). The plate heat exchanger design is more favourable when compactness requirement is a priority. In addition, plate heat exchangers are low costs, simple to maintain, flexible and have high heat transfer efficiencies (Elmaaty, Kabeel & Mahgoub, 2017).

Plate heat exchanger can be divided into gasketed (plate-and-frame), welded or brazed, spiral plate, lamella, and plate-coil exchangers. One of the earliest patents for plate heat exchangers were made by Dr. Richard Seligman, the founder of Aluminium Plant & Vessel Company Limited in 1923. Over the span of a century, the plate heat exchanger has been abundantly used in various industries such as dairy, paper processing, heating, ventilating, air conditioning (HVAC), aerospace, aircraft, and automotive (Kolb, 2018, Jangid, 2018). In an automotive system, the plate heat exchangers are used in several parts such as the radiator, heater, evaporator and condenser (air conditioning), oil cooler (engine and transmission oils), charge air coolers and intercooler.

A plate heat exchanger device requires good structural strength, high heat transfer rate and simple manufacturing processes to avoid failure and malfunctions (Kim, Paek & Kang, 2000). The extended (fins) or interrupted surfaces (corrugations) are added to provide a large contact surface area with a short flow fluids length to enhance the heat transfer efficiency. The plate-fin heat exchanger does not require a gasket, which are

needed in plate-and-frame heat exchangers. The non-gasket plate heat exchangers are easier to handle (Fernández-Seara, Diz & Uhía, 2013) and can be used at higher temperatures and pressures (Li et al., 2011). The geometries of the extended surface can be designed as plain and straight fins (plain triangular and rectangular fins), plain and wavy fins, and interrupted fins (offset strip, perforated, louvered and pin fins), as shown in Figure 2.1 (Ohadi, 2000; Shah & Sekulić, 2003).

The design of plate-fin exchanger increases the surface area by 5 to 12 times, resulting in increased heat transfer coefficient (Shah & Sekulić, 2003). Most plates have hydraulic diameters ranging from 2 to 10 mm with 10 to 100 numbers of plates, resulting in 5 to 50 channels per fluid (Thonon & Breuil, 2001). The selection of proper fin design in plate heat exchanger is important to ensure a uniform fluid flow distribution. Commercially, the interrupted fin design are used due to effective material construction.



**Figure 2.1:** Extended surface of fin geometries for plate heat exchangers (a) plain (triangular) (b) plain (rectangular) (c) wavy (d) offset strip (e) multilouver (f) perforated (Shah & Sekulić, 2003)

### 2.2.2 Materials and Structure of Plate-fin Heat Exchanger

Plate-fin heat exchangers have large surface areas which can offer good heat transfer performance. However, the fin structure of the plate-fin heat exchanger may be affected by thermal resistance, which can reduce performance. Furthermore, louvered fins have high manufacturing costs, and thin fin may be disadvantaged in term of structural strengths (Kim et al., 2000).

Recent studies, summarized in Table 2.1, have reported that heat transfer rates can be improved by replacing conventional heat exchanger fins with metal foam components. Metal foam has significant potential in thermal heat applications because of its highly porous material characteristics. This porous characteristic results in a large surface area, benefiting heat exchange mechanism. The tortuous flow path of metal foam promotes fluid mixing (Nawaz, Bock, Dai & Jacobi, 2010) which may also increase heat transfer coefficient performance (Chein, Yang, Tsai & Lu, 2009). Han et al. (2012) have stated that the specific surface area of foam can reach over  $10,000 \text{ m}^2/\text{m}^3$ , as compared to the surface area of fin of around  $700 \text{ m}^2/\text{m}^3$  (Shah & Sekulić, 2003).

Zhang et al. (2018) have studied the central processing unit (CPU) cooling system for information technology (IT) equipment using different heat sinks. The traditional heat sinks with microchannel was compared to porous Cu heat sinks. The porous Cu heat sink has performed better by reducing CPU temperature by more than  $10 \text{ }^\circ\text{C}$  as compared to traditional heat sinks. At heat flux density of  $100 \text{ W}/\text{m}^2$ , porous Cu heat sink and microchannel heat sink shows CPU surface temperatures of  $82 \text{ }^\circ\text{C}$  and  $96 \text{ }^\circ\text{C}$ , respectively. The heat coefficient of porous Cu has increased by 28.5% from the microchannel heat sink.

**Table 2.1:** Summary of metal foam heat exchanger studies

Heat exchanger design		Outcome of new design	Source
Initial design	New design		
Micro channel water cooling	Porous Cu water cooling	Porous Cu heat sink coefficient increases by 28.5%.	Zhang, Long & Zhang, 2018
Fin-and-tube	Cu foam	The heat transfer capacity is enhanced to 56%-196%.	Hu et al., 2016
Conventional finned tube	Metal foam wrapped tube	Significantly better in heat transfer performance.	Odabae & Hooman, 2012
Single channel, plate- fin and heat-fin	Cu foam heat sink	Cu foam heat sink can reduce up to 20% thermal resistance with increasing porosity of Cu foam.	Chein et al., 2009
Conventional finned plate	Metal foam heat sink	Metal foam heat sink is much improved for heat removal.	Ejlali, Ejlali, Hooman & Gurgenci, 2009
Conventional finned tube	Metal foam filled tube	The heat transfer has three times higher performance.	Zhao, Lu & Tassou, 2006
Hollow tube	Metal foam filled tube	Enhance the heat transfer performance up to forty times.	Lu, Zhao & Tassou, 2006
Flat plate	Aluminium foam	The thermal resistance is two to three times lower.	Boomsma, 2003

Hu et al. (2016) have compared the heat transfer and pressure drops between a fin-and-tube heat exchanger and a copper foam heat exchanger. The heat exchanger was manufactured via brazing using Cu-9.7Sn-9.6Ni-7.0P (wt.%) as the filler. A thermal analysis was conducted for air conditioning system applications. A thermal analysis is essential in designing and optimising heat performance as condensation may accumulate inside the heat exchanger. In the study, it was found that the copper foam heat exchanger enhances the heat transfer capacity by up to 196%.

Odabae et al. (2013) have examined the heat transfer performance of air-cooled fuel cell stacks using a metal foam for the replacement of water-cooled counterparts. The Al foam with a pore density of 20 PPI or 40 PPI was sandwiched between carbon fiber

plates. The increasing pore densities of Al foam and airflow were expected increase the pressure drop, while the increase in air velocity would decrease the thermal resistance of the aluminium foam and graphite plates. It was found that only a half pumping power was needed for an air-cooled fuel cell using foam as compared to water-cooled fuel cell systems. This was due to large pressure drop as the fluid flows across the water-cooled fuel cell system.

Chein et al. (2010) have investigated the thermal resistances of Cu foam heat sink with single-channel, plate-fin and pin-fin heat sinks. Plate-fin and pin-fin heat sink faced problem of pressure drops, which affected the heat coefficients. In this study, the metal foams are placed in the holes of flow passage. It was found that increasing the porosity of metal foam reduces the thermal resistance by up to 20% as compared to non-foam materials.

Ejlali et al. (2009) have compared the heat transfer performance of air condenser using conventional plate-fin and metal foam designs. It was found that the metal foam heat exchanger was superior over the conventional plate-fin designs in term of material weight and pressure drop. The metal foam allowed more airflow in the porous structure, which improved the fluid mixing and heat transfer performance.

Zhao et al. (2006) have applied Brinkman-extended Darcy model to analyse the heat transfer performance of tube heat exchanger filled with metal foam. Similarly, Lu et al. (2006) have employed the same model of Brinkman-extended Darcy model to compare between hollow tube heat and metal foam heat exchangers. Metal foam heat exchangers were fabricated by filling the hollow tube exchanger with metal foams using co-sintering technique. Results showed the high surface high surface area of the metal foam possessed additional advantages for improving heat transfer performance as compared to

conventional heat exchanger, whether in finned tube or hollow tube heat exchanger designs.

Boomsma et al. (2003) have studied the heat transfer performance of compressed aluminium foam heat exchanger and commercial-flat plate heat exchanger. The compressed aluminium foam was installed in a housing and mounted to the heat exchanger. It was found that the heat transfer of aluminium foam has performed relatively well and has decreased thermal resistance as compared to commercial heat exchangers. These past studies have shown the potential of utilizing metal foam to improve heat transfer performance.

The heat transfer process for foam heat exchanger is identical to plate-fin exchanger mechanisms. First, the hot fluid flows into the solid tube. Then, the heat of the fluid is transferred to the interconnected branch of the metal foam and absorbed by the airflows (Haack, Butcher, Kim, & Lu, 2001). Figure 2.2 (a) shows the large surface area of the interconnected branch, which enhances the heat transfer coefficient as compared to the low surface area of louver fin. Figure 2.2 (b) shows the fluid flowing through a porous area of the metal foam heat exchanger. In the porous heat exchanger design, the fluid experiences maximum contact with the interconnected branches surfaces to absorb the heat.

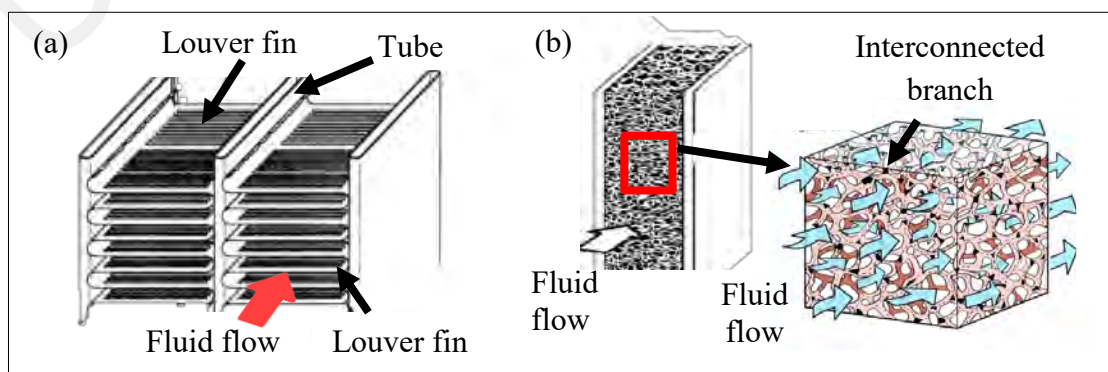


**Figure 2.2:** Type of heat-exchanger (a) louver fin (b) porous fin (Jacobi et al., 2008) and inset is porous metal foam (Zhao, 2012)

Plate heat exchanger can be fabricated from different materials depending on the operating temperature and pressure of the applications. Common heat exchange materials are copper, aluminium, stainless steel, titanium, nickel, and ceramics (Qasem & Zubair, 2018; Shah & Sekulić, 2003). Fernández-Seara et al. (2013) have investigated titanium brazed plate-fin (offset strip) heat exchanger with water-water and 10-30 wt.% ethylene glycol. Francis (2012) has studied brazed aluminium heat exchanger in cryogenic applications. Historically, Shah and Sekulić (2003) have reported that the copper fin-brass tubes of plate-fin heat exchanger has been utilized in the automotive industry since 1910s while aluminium has been used in aerospace applications (since 1940s) and liquefaction of natural gases (since 1950s) due to better mechanical characteristics at low temperatures.

The current work focuses on the use of copper material due to their excellent thermal properties. Copper, being a noble metal, is a transitional element that possesses similar properties of silver and gold. Copper has high electrical and thermal conductivity, good strengths (Shabtay, Ainali & Lea, 2004), excellent malleability, ductility, and corrosion resistance. Copper also is an ideal conductor because of its own intrinsic strength, formability and corrosion resistance. It is applied extensively for architectural components, water supply lines and plumbing fixtures, industrial, chemical plant and electronics (Copper Development Association). The use of copper in foam form makes the component lightweight, yet having increased strength at elevated temperature, making it suitable for heat exchangers application. Copper usually compete with aluminium for automotive applications. Gustafsson & Scheel (2000) have compared the important physical properties of copper and aluminium, and have favoured copper over aluminium as the material for heat exchanger applications.

### 2.2.3 Fabrication of Plate-fin Heat Exchanger

In an automotive vehicle, the radiator (heat exchanger) is a key component of the engine cooling system. Basically, the radiator is used to transfer heat from hot coolant or refrigerant to the outside air. Figure 2.3 shows the radiator core consisting of a set of tubes (refrigerant flow passage) and fins (air flow passage). The hot refrigerant flows in the tubes and passes the heat to the fins. The heat is then carried away by the outside air that flows in between the fins.

In the fabrication of the radiator, the fins and plates are alternately stacked and joined to form a core block before being assembled with tubes and the refrigerant tank to complete the radiator system, as shown in Figure 2.3. Figure 2.4 shows the plate/fin/plate geometry arranged in a sandwich configuration. The plates are positioned alternatively with fins to separate the individual layers. In joining between fins and plate, it is important to ensure a sound joint is made so the heat is transferred effectively. Any flaws in joining could produce high contact resistances and reduces the heat transfer coefficient (Boomsma et al., 2003).

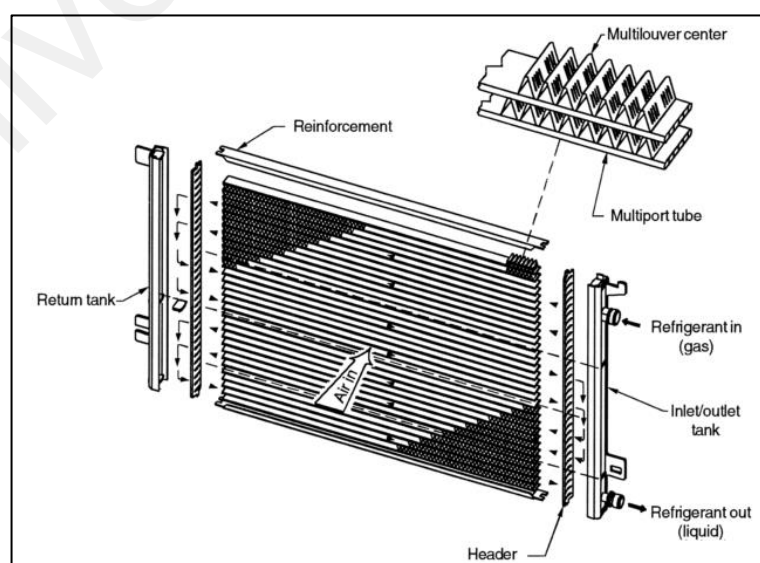


**Figure 2.3:** Automotive cooling system (Shah & Sekulic, 2003)

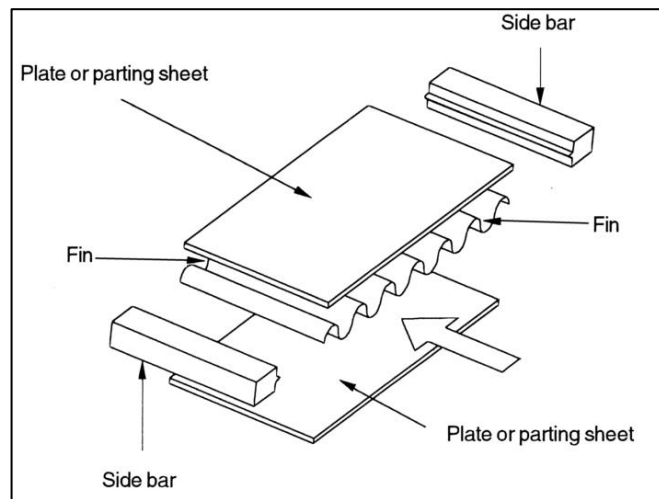


**Figure 2.4:** Component of a plate-fin heat exchanger (Shah & Sekulic, 2003)

Brazing techniques are usually used to join the fins and the plates to form a core block. The core block is then assembled by welding with other parts to form a radiator (Shah, 2003). Alternative methods of joining can also be used such as adhesive bonding, soldering and welding, which are selected based on the applications. Adhesive bonding and soldering are simple processes that require a paste to bond at low melting temperature. The adhesive bonding can be done from room temperature up to 150 °C, while soldering at temperatures < 200 °C depending on the insert material (Heo et al., 2019; Loh et al., 2000). Brazing is usually conducted using a filler metal to join at over 450 °C. Whereas welding technique requires high heat energy to join between metals without using metal inserts or adhesives (Feng et al., 2018).

Previous studies have investigated different joining techniques to fabricate plate heat exchanger with respect to thermal performance, materials and a joining configuration. Alias (2011) have studied the adhesive strength of plate heat exchanger for open cycle liquid desiccant air conditioner system. Cyanoacrylate, silicon sealant, and ethylene vinyl acetate (EVA) hot melt adhesives were compared to join polypropylene (PP) corrugated sheet and solid sheet. The cyanoacrylate adhesive was successfully joined, obtaining 3.68 MPa shear strength from the lap joint test. However, corrugated PP

sheet to solid PP experiences leakage due to the incompatibility of the adhesive on PP material. Loh et al. have (2000) reported that adhesive bonding would form a non-metallic bond which has poor thermal conductivity. This low thermal conductivity increases the thermal resistance and reduces thermal performance. Gejdos et al. (2017) have analysed the damage on high-alloy austenitic steel plate heat exchanger fabricate using soldering methods. It was found that cracks in the solder joint were mostly due to sulphur-based impurities. The presence of sulphur impurities can be reduced through a thorough cleaning process. Lv & Fu (2014) have evaluated the failures of air radiator of more than 30 years of services. It was found that the failure was caused by high-cycle fatigue fracture due to incorrect placement of corrugated plates during fabrication.

Lewinsohn et al. (2014) have evaluated different joining methods of ceramic compact heat exchangers. These heat exchangers are fabricated using tape bonding, preceramic polymers pyrolysis, and brazing using copper (27%) dopped titanium (4%) and silver (69%) filler. The microchannel plates are stacked and bonded using different joining methods. Results showed that the compact heat exchanger using brazing method has formed a stronger joint. Vekariyamukesh et al. (2012) have suggested that good quality brazed aluminium heat exchanger for heating, ventilation, and air conditioning (HVAC) industry could be obtained at a brazing temperature range of 605 °C to 615 °C. Fernandes, Dias and Maia (2010) have reported that stainless steel plates can be brazed using copper or nickel alloys. Sarah et al. (2019) have designed a plate-fin heat exchanger by brazing 316 stainless steel plate and fins that were able to operate at high temperatures and in corrosive environments. The 316 stainless steel brazed plate-fin heat exchanger has comparable performance to a printed circuit heat exchanger in Brayton cycles using supercritical carbon dioxide (sCO<sub>2</sub>) Flex cycle for gas turbine engines.

From the literatures, it was found that a majority of plate-fin heat exchangers were fabricated using the brazing method for joining. Furthermore, the development of lead-free filler metals, such as copper-tin-nickel-phosphorus filler metal, guarantee their non-toxicity and would be harmless to human and the environment. The presence of phosphorus in filler metal makes the brazing process flux-free, thus no cleaning is required (Tapper et al. 2018). In addition, brazing is accurate and able to produce a low thermal resistance joint which is less than 1% of the total thermal resistance (Schampheleire et al., 2014).

### **2.3 Metal Foam**

Naturally porous material such as corals, woods and bones are lightweight and durable structures. These examples from nature has become an inspiration for metallurgist to produce porous metal foam structures (Zhao et al., 2006). Its use has started in the 1960s in the application of metallic foam for the cooling of inter-ballistic missiles components of the US Navy. Commercial usage of metallic foams were available in the early 1980s, and have wide applications such as in transportation, infrastructure and construction, automotive, aerospace and military equipment (Nawaz et al., 2012, Liu et al., 2014). Research and development in metallic foam include utilization in thermal applications, such as in heat exchanger equipment (Abadi et al. 2016a), heat sinks in electronics (Hu et al., 2016), engine combustion, aircraft and automotive systems (Shirzadi et al., 2008). There is a growing demand in metal foam, with a USD 82.0 million share in the global market (Grand View Research, 2017).

The fabrication process plays a vital role in the manufacturing of metal foam, in particular in the metal foam pore density (pore per inch- PPI) and porosity (%). These properties determine the mechanical and thermal properties of metal foam, which affect its functionality in the intended application (Vesenjak et al., 2016). There are several

methods of metal foam fabrication, such as electro-deposition (Kim et al., 2016), powder metallurgy, casting, metal vapour, and metal ions (Xie et al., 2004; Ramos et al., 2012; Wang et al., 2016). The choice of process would depend on the required foam structure, whether open-cell or closed cell. In addition, the metal foam material is selected based on their intended applications. Metal foams material can be fabricated from nickel (Ni) (Ochiai et al., 2006; Sun et al., 2018), iron (Fe) (Alavi et al., 2017), copper (Cu) (Rybar et al., 2016), aluminium (Al) (Saw et al., 2017), or stainless steel (SS) (Tuzovskaya et al., 2012).

The high surface area of metal foam enable the transfer of a high amount of heat with a small volume of metal (Zhao, 2012). The foam structure consists of highly interconnected branches and porosities, which can be closed cell or open-cell structures. Closed-cell metal foam generally has air-filled pores with cell wall barriers, as shown in Figure 2.5(a). In contrast, open-cell metal foam has continuous interconnected branches network formed a cell wall with a node, as shown in Figure 2.5(b). The interconnected branches of foams are surrounded by void spaces which are linked through pores (Tan & Chong, 2016). These voids create a highly porous structure and result in a large ratio of area per unit volume.

Closed-cell metal foams are utilised in structural applications due to their strengths while open-cell metal foams are applied in a functional applications such as in cooling, heating and condensing (Ghosh, 2009). Other applications of open cell structures are in sound absorption and high temperature gas and fluid filtrations. In heat exchanger applications, the fluid medium would pass through the pores and make contacts with the large surface area of metal foam branches (Kim et al., 2016). The high surface area of open-cell metal foam is thus expected to have significant heat transfer capability.

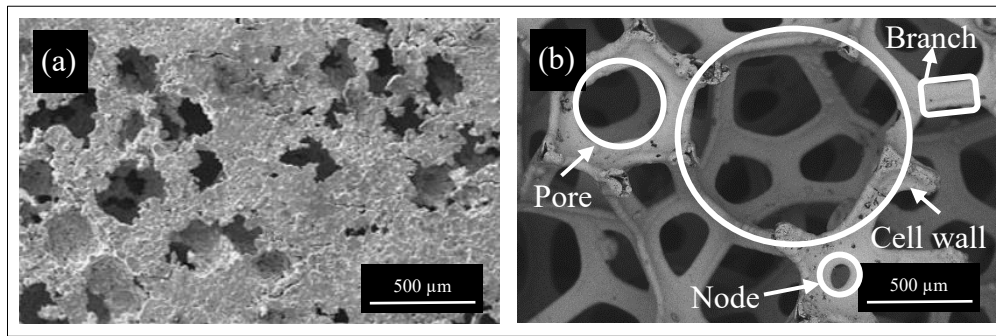


**Figure 2.5:** (a) Closed-cell (El-Hadek & Kaytbay, 2008) (b) Open-cell of metal foam

The intricate shape of the metal foam structure creates an extended surface which produces complex flow paths and increased surface area. The cell of metal foam usually follows a polyhedrons-like cell model with 12 to 14 faces. Each face would have a pentagonal or hexagonal shape depending on the pore density of the metal foam (Joen et al., 2010). Bhattacharya et al. (2002) have suggested that the cross-sectional shape of the metal foam branch can be changed from a circle to an inner concave triangle. As the porosity ( $\epsilon$ ) of metal foam increases, the cross-section shape of the metal foam would more likely to have an inner concave triangle shape, as shown in Figure 2.6. The metal foam is characterized by a pore diameter that correlates to pore density (PPI), the diameter of branches and foam porosity (volume of void divided by the total volume of medium) (Nawaz et al., 2012).

In industrial applications, the distribution of the open cell in the porous metal is often referred to by pore density and relative density (Ghosh 2015). The pore density of a cubic metal foam is typically expressed in units of pore per inch (PPI) (Bhattacharya et al., 2002). Other parameters that can describe the metal foam are its interfacial surface area, cell shape and size, permeability and cubic interconnected branch model. Different pore densities of metal foam can be produced by controlling the manufacturing input parameters (Rybar et al., 2015). Figure 2.7 shows different Cu foams with pore densities of 15 PPI, 25 PPI and 50 PPI.

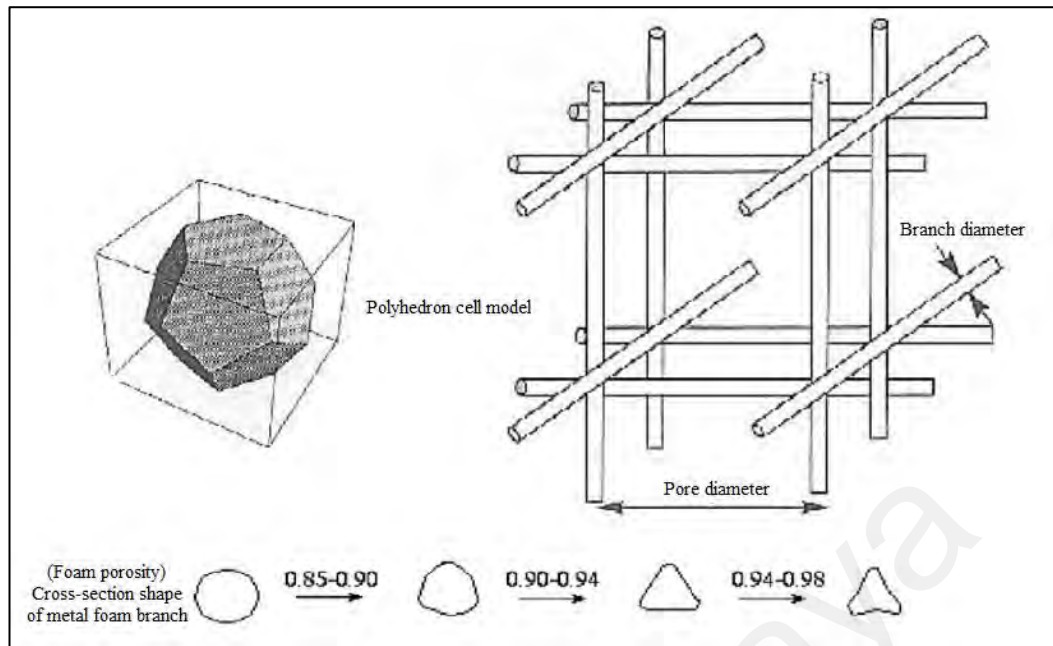


**Figure 2.6:** Polyhedron cell model and cross-section shape of metal foam branch based on foam porosity. (Bhattacharya et al., 2002)

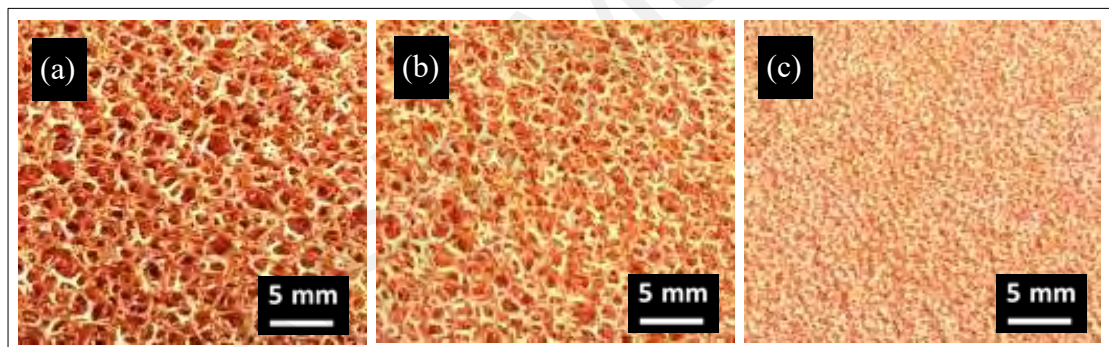


**Figure 2.7:** Cu foam at different pore density (a) 15 PPI (b) 25 PPI (c) 50 PPI

Functional applications of metal foam have mainly focused on thermal management. Tan & Chong (2016) have compared the results of experimental and simulated heat transfer of a three-dimensional (3-D) Cu foam geometrical structure using one-dimensional (1-D) aligned cylinder-bank. The parameters of Nusselt number and root-mean-square (RMS) error show good agreement between the simulation work and experimental results.

Chein et al. (2009) have used an electroforming technique to fabricate Cu foam with different pore densities and porosities by varying the electroforming time duration.

Thermal analysis of the Cu foam showed that an increase in foam porosity would reduce its thermal resistivity.

Mechanical analysis of the metal has been carried out on identify the metal foam failure and behavior mechanisms. Chen et al. (2017) have studied the compression characteristics of open-cell Cu foam by varying the strain rates ( $10^{-2} \text{ s}^{-1}$ ,  $10^{-3} \text{ s}^{-1}$  and  $10^{-4} \text{ s}^{-1}$ ) and Cu foam porosity (90.3%, 95.7% and 96.4%). The results show that the compression strengths, Young's modulus and yield strength of the Cu foam increase with increasing strain rate and decreasing Cu foam porosity. The failure mechanism of the compression deformation shows that the Cu foam experiences layer by layer collapse. This failure occurs due to the formation of stress concentration at the weak branch of Cu foam, as shown by the plastic stage deformation on the compressive stress-strain curve.

Liu et al. (2014) have investigated the effect of strain rates ranging from  $10^{-3} \text{ s}^{-1}$  to  $2400 \text{ s}^{-1}$  on the Cu foam mechanism and behaviour. The compressive stress-strain curves of lotus-type porous Cu consists of a linear elastic stage, a plateau stage and the densification stage for all strain rates. Material with a lower strain rate has less sensitivity towards stress-strain curve until the strain rate exceeds  $1.0 \text{ s}^{-1}$ . The plateau stage of the compressive stress-strain curve would be affected by the high strain rate. At high strain rates, the gases in the pores have insufficient time to escape which directly increase the atmospheric pressure and lead to an increase in the plateau stress.

## **2.4 Brazing Metal Foam as a Joining Method**

The brazing process is an easy and simple joining method that can preserve the metallurgical characteristics of the individual metal components (Schwartz, 2003). It is a suitable technique for joining of porous metal, nonmetals to metals and dissimilar metals. A filler is usually required, which is placed in between the joining interface prior

to the brazing process (Craymer, 2011). The literatures on the types of brazing filler materials are abundant for a variety of applications, as shown in Table 2.2.

Metal foams can be joined either using soldering, welding or brazing. Joining metal foams by soldering has several limitations which includes requirement for non-corrosive flux, non-uniform distribution of solder due to the porous structure of the foam, and restrictions on the use of the joined foam for high-temperature applications due to the low melting point of solder (Nowacki, Grabian and Krajewski, 2014). In contrast, joining of metal foam using welding is prone to deformation and shrinkage in the molten substrate material (Zhang, Chen, Liu & Li, 2013). Furthermore, the molten substrate material may diffuse into the pores and block the path of fluid flow of the porous network, increasing the thermal resistance of the welded metal foam. There is also a possibility of decreased shear strength due to degradation of the metal foam branch in the region of the weld (Kim et al, 2016). The brazing process can overcome the limitations of soldering and welding techniques, especially for high temperature thermal applications. It uses a filler metal that creates the joining bond, without melting the contacting surfaces, which can withstand high temperature operations.

The performance of metal foam heat exchanger have been reported widely in the literatures, but investigations on the joining of metal foam heat exchangers are scarce. Past studies have investigated the failures of the heat exchanger and have reported that the leading causes of the system failure were due to weak joints (Weishaupt, Stevenson, Mc Dougall & Turnquist, 2012; Lv & Fu et al., 2014; Hasap et al., 2015). Several work have discussed the use of brazing in the fabrication of metal foam heat exchangers (Chein et al., 2009; Ribeiro, Barbosa & Prata, 2012; Hu et al., 2016), although the process on joining of the metal foam heat exchanger were not explained in detail.

**Table 2.2:** Summary of brazing studies on various material

Substrate	Filler	Application	Source
<b>Copper-based</b>			
Cu-35Zn-3Pb	Cu-9Sn-7Ni-6P	Radiators of automobiles	Hasap, Noraphaiphaksa & Kanchabomai (2015)
CuCrZr and bronze	Cu-6.4Ni-9.2Sn-6.3P and Cu-9.1Ni-3.6Sn-8.0P	Commutator in the automotive industry	Kalin et al. (2016)
Copper	3.5Ag-72.8Cu-22.8Zn-0.9Cd	Automotive radiator	Tajfar, Ganjeh & Mirnagheri (2016)
<b>Titanium-based</b>			
Ti-6Al-4V	Ti-20Zr-20Cu-20Ni	Aerospace and chemical industries	Komolafe (2014)
Ti600 and Ni-25Si	Ti-Zr-Ni-Cu	Aerospace industry	Li et al. (2017)
Ti <sub>2</sub> AlC ceramics	Pure Al	Heat exchanger or high temperature solid lubricant	Lu, Sun, Zhang, Qi & Hug (2017)
<b>Composite-based</b>			
Sapphire and Inconel 600	63Ag-1.75Ti-35.25Cu	Gas pressure sensor	Zaharinie, Moshwan, Yusof, Hamdi & Ariga (2014)
C/C composite and Nb with Graphene-Cu foam as an interlayer	Ag-Cu-Ti	Thermal structure of aerospace technology	Wang et al. (2017)
Graphene-Cu	Ni-Cr-P-Cu	Commutator in the automotive industry	Zhang, Wang, Liu & He (2014)
<b>Ceramic-based</b>			
Porous Si <sub>3</sub> N <sub>4</sub>	Co <sub>22.5</sub> Si <sub>77.5</sub>	Thermal insulators	Zhuang et al. (2016)
<b>Stainless Steel-based</b>			
Hastelloy C276	Nickel based filler: BNi-2	High temperature fuel cell	Luo et al. (2017)

Hafeez, Chandra and Mostaghimi (2017) have reported that the heat removal performance of brazed foam material is better compared to epoxy-bonded material. In a

heat exchanger process, the stresses of fluid flows could affect the brazing joint strength and compress the metal foam, which leads to heat exchanger failure. Boomsma et al. (2003) have reported that the fluid flow and heat transfer behaviour would be affected when there is an addition of flow resistance near the interface joint due to imperfect brazing. Muley, Kiser, Sunden and Shah (2012) have stated that to enhance the heat transfer performance requires improvement in the joining of the metal foam. Thus, this is the motivation for the current work which will investigate the brazing of Cu foam for use in thermal applications.

#### **2.4.1 Brazing Filler Alloys**

A filler alloys is usually sandwiched in between the joining surface prior to brazing. The brazing filler alloys must have liquidus temperature above than 450 °C but below the solidus temperature of the base (substrate) metal. While the brazing temperature is usually fixed at approximately 56 °C above the liquidus of the filler material. According to American Welding Society (2008), the range selection of brazing temperature is depends on the materials joining, filler alloys, brazing process and joint design.

In the brazing process, as the brazing temperature is reached, the filler alloys melts and spreads to cover the faying surfaces and forms the brazed joint. The brazing temperature is usually lower than the melting temperatures of the base materials, the microstructures of the joined metals would not be affected to a great degree. Investigations into brazing usually focus on the microstructure of the joining interface due to the interactions of the filler alloys with the surfaces of the joined base materials (AWS, 2011).

The capillary action of the filler alloys plays an essential role in the formation of a sound joint by wicking the filler alloys in between of the faying surfaces. A good filler

for braze metals normally yield excellent wetting characteristic by flowing and filling into the thin gap of the brazed surfaces, which is usually incorporated into the brazing configuration to enhance the flow of the filler alloys. This thin braze gap is important in maintaining a robust surface tension and wetting characteristics of the filler. A stronger brazed joint is also obtained indirectly as the braze gap induces mean stresses in the brazed joint between the strong substrate materials and the weaker filler alloys (Craymer, 2011).

Wetting performance is critical in the brazing process as the filler material is required to spread into the joint to wet both surfaces. Wetting behaviour is determined by the balance between the surface tensions of solid-liquid, solid-vapour and liquid-vapour interfaces. The cleanliness of the substrate surface is also a crucial factor for joint surfaces (Jarvis, Voice & Goodall, 2011) as the presence of oxide layers, dirt, grease and other contaminations may prevent good wetting to occur (Schwartz, 2003).

Excessive diffusion of the filler alloys may cause major changes in the properties of the base metals. The selection of filler alloys is critical in determining the quality of the brazed joint. The factors that should be considered in the selection of a filler alloys are the brazing temperature, the substrate materials substrate, the joint configuration and the melting characteristic of the filler (Komolafe, 2014). Usually, the filler alloys is selected based on similar thermal expansion characteristic to the substrate metals (Craymer, 2011). Thus, it is important for the appropriate selection of types and amounts of filler alloys applied to control fluidity of diffusion.

Amorphous filler alloys (also known as metallic glasses) is a non-crystalline material, consisting of eutectic elements combinations of transition metals (nickel, iron, copper or chromium) and metalloids (silicon, boron or phosphorus). It is produced by using a rapid solidification process due to metalloids content at or near the eutectic

concentration (Arentoft, Eriksen & Hansen, 2010). The amorphous filler alloys can be flexibly produced into various shapes due to its ductile properties (Rabinkin, 2000). The production of amorphous filler alloys in foil form has simplified the brazing process and is becoming more favoured compared to the regular powder and paste filler alloys compositions. Amorphous filler alloys undergo rapid solidification process, which is in contrast to the slow solidification process of crystalline filler alloys. Thus, different microstructures are obtained from amorphous filler alloys compared to its crystalline form due to different solidification process.

During crystallization in the rapid solidification process, the molten mixture of amorphous filler alloys instantaneously undergo phase transition from a liquid state to a solid state as it does not have solidus and liquidus temperatures. The rapid cooling in a liquid state causes the filler to begin solidifying without being diffused. The diffusion of the elements is slowed as the nucleation occurs before the liquidus, forming a remote disorder and short-range order amorphous structure. This slow diffusion and nuclei growth results in equiaxed grains with fine microstructures, as shown in Figure 2.8 (a). The instantaneous solidification causes formation of numerous crystal nuclei growth and subsequently hinders further growth which lead to a formation of a uniform and homogenous microstructure (Sevryukov, Fedotov & Polyansky, 2016). Slow solidification of the crystalline filler alloys is then followed by further grain growth of the liquid atom of the solidified molten filler, as shown in Figure 2.8 (b).

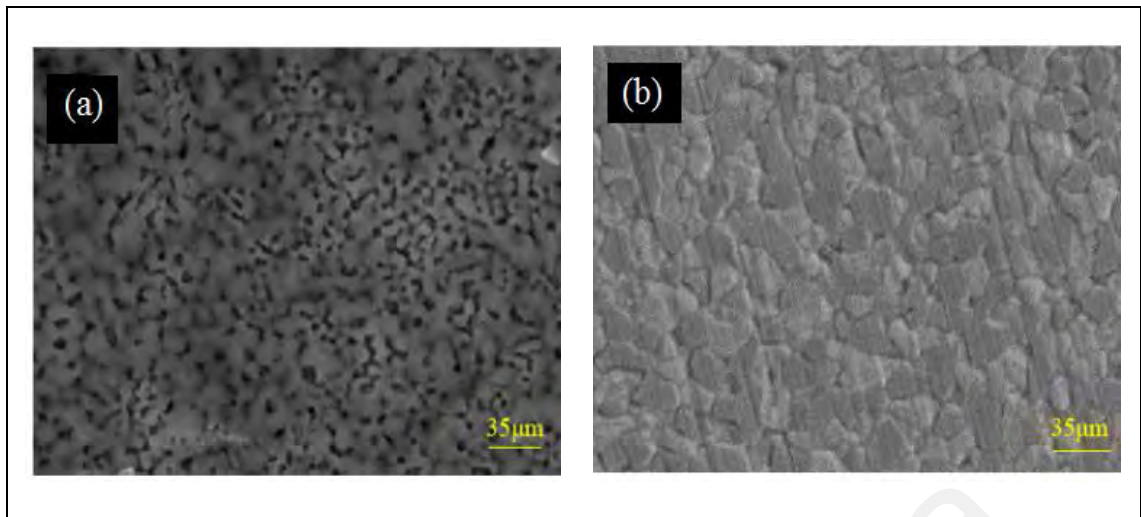


**Figure 2.8:** The microstructure of amorphous filler alloys (Cu-8.27Sn-5.74Ni -7.35P) and crystalline filler alloys (Cu-8.99Sn-6.63Ni -7.57P) (Xu, Ma & Xia, 2019).

The amorphous filler alloys is homogeneous in term of chemical and phase structure due to the composition of nickel, tin and phosphorus of more than 4%. The homogenized elements in amorphous filler alloys results in a narrow brazing temperature range. Furthermore, the amorphous filler alloys are in thin sheet forms, allowing rapid dissolution of filler on the substrates. In comparison, paste fillers require longer time to dissolve during brazing due to their thicker physical form (Weiyuan, Wenjiang & Tiandong, 2013). Fillers in paste or powder forms are challenging to apply into the braze cross-section as they require larger brazing gaps compared to foil filler alloys. Furthermore, paste filler alloys may develop more intermetallic compounds (IMCs) causing coarse grain sizes at the joints. In contrast, amorphous filler alloys possesses higher diffusion property, good filler wettability and capillary characteristic as compared to paste fillers. This characteristic allows the amorphous filler alloys to flow more freely upon melting (Weiyuan et al., 2013). Several studies have evaluated the utilization of filler foil for use in the brazing processes, as listed in Table 2.3.

Copper-phosphide (Cu-P) based filler alloys has been widely recommended and employed for the brazing of Cu (Aminazad, Hadian & Ghasimakbari, 2015). This amorphous filler alloys consists of varying composition weight percentages (wt. %) of

Cu, Sn, Ni and P elements. Each element in the amorphous filler alloys has a specific role, such reducing the melting point by incorporating Sn and P, and increasing strength and corrosion resistance by adding Ni (Şerban, Codrean, Utu & Opris, 2009; Xihui, Xiaoqiang, Min'ai, Shengguan & Zhongli, 2016). The element P act as a dissolvent (Şerban et al., 2009), fluxing agent (de-oxidant) with a self-cleaning effect (Zhong, Zhou, Shen & Ling, 2012) which can eliminate oxides contamination and improve the filler fluidity in a liquid phase (Weiyuan et al., 2013; Li et al., 2011). Furthermore, P promotes good wetting to cope with de-oxidation during the brazing process (Aminazad et al., 2015).

**Table 2.3:** Summary of filler foil from previous studies

Filler Foil	Substrate	Summary	Source
Ni-Cr-Si-B	Ni-NiCr and 18Cr-8Ni steel	The brazing seam consisted of Ni-B divorced eutectic and $\gamma$ -Ni solid solution, which is mainly dissolution and diffusion between NiCr substrate and filler alloys.	Wu, Li and Wang (2012)
Pd Titanium (Ti)	Porous Tungsten (W)	Ti foil fails to braze porous W due to poor brazed joint because serious melted Ti-rich infiltration. The Pd foil has successfully brazed but with limited Pd-rich infiltration (30 $\mu$ m) into the porous W.	Lin, Shu, Chen, Shiue and Shy (2012)
NiCrSiB	ZrO <sub>2</sub> and Ti-6Al-4V	Formation of TiO reaction layer is very crucial in brazing joint by the reaction of active Ti with ZrO <sub>2</sub> . In brazing seam, mainly consists of Ti <sub>2</sub> Ni, Ti <sub>5</sub> Si <sub>3</sub> and $\beta$ -Ti phases. The diffusion of Ni and Cr into TC4 alloy resulting in the formation of $\beta$ -Ti in diffusing zone.	Cao, Song, Li, Zhao and Feng (2013)
Cu-9Sn-7Ni-6P VZ 2250	Cu-35Zn-3Pb	The large thickness of the filler foil resulting smaller thickness of brazing joint and a more uniform combination between Cu <sub>3</sub> P phases and Cu-Zn-Sn phases. This is due to flux, and excess melted Cu <sub>3</sub> P are pressured out of the gap. The high contact pressure allows	Hasap et al. (2015)

Filler Foil	Substrate	Summary	Source
		the flux, excess melted filler and entrapped gas to pressure out through opening brazing point.	
Ti-Zr-Ni-Cu	Ti600 and Ni-25Si	The interaction between filler and substrate in the brazing process has increased the brazing seam. Ti-rich phases were formed near Ti600 alloys such as $Ti_3Al$ , $Ti_2Ni$ , $(Ti,Zr)_2(Ni,Cu)$ and $(Ti,Zr)_2Si$ . The diffusion layer of $Ni_{31}Si_{12}$ layer, $Ti_6Ni_{16}Si_7$ layer, $TiNi_3$ layer and $TiNi$ layer were formed at $Ni_{25}Si$ side.	Li et al. (2017)

Past studies have reported the use of Cu-P based amorphous filler alloys for the brazing of different solid metals. The resultant joint was analysed for the formation of interaction layers, intermetallic compounds and brazed joint strengths. Zhong et al. (2012) have reported that a Cu-7Ni-9Sn-6P amorphous filler alloys has successfully brazed glass to Kovar with a brazed joint strength of 1.6 MPa at 680 °C. Microcracks were found along the glass interface, and the compounds of  $Cu_3P$  and  $Ni_2P$  in the interface layer were believed have reduced the brazed joint strength.

Weiyuan et al. (2013) have studied the formation of Cu/Cu brazing joints using crystalline and amorphous alloys of Cu-9Sn-16Ni- 7P. Results show that amorphous filler alloys is more favoured for quick dissolution into the base metal as compared to crystalline filler. The fast dissolution was due to the thin sheets of amorphous filler alloys resulting in a shortened distance of atomic diffusion.

Hasap et al. (2015) have reported that crack propagation on the Cu-35Zn-3Pb brazed joint using Cu-9Sn-7Ni-6P amorphous filler alloys was caused by a brittle phase of  $Cu_3P$  and formation of cavities. The formations of cavities were due to contact pressures between the substrate surfaces leading to entrapment of gases and molten filler wettability problems.

Kalin et al. (2016) have investigated the brazing of beryllium (Be) and copper-chromium-zirconium (CuCrZr) bronze using different amorphous filler alloys of Cu-6.4Ni-9.2Sn-6.3P (STEMET 1105) and Cu-9.1Ni-3.6Sn-8.0P (STEMET 1101). It was discovered that the brazed was thicker using STEMET 1101 as compared to STEMET 1105. This was because the molten STEMET 1105 had higher fluidity characteristics during brazing since the solidus temperature of STEMET 1105 at 604 °C was lower than STEMET 1101 (618 °C).

Lutfi, Yusof, Ariga, Singh and Hamdi (2016) have conducted the brazing of Cu/Cu with Cu-7.0Ni-9.3Sn-6.3P amorphous filler alloys using hybrid microwave heating. It was found out the formation of the interface layer can be controlled by varying heating susceptor material. Subsequently, Lutfi, Yusof, Singh, Ariga and Hamdi (2017) have reported the interface layer formed from conventional brazing was three times thicker than the interface layer in brazing using hybrid microwave heating.

Several past studies have utilized the Cu-P based amorphous filler alloys for brazing. However, Cu-P based amorphous filler alloys have yet to be used to braze metal foams. Thus, this current work proposes using different compositions wt.% of Cu-P based amorphous filler alloys to braze Cu foam to solid Cu.

#### **2.4.2 Mechanism of Brazing**

The American Welding Society (AWS A3.0:2001) has defined diffusion brazing as “a brazing process that produces coalescence of metals by heating them to a brazing temperature and by using a brazing filler alloys or *in-situ* liquid phase. The brazing filler alloys may be distributed by capillary attraction or may be placed or formed at the faying surfaces. The brazing filler alloys is diffused with the base metal to the extent that the

joint properties have been changed to approach those of the base metal. Pressure may or may not be applied” (AWS, 2011).

Figure 2.9 shows the diffusion brazing process. Firstly, a filler alloys is inserted in between the faying surfaces of two metals substrates. During brazing, the filler distributes within the joint area, starts to wet and fill the joint surface by capillary action. As the brazing temperature and holding time increase, the elements in the molten filler alloys diffuse to the metal substrate, causes the solidus temperature of filler alloys to increase and re-melt. At this stage, the filler alloys is isothermally solidified at the brazing temperature. Lastly, the filler alloys has inter-diffused with the metal substrate to form a homogenous joint. (Jacobson & Humpston, 2005; AWS, 2011)

Brazing involves the heating process of the filler alloys to a liquid phase, then solidification of molten filler alloys below its eutectic (liquidus) temperature. During the solidification process, the nucleation starts to initiate when there is solid formation within the molten filler. It is then followed by a growth step where the liquid phase of the molten filler is solidified until none of the molten filler is left (Bernasko, 2012; Weiyuan et al., 2013). This process explains the joint interface formation between the solid and remaining liquid of filler alloys.

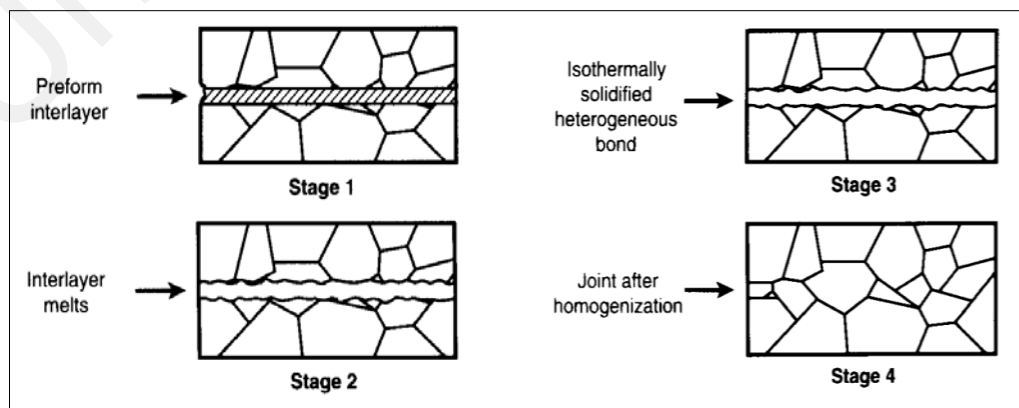


**Figure 2.9:** Illustration of diffusion brazing (Jacobson & Humpston, 2005)

The diffusion brazed joint may change the microstructures and intermetallic compound (IMC) of the filler alloys or it may be composed entirely of the base metals due to high mutual solubility of the filler alloys. IMC is a combination of two or more metallic elements to form a new phase having unique properties, crystal structure and composition. In the joining process, a strong bond of IMC is formed through a chemical reaction between filler alloys and substrate metal at the joint interface. This reaction allows the dissolution of the metal substrate into the molten metal based on the solubility of filler alloys and IMC formation, and the formation of IMC on the metal substrate through a combination of active constituent in the filler alloys and metal substrate. (Jacobson & Humpston, 2005)

Past studies have been conducted on diffusion brazing using different parameters including brazing temperature, holding time, amount of filler alloys and mutual solubility between base metals and filler alloys (AWS, 2011). Zhong et al (2012) have performed vacuum brazing of borosilicate glass and iron-nickel-cobalt alloy (Kovar®) using amorphous filler alloys of Cu-7.0Ni-9.0Sn-6.0P. As the filler melt, the P started to diffuse and oxidise (forming a  $P_2O_5$  compound), creating a brittle IMCs of  $Cu_3P$  and  $Ni_2P$  at the brazed interface joint. This formation of brittle IMC in the brazed joint interface reduces the brazed joint strength.

Hasap, Noraphaipaksa and Kanchanomai (2014) have investigated the microstructure and fracture surface of Cu-alloy (Cu-35Zn-3Pb) brazed joint interface using amorphous filler alloys of Cu-9.0Sn-7.0Ni-6.0P. The microstructure of Cu-alloy brazed joint interface showed a grey phase formation which consisted of IMC of  $Cu_3P$  phase in the filler region at the centre of the brazed joint interface. The formation of  $Cu_3P$  was due to P having good solubility in Cu. The formation IMC of Cu-Zn-Sn phase (light grey phase) in the diffusion layer of the brazed joint interface was also observed. The Cu-

Zn-Sn phase was due to the diffusion of Zn (in the substrate) into the brazed joint interface. The hardness values (HV) of Cu<sub>3</sub>P and Cu-Zn-Sn phases were 286 HV and 133 HV, respectively. The differences in HV values indicate that Cu<sub>3</sub>P phase was harder and more brittle than Cu-Zn-Sn phase. The brittleness of Cu<sub>3</sub>P phase would contribute to crack propagation and lead to fracture.

Xihui et al. (2016) have utilized amorphous filler alloys of Cu-5Sn-3Ni-6P-0.2Fe to braze Fe-20.18Cr-4.98Al-0.48Ti-0.50Y<sub>2</sub>O<sub>3</sub> (MGH956). It was reported that the filler region at the middle of the brazed joint interface formed a combination of grey phase, worm-like shape grey phase and bright phase. The grey phase showed IMCs of Cu<sub>3</sub>P, (Fe,Ni)<sub>3</sub>P and FeCr and the worm-like shape grey phase was made up of IMCs of (Fe,Ni)<sub>3</sub>P and FeCr, while the bright phase indicated Cu solid solution.

Lutfi et al. (2016) have conducted a brazing process of Cu/Cu using amorphous filler alloys of Cu-7.0Ni-9.3Sn-6.3P using a modified domestic microwave oven with different susceptors (SiC or graphite) for 480 s of heating time. It was observed that a single layer of IMC was formed at the joint interface without voids or cracks. Excessive growth of IMC can be minimised by fast heating. It was shown that the thickness of IMC obtained by heating in SiC susceptor was three times thinner than heating in graphite susceptor. The hardness value of the IMC layer using graphite susceptor was higher than the hardness values of IMC produced in the brazing using SiC susceptor. A high hardness value indicated that that the graphite susceptor produced more brittle IMC as compared to those produced using SiC susceptor. The IMC of Cu<sub>3</sub>P was shown as a grey phase and a nickel-enriched area was formed in the middle of joint interface.

Kalin et al. (2016) have carried out brazing of Be and Cu-Cr-Zr bronze using different amorphous filler alloys of Cu-6.4Ni-9.2Sn-6.3P (STEMET 1105) and Cu-9.1Ni-3.6Sn-8.0P (STEMET 1101). It was reported the IMCs found in the brazed joint interface

were  $\text{Be}_2\text{Cu}$  phase (solid solution of Be in Cu), a solid solution of Ni and Be in Cu (Cu, Ni, Be), a solid solution of P in Cu ( $\text{Cu}_3\text{P}$ ,  $\text{Cu}_2\text{P}$ ) and IMC of P with Cu and Cr [(Cu, P), (CrP)]. The IMC of  $\text{Cu}_3\text{P}$  phase was observed to accumulate in the filler region of brazed joint interface, shown as a grey phase. Brazing using STEMET 1105 filler showed a fine and well distributed phase of phosphide at the brazed joint interface. However, STEMET 1102 filler showed large grains with different shapes of phosphide phase, which may reduce the joint strength. The highest shear strength values obtained for Be/CuCrZn brazed joint using STEMET 1105 filler and STEMET 1101 filler were 230 MPa and 261 MPa, respectively.

Zhang et al. (2016) have investigated the brazed joint interface of Cu/Cu using amorphous filler alloys Cu-9.3Sn-15.7Ni-6.5P. The microstructure obtained showed the brazing interface joint consisting of dark grey phase, grey phase and bright regions. EDX point analysis on the dark grey phase showed P-enriched and Ni-enriched with an IMC of  $(\text{CuNi})_2\text{P}$  phase. The grey phase and bright phase showed P-enriched ( $\text{Cu}_3\text{P}$  IMC) and Sn-enriched ( $\text{Cu}_{13.7}\text{Sn}_{86.3}$ ), respectively. The brittle phases of  $\text{Cu}_3\text{P}$  and  $(\text{CuNi})_2\text{P}$  resulted in a brittle fracture in the tensile tests. Thus, the use of amorphous filler alloys of Cu-Sn-Ni-P produced brittle IMC phases of  $\text{Ni}_2\text{P}$ ,  $\text{Cu}_3\text{P}$  and  $(\text{CuNi})_2\text{P}$ . This current work would investigate the brazing of Cu/Cu foam using different wt.% of Cu-Sn-Ni-P amorphous filler alloys.

## **2.5 Current Research on Foam Brazing**

Although there are many existing applications of metal foam as interlayer joining and heat transfer components, studies on the joining of open-cell metal foam still remain inadequate. Metal foams have been used in interlayer joining to enhance the joining strength between metals. Sun et al. (2018) have conducted the brazing of ceramic ( $\text{Al}_2\text{O}_3$ ) and stainless steel (1Cr18Ni9Ti) using Ag-28Cu-3Ti filler with and without 0.2 mm Ni

foam as an interlayer. It was found that the shear strength of Al<sub>2</sub>O<sub>3</sub> and 1Cr18Ni9i joint with Ni foam interlayer has improved by 292% (from 18.4 MPa to 72.1 MPa) as compared to the shear strength of the joint without Ni foam. The residual thermal stress of brazed Al<sub>2</sub>O<sub>3</sub>/1Cr18Ni9i was higher (449.9 MPa) as compared to brazed Al<sub>2</sub>O<sub>3</sub>/Ni foam/1Cr18Ni9i (74.7 MPa).

Wang et al. (2017) have conducted the brazing of C/C with Nb using Ag-26.7Cu-4.6Ti (wt.%) filler with different interlayer foams of 0.3 mm thickness (pure Cu foam or graphene (G)-Cu foam). It was found that the G-Cu foam has effectively inhibited the intense reaction of Cu foam and filler. The use of G into the Cu foam has resulted in a homogenous distribution of the filler on the joint interface and has significantly enhanced the joint strength between C/C and Nb.

Many researchers have shown interest in metal foam heat exchanger with numerous studies on its applications, as discussed in Section 2.2.2. However, research on metal foam joining are still limited, and the knowledge of different metal foam materials, fillers, joining techniques, joining mechanism and joining strengths still requires further studies.

Nevertheless, studies on metal foam joining have been increasing in recent years. Ubertalli et al. (2017) have studied the joining of AA6016 (Al0.25Mg1.0Si)/Al foam/AA6016 using different fillers of Zn (250 µm thickness) and Zn + 2 % Al (350 µm thickness) with 5 min holding time at 430 °C and 1 min holding time at 420 °C, respectively. The joining using Zn + 2 % Al filler shows higher stiffness with the diffusion of Al-rich and Zn rich in the joining area. The Zn + 2 % Al filler was found to spread non-homogenously on Al foam and was concentrated on the joint area with 800 µm thickness.

Song et al. (2015) have fabricated a steel/aluminium foam/steel sandwiched brazed joint using aluminium-silicon based alloy filler. It was found that increasing the brazing time for an additional 10 min resulted in the decrease of the shear joint strength due to formation of a brittle phase. The highest shear strength obtained was 6.26 MPa for the joint produced at 620 °C for 10 mins brazing time.

Nannan et al. (2013) have carried out brazing of aluminium (Al) foam-Al foam using Al86SiMg filler by varying the vacuum pressure ( $6.63 \times 10^{-3}$  Pa and 5.0 Pa) and the amount of filler layer (monolayer and multilayer). The microstructure analysis of the resultant joint showed Al foam-Al foam has much better wetting and spreading characteristics in high vacuum. Based on the magnesium phase diagram, the process of magnesium sublimation [magnesium (solid) changes into magnesium (gas)] began at 200 °C at  $10^{-3}$  Pa. The magnesium (gas) would react with oxygen and moistures and prevents the specimen from oxidation. Magnesium sublimation normally occurs at 400 °C at 1 Pa that may cause oxidation on the contact surface which influences joint strength. The joint bending strength of brazed Al foam-Al foam was the highest for the multilayer filler in high vacuum, followed by the joint produced with multilayer layer in a low vacuum and then with monolayer filler in high vacuum.

Jarvis et al. (2011) have conducted the brazing of nickel (Ni) foam to Ti6Al4V (Ti: titanium, Al: aluminium, V: vanadium) using Ti15Cu25Ni with different binder systems of polyvinyl alcohol (PVA), polyvinyl butyral (PVB) and polyethylene glycol-polymethyl methacrylate (PEG-PMMA). Shear test results of the joints show that crack deformations were formed in a majority of the Ni foam area for joints produced with PVA and PVB binders. While the joint produced with PEG-PMMA binder has shown a line crack deformation on the Ni foam. These results suggest that joint failures tend to occur through the foam instead of in the joint interface.

Past studies have shown that most metal foam joining was carried out using aluminium (Al) foam, and there is still a lack of research in Cu foam joining. The focus on Al foam was due to its good thermal conductivity, lightweight and easy to join. However, there are studies on the performance of heat exchanger using Cu foam materials (Chein et al., 2009; Tan & Chong, 2016; Zhang, Long & Zhang, 2018). Cu has high thermal conductivity, high coefficient of thermal expansion, and good mechanical properties making it a promising material for foam brazing applications (Han et al., 2012). Cu are used in various applications, including plumbing, cooling, heating, air-conditioning, fire sprinklers, and solar heating (Zhang et al., 2010). This current work would expand the use of Cu in the form of metal foam, for use in heat exchanger applications.

## **2.6 Corrosion Behaviour of Brazing Joints**

The use of heat in brazing would affect the metallurgical properties of the metals. It is expected that changes would occur in their metallurgical properties such as crystal structure arrangements and chemical composition. Changes in chemical composition includes the distribution of solid solution and microstructural intermetallic phases, formed due to dissolution of elements into solid solutions, and solute precipitation from a solid solution during heating and cooling process. Changes to metallurgical and chemical compositions would influence the corrosion behaviours of the brazed metals (De Leeuw, 1999). The interactions of molten filler alloys and substrate to form the brazed joint interface may be prone to corrosion in the presence of moisture, corrosive or aggressive environment (Montemor, 2016). Weishaupt et al. (2012) have studied 65Cu-35Zn radiators and have found that the chlorides on the radiators have initiated pitting corrosions. This corrosion weakened the joints in the radiators and would lead to radiator failure.

### 2.6.1 Electrochemical Potentiodynamic Polarisation

Corrosion can be evaluated using electrochemical measurement such as electrochemical potentiodynamic polarisation, which gives a general information on corrosion resistance and susceptibility (Zupancic, Legat & Funduk, 2006). Electrochemical methods were successfully conducted in several studies on corrosion of brazed materials.

Zupancic et al. (2006) have carried out an investigation on corrosion resistance of brazed and laser-welded cobalt-chromium alloy using electrochemical analysis. From the potentiodynamic polarisation curves, the brazed cobalt-chromium has a more noble corrosion potential ( $E_{\text{corr}}$ ) than laser-welded cobalt-chromium. The brazed cobalt-chromium showed higher corrosion current density ( $I_{\text{corr}}$ ) indicating that the brazed joint has lower corrosion resistance compared to laser-welded joint. This result was due to the passivation ability of laser-welded cobalt-chromium that has enhanced its corrosion resistance.

Elrefaey, Wojarski and Tillmann (2010) have evaluated the corrosion behaviour of titanium alloy (Ti)-carbon steel (St) brazed joint interface using Ag-34Cu-2Ti filler alloys at different brazing temperatures (850 °C, 880 °C and 930 °C) and holding times (5 min and 15 min). Potentiodynamic polarisation measurements were carried out for St, Ti, Ag-34Cu-2Ti filler, Ti/St at 850 °C brazing temperature with 5 min holding time (hereinafter referred to as Ti/St-850-5), Ti/St-850-15, Ti/St-880-15 and Ti/St-930-15. The corrosion potentials show a more noble value from Ag-34Cu-2Ti filler to Ti as compared to Ti/St brazed joint interface. In term of  $I_{\text{corr}}$ , Ti showed the highest corrosion resistance, followed by Ag-34Cu-2Ti filler. Ti/St brazed joint at high brazing temperature showed better corrosion resistance as compared to Ti/St brazed joint at low brazing temperature. St has the lowest corrosion resistance. The microstructure of Ti/St-930-15 brazed joint interface exhibited a Cu-Ti IMC in the diffusion layer resulting in increased corrosion

resistance than other brazed joints. At high brazing temperature, Ti would migrate from the substrate to the brazed area, forming Cu-Ti IMC phase, which would create a passive film in polarisation test and yield a low  $I_{\text{corr}}$  value (low corrosion rate and high corrosion resistance).

Rahmani and Meletis (2019) have investigated the corrosion behaviours of Cu, silver (Ag), brazed Cu-60Ag and brazed Cu-6Ag in electrolytes in the presence and absence of benzotriazole (BTA) as a corrosion inhibitor to protect the metals. The addition of BTA has shifted the  $E_{\text{corr}}$  of Cu to a noble value but the result was in the opposite direction for Ag. The addition of BTA has influenced the  $I_{\text{corr}}$  to yield a lower corrosion rate of Cu and Cu alloy. This resulted in the brazed Cu-6Ag having better corrosion resistance than brazed Cu-60Ag in the presence of BTA. The kinetically-induced responses of  $I_{\text{corr}}$  is controlled by  $\alpha$ -Cu phase, which are prevalent in high Cu alloy. While the thermodynamically-induced responses of  $E_{\text{corr}}$  is overcome by  $\beta$ -Ag phase. This explained why the brazed Cu-6Ag has high corrosion resistance and noble  $E_{\text{corr}}$  as compared to Cu-60Ag with BTA addition.

Generally, evaluations of the corrosion behaviour on Cu/Cu foam are still lacking, thus there is a need to include corrosion analysis in this study on Cu/Cu foam brazed joints.

### **2.6.2 Corrosion of Copper**

Copper are used in brazing joints for industrial, heat exchanger, and plumbing applications due to its corrosion resistance, excellent electrical and thermal conductivity, and has good mechanical workability (Al-Abdallah, Maayta, Al-Qudah & Al-Rawashdeh, 2009; Aminazad et al., 2015). However, Cu may deteriorate, especially in corrosive environments that are high in moistures, pollutants and temperatures (Clarelli, Filippo &

Natalini, 2014). Corrosion may form in these conditions, and reduces the performance of the material (e.g reduction of heat transfer performance in heat exchanger applications).

For Cu brazed joints, corrosion may also depend on the filler alloys, the brazing temperature and the atmospheric conditions during the brazing process (Aminazad et al., 2015). In less polluted environments, Cu would normally react with oxygen to form a thin layer of cuprite on the surface of copper, as shown in reaction 2.1 (Clarelli et al., 2014). The formation of cuprite, also known as copper (I) oxide or copper (II) oxide, can protect the copper from further oxidation.



Warraky, Shayeb and Sherif (2004) have stated that the presence of anions such as chloride ( $\text{Cl}^-$ ), bicarbonate ( $\text{HCO}_3^-$ ), nitrate ( $\text{NO}_3^-$ ), sulphate ( $\text{SO}_4^{2-}$ ) and perchlorate ( $\text{ClO}_4^-$ ) could initiate pitting corrosion. However,  $\text{Cl}^-$  and  $\text{SO}_4^{2-}$  were found as the main agents in pitting corrosion. The pitting initiation is due to the tendency of  $\text{Cl}^-$  ion to form an unstable layer ( $\text{CuCl}$ ) and soluble chloride complexes ( $\text{CuCl}_2^-$ ). The corrosion problems of Cu has been a topic of interest for many researchers as Cu and its alloys are frequently used in piping and plumbing, including thermal applications (Al-Abdallah et al., 2009). The reactions of Cu in sodium ( $\text{NaCl}$ ) ions are as follows (Lilja, 2013):

- Anodic reactions



- Cathodic reduction



- Total Cu corrosion reaction



From the reactions above, the presence of chloride ion ( $Cl^-$ ) and oxygen would initiate the corrosion process. Environmental condition such as the presence of aggressive ions, saline water and corrosive liquids may negatively affect the copper. Therefore, the current work attempts to present a detailed analysis on the corrosion of brazed Cu foam using Cu-Sn-Ni-P filler alloys.

## 2.7 Summary

The feasibility of Cu foam in thermal applications has been widely discussed due to its large contact surface area characteristics. The high thermal conductivity and good strength of Cu also makes it a potential medium in heat exchanger applications. Based on the literatures, the brazing process is a suitable method that is easy and safe to implement for joining Cu foam through a bond formation using filler alloys. The amorphous filler alloys have been reported as flexible, easy to fill in braze cross-section, have good wettability and results in high joint strengths. As the study on the brazing of Cu foam is yet to be explored widely, this current work will attempt to evaluate the mechanical and microstructural properties of brazed Cu/Cu foam/Cu. In addition, the corrosion behaviour of brazed Cu/Cu foam/Cu joints and its correlation with the mechanical and microstructural properties of brazed Cu/Cu foam/Cu would also be investigated.

## CHAPTER 3 : METHODOLOGY

### 3.1 Introduction

This chapter describes the material, experimental methods and evaluation techniques used in this study. This study uses method of one-factor-at-a-time (OFAT) which varies one parameter while keeping all other parameters constant at a time (Heiman, 2008). The OFAT approaches could provide initial measurement ranges and ascertain the optimal selected condition for each analysed parameter (Subramaniam, Mazuki, Shukor & Ahmad, 2019). The high numbers of the experiment in the OFAT method can avoid any omitted conditions (Saber, 2010) to obtain the accurate outcome (Heiman, 2008). Besides, there is still a lack of literature in Cu foam joining using amorphous filler alloys. Hence, the utilisation of OFAT method will significantly contribute to the foam joining research area.

In general, this study focuses on the brazing of Cu/Cu foam/Cu using different Cu-Sn-Ni-P amorphous filler alloys, namely, Cu-4.0Sn-9.9Ni-7.8P, Cu-9.7Sn-5.7Ni-7.0P and Cu-9.0Sn-7.0Ni-6.0P (hereinafter referred to as filler A, filler B and filler C, respectively). Different foam pore densities (15 PPI, 25 PPI and 50 PPI) were evaluated, (hereinafter referred to as foam A, foam B and foam C, respectively). The unit of PPI (pore per inch) represents the number of pores in a square inch of Cu foam, as received from the manufacturer.

This work is divided into two-phases which is 1) brazing of Cu/Cu foam/Cu and 2) evaluation of corrosion behaviour of brazed Cu/Cu foam/Cu for foam A (hereinafter referred to as Cu/Cu foam A/Cu). In phase 1, preliminary investigations on brazing holding time of Cu/Cu foam A/Cu using filler B was conducted. Experimentation on different holding times (5 min, 10 min and 15 min) at different brazing temperatures were carried out to optimise the holding time for Cu/Cu foam/Cu brazing.

Next, the brazing of Cu/Cu foam/Cu in phase 1 is separated into part A and part B, to focus on mechanical properties and microstructure analysis, respectively. In part A, the brazing of Cu/Cu foam/Cu was conducted using filler A, filler B, and filler C at different brazing temperatures (660 °C, 680 °C, 700 °C and 720 °C) with foam A, foam B and foam C. The compressive strength of nonbrazed and brazed Cu/Cu foam/Cu were compared. Determination of the brazed joint interface strength of Cu/Cu foam/Cu was carried out using a shear test. Additional data of brazed Cu/Cu foam/Cu using filler A and filler C at a brazing temperature of 640 °C with different foams was included.

In part B, the brazing of Cu/Cu foam/Cu was conducted using filler A, filler B, and filler C with foam A, foam B and foam C at a fixed brazing temperature of 660 °C (for filler A and filler C) and 680 °C (for filler B). The microstructures of Cu/Cu brazed joint interface using different amorphous filler alloys (filler A, filler B, and filler C) were compared. The hardness values on the brazed joint interface of Cu/Cu foam/Cu were measured using Vickers hardness testing. The microstructures and phase determinations of Cu/Cu foam/Cu brazed joint interfaces were analysed using SEM (point, line and mapping), EDX and XRD, respectively.

In phase 2, the corrosion behaviour of the filler and Cu/Cu foam A/Cu brazed joint interface was investigated. The corrosion characteristic of the crystalline filler A, crystalline filler B, and crystalline filler filler C was analysed using electrochemical potentiodynamic polarisation. The microstructures of post-immersed Cu/Cu foam A/Cu brazed joint interface using different fillers (filler A, filler B and filler C) were observed. The overall structure of the research work is shown in Figure 3.1

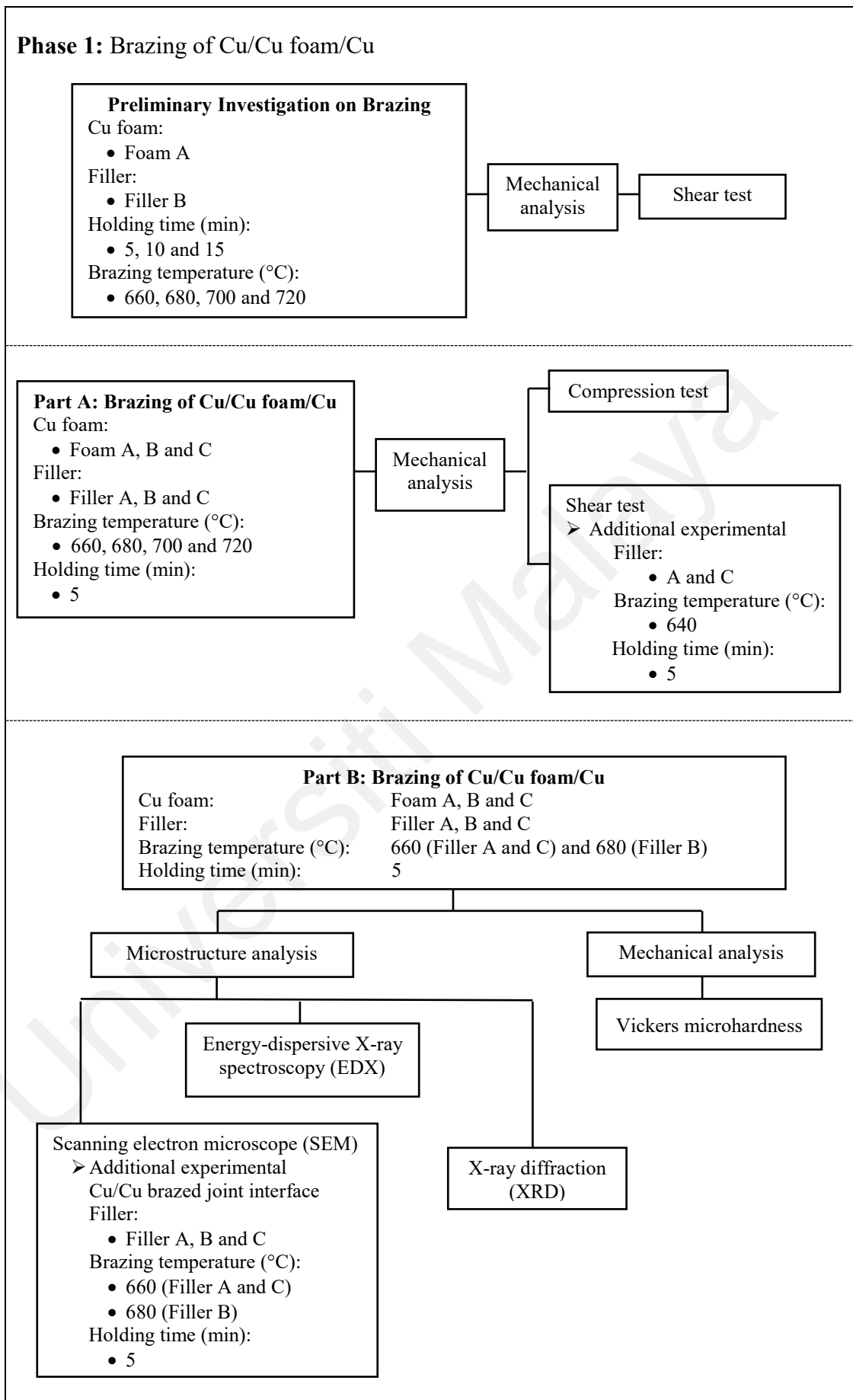


**Figure 3.1:** Summary of overall work

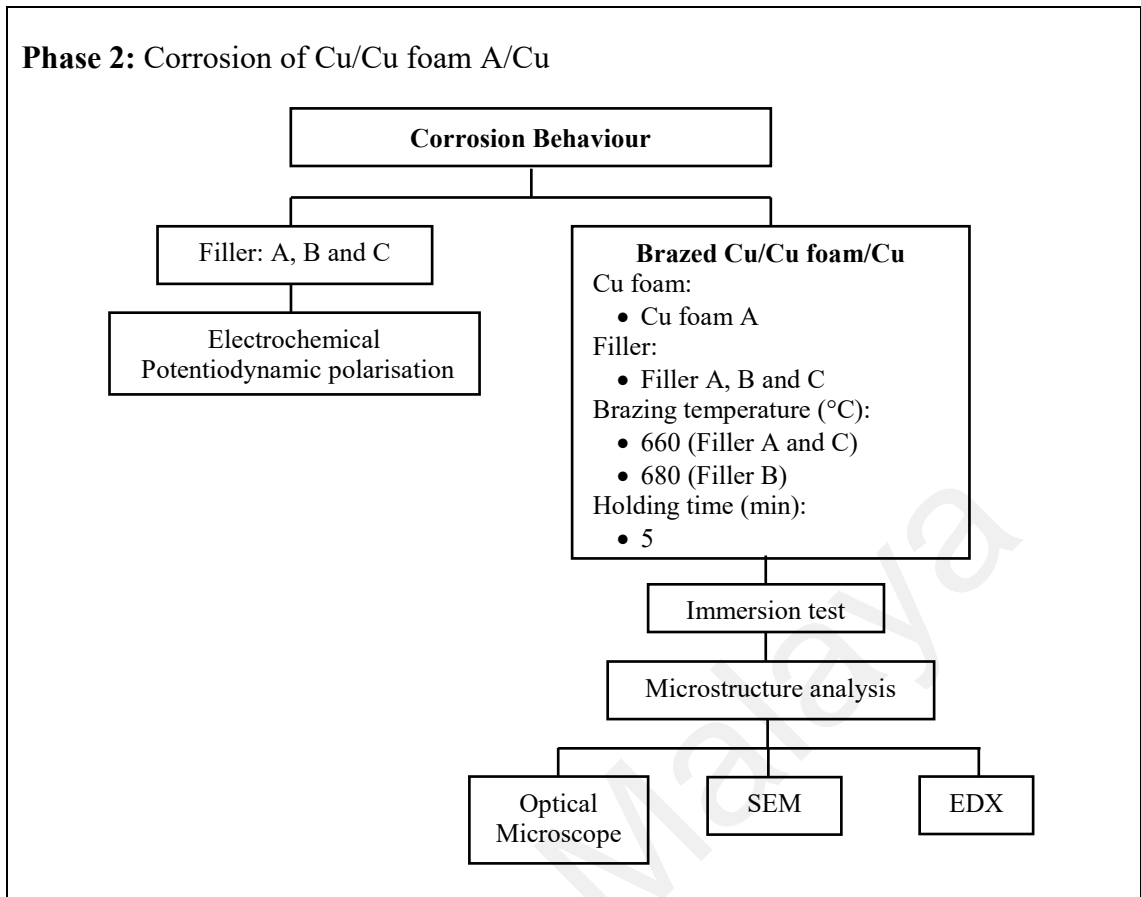


**Figure 3.1 (continued):** Summary of overall work

### 3.2 Materials

All materials (Table 3.1) in current work were used as received from the manufacturer.

**Table 3.1:** Materials used in this work

Name	Details	Manufacturer
<b>Materials</b>		
Cu substrate	Purity: 99.9 % <sup>1</sup> Thickness: 3 mm	Purchased from C & W Hardware, Kuala Lumpur, Malaysia
Cu foam	Pore density <sup>2</sup> : 15 PPI, 25 PPI and 50 PPI Thickness: 7 mm	Duranice Applied Materials, Dalian, China
Amorphous Filler Alloys (wt. %) <sup>3</sup>	Filler A: Cu-4.0Sn-9.9Ni-7.8P T <sub>s</sub> : 610 °C, T <sub>L</sub> : 645 °C	Metglas® Inc., Conway, USA <sup>4</sup>
	Filler B: Cu-9.7Sn-5.7Ni-7.0P T <sub>s</sub> : 610 °C, T <sub>L</sub> : 645 °C	Metglas® Inc., Conway, USA <sup>4</sup>
	Filler C: Cu-9.0Sn-7.0Ni-6.0P T <sub>s</sub> : 610 °C, T <sub>L</sub> : 645 °C	Vacuumschmelze GMBH & Co., Hanau, Germany <sup>4</sup>

Notes: <sup>1</sup> EDX analysis on Cu composition in **Appendix A.2**, <sup>2</sup>pore density value and <sup>3</sup>details on Cu-Sn-Ni-P wt. % of the amorphous filler were obtained from the manufacturer and <sup>4</sup>amorphous fillers were donated by Professor Tadashi Ariga from Tokai University, Japan.

### 3.3 Copper Foam

Three types of open-cell Cu foams with nominal pore densities of 15 PPI, 25 PPI and 50 PPI were supplied by the manufacturer (Duranice Applied Materials (Dalian) Co., Ltd) and has been used as received. The foams were fabricated using an open cell polyurethane foams replication method. The method involves an electroplating process where the surface of polyurethane foam is coated with a thin layer of metal (eg: Ni) by sputtering, making it conductive. Then Cu is deposited by electroplating on the polyurethane foam to form an open-cell Cu foam structure (Alavi et al., 2017).

The geometrical and physical structures of the Cu foam were characterised using a digital microscope (Keyence, Osaka, Japan) to measure the diameters of pores, cell walls and Cu foam branches. Thirty measurements for each Cu foam pore density [three different specimens for each Cu foam pore density (ten measurements for each specimen)] were taken. Then, the average values from the thirty measurements were calculated for diameters of pore, cell walls and Cu foam branches. The measurements of best fitting sphere were conducted on the 2D images (**Appendix B.1**). This method was adopted from the method used by Alavi et al., 2017.

The percentages of porosity of the Cu foam were determined using Archimedes' principle, utilizing the concept of mass displacement (Jamadon et al., 2016; Mirzaei & Paydar, 2017). Water was used as a media and the porosity percentage was calculated using Archimedes' equation as follows:

$$P(\%) = \frac{W_{as} - W_d}{W_{as} - W_s} \quad (3.1)$$

Where P represents the porosity percentage,  $W_{as}$  is the weight of Cu foam after submerged,  $W_d$  is the weight of dry Cu foam and  $W_s$  is the weight of Cu foam while submerged.

### 3.4 Brazing Process

The brazing process was conducted according to AWS Standard C3.6M using a laboratory furnace VMK-Vacuum instrument (Linn High Therm, Eschenfelden, Germany). The Cu foam of 7 mm thickness was cut into square specimens measuring 10 x 10 mm using wire EDM. Similarly, EDM wire cut was used to prepare the 3 mm thick Cu as a substrate with dimensions of 15 x 15 mm (top) and 20 x 20 mm (base). The thickness value of Cu foam was selected based on previous studies in heat performance, which ranged from 5mm (Odabae et al., 2013) to 15 mm (Tan & Chong, 2016).

The Cu substrate plates were grounded with 600 and 800 SiC abrasive paper. The plates, fillers and foam were then stacked into a jig, as shown in Figure 3.2, composed of the Cu base plate, a 40  $\mu$ m filler alloys sheets, the Cu metal foam, another 40  $\mu$ m filler alloys sheet and the Cu top plate. This configuration provides a protective structure with a great energy absorption capability, excellent strength and high resistance to shock (Zhou, Su, Wang, Shu & Zhao, 2016). Finally, the specimen was clamped and placed into the furnace for the brazing process. The brazing procedure is summarized in Figure 3.3.

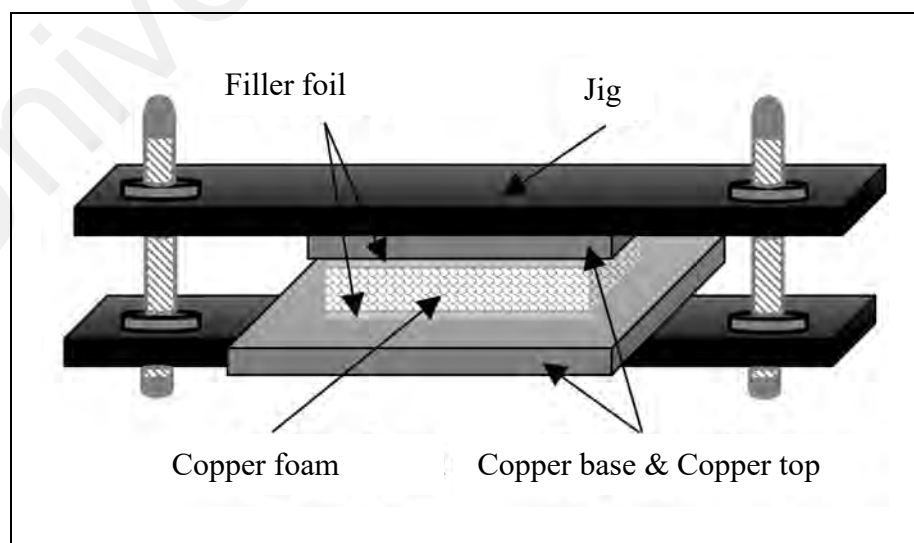


**Figure 3.2:** Schematic diagram of specimen arrangement

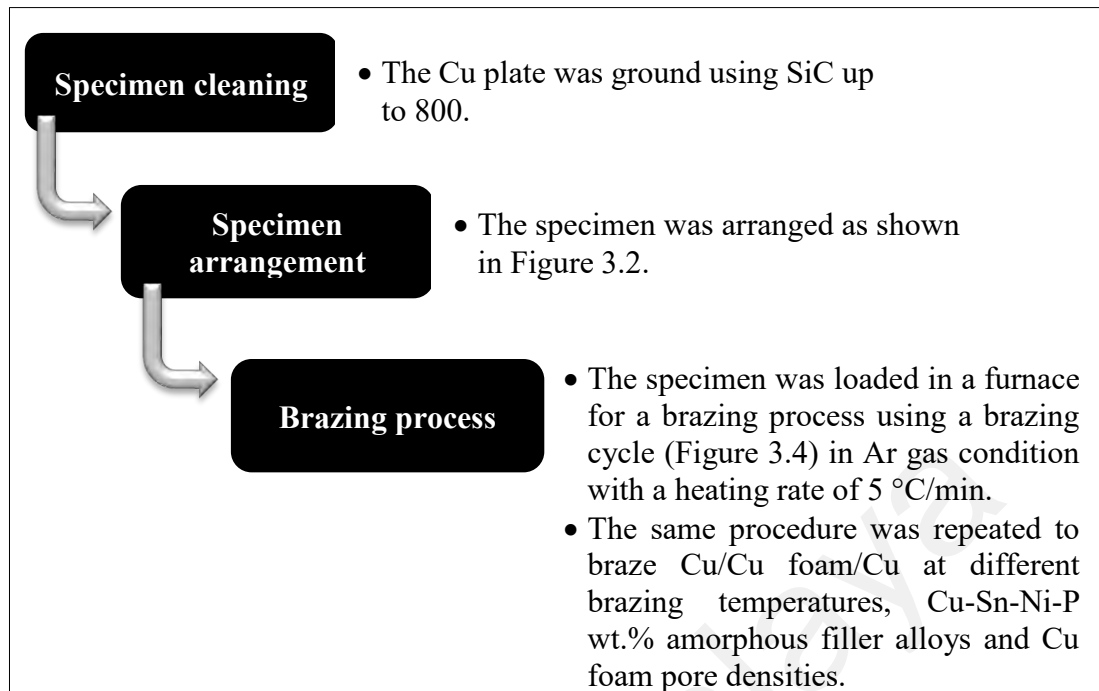


**Figure 3.3:** Summary of Cu/Cu foam/Cu brazing process

The brazing process was carried out under argon (Ar) gas atmosphere with a uniform heating rate of 5 °C/min and 5 min holding time using a brazing cycle as shown in Figure 3.4. The Ar gas was used to avoid oxidation during brazing at high temperature. The formation of oxide on the specimen's surface would reduce the wettability of the filler, resulting in a weak joint. The short holding time of 5 mins was selected to minimize the energy used (Zhong et al., 2012) without jeopardizing the mechanical strength of the joint. The brazing cycle consisted of a preheating stage at 350 °C for 30 min. Zaharinie (2015) has reported that a preheating stage of 350 °C for 30 min would not affect the grain growth as the preheating temperature was less than the targeted annealing temperature range. The preheating may soften and assist in the full melting of the filler alloys during brazing. The uniform heating rate and preheating phases were fixed at 5 °C/min and 30 min, respectively because Cu is usually difficult to join rapidly due to its high thermal conductivity (Srinath, Sharma & Kumar, 2011). Finally, the specimen was cooled at a slow rate of 5 °C/min to avoid formation of residual stresses and allow the intermetallic compound phases to achieve a stable equilibrium (Ubertalli et al., 2017).

This procedure was adopted for the Cu/Cu foam/Cu brazing at different Cu-Sn-Ni-P wt. % amorphous filler alloys, brazing temperatures and Cu foam pore densities. The Cu-Sn-Ni-P amorphous filler alloys was chosen because of its suitability to braze coppers. The wt. % and element contents of the amorphous filler alloys determines the melting temperature range (between solidus and liquidus temperature). Each of the element play a vital role as stated in section 2.4.1. The solidus and liquidus temperatures of filler A, filler B and filler C were provided by the manufacturer as listed in Table 3.1. The range of brazing temperatures (660 °C, 680 °C, 700 °C and 720 °C) were selected based on the approximate 56 °C above liquidus temperature of all amorphous filler alloys (AWS, 2011). The pore densities (ranging from 15 PPI to 50 PPI) of Cu foam were chosen due to their influence in heat rate performance. Mancin, Zilio, Diani and Rosetto (2012) have found that very high pore density (60 PPI and above) in foam metal would cause a pressure drop in the heat exchanger and requires more pumping power.

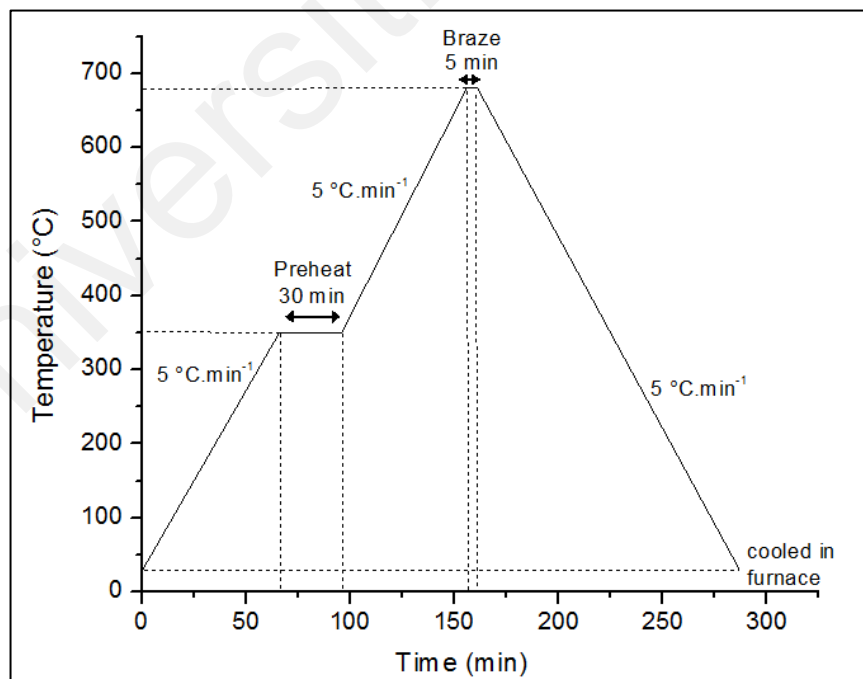


**Figure 3.4:** Brazing cycle of Cu/Cu foam/Cu

### 3.5 Mechanical Testing

#### 3.5.1 Shear Test of Cu/Cu foam/Cu Brazed Joint Interface

Shear test, schematically shown in Figure 3.5, was performed to evaluate the brazed joint strength. The improper and weak brazing joint could affect the heat efficiency of heat exchanger. The shear test was conducted using an Instron Universal Testing Machine 3369 equipped with Bluehill 2.0 software (Instron Inc., Norwood, USA). A 50 kN load cell was fitted operating in displacement control mode at a cross-head speed of 1mm/min for the shear test, conducted at room temperature.

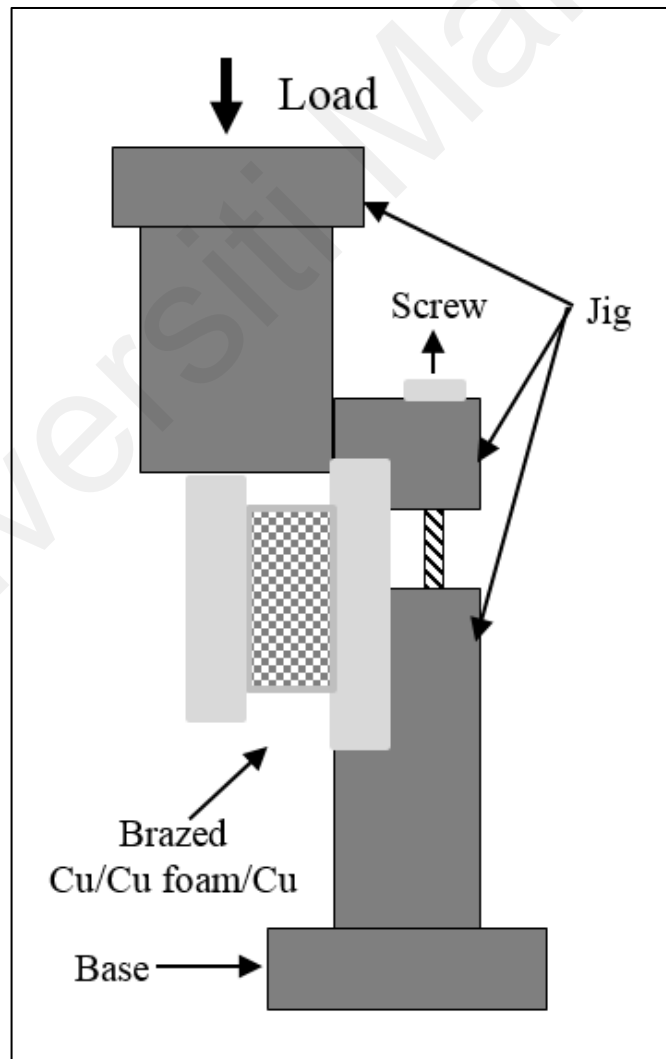


**Figure 3.5:** Schematic diagram of the shear test for Cu/Cu foam/Cu

The data result of shear strength value were obtained with applied force over cross-sectional area. The value was calculated and generated by the Bluehill 2.0 software from the shear test. The cross-sectional area of Cu foam (length time by width) was selected instead of intact joint area (foam branches). The cross-sectional area of Cu foam was used because the Cu foam is made up from hollow structure of interconnected branches (Figure B3, **Appendix B.1**). Next, the Cu substrate (base) surface from Cu/Cu foam/Cu shear-fracture, in this shear test, was analysed using XRD for phase determination. Details XRD analysis was stated in section 3.6.3; page 57.

### **3.5.2 Compression Test of Cu/Cu foam/Cu**

The compression test, schematically shown in Figure 3.6, was conducted because in the heat exchanger application, the fluid (to cool down the hot coolant) flow force may suppress the foam by flowing within the porous foam structure. The investigation on compressive strength and compressive behaviours could overcome the undesirable destruction of Cu foam.

The sample of nonbrazed Cu/Cu foam/Cu and brazed Cu/Cu foam/Cu using amorphous filler alloys were compared. The test was performed in accordance to ISO Standard 13314:2011 using an Instron Universal Testing Machine 3369 equipped with Bluehill 2.0 software (Instron Inc., Norwood, USA). A 50 kN load cell was fitted operating in displacement control mode at a cross-head speed of 1 mm/min. The compression tests were conducted at room temperature. The data result of compressive strength value were obtained with applied force over cross-sectional area. The value was calculated and generated by the Bluehill 2.0 software from the compressive test. The cross-sectional area of Cu foam (length time by width) was selected instead of the solid interconnected branches only (Figure B3, **Appendix B.1**).

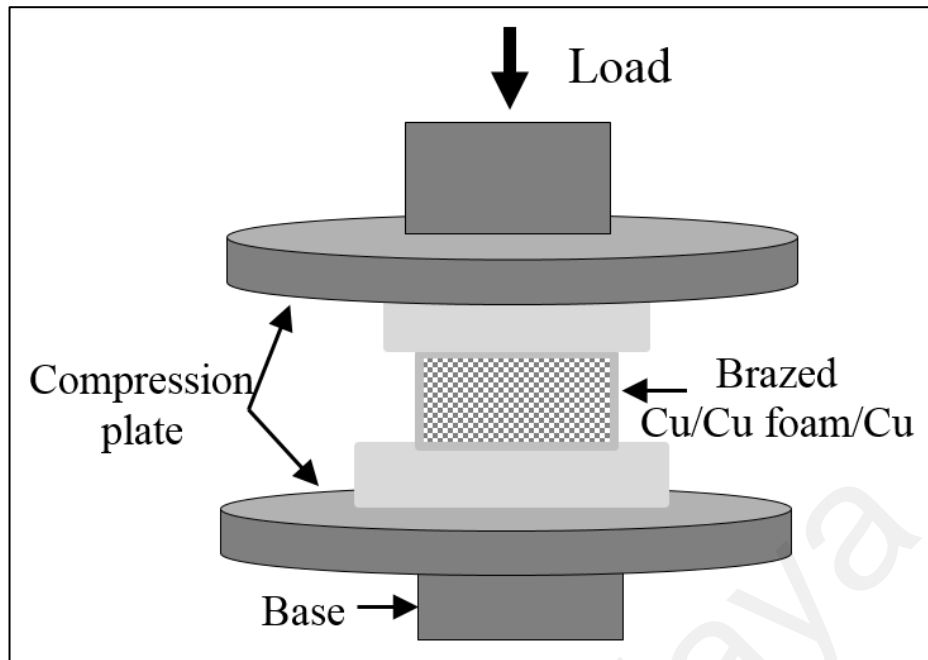


**Figure 3.6:** Schematic diagram of compression test for Cu/Cu foam/Cu

### 3.5.3 Vickers Microhardness Test

Vickers Microhardness test was conducted according to ASTM Standard E384 using DUH-211S Shimadzu Dynamic Ultra Micro Hardness Tester (Shimadzu Corp., Tokyo, Japan). The surface of the sample was prepared by grinding using SiC abrasive paper.

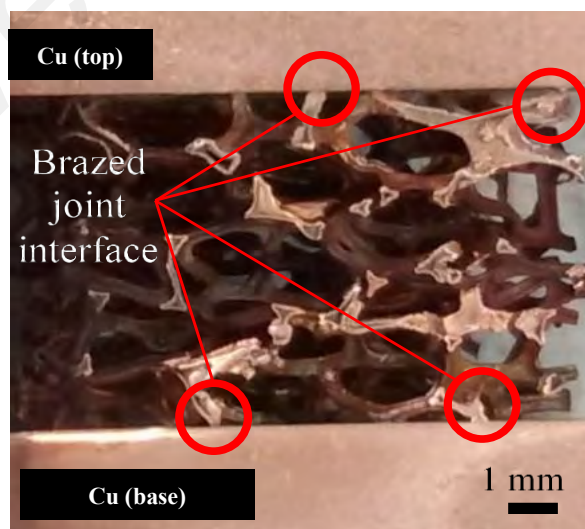


**Figure 3.7:** Cu/Cu foam/Cu brazed joint interface using filler B with foam A at 680 °C

A selection of brazed joints interface of Cu/Cu foam were chosen (Figure 3.7) for diamond indentation in the microhardness test. The microhardness measurements were made with an indentation load of 100 mN and rate of 10 mN/s for 5 s. The hardness values (HV) were obtained from the DUH analysis software from which the average HV was calculated.

### **3.6 Material Characterisation**

#### **3.6.1 Microscopic Evaluation**

The geometrical properties of Cu foam were determined using a Keyence VHX-5000 series digital microscope (Keyence, Osaka, Japan) with a 100x magnification capability. The average diameter values of branches, pores and cell walls of Cu foam were calculated by taking the average of measurements at 30 different locations on the captured images. For the immersion test, an optical microscope (Olympus, Tokyo, Japan) was used to obtain the images of post-immersed uncleaned brazed Cu/ Cu foam/Cu.

#### **3.6.2 Scanning Electron Microscope (SEM) and Energy-dispersive X-ray spectroscopy (EDX)**

Scanning electron microscope (SEM) micrographs of the interface joints and cross-sections of brazed Cu/Cu foam/Cu were acquired using a JEOL JSM 6360A (Tokyo, Japan). In addition, Energy-dispersive X-ray spectroscopy (EDX) analysis was carried out to obtain elemental composition (%) of the samples to evaluate for possible phase formations. The EDX apparatus was equipped with Elemental analysis software JEOL JED-2300 (Tokyo, Japan).

Prior to SEM and EDX analysis, the Cu/Cu foam/Cu braze specimens were metallurgically prepared by surface grinding using increasingly finer SiC abrasive papers

(600, 800, 1200 grit sizes) to expose the joint interface, as shown in Figure C1 in **Appendix C**. They are then polished with 3  $\mu\text{m}$  and 2  $\mu\text{m}$  diamond suspension (Buehler, Illinois, United States) and etched according to ASTM No. 30 by using a mixture of ammonia (30%) and hydrogen peroxide (3%). The etching was carried out by swirling the sample in the etching solution for 10 s.

### 3.6.3 X-ray Diffraction (XRD)

XRD analysis was conducted to determine the molecular structure of Cu/Cu foam shear-fracture. The analysis was made on the Cu substrate surface (base) from the shear test of the brazed sample, as illustrated in Figure 3.8, using a Lab X, XRD-6100, Shimadzu (Kyoto, Japan). The range of  $2\theta$  was from  $20^\circ$  to  $90^\circ$  using continuous scan with a  $2\theta$  step size of  $0.02^\circ$  and Cu- $k\alpha$  radiation at  $\lambda = 1.54 \text{ \AA}$ . The raw data was analysed using X'Pert Highscore software with Inorganic Crystal Structure Database (ICSD), as shown in **Appendix A.3**.

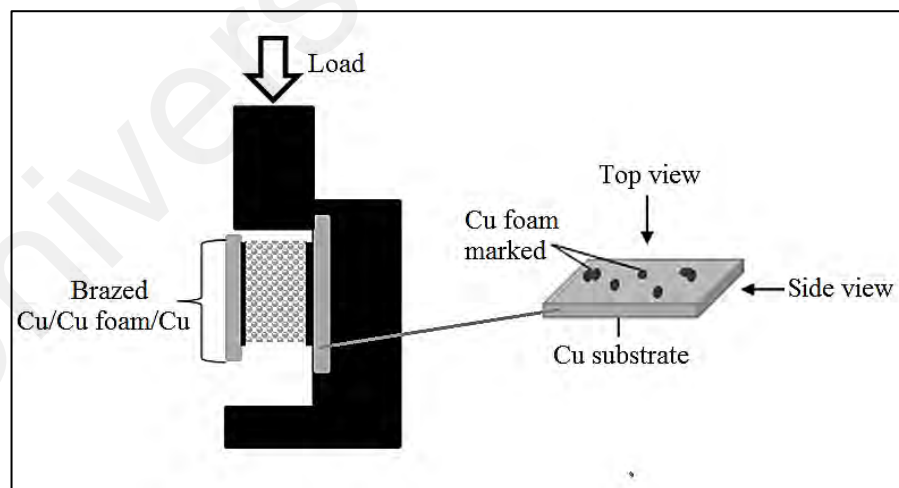


**Figure 3.8:** Schematic diagram of Cu substrate surface (base) from the shear test of brazed Cu/Cu foam/Cu

## 3.7 Corrosion

### 3.7.1 Electrochemical Potentiodynamic Polarisation

For the electrochemical analysis, the amorphous filler alloys specimens were first melted and cooled to imitate the brazing process. They are then analysed in the electrochemical set-up, shown in Figure 3.9. The potentiodynamic polarisation tests were performed in 3.5% sodium chloride (NaCl) electrolyte by using potentiostat (Biologic SP-150, Claix, France) equipped with EC-Lab software V10.44. Saturated calomel electrode (SCE) and platinum (Pt) mesh were used as a reference electrode and counter electrode, respectively.

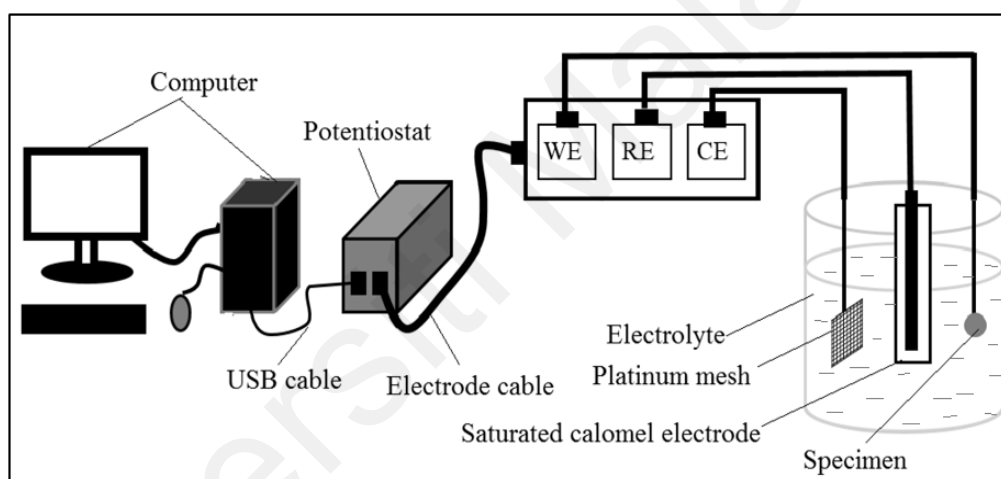


**Figure 3.9:** Schematic diagram of electrochemical set-up

The scan rate was fixed at 0.2 mV/s with 15 min of open circuit potential (OCP). The corrosion potential ( $E_{\text{corr}}$ ) and corrosion current density ( $I_{\text{corr}}$ ) were obtained by extrapolating linear Tafel line of the anode and cathode polarisation curves using Tafel fit analysis of EC-Lab software (**Appendix B.3**).

### 3.7.2 Immersion Test

Brazed Cu/Cu foam A/Cu samples for the immersion test were prepared under Ar gas atmosphere with 5 °C/min heating rate (as outlined in Section 3.4). The samples were prepared using different Cu-Sn-Ni-P amorphous filler alloys at brazing temperatures of

660 °C (filler A and filler C) and 680 °C (filler B). These microstructure samples (without etched) were observed using SEM and EDX before undergone the immersion test. These samples were referred to as pre-immersed samples.

The subsequent immersion test was carried out based on ASTM Standard G-31. A 3.5% (wt.%) sodium chloride (NaCl) (99.97% purity, Bendosen laboratory) was prepared as a media for the immersion test. The specimens were hanged and immersed in the NaCl media for seven days (Figure 3.9). After seven days, these post-immersed samples were observed using optical microscope, SEM and EDX. Next, the post-immersed samples were cleaned according to ASTM Standard G1-90 using sulphuric acid (H<sub>2</sub>SO<sub>4</sub>) [AJAX-Finechem (Univar), Carribbean DV, Australia] before undergone SEM and EDX for microstructure analysis. The chemical cleaning was prepared by diluting 50 ml of the H<sub>2</sub>SO<sub>4</sub> (specific gravity 1.84) with distilled water to make a 500 ml of solution.

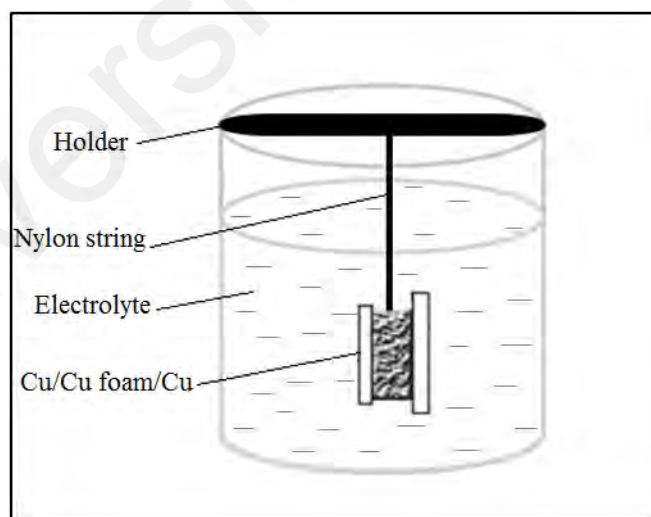


**Figure 3.10:** Schematic diagram of immersion test (Initial: 0 day)

## CHAPTER 4 : RESULTS AND DISCUSSION

### 4.1 Introduction

This chapter presents the results and discussions of the experiments conducted. Firstly, the percentage of porosities of the three Cu foams were calculated from the images captured using the digital microscope. The brazing experiments of Cu/Cu foam/Cu were conducted at four different brazing temperatures ( $T_{br}$ ) of 660 °C, 680 °C, 700 °C and 720 °C. Three different Cu-Sn-Ni-P wt.% amorphous filler alloys were used, namely, Cu-4.0Sn-9.9Ni-7.8P, Cu-9.7Sn-5.7Ni-7.0P and Cu-9.0Sn-7.0Ni-6.0P (hereinafter referred to as filler A, filler B and filler C, respectively). The Cu foam were classified according to their pore densities of 15 PPI, 25 PPI and 50 PPI (hereinafter referred to as foam A, foam B and foam C, respectively).

A preliminary brazing process was conducted to determine the optimal brazing holding time. The compressive strength ( $\sigma_{comp}$ ) and shear strength ( $\tau_{shear}$ ) values of Cu/Cu foam/Cu were determined for brazing using different amorphous filler alloys with different Cu foam pore densities at different brazing temperatures. The microstructure analysis was conducted for brazed Cu/Cu foam/Cu using different amorphous filler alloys with different Cu foams pore densities at a constant temperature of 660 °C (filler A and filler C) and 680 °C (filler B). The microstructure evaluation included analysis on the joint interface, cross-sectional areas, intermetallic compounds (IMC) and phase determination. Corrosion characteristics of Cu-Sn-Ni-P wt.% fillers were conducted by potentiodynamic polarisation technique. Finally, the corrosion behaviours of Cu/Cu foam/Cu brazed joints using different Cu-Sn-Ni-P wt.% amorphous filler alloys for Cu foam A were evaluated.

## 4.2 Characterisation of Copper Foam

The cellular structures of Cu foam A, foam B and foam C are shown in Figure 4.1. Their geometrical and physical structures are characterised and tabulated in Table 4.1. The diameters of pore, cell walls and Cu foam branches were measured using a digital microscope, as described in **Appendix B.1**. The porosity percentages of the Cu foams were calculated using Archimedes' principle (**Appendix B.2**). Archimedes' principle can be used in a mass displacement method to obtain the porosity percentage of metal foam (Jamadon et al., 2016; Mirzaei and Paydar, 2017).

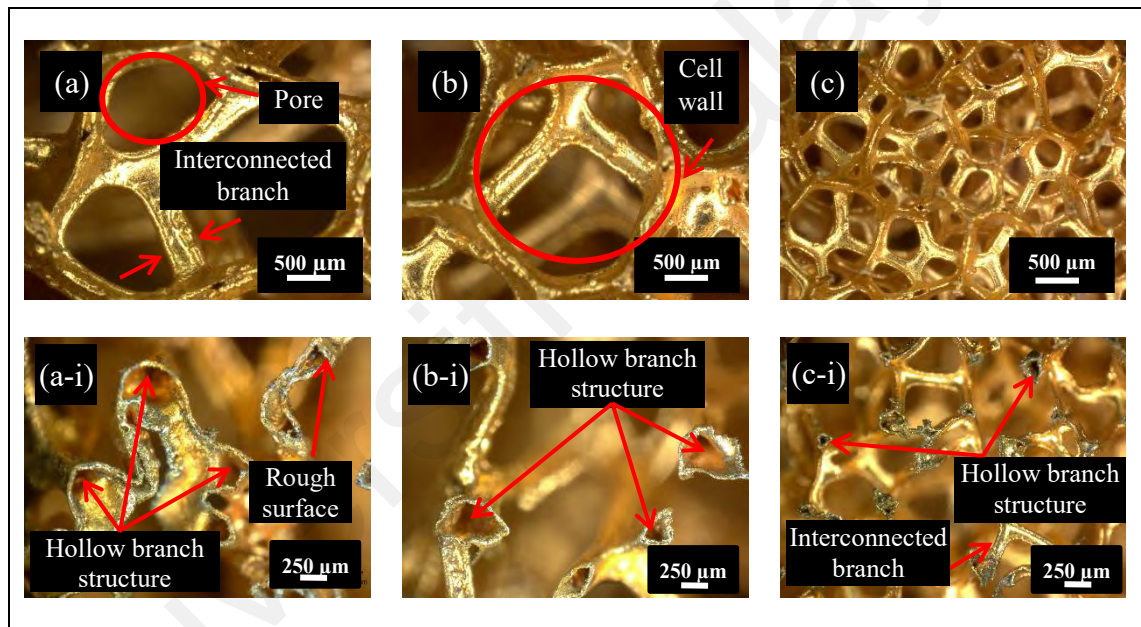


**Figure 4.1:** Digital microscope image of Cu foam and cross-sectional view of Cu foam interconnected branch (a & a-i) Foam A (b & b-i) Foam B (c & c-i) Foam C

**Table 4.1:** Characterisation of Cu foam

Number of pores per inch (PPI) <sup>1</sup>	15	25	50
Pore diameter (mm)	$1.10 \pm 0.17$	$0.86 \pm 0.19$	$0.38 \pm 0.07$
Cell diameter (mm)	$2.54 \pm 0.19$	$1.84 \pm 0.51$	$0.82 \pm 0.12$
Branch diameter (mm)	$0.58 \pm 0.06$	$0.50 \pm 0.06$	$0.22 \pm 0.02$
Porosity (%)	$89.63 \pm 0.1$	$90.52 \pm 1.0$	$91.98 \pm 0.3$

<sup>1</sup> Nominal value by the manufacturer (Duranice Applied Materials (Dalian) Co., Ltd)

Foam C has the highest porosity percentage, followed by foam B and foam A. This is reflected in the amounts of void spaces in foam C, as shown in Figure 4.1. Foam C consisted of small diameters of interconnected branches, resulting in a large surface area. Cross-sectional view of Cu foam interconnected branches showed a hollow cylindrical core structure, contributing to the lightweight properties of the Cu foam. A similar study of Ni foam has reported that the hollow structure was the result of the fabrication process *via* electro-deposition methods (Heo et al., 2019).

Digital images and measurements show the decrease in sizes of the pores, cell walls and Cu foam branches from foam A, foam B and foam C, accordingly. However, the number of Cu foam interconnected branches had increased from foam A to foam B and finally foam C, increasing the surface area of the foam. It has been reported that the increase in Cu foam pore density would result in the increase in total heat transfer and pressure drop. Hu et al. (2016) has reported that the increase Cu foam from 5 PPI to 15 PPI yield total heat transfer rate and pressure drop increment by 67% and 62%, respectively.

#### **4.3 Characterisation of Cu-Sn-Ni-P Amorphous Filler Alloys**

Figure 4.2 shows the XRD peak pattern of Cu-Sn-Ni-P amorphous filler alloys, showing broad peak curves at approximately 2 Theta of 35° to 52° for filler A, filler B and filler C. There were no narrow and sharp of diffraction peaks to indicate any crystallisation and the diffraction peaks indicate that all forms of the constituent in the filler were amorphous.

The broad peak formation points to the random atomic arrangement of amorphous materials in three-dimensional (3D) phase that do not own a periodicity. This arrangement causes the X-ray to scatter, causing a wide range of 2 Theta (Cullity, 1956).

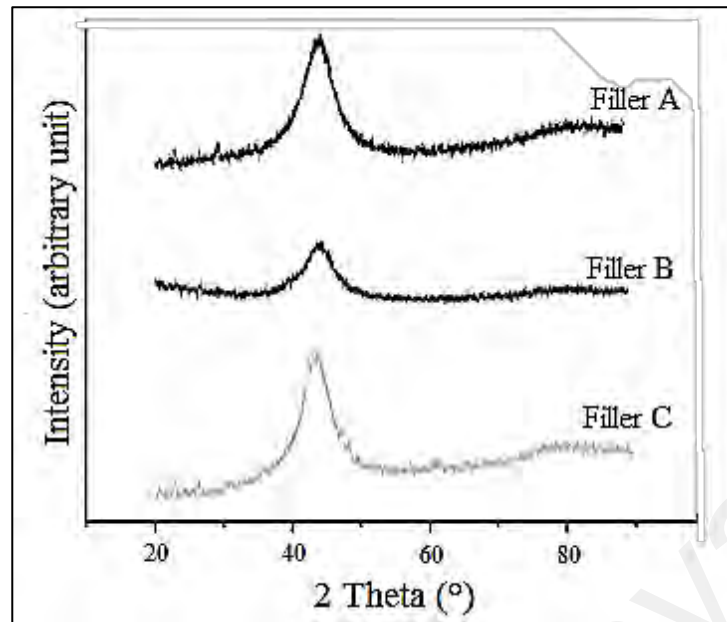


**Figure 4.2:** XRD pattern of Cu-Sn-Ni-P amorphous filler alloys

Similar XRD broad diffraction peak patterns for amorphous filler have been reported by other researchers, such as for Ti-25Zr-15Ni-20Cu filler (Zou, Jiang, Zhao & Chen, 2009) and Cu-15.7Ni-9.3Sn-6.5P filler (Zhang et al., 2016).

#### 4.4 Preliminary Investigation on Brazing Holding Time

A preliminary investigation of Cu/Cu foam A/Cu brazing using filler B was conducted to evaluate different holding times and brazing temperatures. This was done to optimise the brazing holding time for the subsequent experimentation on Cu/Cu foam/Cu brazing. The resultant brazed joints were evaluated for their shear strengths. Figure 4.3 shows the shear strengths of Cu/Cu foam A brazed joints using filler B. It was found that the shear strengths of Cu/Cu of foam A increases as the brazing temperature increased from 660 °C to 680 °C, but declined as the temperature reaches 700 °C. Further increase in brazing temperature to 720 °C did not show any significant rise in the shear strength of Cu/Cu foam A. The highest shear strength for Cu/Cu foam A brazed joint was obtained at a brazing temperature of 680 °C for all brazing holding time, indicating that this brazing temperature was sufficient for the filler to diffuse into the brazed joint interface.

Increasing the temperature over 700 °C would result in weak interactions of the atoms in the filler to form better brazed joint.

It was found that the shear strengths of Cu/Cu foam A decreases as the brazing time increases from 5 min, 10 min and 15 min. This reduction in shear strengths was probably due to the prolonged brazing holding time which could have likely to cause vapourisation and formation of brittle compounds on the brazed joint interface (Zhong et al., 2012). Furthermore, increasing the brazing time over 5 min may degrade the Cu foam (Jacobson & Humpston, 2005). At elevated brazing temperature with prolonged brazing time, the hollow branch structure of the Cu foam (Figure 4.1) may collapse and degrade, reducing the shear strength of the joint. As reported by Wang et al. (2017), intense reaction between filler (Ag-Cu-Ti) and Cu foam would collapse the Cu foam structure during brazing. Hence, the brazing time of 5 min was fixed for next investigation.

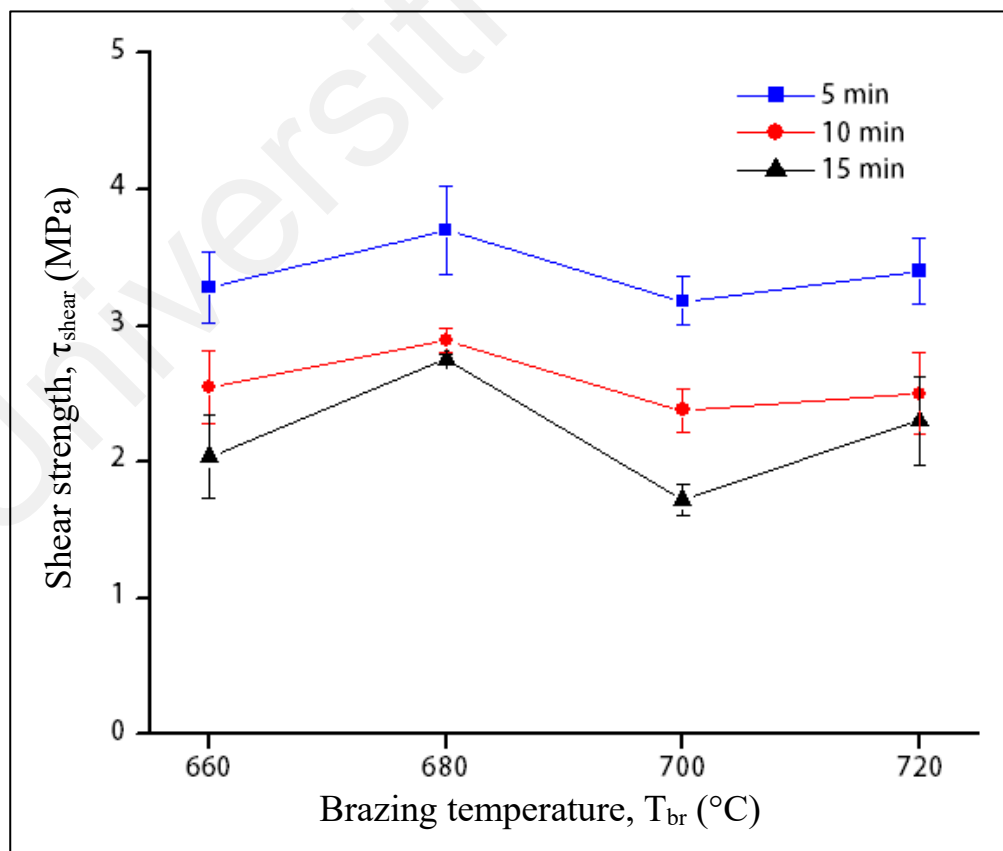


**Figure 4.3:** Shear strength of brazed Cu/Cu foam A using filler B at different holding time

#### **4.5 Mechanical Evaluation of Brazed Cu/Cu foam/Cu using different Cu-Sn-Ni-P Amorphous Filler Alloys at 5 min brazing holding time**

The compressive strength and shear strength of brazed Cu/Cu foam/Cu joint were evaluated for different amorphous fillers (filler A, filler B and filler C) with different Cu foam pore densities (foam A, foam B and foam C) at different brazing temperatures of 660 °C, 680 °C, 700 °C, 720 °C.

The compressive strength tests were conducted to compare the mechanical properties of nonbrazed Cu/Cu foam/Cu and brazed Cu/Cu foam/Cu. Shear strength evaluations were conducted for the brazed Cu/Cu foam. These tests are important to determine the mechanical properties of Cu foam and brazed Cu/Cu foam brazed joint to withstand the load of the fluid flow mass in heat exchanger applications (Heo et al., 2019).

##### **4.5.1 Effect of Brazing Temperature, Amorphous Filler and Cu Foam Pore Density on Compressive Strength of Cu/Cu foam/Cu**

Figure 4.4(a) shows the increase in compressive strengths of Cu/Cu foam/Cu using filler A as the brazing temperatures increases from 660 °C to 680 °C, followed by a decline at 700 °C and 720 °C. This indicate that a brazing temperature of 680 °C is the most favourable for filler A to braze Cu/Cu foam/Cu and produce the highest compressive strength. Beyond 680 °C brazing temperature, the formation of interface brazed joint microstructure would be affected which reduces its compressive strength.

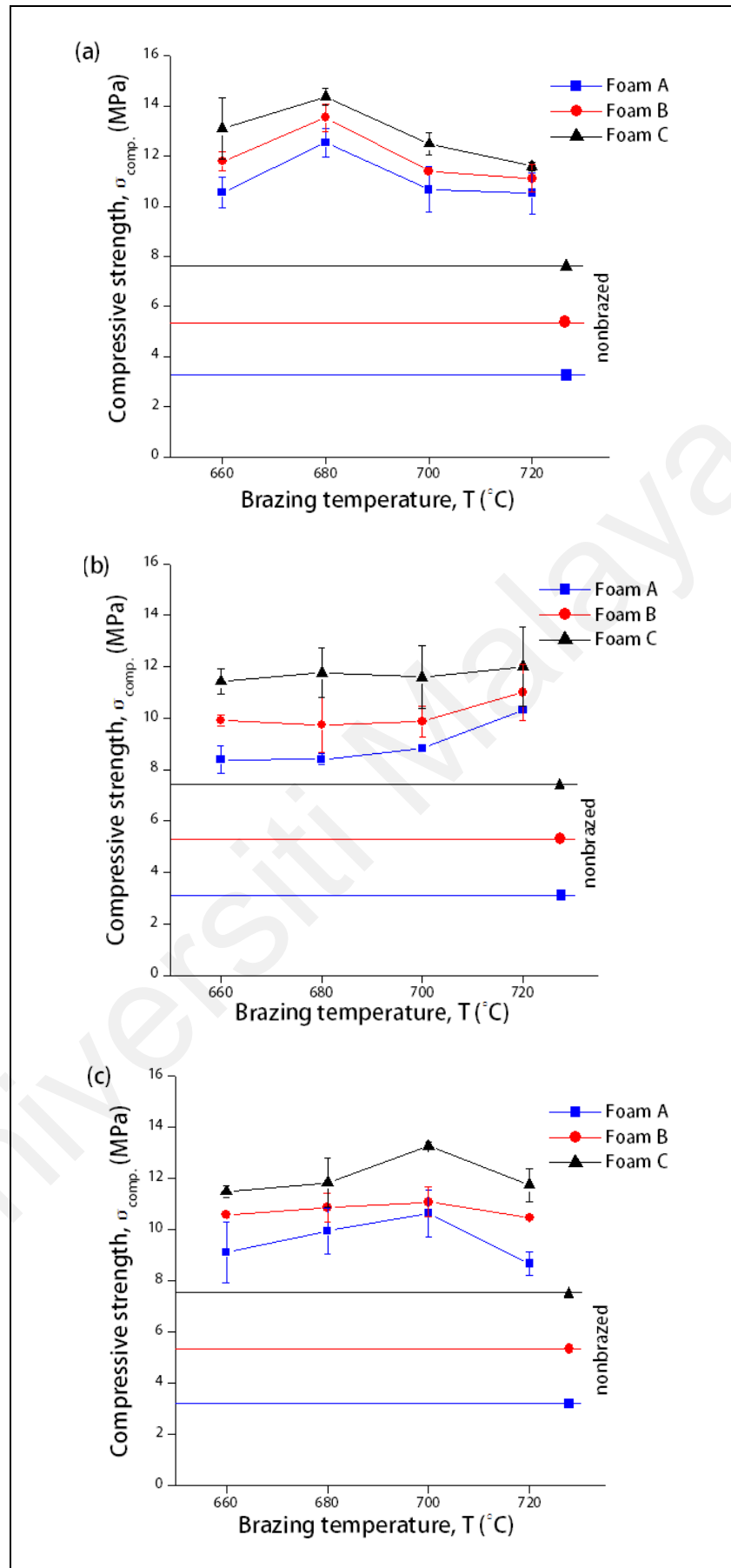


**Figure 4.4:** Compressive strength ( $\sigma_{comp.}$ ) of Cu/Cu foam/Cu using (a) filler A (b) filler B (c) filler C with different Cu foam at different brazing temperature

Figure 4.4(b) shows a constant compressive strength value of Cu/Cu foam/Cu using filler B as the brazing temperatures increases from 660 °C to 700 °C, followed by an increase at 720 °C. This could be due to the ability of filler B to flow to the Cu foam via capillary action. At elevated temperature, the filler B will melt, then spread and flow through the narrow spaces of the Cu foam. Increasing the brazing temperature enabled sufficient heat input to provide the required energy to break the atomic bonds in filler B, allowing it to flow freely and coat the Cu foam branch. This has resulted in the increase in compressive strengths.

A similar trend was observed for Cu/Cu foam/Cu using filler C. Figure 4.4(c) shows a constant compressive strength values for brazing temperatures of 660 °C to 680 °C, which increases as the brazing temperature increased to 700 °C, but declined as the temperature rised to 720 °C.

The pore density of Cu foam has a significant effect on the compressive strength performance. Figure 4.4 shows the compressive strengths of Cu/Cu foam/Cu increase from foam A to foam B and finally foam C. The highest compressive strength of foam C can be attributed to the abundance of branching structure (Figure 4.1). The increase in compressive strengths with the increase in Cu foam pore densities correlate to the rise in the density and porosity, as tabulated in Table 4.1. Figure 4.5 shows the high number of branches in foam C as compared to foam B and foam A. This interconnected branch would able to resist the applied load better than foams with lesser interconnected branches. As mentioned in Section 4.2, the increase in the amounts of Cu foam branches in foam A, foam B and foam C, would correspondingly increase their compressive strength values.

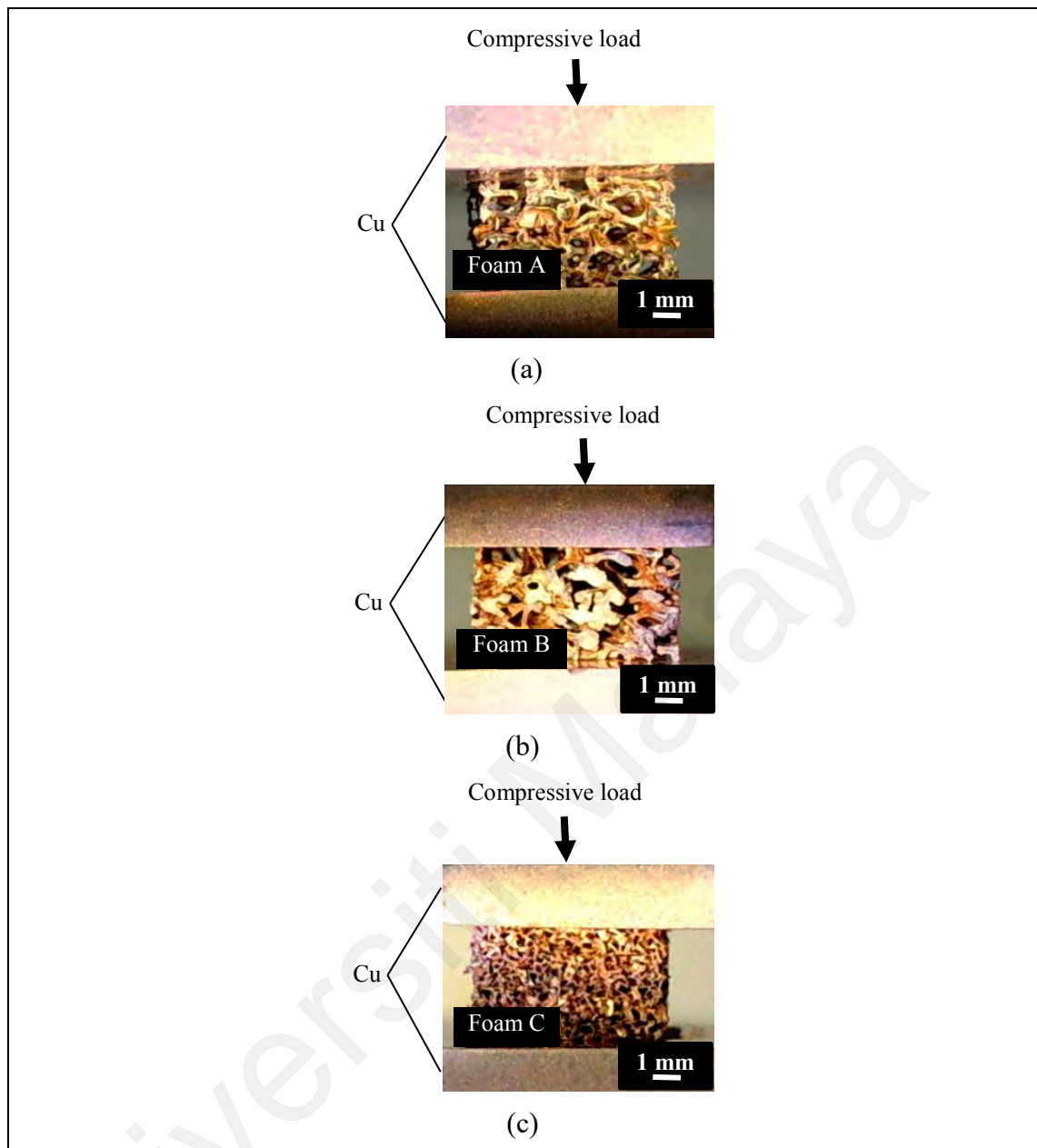


**Figure 4.5:** Compressive load exerted on Cu/Cu foam/Cu with (a) foam A (b) foam B and (c) foam C

Overall, brazed Cu/Cu foam/Cu using a filler A yielded the highest compressive strength at a brazing temperature of 680 °C for foam A (12.5 MPa), foam B (13.5 MPa) and foam C (14.4 MPa). This is followed by brazed Cu/Cu foam/Cu at 720 °C using filler B for foam A (10.3 MPa), foam B (11.0 MPa) and foam C (12.0 MPa).

The lowest compressive strength obtained was for brazed Cu/Cu foam/Cu at 720 °C using a filler C with foam A (10.6 MPa), foam B (11.1 MPa) and foam C (13.3 MPa).

Generally, the differences in the compressive strengths of brazed Cu/Cu foam/Cu would depend on the amorphous filler, brazing temperature and Cu foam pore density.

In comparison, the compressive strengths of nonbrazed Cu/Cu foam/Cu for foam A, foam B and foam C were 3.23 MPa, 5.31 MPa and 7.74 MPa, respectively as shown as a straight line in Figure 4.4. The compressive strength of nonbrazed samples were lower than the values obtained for brazed Cu/Cu foam/Cu (ranged from 10.3 MPa to 14.4 MPa). The percentage increment of compressive strength between nonbrazed and brazed Cu/Cu foam/Cu shows average percentage increments calculated were 108.93%, 75.81% and 52.06% for foam A, foam B and foam C, respectively. The result presents that using filler in the brazed Cu/Cu foam/Cu would significantly enhance its compressive strength performance.

During brazing, the molten filler flows towards the Cu foam branches and would coat them during solidification. The coated branches is indicated by the changes in colour of the Cu foam (**Appendix C**). The solidified filler on the Cu foam branches would increase the compressive strength of the brazed Cu/Cu foam/Cu as compared to the nonbrazed Cu/Cu foam/Cu.

Figure 4.6 shows the compressive stress-strain curve for a nonbrazed Cu/Cu foam/Cu (without filler). Generally, a compressive stress-strain curve of porous materials can be divided into three regions which are linear elastic, plateau and densification (Gnyloskurenko et al., 2005; Liu et al., 2014; Haidar and Sekh, 2018). In the linear elastic region, the stress gradually increases with increasing strain, at a low strain range ( $< 0.015$ ). Here, the compressive stress concentration reaches the yield strength of the Cu foam cell wall and leads to a reduction of Cu foam pore size.

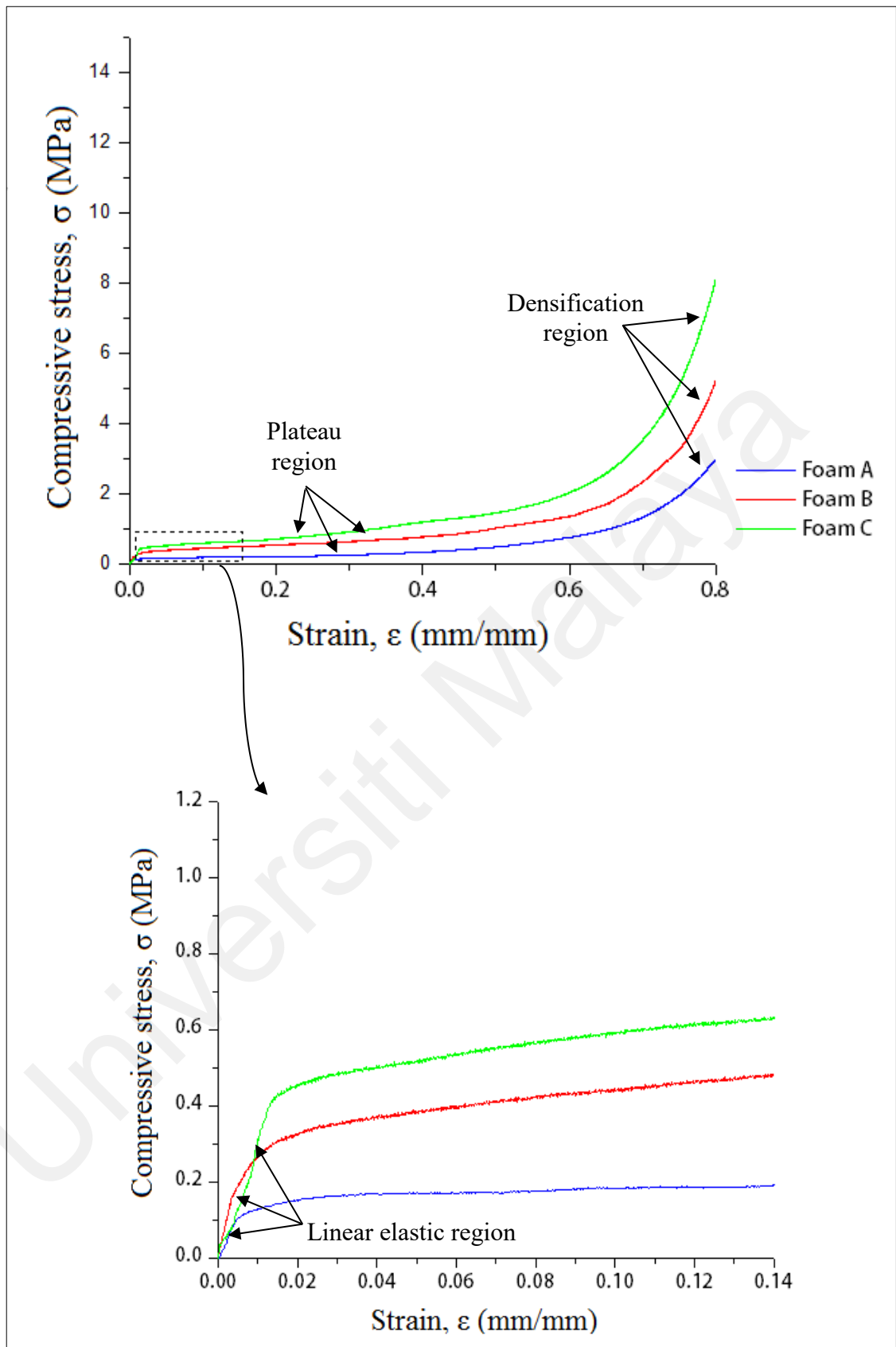


**Figure 4.6:** Compressive stress-strain curve of nonbrazed Cu/Cu foam/Cu and the inset shows an elastic curve at strain range of 0 - 0.14 $\epsilon$

Beyond the elastic region, the plastic deformation of the nonbrazed Cu/Cu foam/Cu is indicated by a plateau region. A long and smooth plateau region corresponds to a ductile behaviour with nearly constant stress. It can be theorised from this result that nonbrazed Cu/Cu foam/Cu can still absorb the energy of the impact even though it was in a state of compressive deformation. The compressive stress–strain curve also illustrates the ability of foam C to absorb excess energy because of its high-stress amplitude. The continual deformation causes the reduction in pore size and porosities of Cu foam (Liu, Tan, Wu & He, 2010). Finally, a sharp increase in densification with increasing strain indicating compaction on the Cu foam branches. When the Cu foam becomes sufficiently compact, the cell wall would collapse with further load application.

The compressive stress-strain curve of nonbrazed Cu/Cu foam/Cu (Figure 4.6) and brazed Cu/Cu foam/Cu using different amorphous fillers (Figures 4.7 to 4.9) with different Cu foam pore densities were compared. The brazing temperature was selected based on the highest compressive strength, as discussed previously (Figure 4.4).

The linear elastic region of brazed Cu/Cu foam/Cu shows brazing using filler B and C yielded the lowest strain range ( $<0.005$ ), followed by filler A ( $<0.01$ ). In comparison, the linear elastic region of the nonbrazed Cu/Cu foam/Cu shows the strain range is  $<0.015$ . The presence of fillers reduces the linear elastic region with increasing stress.

The compressive stress-strain curve of brazed Cu/Cu foam/Cu using filler A (Figure 4.7) and filler B (Figure 4.8) with a foam C shows a primary (first) and secondary plateau regions. The first and secondary plateau regions appear in the stress-strain curve due to the deformation of foam C is considered to occur in the high porosity layer, and then shifted to the low porosity layer, respectively.

Initially, the deformations started in the high porosity layer present primary maximum stress in the first plateau region. The continual deformation causes the reduction in foam porosity and pore size leads to the initial point of densification for the high porosity layer. However, at this point, it is considered as the endpoint of the first plateau region because the second plateau region appeared indicates the deformation of the low porosity layer. At this stage, the deformation of Cu foam shifted to the low porosity layer, which known as the transition region. The transition step for a deformation of Cu foam low porosity layer occurs due to the Cu foam high porosity layer has been collapsed in the early stage. After that, the densification of the Cu foam low porosity layer started. The sharp increase of the curve in the densification region indicates the Cu foam branches become sufficiently collapse and compact. On the contrary, a second plateau region for the brazed Cu/Cu foam/Cu using a filler C with a foam C (Figure 4.9) was not observed. The result shows that the filler probably plays a role for different plateau regions step to occur as no second plateau region is observed for a nonbrazed sample (Figure 4.6). While filler C may not affect the structure of the foam C since none of the second plateau regions is observed compared to filler A and filler B.

Hangai, Utsunomiya, Kuwazuru, Kitahara and Yoshikawa (2015) have reported similar plateau regions in the compressive stress-strain curve for the deformation behaviour study of functionally graded aluminium foams. Authors improved the aluminium foam by adding a blowing agent titanium(II) hydride ( $TiH_2$ ) using friction stir welding method. The result shows different steps in the plateau region in the compressive stress-strain curve with the addition of  $TiH_2$ . Authors found that the combination of high porosity and low porosity layers of foam can control the foam deformation.

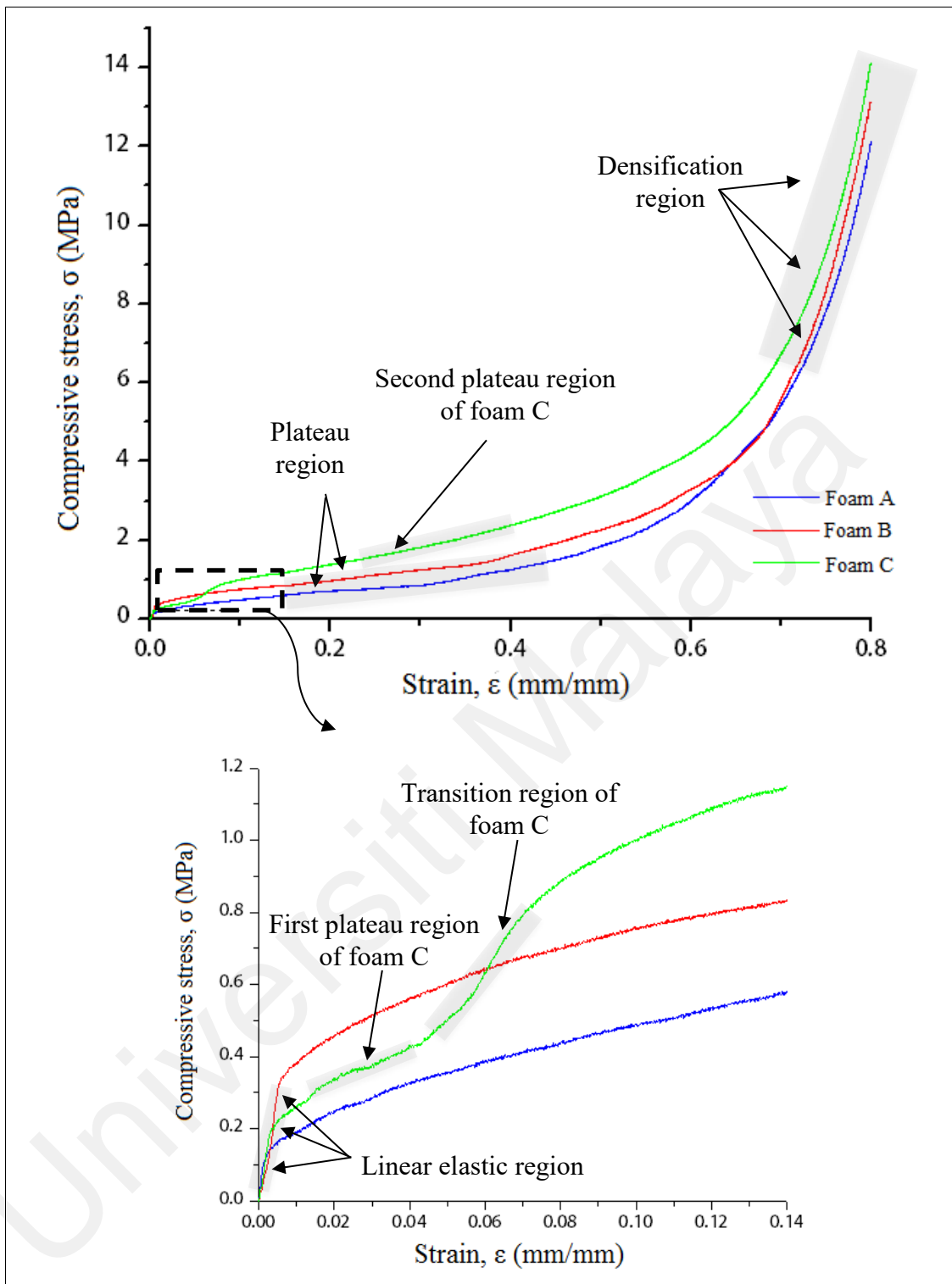


**Figure 4.7:** Compressive stress-strain curve of brazed Cu/Cu foam/Cu using filler A at 680 °C with different foam and inset shows an elastic curve at strain range of 0 - 0.14 $\epsilon$

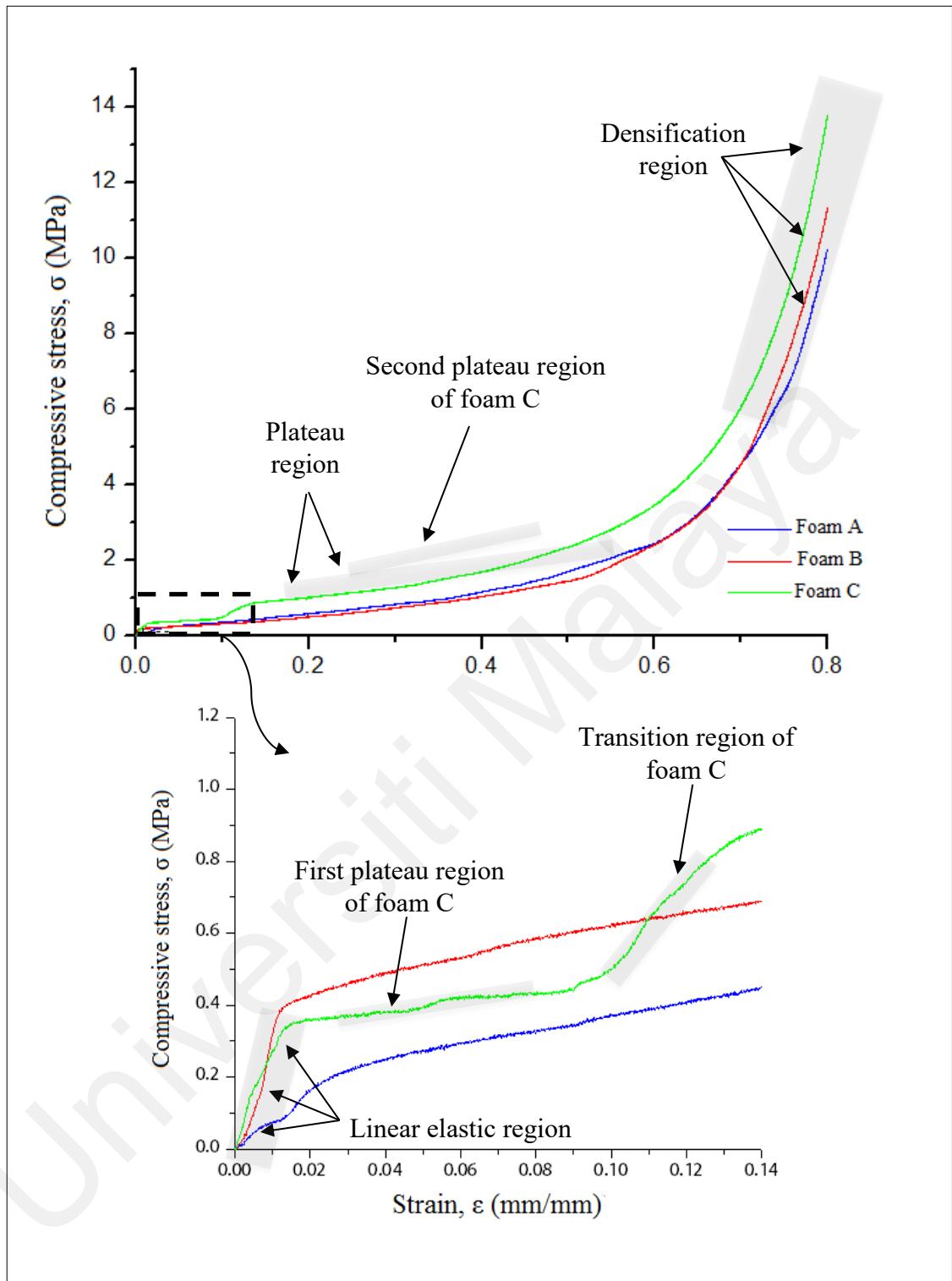


**Figure 4.8:** Compressive stress-strain curve of brazed Cu/Cu foam/Cu using filler B at 720 °C with different foam and inset shows an elastic curve at strain range of 0 - 0.14 $\epsilon$

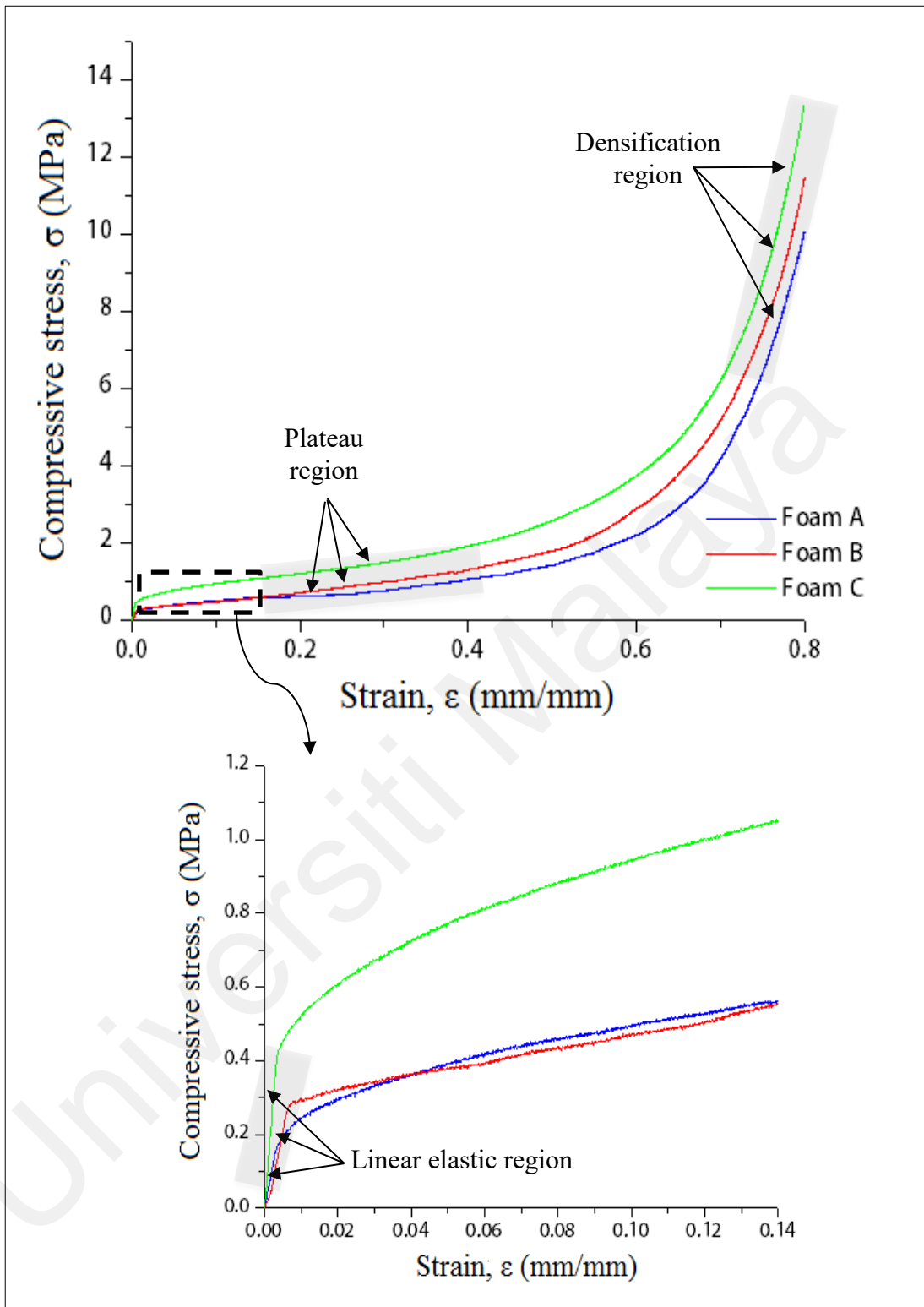


**Figure 4.9:** Compressive stress-strain curve of brazed Cu/Cu foam/Cu using filler C at 700 °C with different foam and inset shows an elastic curve strain range of 0 - 0.14 $\epsilon$

#### **4.5.2 Effect of Brazing Temperature, Amorphous Filler and Cu Foam Pore Density on Shear Strength of Cu/Cu foam/Cu**

For the shear tests, an additional Cu/Cu foam/Cu specimen was prepared at 640 °C brazing temperature. The brazing of Cu/Cu foam/Cu was conducted at 640 °C to ascertain the highest shear strength results, based on the liquidus temperatures of filler A (610 °C) and filler C (600 °C) (Table 3.1).

Figure 4.10(a) shows the increase in shear strength of Cu/Cu foam (filler A) as the brazing temperature increases from 640 °C to 660 °C. However, as the brazing temperature increases to 680 °C, the shear strength started to decline. Reductions in shear strengths were continued to be seen for all Cu foam pore density as the brazing temperature increases from 700 °C to 720 °C.

Similarly, the shear strengths of Cu/Cu foam using filler B increase as the brazing temperature increases from 660 °C to 680 °C, as shown in Figure 4.10(b). A decrease in shear strength was seen as the brazing temperature increases to 700 °C, with an insignificant increase as the brazing temperature reaches 720 °C. The highest shear strength obtained for Cu/Cu foam using filler B is at a brazing temperature of 680 °C for all Cu foam pore density. For filler C, the shear strengths of Cu/C foam increase as the brazing temperature increases from 660 °C to 680 °C [Figure 4.10(c)], but decreases as the brazing temperature increases to 720 °C.

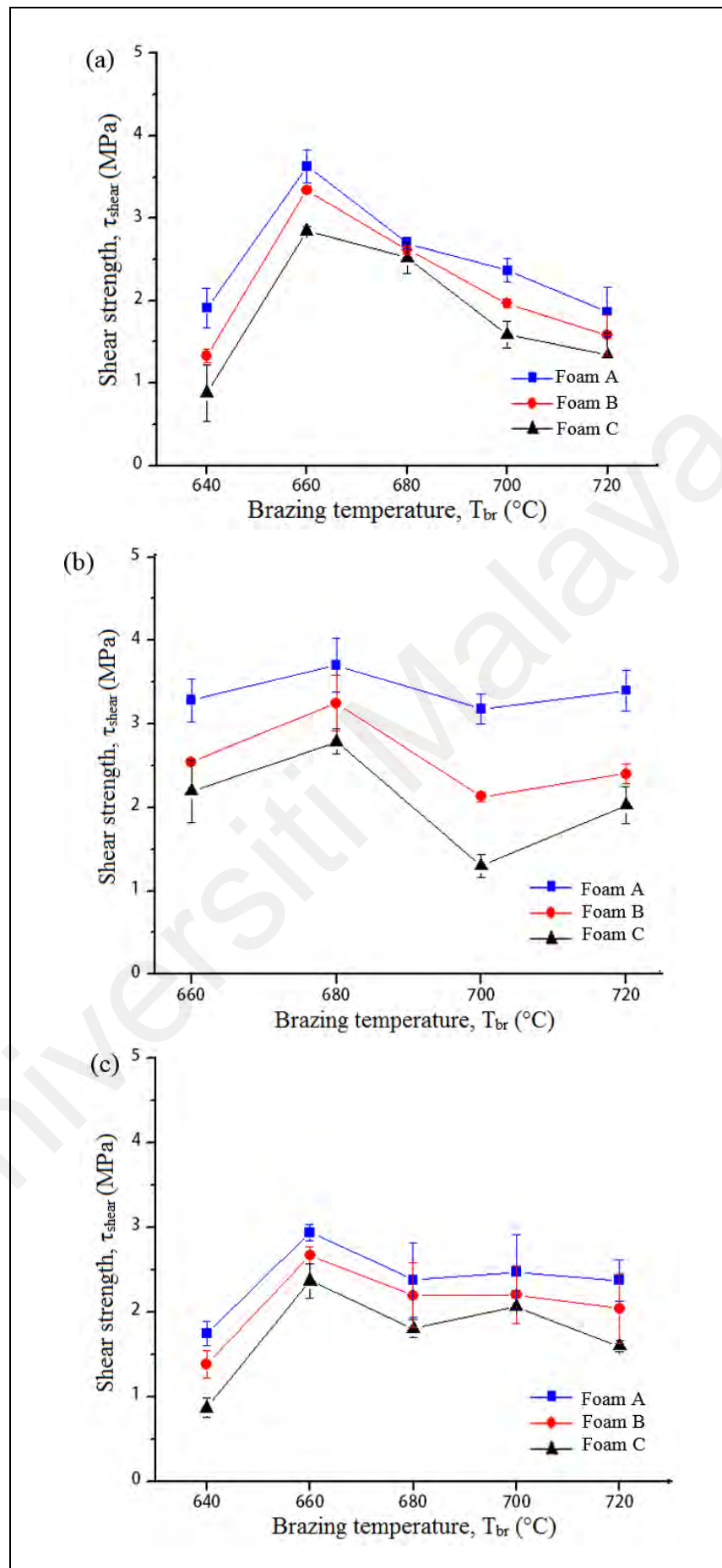


**Figure 4.10:** Shear strength of Cu/Cu foam using (a) filler A (b) filler B (c) filler C

The highest shear strengths of brazed Cu/Cu foam/Cu using filler A, filler B and filler C were obtained at brazing temperatures of 660 °C, 680 °C and 660 °C, respectively. The different brazing temperature to be more effective in shear strength is due to the different elements composition in the amorphous filler alloys. Each of the amorphous filler alloys have different solidus and liquidus temperature that will affect the melting range of amorphous filler alloys. The melting range of filler A, B and C are 35 °C, 52 °C and 30 °C, respectively based on the solidus and liquidus temperature provided by manufacturer (Table 3.1). The filler B owns wide melting range has yields highest shear strength at higher brazing temperature  $T_{br}$  (680 °C) compared to filler A and filler C. Even though the filler B and C have similar liquidus temperature of 643 °C and 645 °C, respectively, the optimum brazing temperature was different due to dissimilar melting range. The wide melting range apparently need more energy to break a bond of atom in filler B to diffuse between Cu/Cu foam brazed joint interfaces in forming a strong joint. This is probably the filler B need higher brazing temperature to possess a good formation of metallurgical combination because of sufficient atom diffusion in the interface. However, a continually increasing of brazing temperature may enhance a coarseness of microstructure resulting in decreasing of the shear strength (Zhong et al., 2012).

Zhong et al. (2012) have studied the shear strengths of glass/metal (iron-nickel-cobalt alloy: Kovar®) using Cu-9.0Sn-7.0Ni-6.0P filler at brazing temperatures of 660 °C to 700 °C. It was found that the shear strengths of the joint would increase as the brazing temperature increases from 660 °C (6 MPa) to 680 °C (11.6 MPa). Furthermore, increasing the brazing temperature up to 700 °C had reduced the shear strengths of the joint. The filler used has the same composition of the filler (filler C) used in this study. However, the current study has found the highest shear strengths were obtained at a brazing temperature of 660 °C (2.9 MPa- foam A, 2.7 MPa- foam B, 2.4 MPa- foam C).

The difference in brazing temperatures between Zhong et al. (2012) and the current study was due to different joining materials involved.

Figure 4.10 shows Cu/Cu foam A resulted in the highest shear strength for all filler types (3.6 MPa filler A at 660 °C , 3.7 MPa filler B at 680 °C and 2.9 MPa, filler C at 660 °C ). This is followed by Cu/Cu foam B using filler A at 660 °C (3.3 MPa), filler B at 680 °C (3.3 MPa) and filler C at 660 °C (2.7 MPa). The lowest shear strengths obtained were 2.9 MPa (filler A at 660 °C), 2.8 MPa (filler B at 680 °C) and 2.4 MPa (filler C at 660 °C).

Increasing the Cu foam density was found to have reduced the shear strengths of the joint. Foam C has a higher porosity and smaller pore sizes as compared to foam A, but has lower shear strength. The interconnected structure with small diameter branches resulted in a large surface area between Cu and Cu foam C (Figure 4.1). However, this large surface area did not result in increased shear strength properties as the molten filler has to spread in more hollow spaces in foam C. This observation is similar to past results which have found highly porous metal yielded low shear strengths. For example, Wan et al. (2012) have conducted shear tests on porous metal fibre sintered sheet (PMFSS) at different porosities. Increasing the porosity of PMFSS from 70% to 90% resulted in decreased the shear strengths from 7.7 MPa to 0.9 MPa.

Figures 4.11 to 4.13 show shear stress-strain curves of brazed Cu/Cu foam/Cu using filler A, filler B and filler C, respectively. The brazing temperature was selected based on the highest shear strength (Figure 4.10). Generally, a shear stress-strain curve of Cu/Cu foam brazed joint can be divided into four regions which are elastic, plateau, densification and tearing (Kaya, 2020). Initially, the elastic region takes place when the stress gradually increases with increasing strain between the stress load and brazed sample. The continual deformation presented a hardening plateau region where the stress

is nearly constant with increasing strain. Fluctuate and noise curves correspond to the solid and void spaces of the brazed joint interface between the Cu substrate surface and porous structures of the Cu foam interconnected branches. Beyond the plateau region, a larger slope and sharp increase with increasing strain is indicated by a densification region. At this region, the deformation of the brazed joint sample is subjected to compressive loading instead of shearing loading. Finally, a lower slope with nearly constant stress in the shear stress-strain curve is denoted as tearing region. Kaya (2020) has reported similar shear stress-strain curve for a 316L open-cell stainless steel (SS) foam. The SS foam owns high ductility and experiences a high plasticity.

The plateau region and enlarge area under the shear stress-strain curve (Figures 4.11 to 4.13) indicate the Cu/Cu foam brazed joint interface owns a high ductility property. The brazed joint of Cu/Cu foam capable of absorbing energy before the sheared off occur. The brazed Cu foam has a lower shear energy absorption capacity found from the shear stress-strain curve, compared to the compressive energy absorption capacity (compressive stress-strain curve Figures 4.7 to 4.9). This is might be due to the filler presence to join Cu and Cu foam.

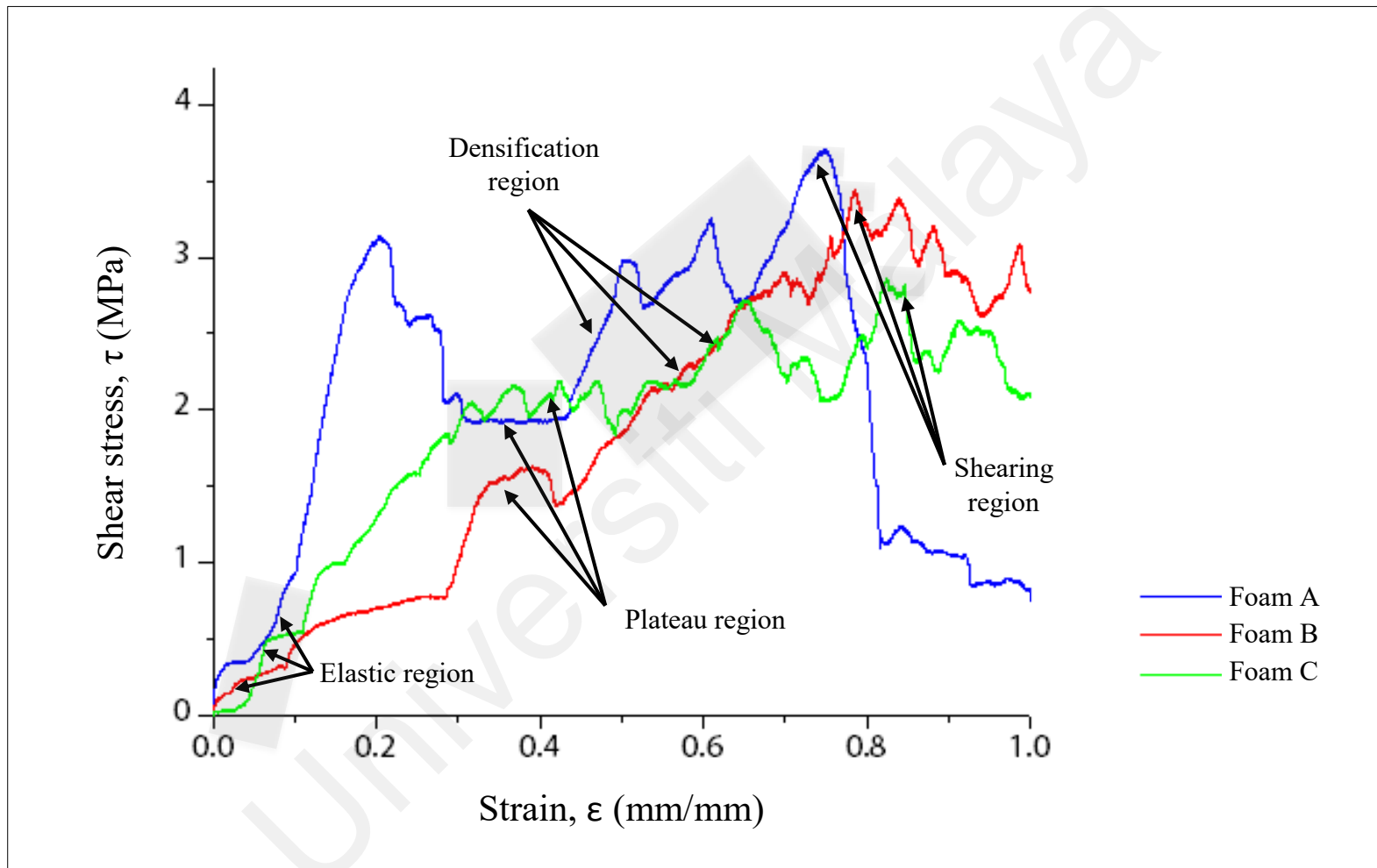


**Figure 4.11:** Shear stress-strain curve of brazed Cu/Cu foam/Cu using filler A at 660 °C with different foam

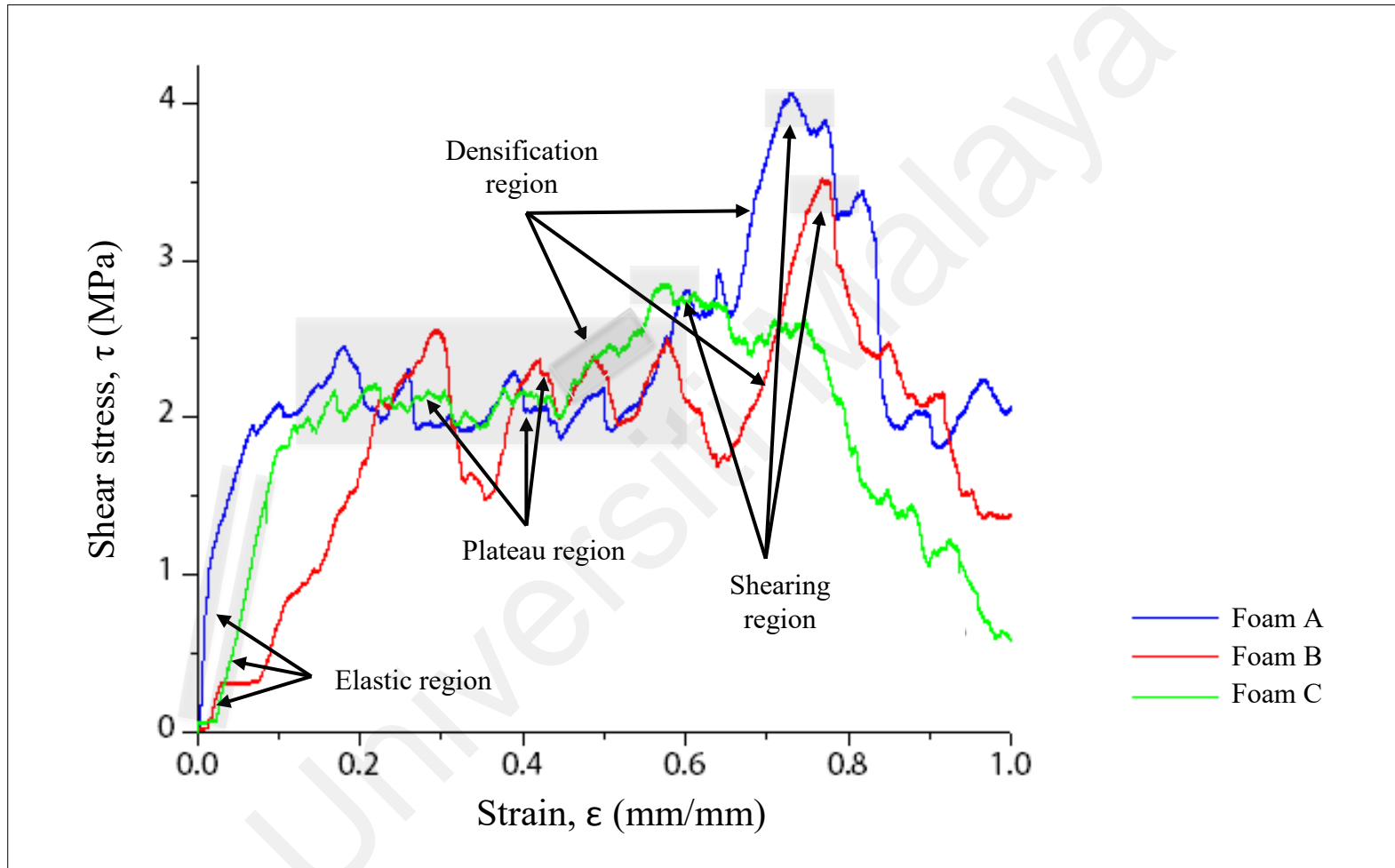


**Figure 4.12:** Shear stress-strain curve of brazed Cu/Cu foam/Cu using filler B at 680 °C with different foam

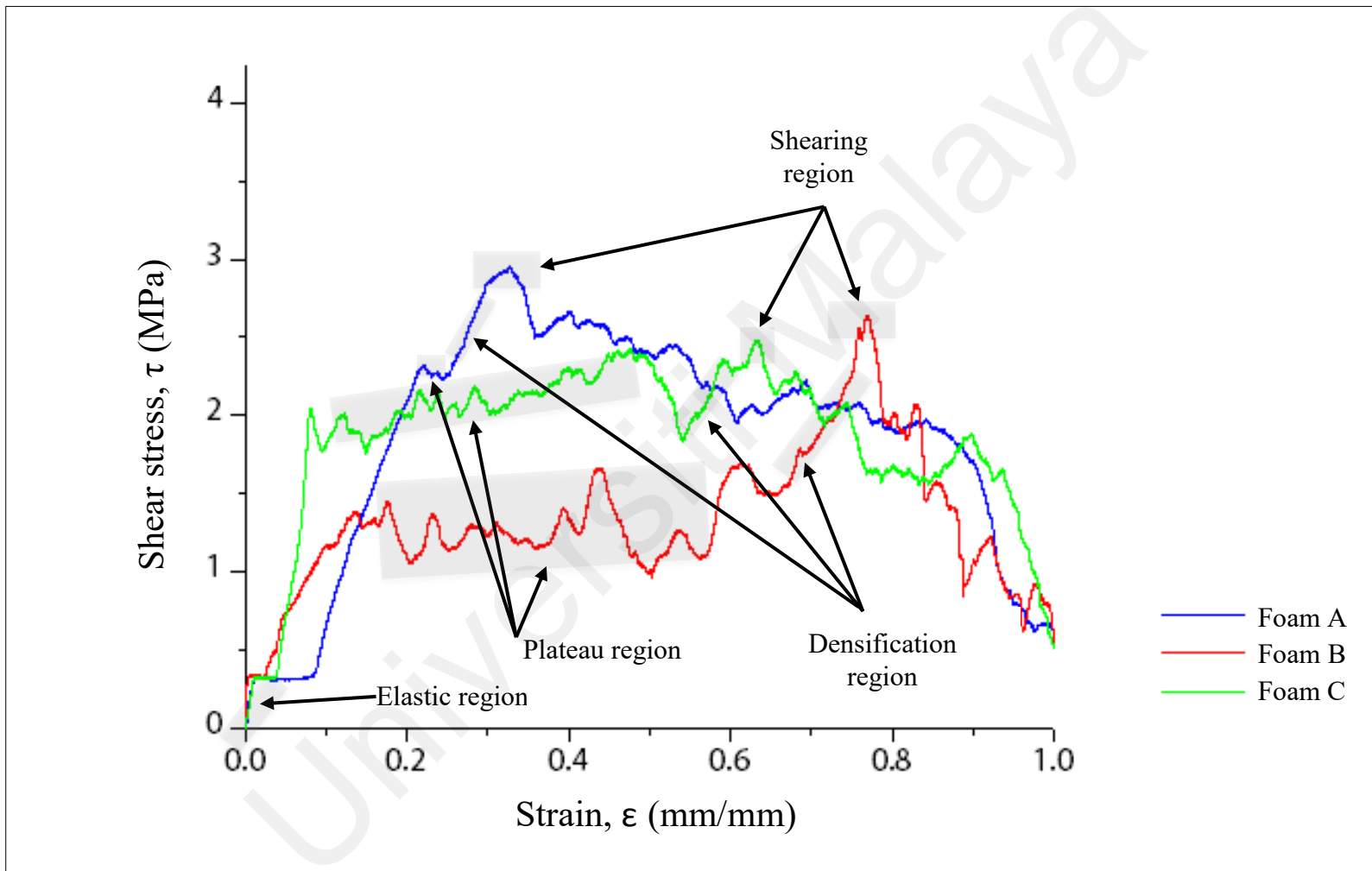


**Figure 4.13:** Shear stress-strain curve of brazed Cu/Cu foam/Cu using filler C at 660 °C with different foam

### 4.5.3 Comparison on Compressive and Shear Strength of Brazed Cu/Cu foam/Cu

The compressive strength and shear strength play vital roles in Cu/Cu foam/Cu brazed joint. The strength of Cu foam and a strong brazing joint are required properties in heat exchanger applications (Boomsma et al., 2003). The compressive strength of Cu/Cu foam/Cu is needed to accommodate strong mass fluid flow during heat exchanger operation. While the shear strength determines the contact joining quality between substrate and the foam which affect the thermal conduction due to the thermal resistance at the joining interface (Heo et al., 2019).

Based on previous discussions, the highest compressive strengths of Cu/Cu foam/Cu using filler A, filler B and filler C were obtained at high brazing temperatures of 680 °C, 720 °C and 700 °C, respectively. However, the highest shear strengths of Cu/Cu foam/Cu using filler A, filler B and filler C were obtained at low brazing temperatures of 660 °C, 680 °C and 660 °C, respectively. The compressive and shear strength values are summarized and tabulated in Table 4.2. Lower brazing temperatures minimise operational costs by saving time and energy. AWS (2011) has stated that lower brazing temperature minimises heating effects such as annealing, grain growth and distortion of the substrate. Moreover, lower brazing temperature reduces the interactions between substrate and filler alloys, overcoming possible erosions of the substrate.

The compressive strength values obtained ranged from 10.3 MPa to 14.4 MPa (as discussed in section 4.4.1). While the shear strength values ranged from 2.4 MPa to 3.7 MPa (as discussed in section 4.4.3). Shah and Sekulić (2003) have reported that the plate-fin heat exchanger is designed for a moderate operating pressure which is less than 700 kPa. Hudson Products Corporation (2007) has developed the air-cooled heat exchanger with an airflow pressure of 345 kPa to 689 kPa.

**Table 4.2:** Highest compressive strength and highest shear strength of brazed Cu/Cu foam/Cu

Foam	Filler					
	A		B		C	
	$\sigma_{\text{comp}}$ at 680 °C	$\tau_{\text{shear}}$ at 660 °C	$\sigma_{\text{comp}}$ at 720 °C	$\tau_{\text{shear}}$ at 680 °C	$\sigma_{\text{comp}}$ at 700 °C	$\tau_{\text{shear}}$ at 660 °C
A	12.54	3.63	10.32	3.70	10.65	2.94
B	13.54	3.34	11.01	3.25	11.09	2.67
C	14.37	2.85	12.00	2.79	13.27	2.37

Note:  $\sigma_{\text{comp}}$  is a compressive strength (MPa) and  $\tau_{\text{shear}}$  is a shear strength (MPa).

The shear strength in the current study is adequate to withstand the pressure of fluid flow in plate-fin heat exchanger application. Hence, in the next section of evaluations, the brazing temperatures that result in the highest shear strengths would be chosen for further evaluation. Thus, the next discussion would be on brazed Cu/Cu foam/Cu with different Cu foam pore densities using filler A, filler B and filler C at brazing temperatures of 660 °C, 680 °C and 660 °C, respectively.

#### 4.5.4 Microhardness of Cu/Cu foam Brazed Joint Interface

Figure 4.14, figure 4.15 and figure 4.16 show the diamond shaped indentations mark on Cu/Cu foam brazed joint interface using filler A, filler B and filler C, respectively. These indentation marks were made at different regions of Cu/Cu foam brazed joint interface to evaluate the hardness values on Cu foam, filler and Cu substrate (base) regions. A black region indicates the Cu foam pore area, while a grey region shows the filler area, as labelled in Figure 4.14(b). Light brown areas indicate Cu foam and Cu substrate at the brazed joint interface regions.

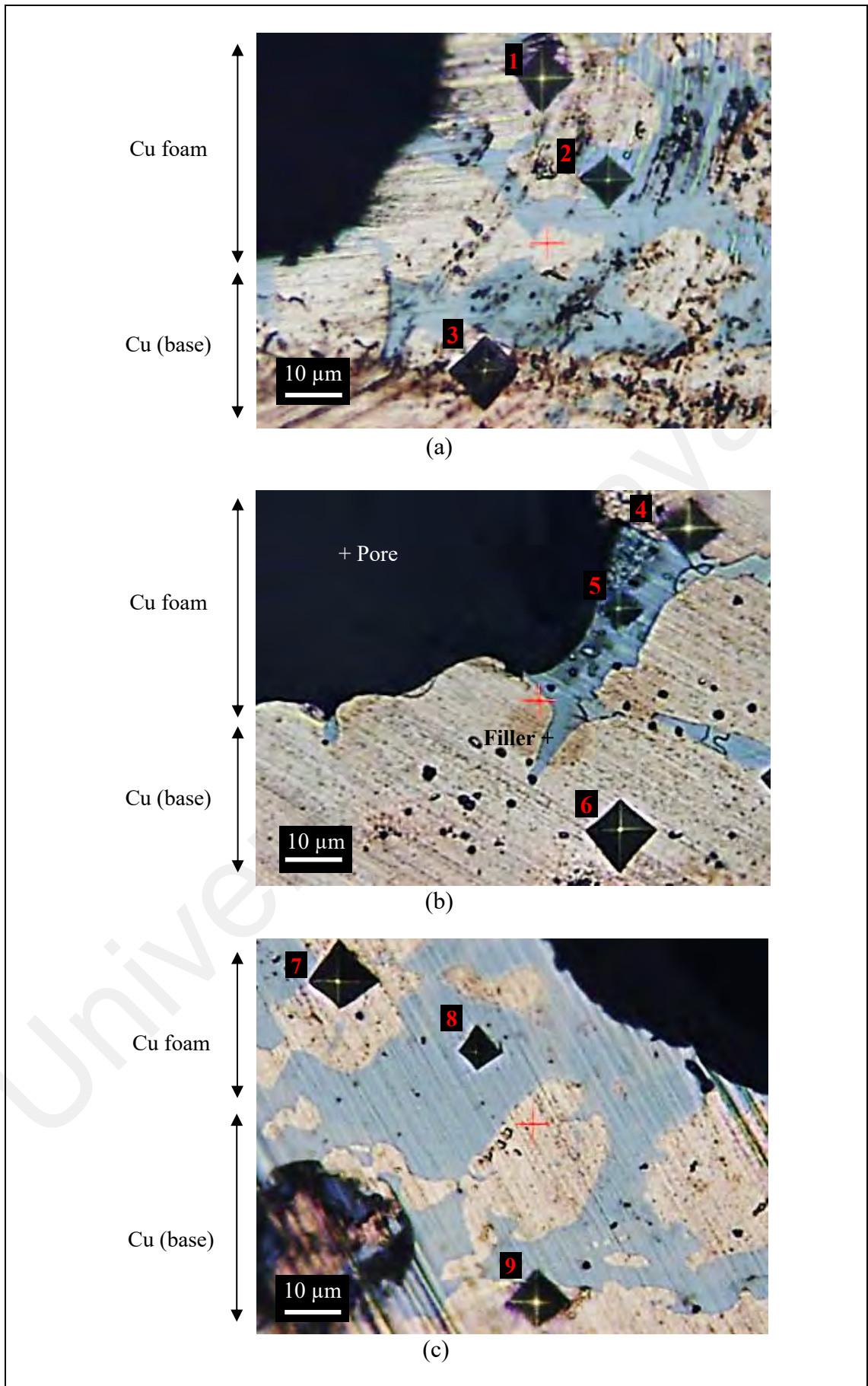


**Figure 4.14:** Micro-hardness test for Cu/Cu foam brazed joint interface joint using filler A with (a) foam A (b) foam B and (c) foam C at  $T_{br}$  of 660 °C

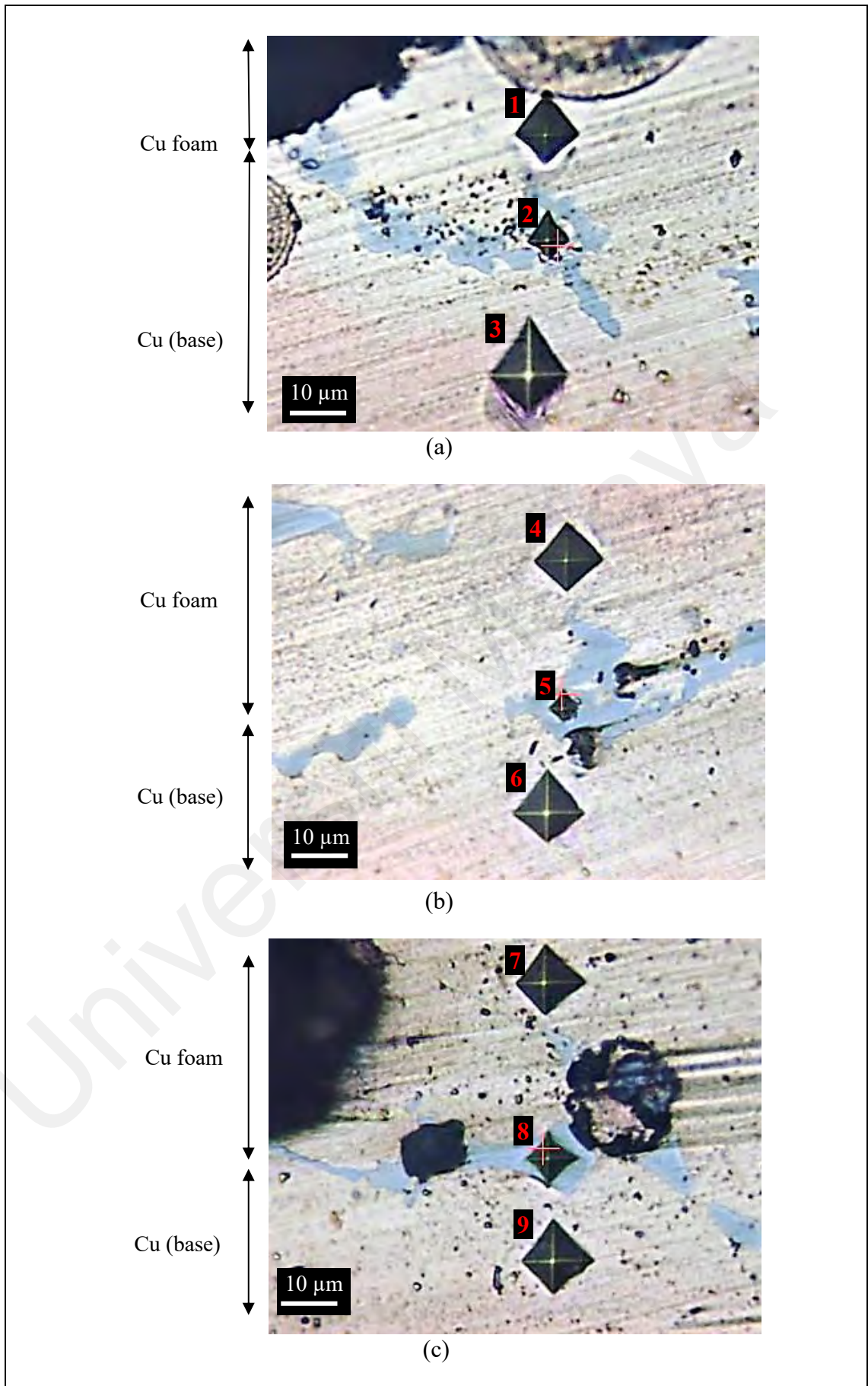


**Figure 4.15:** Microhardness test for Cu/Cu foam brazed joint interface joint using filler B with (a) foam A (b) foam B and (c) foam C at  $T_{br}$  of 680 °C

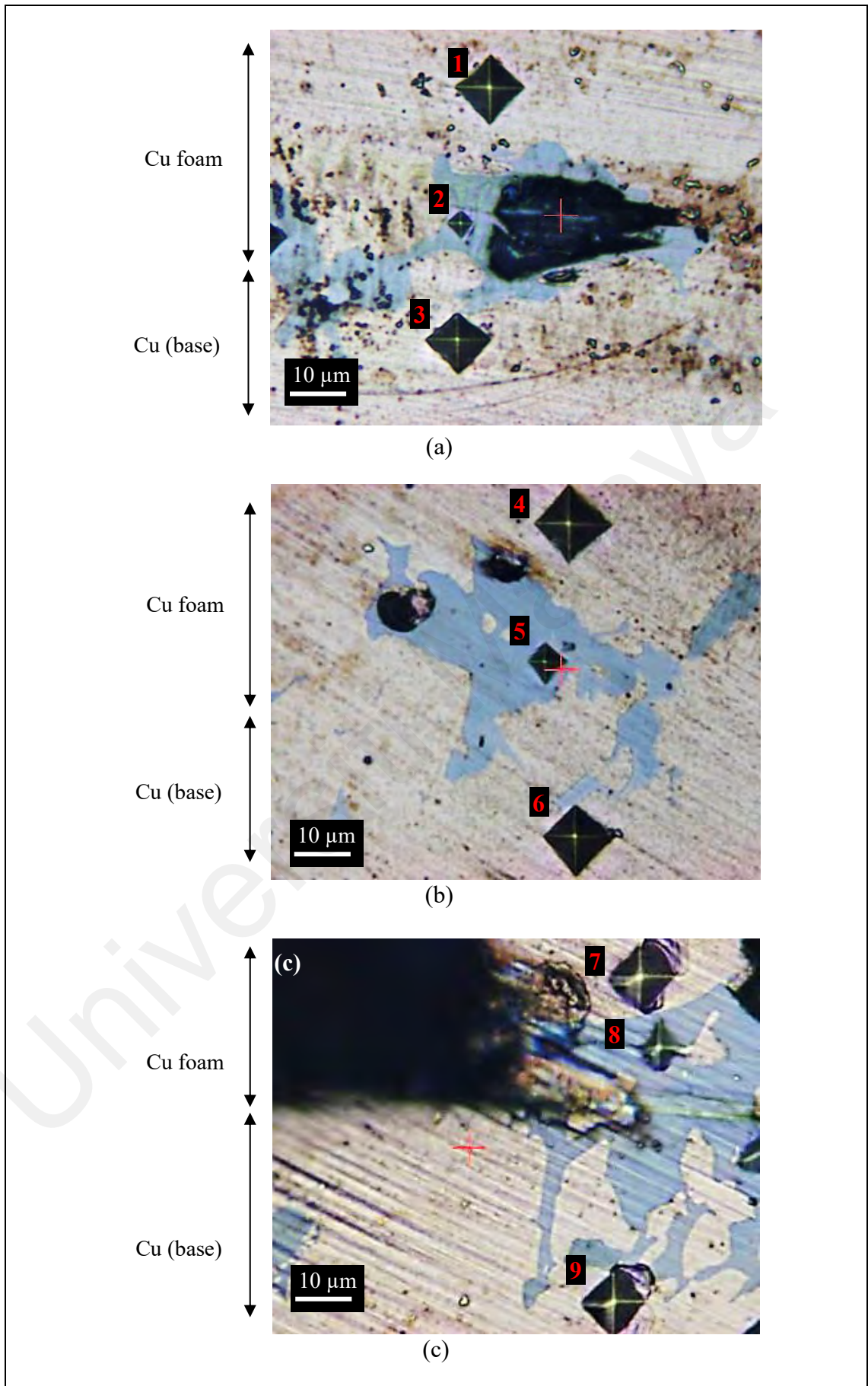


**Figure 4.16:** Microhardness test for Cu/Cu foam brazed joint interface joint using filler C with (a) foam A (b) foam B and (c) foam C at  $T_{br}$  of 660 °C

The HV of indentation marks (Figure 4.14 to Figure 4.16) are plotted in Figure 4.17 for comparison. The numbered indentation (x-axis) for foam A (1, 2 and 3), foam B (4, 5 and 6) and foam C (7, 8, 9) are labelled based on the locations in figure 4.14 (filler A), figure 4.15 (filler B) and figure 4.16 (filler C). Generally, all specimens have similar HV values at the brazed joint interface of Cu foam and Cu substrate regions. High HV values were obtained at the filler region (grey areas) as compared to the Cu foam and Cu substrate of the brazed joint interface regions. These high HV values indicate the presence of hard intermetallic compound (IMC) at the brazing interface. The presence of IMC may result in brittle failure which can lower the brazing joint shear strengths (Elrefaey & Tillmann, 2008).

The hardness results show that the HV values at Cu foam and Cu substrate of the brazed joint interface region were lower than the filler region (Figure 4.17). This suggests that any crack initiation would likely occur at the filler region first and propagate at the Cu foam and Cu substrate of the brazed joint interface regions. It was also found that the HV values for all regions increase with decreasing diameter and thickness of the Cu foam branch. Thus, foam C, with the smallest diameter and thickness of Cu foam branch has the highest HV value, followed by foam B and finally foam A, as shown in Table 4.1. The increase in HV values based on the Cu foam correlate to shear strength of brazed Cu/Cu foam A, Cu/Cu foam B and Cu/Cu foam C.

Similar HV values are expected for both the Cu and the Cu foam on the brazed joint interface. Lutfi et al. (2016) have reported similar HV (161 HV) on the brazed joint interface of Cu/Cu using filler C. However, the current work shows a different HV value for the filler region. This is due to the structural differences between Cu foam and solid Cu. The filler would tend to flow into the Cu foam (as shown in Cu substrate surface from the brazed sample shear-fracture (Figure 4.14 to Figure 4.16) due to the hollow and

porous structure of the foam (Figure 4.1). The lowest HV value was recorded for brazed Cu/Cu foam using filler A. It is then followed by increasing HV values for brazed Cu/Cu foam using filler B and filler C at filler regions. High HV values at the filler region are expected due to additions of new elements.

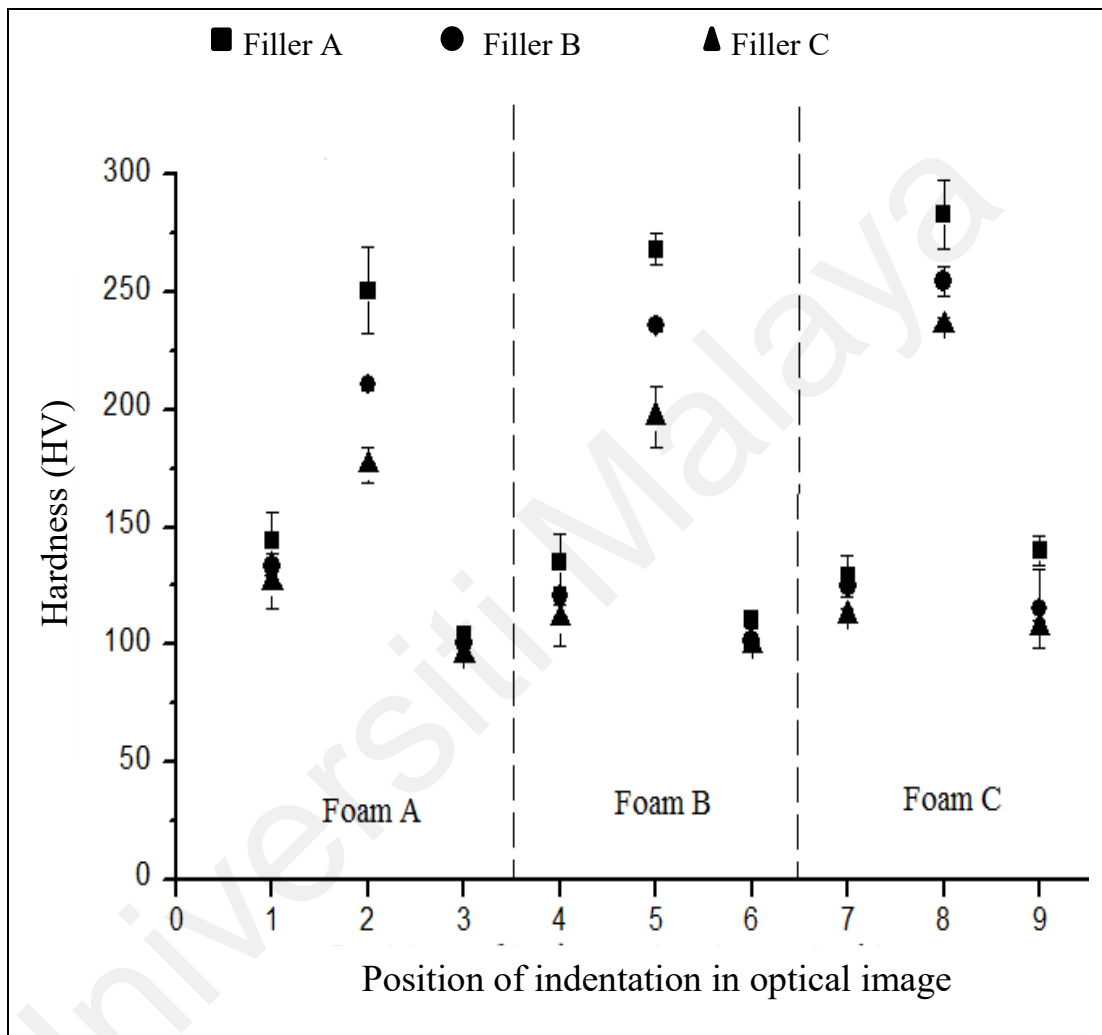


**Figure 4.17:** Hardness value (HV) of Cu/Cu foam brazed joint interface based on indentation position in Figure 4.14 to Figure 4.16. Note: Cu foam area (1, 4 and 7), filler region (2, 5 and 8) and Cu area (3, 6 and 9).

## **4.6 Microstructure of Brazed Cu/Cu foam/Cu using Cu-Sn-Ni-P Amorphous Filler Alloys**

The shear-fracture, microhardness and microstructure of the interface of the Cu/Cu foam/Cu brazed joint were evaluated using different fillers (filler A, filler B and filler C) with different Cu foam pore densities (foam A, foam B and foam C). The brazing temperatures were fixed at 660 °C for filler A and filler C, while 680 °C was set for filler B based prior discussion on highest shear strength parameters.

### **4.6.1 Shear-Fracture of Brazed Cu/Cu foam**

The Cu substrate surface from the Cu/Cu foam shear-fracture, obtained from the shear test shown in Figure 3.8, was observed using SEM. Figures 4.18, 4.19 and 4.20 show the microstructures of the Cu substrate surface (top view) obtained from the Cu/Cu foam shear-fracture using filler A, filler B and filler C, respectively. From the images, it can be deduced that the shear-fracture of brazed Cu/Cu foam experienced a mixture of ductile and brittle fracture. The enlarge area under the shear stress-strain curves of the brazed Cu/Cu foam (Figures 4.11 to 4.13) and tear regions in BSE images (Figures 4.18 to 4.20) show evidence of ductile behaviour. BSE images show multiple cracks formation were found perpendicular to the stress loading direction, then continue propagating to develop tear region, followed by brittle cleavages. Several tear regions were observed as smooth fractures probably due to shear band formation and sliding (Yang, Shao & Yao, 2019). There are significant differences in BSE image of the Cu substrate surface from the Cu/Cu foam shear-fracture of foam A, foam B and foam C. As seen on the low magnification BSE (500 µm scale) of Figure 4.18, 4.19 and 4.20, a greater proliferation of patch marks on the Cu fractured surface were observed as the pore density of Cu foam was increased (from foam A to foam B to foam C). The increased number of patch marks on foam C

indicate high amounts of Cu foam branches were brazed with the Cu substrate. However, high amounts of brazed branches are not an indication of strong bond formation.

Based on previous results, low shear strength was obtained in the brazing joint of Cu/Cu foam using 40  $\mu\text{m}$  filler for foam C (having large amounts of branches) as compared to foam A (smaller amounts of branches). This was due to the small pore sizes and hollow structures of the Cu foam C interconnected branches. Figure 4.19 and Figure 4.20 show the Cu substrate surface from the Cu/Cu foam shear-fracture consisted a vacant area due to the hollow structure of Cu foam. This vacant area was surrounded by fractured Cu foam, indicating the foam has a hollow structure, as shown in Figure 4.1. These vacant area is due to the hollow foam structure that can be observed for foam B and C, shown in Figure 4.19 and Figure 4.20. Nevertheless, vacant area can also be the result of voids in Cu foam structure.

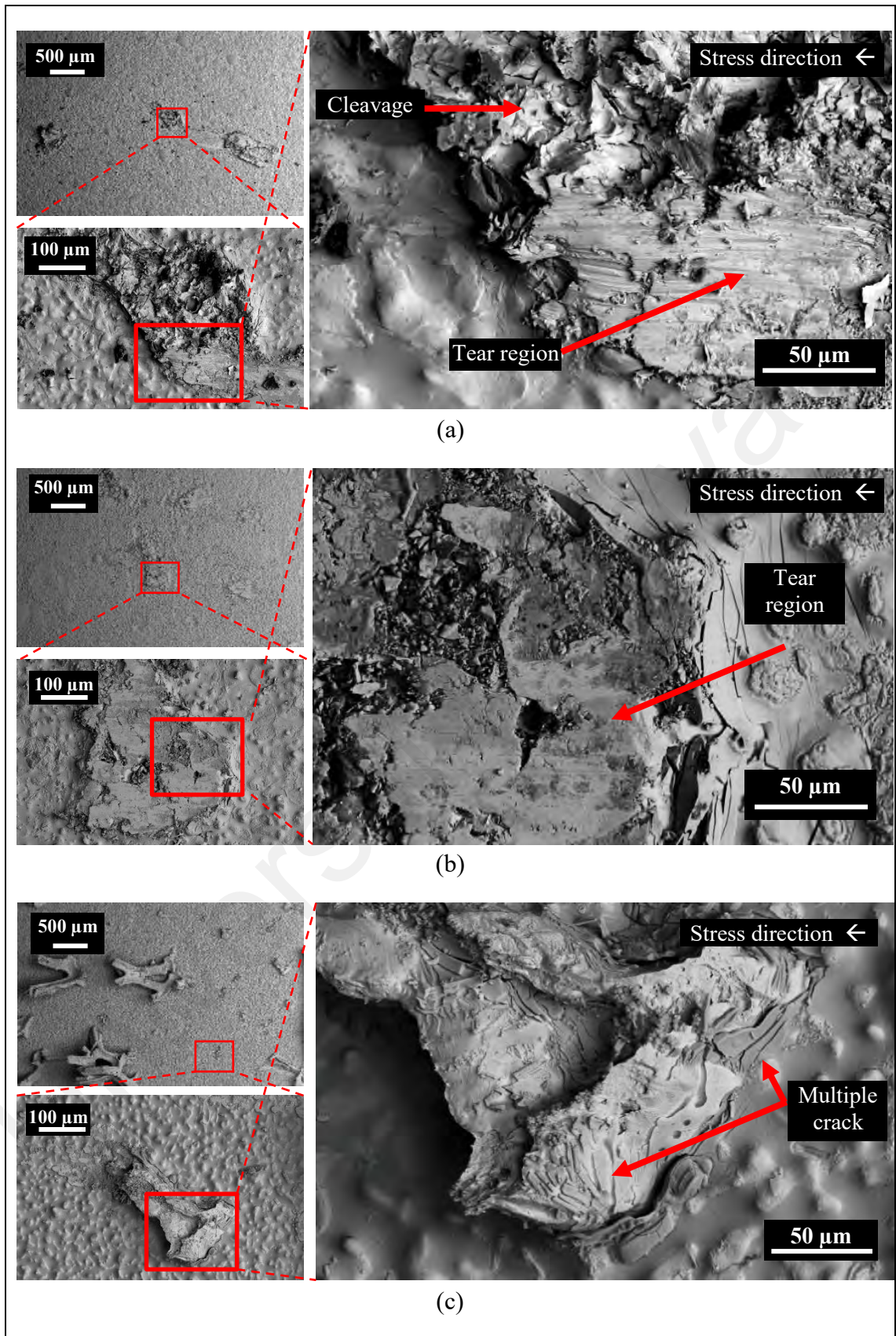


**Figure 4.18:** Top view of Cu substrate surface from shear test of brazed Cu/Cu foam using filler A with (a) foam A (b) foam B and (c) foam C at  $T_{br}$  of 660 °C

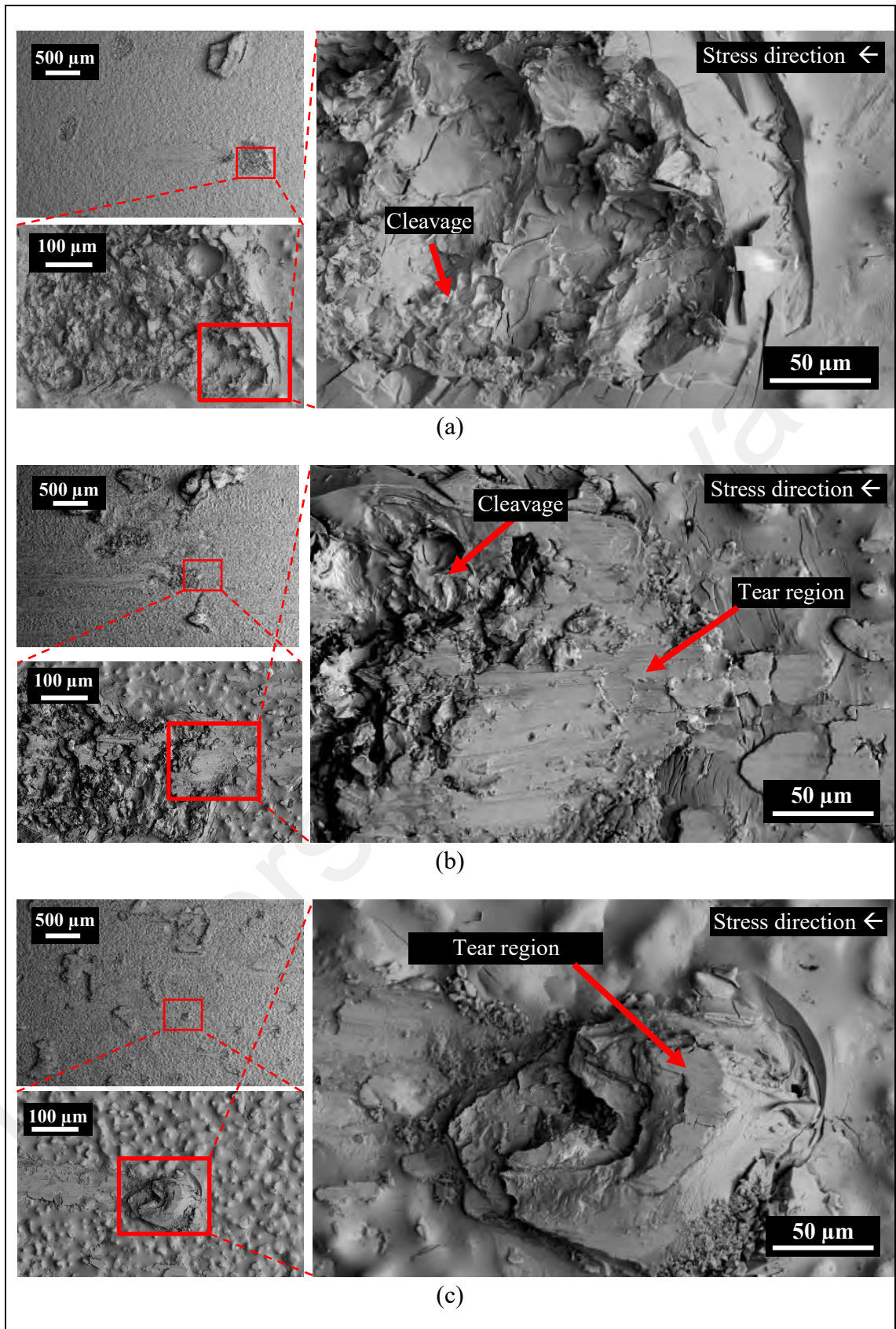


**Figure 4.19:** Top view of Cu substrate surface from shear test of brazed Cu/Cu foam using filler B (a) foam A (b) foam B and (c) foam C at  $T_{br}$  of 680 °C

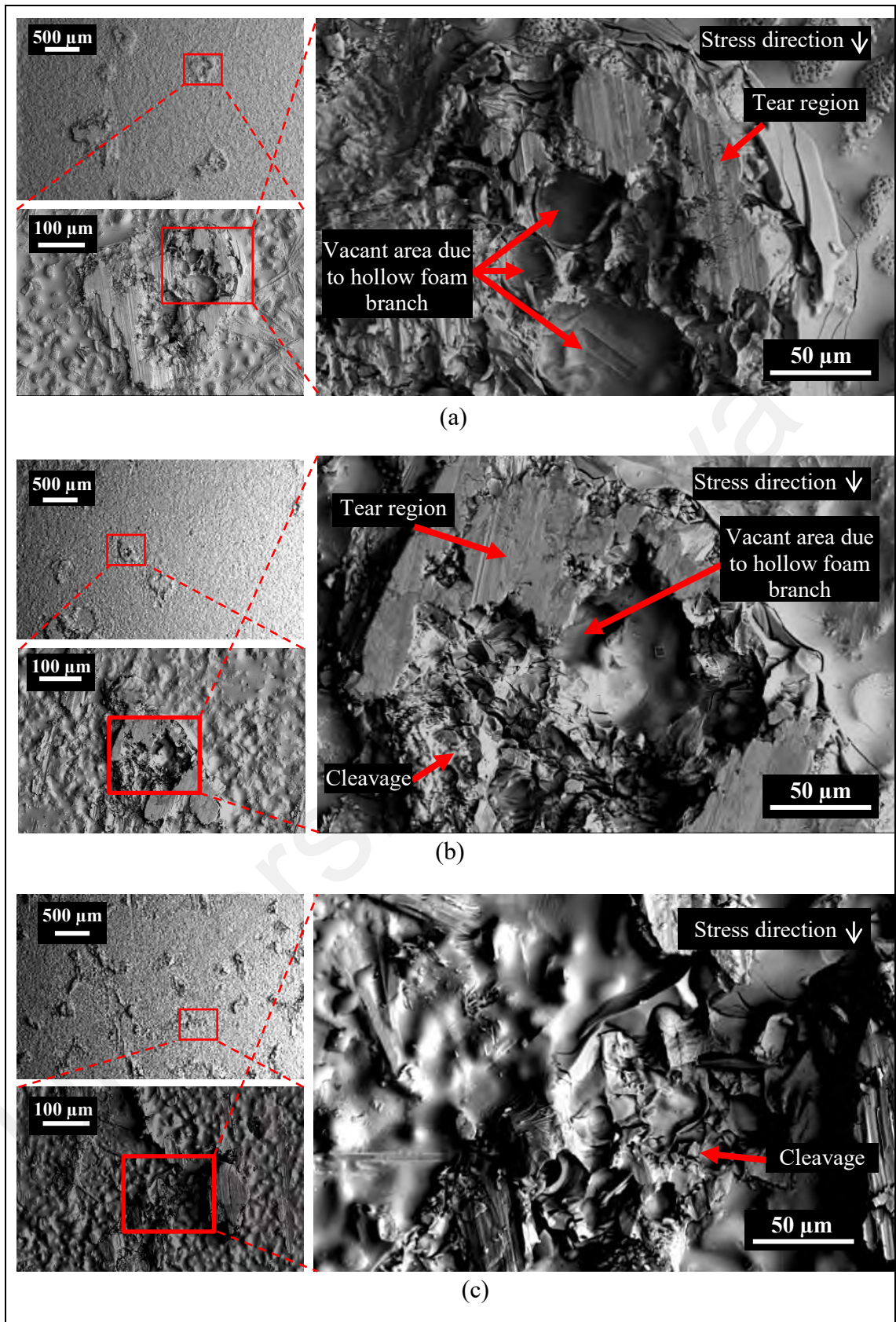
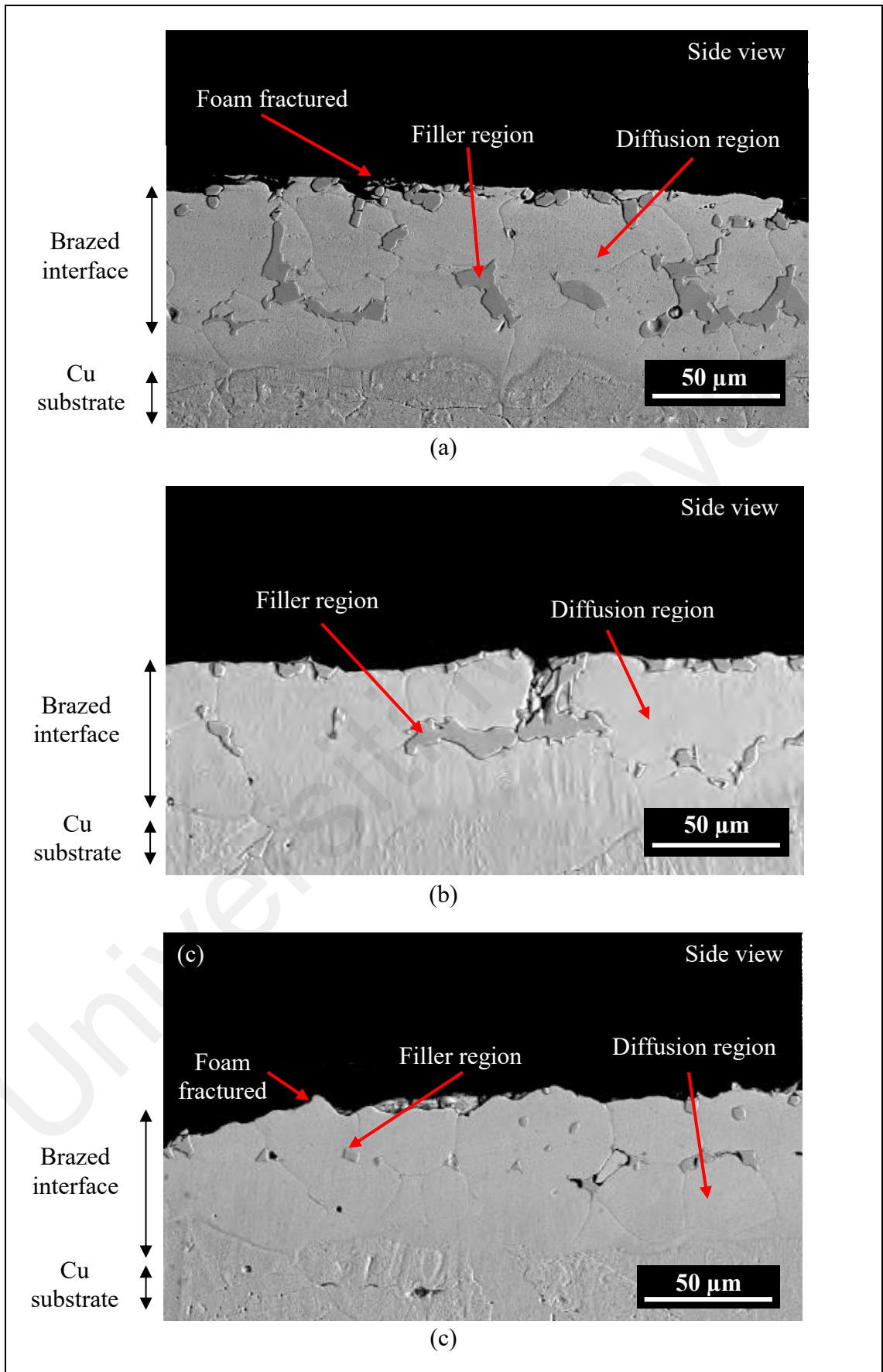


**Figure 4.20:** Top view of Cu substrate surface from shear test of brazed Cu/Cu foam using filler C with (a) foam A (b) foam B and (c) foam C at  $T_{br}$  of 660 °C

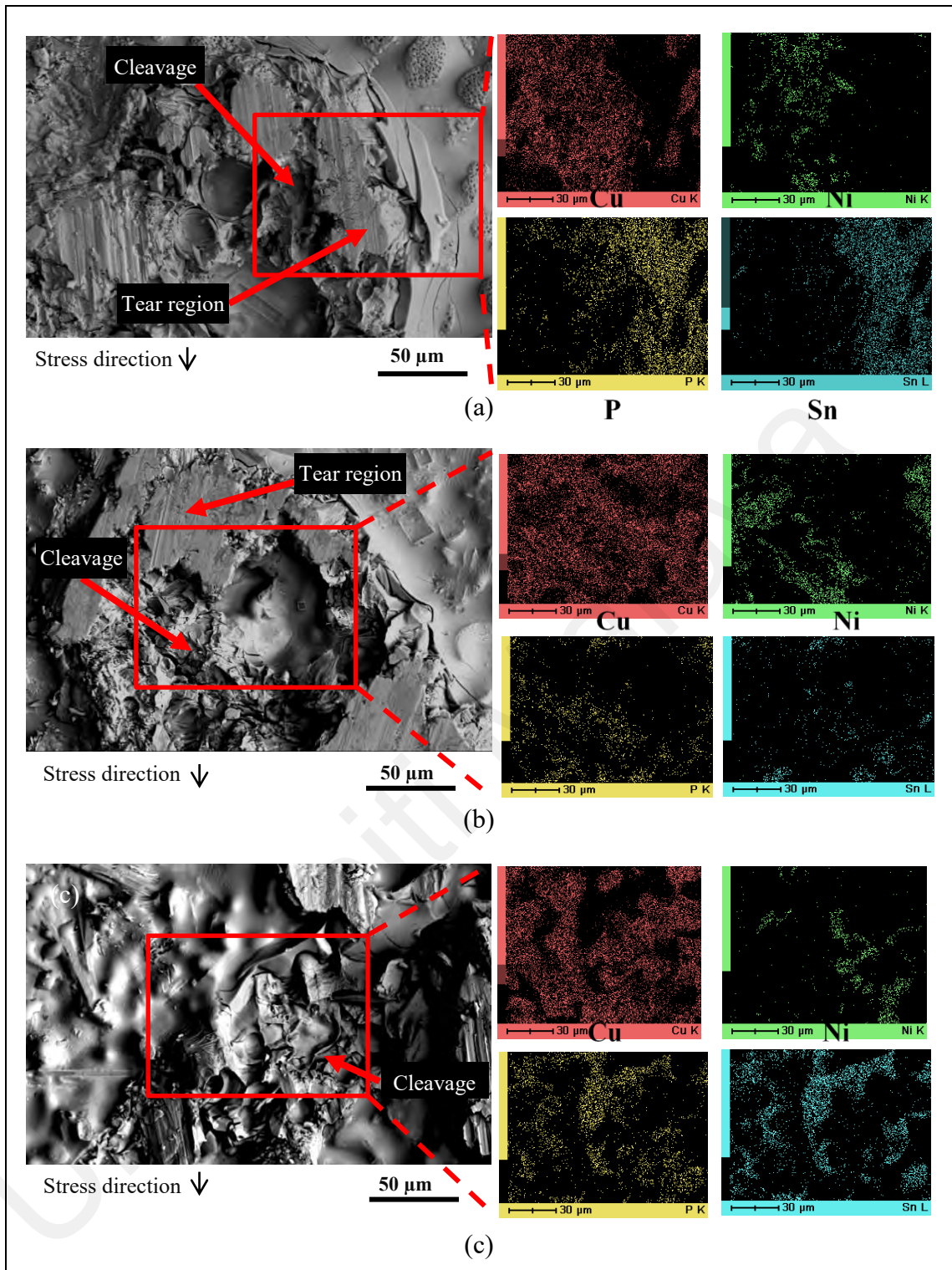
Side-view images of Cu substrate surface from the Cu/Cu foam shear-fracture using filler C were also captured as shown in Figure 4.21. Followed by a mapping analysis on the top view of Cu substrate surface (Figure 4.22) from the Cu/Cu foam shear-fracture to determine the influence of filler elements on the shear-fracture of the Cu/Cu foam joint.

Figure 4.21 shows dark grey (island-shaped) and light grey areas indicating the filler and the diffusion regions, respectively. The diffusion region, shown as a brighter area than the Cu substrate, is an interaction layer between Cu/filler and Cu foam/filler which are formed during brazing. BSE images have shown that the crack formation has propagated along the filler region. Higher amounts of filler region were observed for the brazed joint interface Cu/Cu foam A as compared to the brazed Cu/Cu foam B and Cu/Cu foam C. In contrast, Cu foam C has a higher number of branches, which are reflected in the accumulation of filler region, as observed on the Cu substrate surface of the Cu/Cu foam shear fracture. The distribution of the filler region was non-homogeneous, as expected from the highly porous interconnected structure of the Cu foam. The highest shear strength obtained in brazed Cu/Cu foam A can be attributed to the large formation of filler regions.

Figure 4.22 (inset) shows the mapping analysis of the top view of Cu substrate surface from the Cu/Cu foam shear-fracture using a filler C. The tear region shows high concentration of Cu and nickel (Ni) with lower concentration of phosphorus (P). The tear region was observed on the brazed joint interface of Cu foam branches. The cleavage fracture was formed on the filler region of the Cu/Cu foam brazed joint interface, which had concentrations of Cu, P and Ni. High concentrations of tin (Sn) and P were observed on the vacant area on the Cu substrate surface from the Cu/Cu foam shear-fracture (void space of Cu foam that being brazed to Cu substrate).



**Figure 4.21:** Side view of Cu substrate surface from shear test of brazed Cu/Cu foam using filler C with (a) foam A (b) foam B and (c) foam C at  $T_{br}$  of 660 °C



**Figure 4.22:** Top view mapping analysis of Cu substrate surface from shear test of brazed Cu/Cu foam using filler C with (a) foam A (b) foam B and (c) foam C at  $T_{br}$  of 660 °C

Ni and P have good solubility properties allowing it to disperse over the tear region, cleavage fracture and nonbrazed areas. The mapping analysis have identified Ni and P on the Cu foam branches, which indicated that they tend to flow onto the Cu foam

branches during brazing and would strengthen the branches. This was supported by the results of compressive strength of brazed Cu/Cu foam/Cu as compared to nonbrazed Cu/Cu foam/Cu, as discussed in section 4.4.1. The cleavage fracture, which is an indication of brittle behaviour, are due to the presence of P and Ni in the brazed joint interface. Less concentration of P and Ni in tear region of Cu foam branch fracture denoted as a ductile agrees with enlarge area under the shear stress-strain curve behavior.

#### 4.6.2 Brazed Joint Interface of Cu/Cu Foam

Figure 4.23 shows the Cu/Cu foam/Cu brazed joint interface joint at several magnifications. BSE image shows the brazed interface consisted of filler regions (grey island-shaped like) and diffusion regions (light grey).

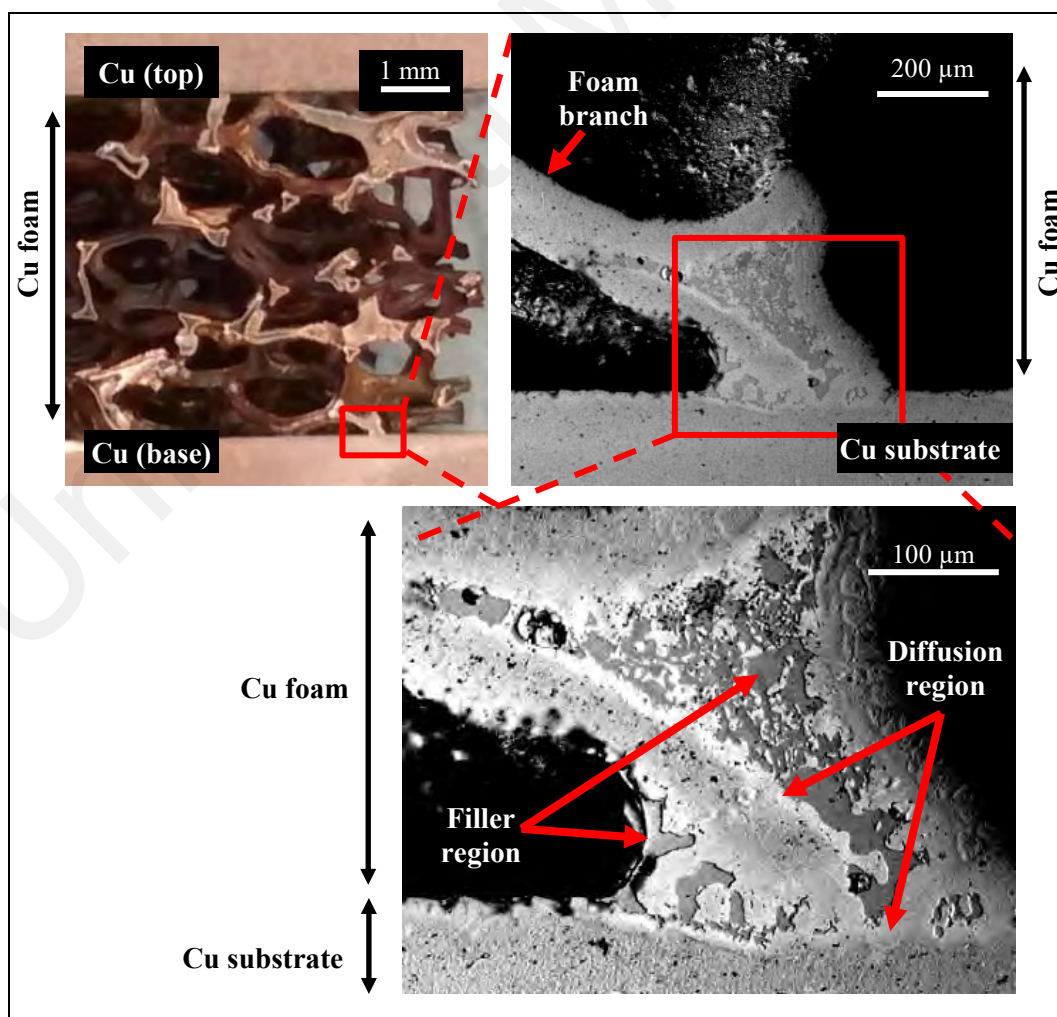


**Figure 4.23:** Brazed joint interface of Cu/Cu foam using filler B with foam A at 680 °C

During brazing, the filler is expected to melt at the brazing temperature and spread on the faying surfaces of the Cu substrate and Cu foam. As the brazing temperature increases, the molten filler would spread up into the Cu foam branch via capillary force to coat the interconnected foam branches. Upon solidification, formation of grey island-shaped like and light grey regions can be observed at Cu/Cu foam brazed joint interface joint and on the interconnected branches of Cu foam.

The grey island-shaped like areas, identified as the filler region, consisted of a brazing residual layer. This layer influences the brazed joint strength due to large accumulation of brittle compounds. The filler regions are formed during cooling and solidification process when it has not yet reacted with the substrate metal (Xu et al., 2019). On the other hand, the diffusion region (indicated by the light grey areas) shows the interaction of Cu-Sn-Ni-P amorphous filler alloys with Cu substrate and Cu foam.

Figure 4.24 shows the formation of filler region and diffusion region concentrated at the Cu/Cu brazed joint interface and were homogeneously distributed in a straight line. This is in contrast with the non-homogenous region on the Cu/Cu foam brazed joint interface where the filler was able to spread and coat the Cu foam branches (Figure 4.25 to Figure 4.27). Similar results were obtained by Ubertaini et al. (2017) in which the non-homogeneous spread of filler and diffusion region on the metal foams was observed.

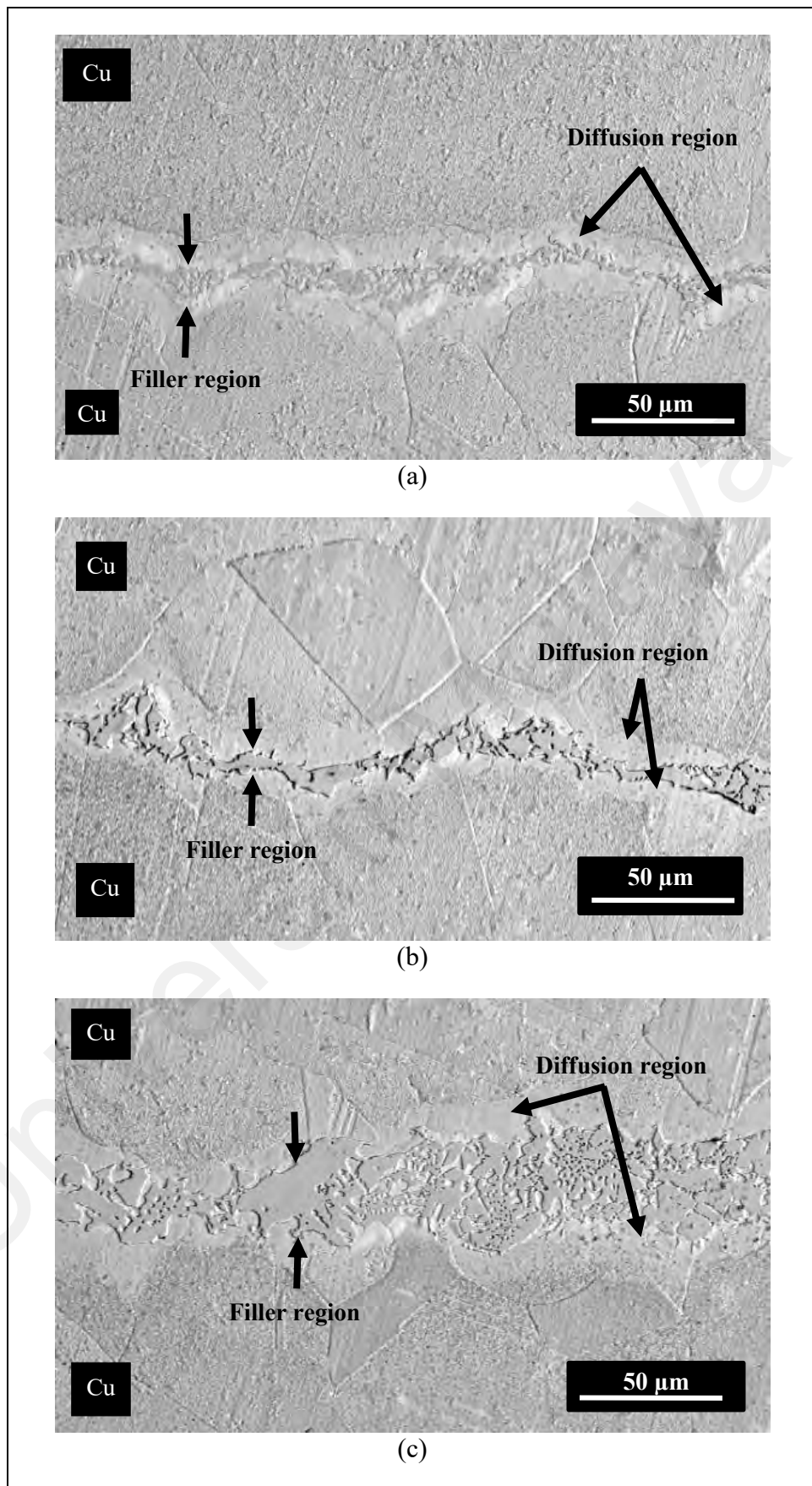


**Figure 4.24:** Microstructure of Cu/Cu brazed joint interface using (a) filler A (b) filler B and (c) filler C

Figure 4.25, Figure 4.26 and Figure 4.27 show the microstructures of Cu/Cu foam brazed joint interface using filler A, filler B and filler C, respectively. The thicknesses of filler and diffusion regions differs according to the types of fillers. The brazed joint interface of Cu/Cu foam using filler A was thicker than those of fillers B and C. This difference in thickness was probably due to the higher wt. % of phosphorus and nickel in filler A as compared to filler B and filler C.

Spherical shaped cavities were observed in the Cu/Cu foam brazed joint interface for all fillers. The formation of cavities were most likely due to entrapped oxide and gases in the open-cell structure of Cu foam (Hasap et al., 2014) . These cavities may cause crack initiations which would influence the brazing joint strengths. From the BSE images, the number of cavities increases with increase in foam density. The presence of entrapped gases would slow the flow of filler and contributes to further formation of cavities (Aminazad et al, 2015). Furthermore, the non-homogeneous porous structure of Cu foam can be difficult for the filler to flow through, which results in cavity formation. Thus, the increase in cavities with increasing pore density contributes to the decreased shear strength of the brazed joint.

The brazed joint interface of Cu/Cu foam (ranged from 51.9  $\mu\text{m}$ -94.3  $\mu\text{m}$ ) in Figure 4.25 to Figure 4.27 were found to be thicker than the brazed joint of Cu/Cu (ranged from 37.7  $\mu\text{m}$ -68.9  $\mu\text{m}$ ) in Figure 4.24. The increased thickness of brazed joint interface for Cu/Cu foam was due to the ability of the molten filler to flow into the porous structure of Cu foam branch via capillary action. Furthermore, the hollow and porous structures of Cu foam branches (Figure 4.1) would enhance the dissolution of Cu foam into the molten filler and increase the width of the brazed joint interface (Jacobson & Humpston, 2005).

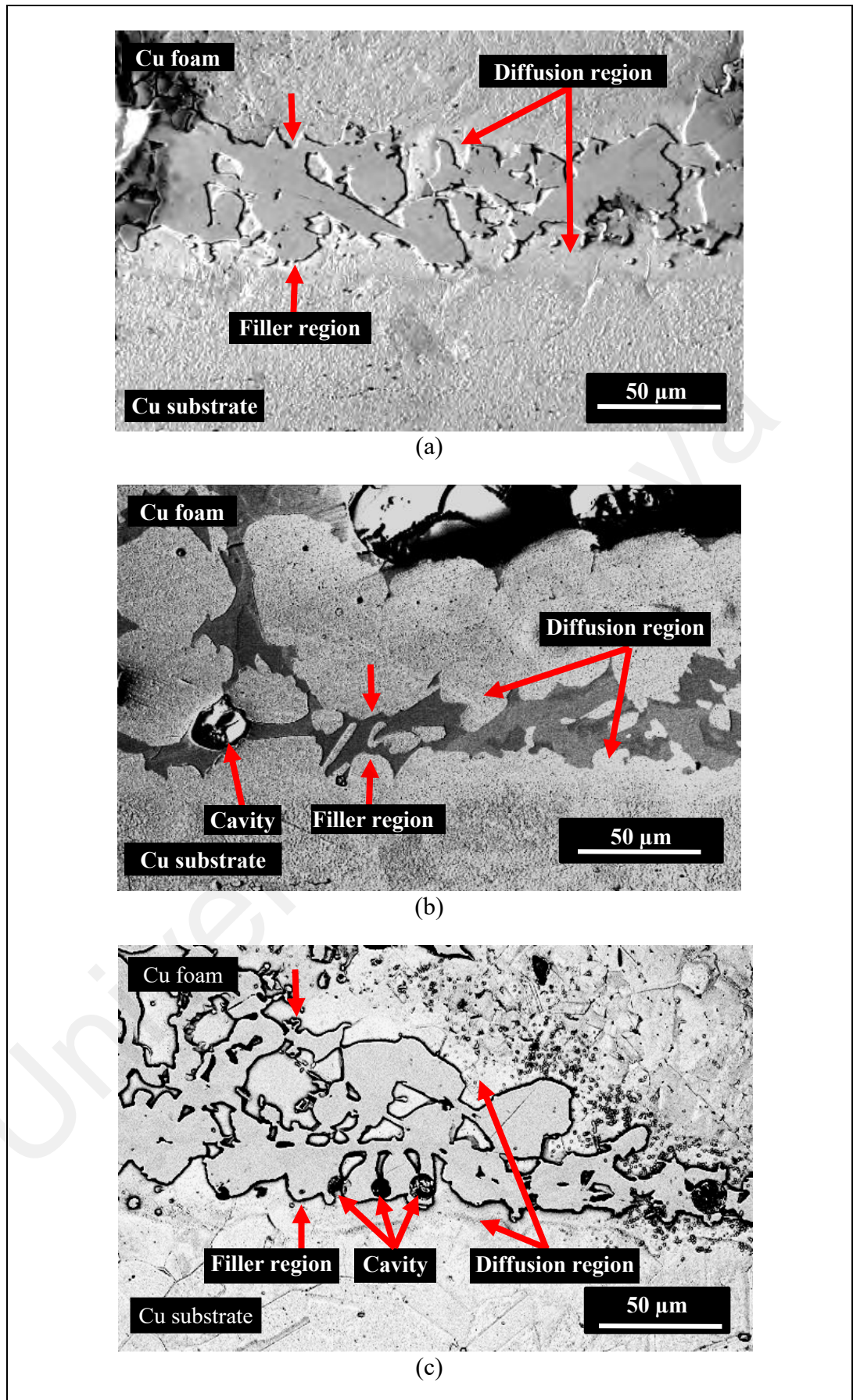
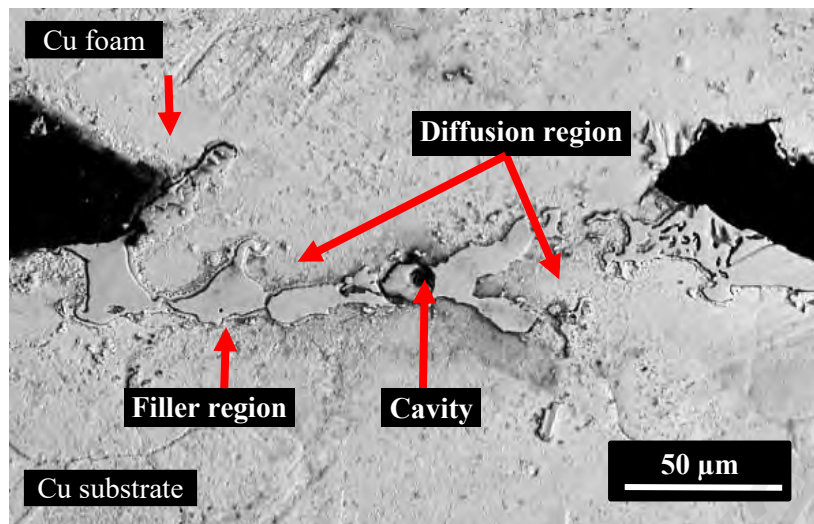
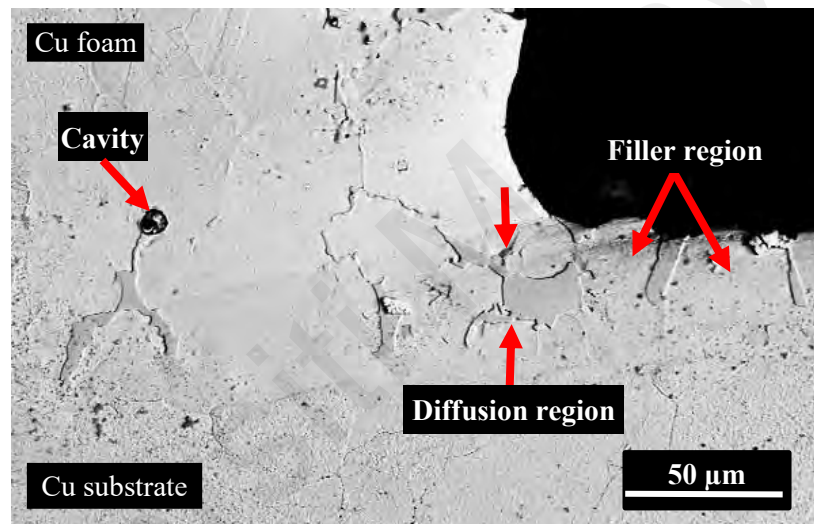


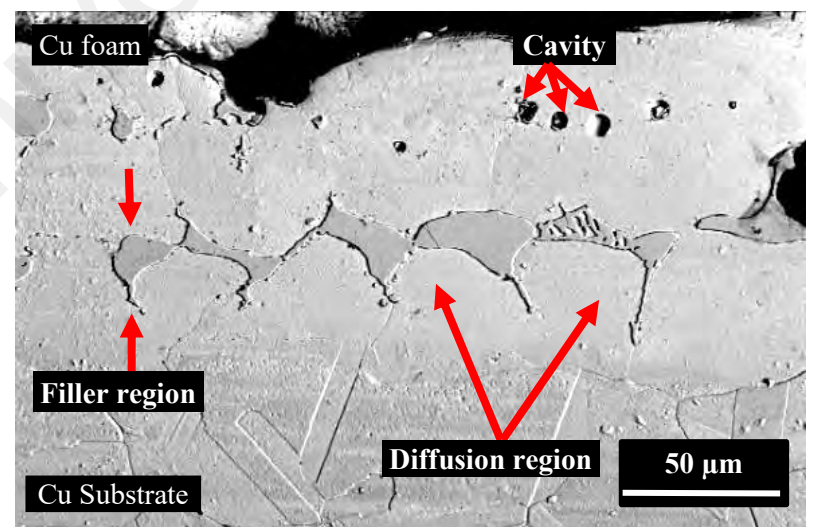
**Figure 4.25:** Microstructure of Cu/Cu foam brazed joint interface joint using filler A with (a) foam A (b) foam B and (c) foam C



(a)

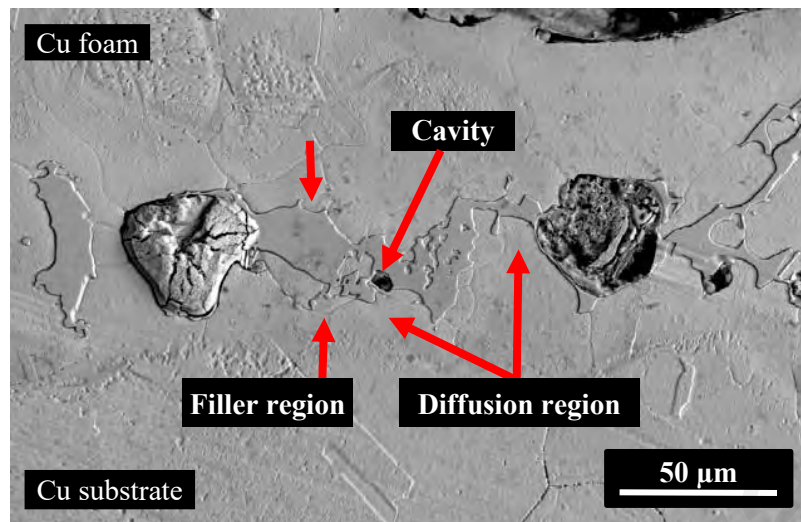


(b)

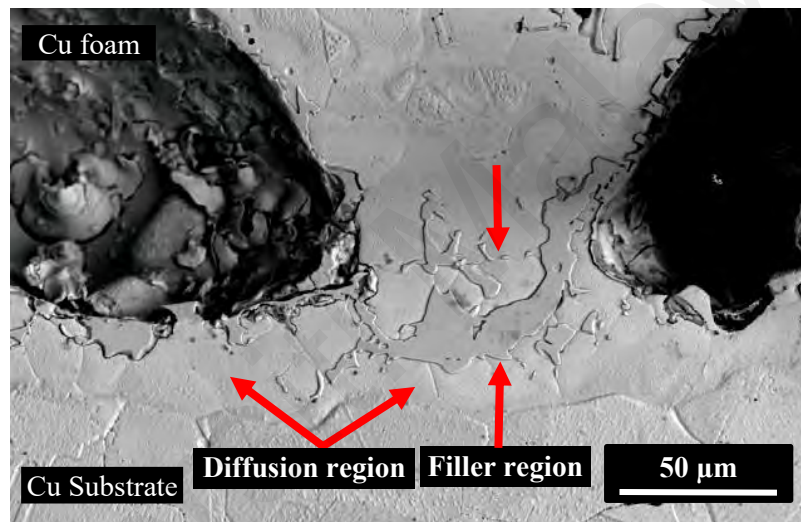


(c)

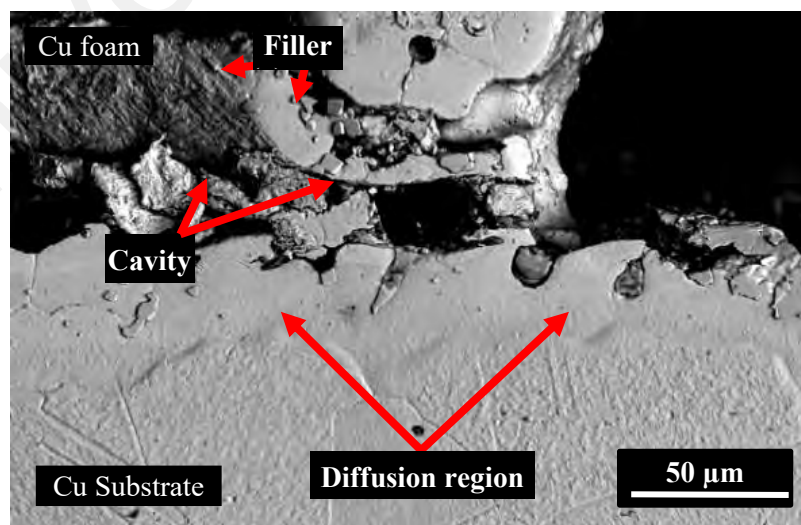
**Figure 4.26:** Microstructure of Cu/Cu foam brazed joint interface using filler B with (a) foam A (b) foam B and (c) foam C



(a)



(b)



(c)

**Figure 4.27:** Microstructure of Cu/Cu foam brazed joint interface using filler C with (a) foam A (b) foam B and (c) foam C

Figure 4.28 displays the XRD peak pattern for the Cu shear-fracture surface of Cu/Cu foam. The phases of Cu, Cu<sub>3</sub>P, Ni<sub>3</sub>P and Cu<sub>6</sub>Sn<sub>5</sub> phases have been identified for all Cu shear-fracture surface of Cu/Cu foam using different fillers with different Cu foam pore density. The XRD peak pattern of Cu (ICSD with PDF No. 98-062-7113), Cu<sub>3</sub>P (ICSD with PDF No. 98-062-8629), Ni<sub>3</sub>P (ICSD with PDF No. 98-064-6109) and Cu<sub>6</sub>Sn<sub>5</sub> (ICSD with PDF No. 98-010-6530) (**Appendix A.3**) are visible in Figure 4.28.

The Cu has become a dominant peak as all Cu peaks pattern list in ICSD database were appeared at 2 Theta of 43.33°, 50.46°, 74.15° and 89.97°. The presence of Cu can be traced from the Cu substrate and filler. Next, the solely individual phase of Cu<sub>3</sub>P peak [36.00° and 46.14°- Figure 4.28(a); 39.08°, 47.31°- Figure 4.28(b)] and Cu<sub>6</sub>Sn<sub>5</sub> peak [26.38° and 48.32°- Figure 4.28(b); 44.84°- Figure 4.28(c)] have strengthened all of the overlapped peaks of Cu<sub>3</sub>P and Cu<sub>6</sub>Sn<sub>5</sub>. On the other hand, the individual peak of Ni<sub>3</sub>P was missing due to overlapping with other phases.

Several possible dominant reactions were suggested by the XRD pattern during the crystallization of Cu-6Ni-10Sn-7P amorphous filler alloys study by Liu et al. (1990). The crystallisation product of metastable phase trigonal Ni<sub>2.55</sub>P appeared first, followed cubic  $\gamma$ -brass phase (Cu, Ni)<sub>3</sub>Sn. Then, the stable phases of  $\alpha$ -Cu and hexagonal Cu<sub>3</sub>P simultaneously occurred. The metastable and remaining amorphous phase react to form a stable phase of tetragonal Ni<sub>3</sub>P or written as (Ni, Cu)<sub>3</sub>P due to a great amount of Cu in Ni<sub>3</sub>P. Liang et al. (2017) reported the formation of Cu-Sn solid solution may enhance through a thermodynamical favour. The elevated brazing temperature (660 °C) during Cu/Cu foam/Cu brazing improve the Cu and Sn reaction to form a Cu<sub>6</sub>Sn<sub>5</sub> phase.

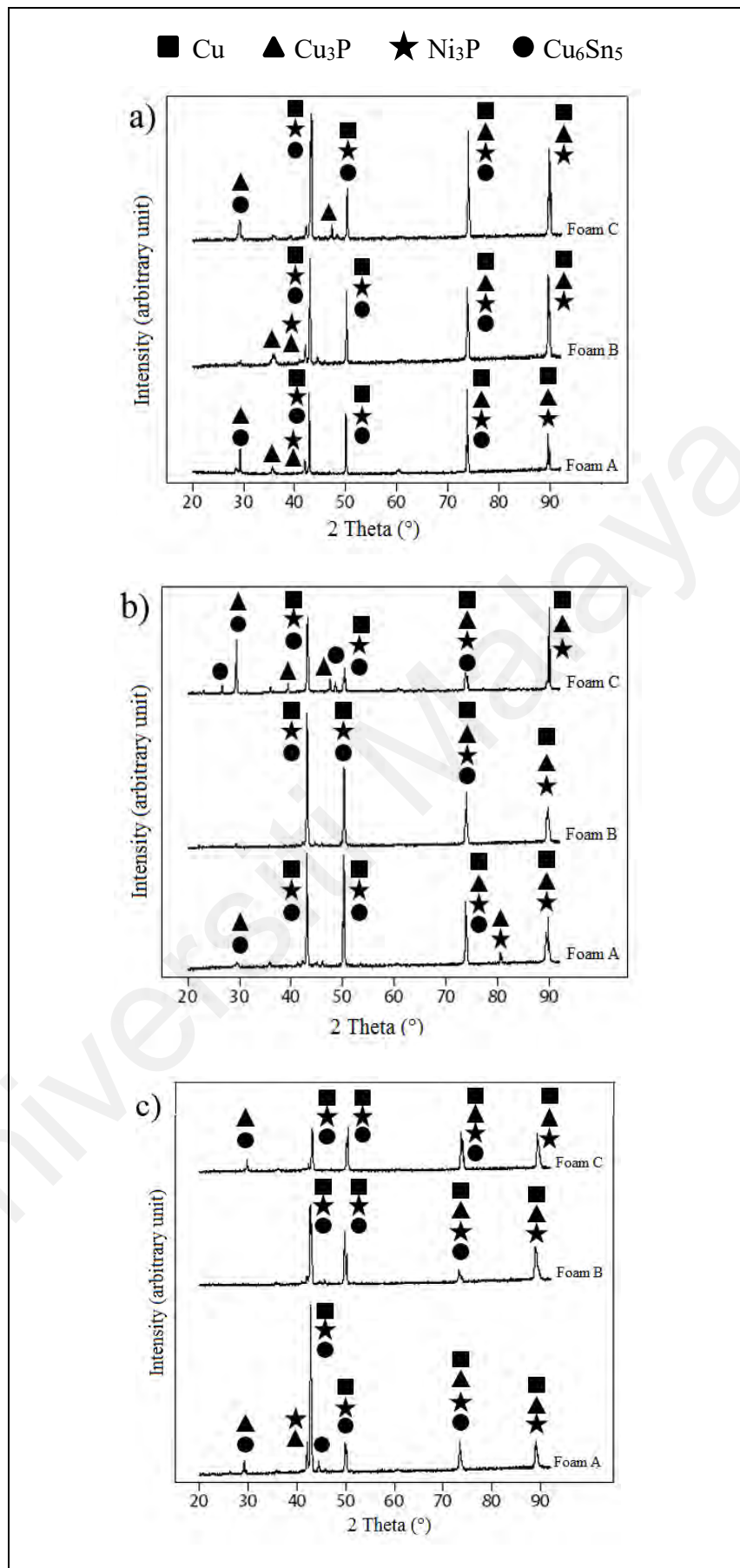


**Figure 4.28:** X-ray diffraction (XRD) pattern of Cu substrate surface from shear test of brazed Cu/Cu foam using (a) filler A (b) filler B and (c) filler C

Figure 4.29 to Figure 4.31 show the EDX analysis for Cu/Cu foam brazed joint interface which consisted of filler region (grey island-shaped) and diffusion region (light area). The insets of Figure 4.29 to Figure 4.31 show the mapping images of Cu/Cu foam brazed joint interface for Cu, Ni, P and Sn elements, indicated in red, light blue, green and purple coloured regions, respectively.

The large grey island-shaped like regions were enriched with Cu and P, as shown in Figure 4.29 (point 1, 3 and 5), Figure 4.30 (point 7) and Figure 4.31 (point 13-15 and 20) while the small grey island-shaped like regions were enriched with Ni and P as shown in Figure 4.30 (point 10-12) and Figure 4.31 (point 19). The correlation of mapping intensities of Ni and P has found that these elements have accumulated at the filler region (grey island-shaped like) of Cu/Cu foam brazed joint interface as shown in the inset of Figure 4.29 to Figure 4.31. The results of the mapping intensity have confirmed the presence of  $\text{Ni}_3\text{P}$  and the overlapped XRD peak pattern of  $\text{Ni}_3\text{P}$ .

Cu-enriched locations were identified at points of 2, 4 and 6 (Figure 4.29) in the diffusion region (light grey areas). The Sn-enriched locations were observed near the rough surface and cavities of the brazed joint interface, as shown in Figure 4.30 (point 8 and 9) and Figure 4.31 (point 16-18). During the brazing process, the low melting point and active element of Sn tends to diffuse out from the filler and flow into the Cu foam resulting in solid diffusion. The reactions between Sn and Cu-based (foam and substrate) results in  $\text{Cu}_6\text{Sn}_5$  liquid phase formation. All the EDX analysis corroborate the peak phases obtained in the XRD results.

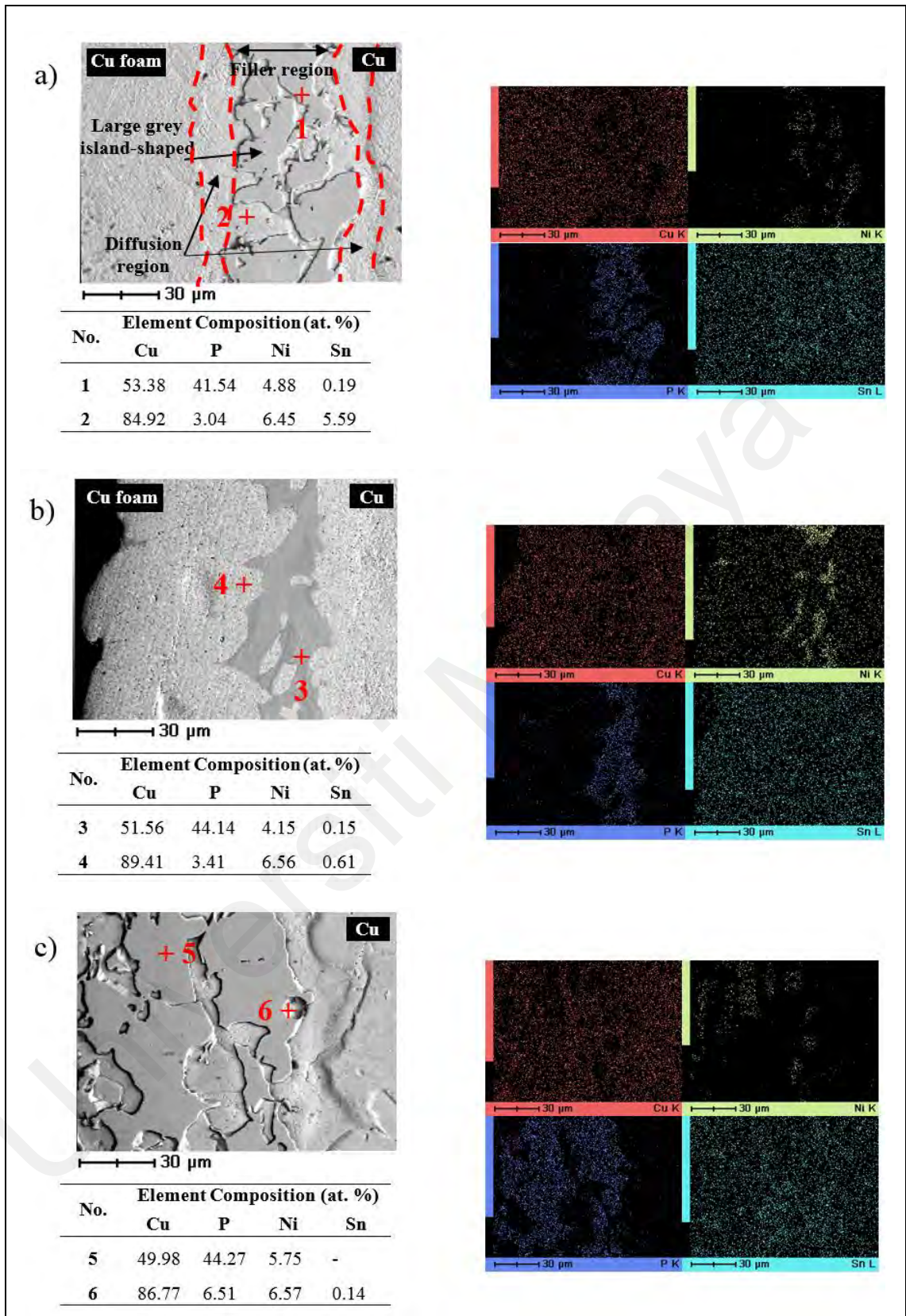


**Figure 4.29:** Elemental composition and mapping analysis on Cu/Cu foam brazed joint interface using filler A with (a) foam A (b) foam B and (c) foam C

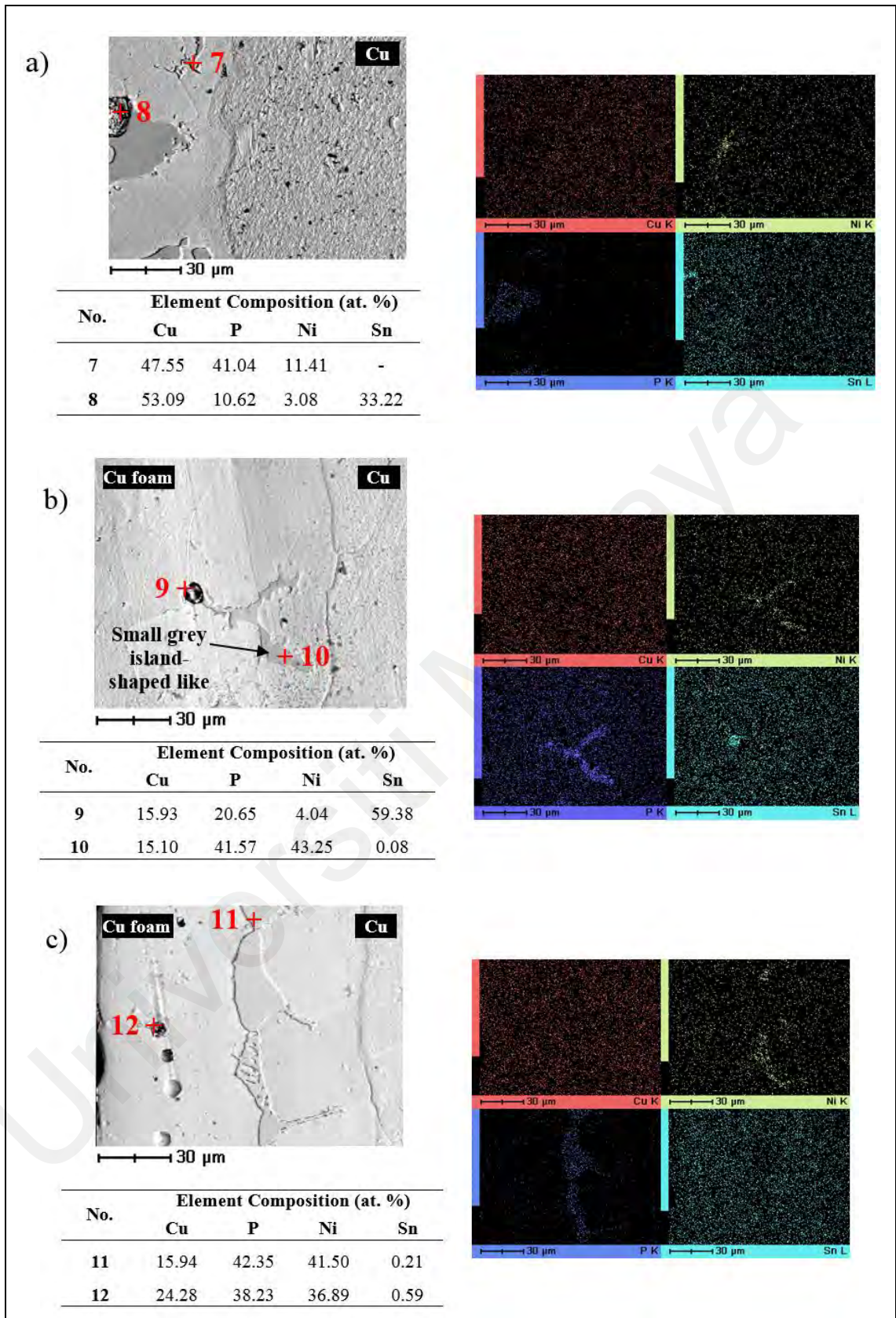


**Figure 4.30:** Elemental composition and mapping analysis on Cu/Cu foam brazed joint interface using filler B with (a) foam A (b) foam B and (c) foam C

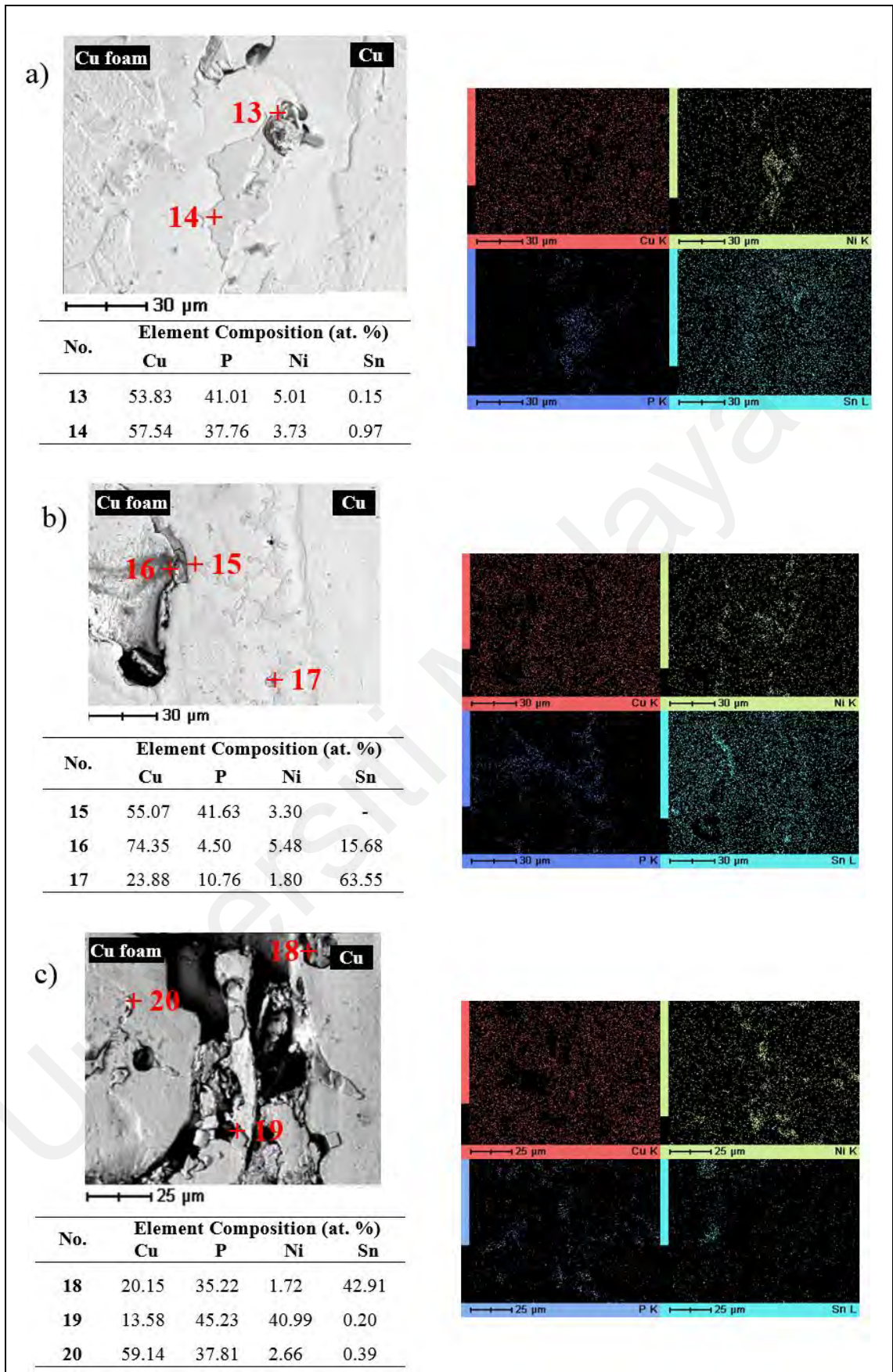


**Figure 4.31:** Elemental composition and mapping analysis on Cu/Cu foam brazed joint interface for filler C with (a) foam A (b) foam B and (c) foam C

Table 4.3 shows a summary of the atomic percentages (at.%) of elemental compositions based on the points in Figures 4.29, 4.30 and 4.31. As shown previously in Figure 4.25, a thicker filler region in the brazed joint interface was observed for the Cu/Cu foam using filler A, consisting of large grey island-shaped like locations enriched with Cu and P. Filler A consisting of Cu-4.0Sn-9.9Ni-7.8P (wt.%) has high wt.% of Ni and P. However, the Ni-enriched points in the brazed joint interface was barely noticeable as compared to the P-enriched point.

Cu/Cu foam using filler B and filler C have thinner filler regions (Figure 4.26 and 4.27, respectively) in the brazed interface joint, which are represented as small grey island-shaped areas consisting of 1) Ni and P-enriched point and 2) P-enriched point. Noted that, filler B and filler C made up of Cu-9.7Sn-5.7Ni-7.0P (wt.%) and Cu-9.0Sn-7.0Ni-6.0P (wt.%), respectively. Points of Ni and P-enriched were identified in the brazed joint interface of Cu/Cu foam filler B and filler C even though these fillers had lesser wt.% of Ni compared to filler A. This was probably due to the formation of thinner filler region in Cu/Cu foam brazed joint interface using filler B and filler C which are manifested in the Ni and P-enriched points. P-enriched points were observed in the brazed joint interfaces of Cu/Cu foam using filler A, filler B and filler C. P was well dispersed as it has good interaction and solubility properties, making it easy to diffuse into the substrate joints (Hasap et al., 2014 and Lutfi et al., 2016).

The XRD peak pattern (Figure 4.30) shows the presence of  $\text{Ni}_3\text{P}$  and  $\text{Cu}_3\text{P}$ , which can be correlated with the Ni and P-enriched points, and P-enriched point from the EDX elemental composition in Table 4.3. As  $\text{Ni}_3\text{P}$  and  $\text{Cu}_3\text{P}$  are brittle phases, their prevalence may reduce the strength of the brazed joint (Zhang et al., 2016).

Sn-enriched points were found in brazed joint interface Cu/Cu foam with a high pore Cu foam density. The high Cu foam pore densities of foam B and foam C have highly

porous structures resulting in increased formation of cavities during the brazing process (see Figure 4.25 to Figure 4.27). As the brazing temperature increases, Sn would tend to diffuse out from the filler and bind near the cavities. Sn-enriched points are easily identifiable at the brazed joint interface of Cu/Cu foam with a high pore density Cu foam. However, wt.% value would also influenced the formation of Sn-enriched points. Figure 4.29(c) shows a cavity at point 6 but no Sn-enriched region was found for Cu/Cu foam brazed joint interface using filler A. The low Sn wt.% (4.0%) in filler A would probably be insufficient for the formation of the Sn-enriched as compared to filler B (Sn: 9.7%) and filler C (Sn: 9.0 %).

Universiti Malaysia

**Table 4.3:** Summary of elemental composition at Cu/Cu foam brazed joint interface using different fillers and foams based on points in Figure 4.29, 4.30 and 4.31

Elemental composition (at.%)															
Filler	Foam A					Foam B					Foam C				
	Point	Cu	P	Ni	Sn	Point	Cu	P	Ni	Sn	Point	Cu	P	Ni	Sn
A	1	53.38	41.54	4.88	0.19	3	51.56	44.14	4.15	0.15	5	49.98	44.27	5.75	-
	2	84.92	3.04	6.45	5.59	4	89.41	3.41	6.56	0.61	6	86.77	6.51	6.57	0.14
B	7	47.55	41.04	11.41	-	9	15.93	20.65	4.04	59.38	11	15.94	42.35	41.50	0.21
	8	53.09	10.62	3.08	33.22	10	15.10	41.57	43.25	0.08	12	24.28	38.23	36.89	0.59
C	13	53.83	41.01	5.01	0.15	15	55.07	41.63	3.30	-	18	20.15	35.22	1.72	42.91
	14	57.54	37.76	3.73	0.97	16	74.35	4.50	5.48	15.68	19	13.58	45.23	40.99	0.20
						17	23.88	10.76	1.80	63.55	20	59.14	37.81	2.66	0.39

**Note:**  Diffusion region Cu-enriched  Filler region P-enriched  Filler region Ni and P enriched  Filler region Sn-enriched

### **4.6.3 Surface Diffusion of Filler across the Brazed Cu/Cu foam/Cu**

The analysis on surface diffusion of filler across the brazed Cu/Cu foam/Cu was conducted to evaluate the fluidity of the filler. Figure 4.25 to Figure 4.27 show the filler has flowed into the Cu foam other than accumulating at the brazed joint interface. Surface diffusion analysis was also conducted to determine reason of the increase in compressive strength value of brazed Cu/Cu foam/Cu as compared to nonbrazed Cu/Cu foam/Cu.

#### **4.6.3.1 Microstructure of Cross-Section Brazed Cu/Cu foam/Cu using different Amorphous Fillers with Foam A**

Figures 4.32, 4.33 and 4.34 show the images of brazed Cu/Cu foam/Cu using Cu foam A (hereinafter as Cu/Cu foam A/Cu) and different fillers (filler A, filler B and filler C), respectively. EDX line scanning analysis was carried out on 6 selected areas (labelled 1 to 6) to evaluate the brazed joint interface area of Cu top/Cu foam A (area 1), Cu foam (area 2-5) and Cu bottom/Cu foam A (area 6) as shown in the inset Figures 4.32, 4.33 and 4.34. Elements of Cu (red), P (blue colour), Ni (green colour) and Sn (light blue colour) were identified on the brazed joint interface and Cu foam surface at several locations. EDX point analysis was also conducted on each area to obtain the elemental compositions (at.%) and are listed in Tables 4.4, 4.5 and 4.6 for Cu/Cu foam A/Cu using filler A, filler B and filler C, respectively. Table 4.7 shows a summary of all elemental composition evaluation based on the points in inset Figures 4.32, 4.33 and 4.34. As discussed in Section 4.5.3, the filler region is easily recognizable due to its a grey island-shaped feature on the surface of Cu and Cu foam. EDX line scanning analysis has shown that on the Cu foam surface, the filler region consisted of high counts of P and Ni elements, while a high count of Sn element are found either on the boundaries of Cu (top/substrate) or along the hollow boundaries of the Cu foam.

**Table 4.4:** Elemental composition across brazed Cu/Cu foam A/Cu using filler A based on points label in Figure 4.32

Point	Element Composition (at. %)			
	Cu	P	Ni	Sn
A	12.17	44.78	42.83	0.22
B	77.62	17.44	3.86	1.07
C	84.12	9.71	5.88	0.29
D	92.98	0.93	6.02	0.07
E	85.00	5.19	9.51	0.30
F	4.88	41.54	4.88	0.19

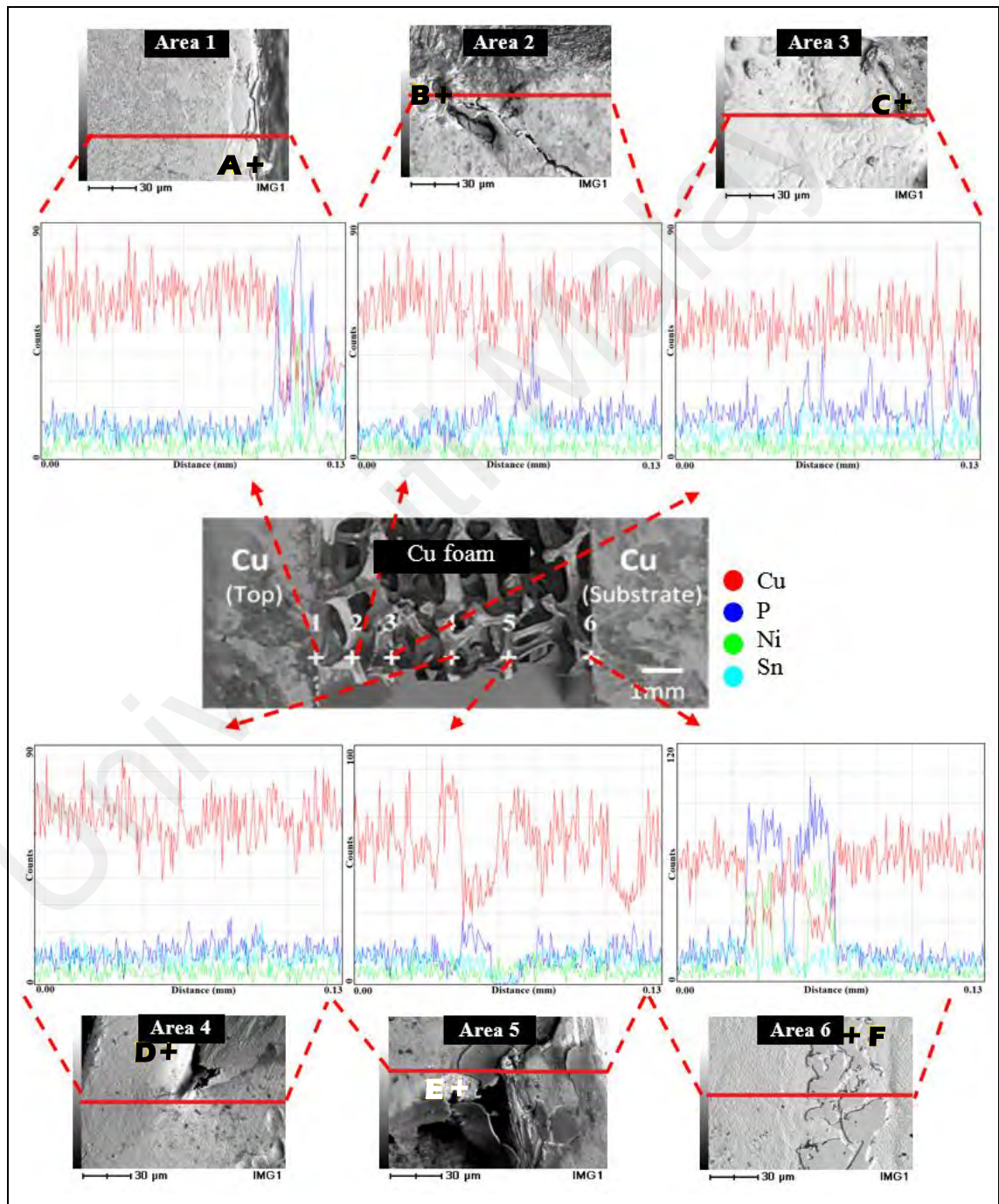


**Figure 4.32:** EDX line scanning analysis at selected area across brazed Cu/Cu foam A/Cu using filler A

**Table 4.5:** Elemental composition across brazed Cu/Cu foam A/Cu using filler B based on points label in Figure 4.33

Point	Element Composition (at. %)			
	Cu	P	Ni	Sn
A	50.30	45.76	3.72	0.22
B	12.99	44.75	42.25	-
C	95.34	0.20	3.97	0.48
D	16.25	44.47	39.18	0.11
E	11.58	45.02	43.40	-
F	47.55	41.04	11.41	-

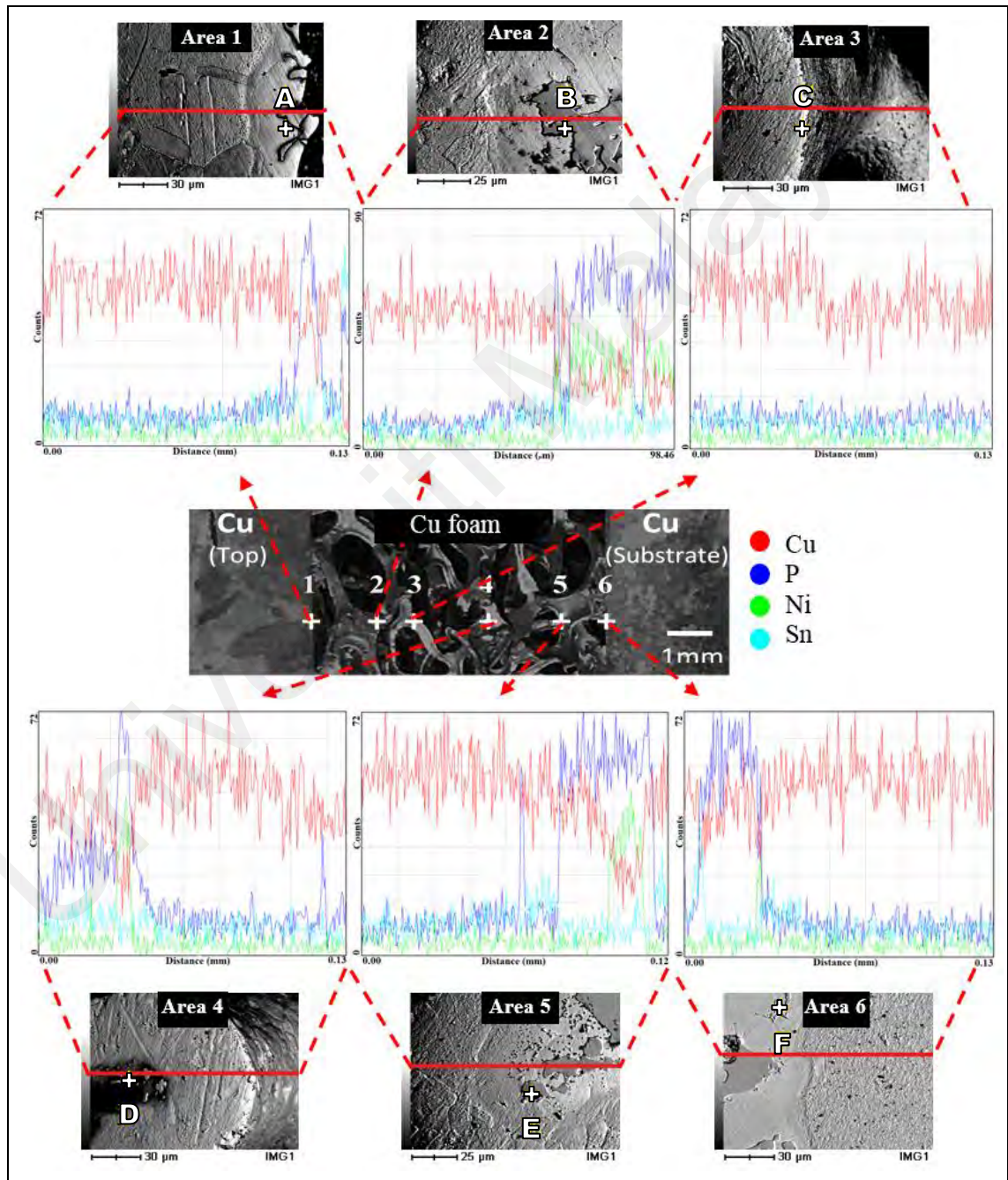


**Figure 4.33:** EDX line scanning analysis at selected area across brazed Cu/Cu foam A/Cu using filler B

**Table 4.6:** Elemental composition across brazed Cu/Cu foam A/Cu using filler C based on points label in Figure 4.34

Point	Element Composition (at. %)			
	Cu	P	Ni	Sn
A	14.42	43.95	41.33	0.30
B	11.01	44.72	43.92	0.35
C	36.05	51.53	3.52	8.89
D	16.25	44.47	39.18	0.11
E	19.33	66.85	1.89	11.93
F	53.83	41.01	5.01	0.15

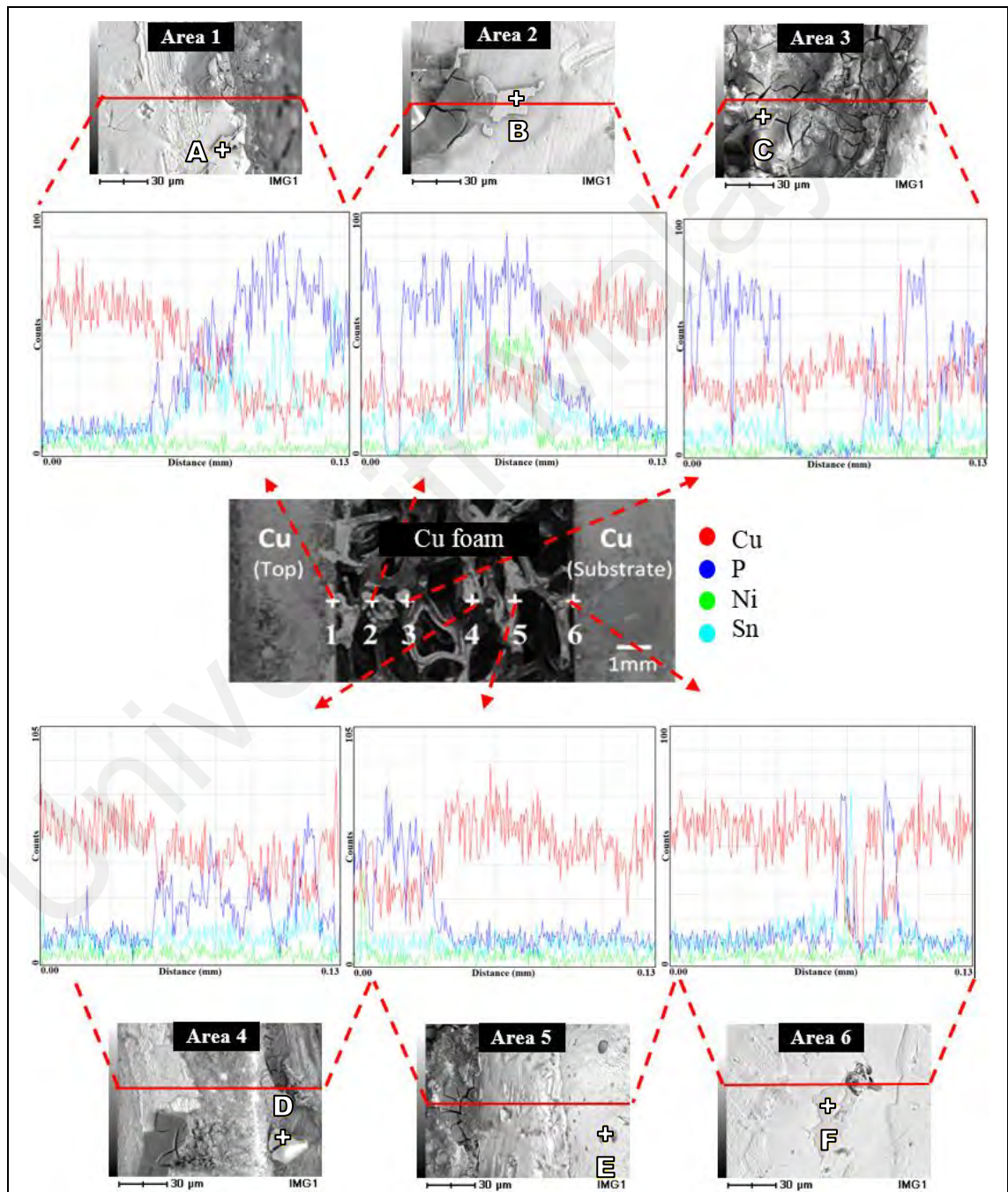


**Figure 4.34:** EDX line scanning analysis at selected area across brazed Cu/Cu foam A/Cu using filler C

P-enriched and Ni-enriched regions were found on the Cu foam based on the elemental composition (at.%) from the EDX point analysis. This shows that the filler was able to flow in the narrow and porous structure of the Cu foam due to capillary force action. This wetting phenomenon occurred through the adhesion movement of filler that was greater than the cohesive force on the brazed joint interface. The filler that consisted of Ni wt.% and P wt.% elements allowed it to flow and diffuse into the base metal. This diffusion brazing process would directly increase the joint strength from the diffusion of Ni and P (AWS, 2011). Jacobson and Humpston (2005) stated that phosphorus is a fast-diffusing element that would diffuse out from the filler at the brazing temperature and would disperse widely in the base metals. In this case, the porous structure of Cu foam would contribute to increase dispersing of P onto the Cu foam. This dispersion was evident as the P and Ni element at.% were found on the middle of Cu foam, as shown in Table 4.7. The filler diffusion in the Cu foam and coated its surface would strengthen the Cu foam branches. This is shown in the increase of the average compressive strength of brazed Cu/Cu foam A by 108.93% as compared to non-brazed Cu/Cu foam A.

EDX line scanning analysis of Cu/Cu foam A/Cu using filler C show high peak counts for all areas. This is confirmed from the EDX point analysis showing the high values of P at.% (more than 40%) and Ni, as shown in Table 4.7. For filler B, the P at.% values found at point A, B, D, E and F are 45.76%, 44.75%, 44.47%, 45.02% and 41.04%, respectively. Whereas, for filler A, the P at.% values at point A, B and F are 44.78%, 17.44% and 41.54%, respectively. However, the value of Ni at.% was found to be lower than P at.%. The increased P at.% value is due to its good interaction and solubility (Hasap et al., 2014 and Lutfi et al., 2016), making it easy to diffuse into the Cu foam.

**Table 4.7:** Summary of elemental composition across brazed Cu/Cu foam A/Cu using different fillers based on points in Figures 4.32, 4.33 and 4.34

Point	Filler A				Filler B				Filler C			
	Element Composition (at. %)											
	Cu	P	Ni	Sn	Cu	P	Ni	Sn	Cu	P	Ni	Sn
<b>A</b>	12.17	44.78	42.83	0.22	50.30	45.76	3.72	0.22	14.42	43.95	41.33	0.30
<b>B</b>	77.62	17.44	3.86	1.07	12.99	44.75	42.25	-	11.01	44.72	43.92	0.35
<b>C</b>	84.12	9.71	5.88	0.29	95.34	0.20	3.97	0.48	36.05	51.53	3.52	8.89
<b>D</b>	92.98	0.93	6.02	0.07	16.25	44.47	39.18	0.11	16.25	44.47	39.18	0.11
<b>E</b>	85.00	5.19	9.51	0.30	11.58	45.02	43.40	-	19.33	66.85	1.89	11.93
<b>F</b>	4.88	41.54	4.88	0.19	47.55	41.04	11.41	-	53.83	41.01	5.01	0.15

P & Ni elements
  P and/or Ni -enriched

Overall, filler A has less diffusion distance to penetrate into the Cu foam as compared to fillers B and C, as shown in Table 4.7. This is probably due to the lower Sn wt.% and higher P wt.% and Ni wt.% in filler A have suppressed the filler A ability to flow into the Cu foam. The high P wt.% and Ni wt.% in filler A require higher brazing temperatures to enhance the wettability performance of P and Ni. However, excessively high brazing temperatures would result in the destruction of Cu foam branches, reducing the shear strength of Cu/Cu foam brazed joint interface.

#### **4.6.3.2 Brazed Cu/Cu foam/Cu using different fillers with different Cu Foams**

EDX point analysis were conducted on the brazed Cu/Cu foam/Cu for different fillers and different Cu foam pore densities. The location of the point labels are listed in Table 4.8 and the result of the EDX analysis is tabulated in Table 4.9.

The behaviours of the filler diffusion of foam B and foam C (Table 4.9) follow the diffusion behaviour for foam A, as discussed earlier. However, in foam A, the P-enriched and Ni-enriched on the Cu foam were only found up to point 2, while for fillers B and C, the P at.% and Ni at.% were found near the middle of the Cu foam.

Table 4.9 also shows the increase Cu foam pore density causes less diffusion of filler in the Cu foam. Increasing pore density would increase the resistance for filler wettability due to a large number of foam branches. This results in reduced penetrable distance of filler penetrable in the Cu foam. This is shown in the results for foam C (high pore density) compared to foam A (low foam density), shown in Table 4.8, and Table 4.9.

**Table 4.8:** Points label across brazed Cu/Cu foam/Cu using different fillers with different Cu foam pore density

Filler	Cu foam	Brazed specimens				1mm	
		Cu top	Cu foam		Cu base		
	A	1 +	2 +	3 +	4 +	5 +	6 +
A	B	+	+	+	+	+	+
	C	1 +	2 +	3 +	4 +	5 +	6 +
	A	1 +	2 +	3 +	4 +	5 +	6 +
B	B	1 +	2 +	3 +	4 +	5 +	6 +
	C	+	+	+	+	+	+
	A	+	+	+	+	+	+
C	B	+	+	+	+	+	+
	C	+	+	+	+	+	+

**Table 4.9:** Summary of elemental composition across brazed Cu/Cu foam/Cu using different fillers with different Cu foam pore density as label in Table 4.8

Cu foam	Point	Filler A				Filler B				Filler C			
		Element Composition (at. %)											
		Cu	P	Ni	Sn	Cu	P	Ni	Sn	Cu	P	Ni	Sn
A	1	12.17	44.78	42.83	0.22	50.30	45.76	3.72	0.22	14.42	43.95	41.33	0.30
	2	77.62	17.44	3.86	1.07	12.99	44.75	42.25	-	11.01	44.72	43.92	0.35
	3	84.12	9.71	5.88	0.29	95.34	0.20	3.97	0.48	36.05	51.53	3.52	8.89
	4	92.98	0.93	6.02	0.07	16.25	44.47	39.18	0.11	16.25	44.47	39.18	0.11
	5	85.00	5.19	9.51	0.30	11.58	45.02	43.40	-	19.33	66.85	1.89	11.93
	6	4.88	41.54	4.88	0.19	47.55	41.04	11.41	-	53.83	41.01	5.01	0.15
B	1	87.28	5.12	6.13	1.47	6.73	51.54	1.01	40.72	29.66	32.76	37.26	0.31
	2	9.08	46.61	43.39	0.91	76.05	17.38	6.55	0.02	33.18	61.75	2.30	2.76
	3	87.47	0.93	8.11	3.49	88.13	3.61	8.22	0.04	87.39	3.98	8.34	0.29
	4	90.87	4.19	4.81	0.14	31.98	66.01	2.01	-	93.00	0.14	6.53	0.33
	5	0.25	35.13	27.53	0.25	76.98	14.93	6.77	1.32	53.92	42.04	3.92	0.12
	6	43.70	25.52	12.89	17.89	64.11	29.57	4.28	2.04	32.13	45.55	14.60	7.72
C	1	13.52	45.45	40.82	0.22	13.64	45.16	41.16	0.04	12.24	43.84	43.70	0.22
	2	3.76	58.83	0.74	36.68	54.60	41.59	3.81	-	26.83	55.55	10.62	7.00
	3	91.85	-	8.15	-	89.89	1.96	8.14	-	91.88	0.44	7.37	0.31
	4	93.91	0.24	5.84	-	81.96	9.35	8.29	0.40	88.77	3.06	7.59	0.59
	5	25.98	39.17	33.91	0.93	1.88	62.11	1.99	34.02	15.29	40.57	42.55	1.58
	6	49.98	44.27	5.75	-	15.94	42.35	41.50	0.21	13.58	45.23	40.99	0.20

#### 4.7 Diffusion Mechanism of Cu-Sn-Ni-P Amorphous Filler Alloys into Cu Foam

A diffusion mechanism of filler (consists of Cu, Sn, Ni and P elements) in different Cu foams of foam A, B and C is proposed schematically in Figure 4.35. In the brazing process, the molten filler would interact with Cu and Cu foam to form a diffusion region and a filler region. As the temperature increases, the filler would migrate through the interconnected branch of Cu foam and coat a portion of the Cu foam interconnected branch. Figure 4.1 shows that foam C has smaller pore sizes and higher number of interconnected branches with a small diameter of Cu foam branches. This structure results in high surface area for the joint contact between Cu and Cu foam. However, this large surface area of foam C was not a decisive factor to form a strong bond due to the small diameter size of the Cu foam C interconnected branches as compared to foam A.

The amounts of filler is important for filler diffusion into the Cu foam to form a sound brazing joint. During the brazing process, increasing the temperature causes the filler to start melting and diffuse into Cu foam through the branches. However, high numbers of Cu foam branches may worsen the wettability of the filler to diffuse into the Cu foam. Thus, the 40  $\mu\text{m}$  thickness of filler has better wettability on Cu foam A (less branches) as compared to Cu foam C (more branches), as illustrated in Figure 4.35.

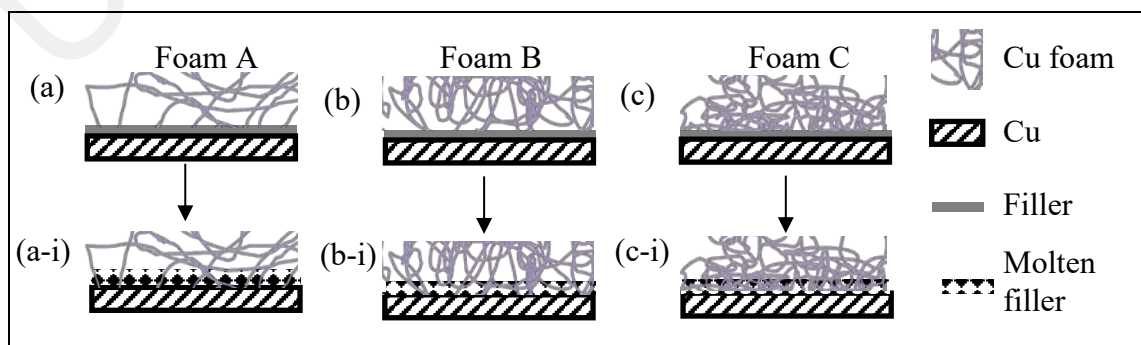


**Figure 4.35:** Illustration of filler before brazing (a to c) and molten filler during brazing (a-i to c-i)

The diffusion of different wt.% of Cu-Sn-Ni-P fillers in the Cu foam was elaborated in section 4.5.4, describing the migration of P and Ni elements from the filler into the Cu foam interconnected branch. Furthermore, the wt.% elements of Cu, Sn, Ni and P would determine the solubility of filler to form brazed joint interface and diffusivity in the Cu foam.

Figure 4.36 shows the proposed diffusion mechanism of Cu-Sn-Ni-P amorphous filler alloys for brazing of Cu/Cu foam/Cu. Initially, the Cu-Sn-Ni-P amorphous filler alloys is sandwiched between the Cu and Cu foam for brazing [Figure 4.36(a)]. Then, the specimens are heated from room temperature to above liquidus temperature of Cu-Sn-Ni-P amorphous filler alloys (ranging of 660 °C to 720 °C). The interstitial diffusion is taking place when the temperature reached at liquidus temperature. The atoms diffuse out from its lattice become the interstitial atoms and move freely.

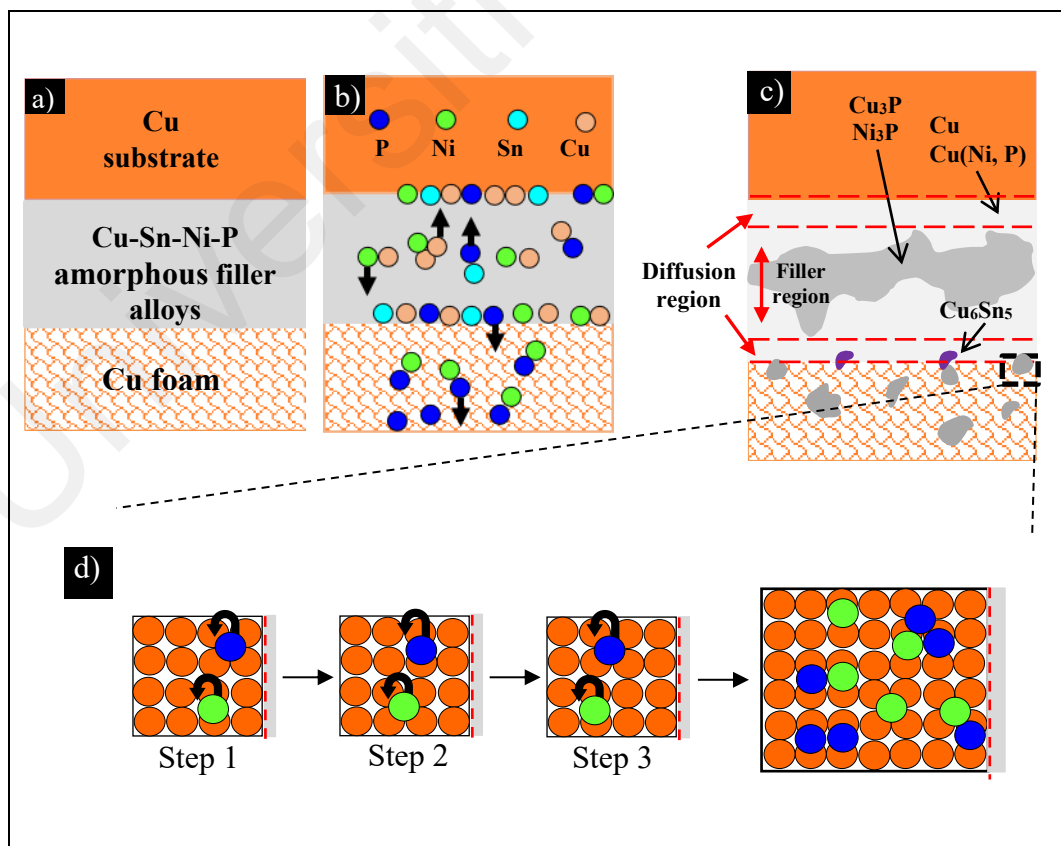


**Figure 4.36:** Proposed diffusion mechanism of Cu-Sn-Ni-P amorphous filler alloys

Once the brazing temperature approaches the liquidus temperature, the filler would have melted completely and begins to react with Cu foam and Cu substrate to form a brazed joint interface [Figure 4.36(b)]. The completely molten filler would have a more homogenous composition and be able to infiltrate the void spaces in between the interconnected branches of Cu foam *via* capillary action.

At elevated temperatures, shown in Figure 4.36(c), some of the P will evaporate due to high-vapour properties of P resulting in enriched Cu and Sn along the boundaries of Cu foam and cavities (Zhong et al., 2012). In addition, P and Ni in the filler would diffuse into the Cu foam and Cu to form the diffusion region due to difference in concentration gradient which would move from a high concentration to low concentration regions (Zhang et al., 2010). The  $\text{Cu}_3\text{P}$  and  $\text{Ni}_3\text{P}$  in the filler would have reacted to form a joint. The low atomic diameters of P and Ni enables further diffusion into Cu foam and movements from one surface atom to another surface atom of the porous Cu foam [Figure 4.36(d)].

#### **4.8 Corrosion Behaviour on Cu-Sn-Ni-P Filler and Cu/Cu foam/Cu Brazed Joint Interface using different Filler with Foam A**

Amorphous filler A, B and C were heated and cooled down using the same procedure for brazing Cu/Cu foam/Cu. This was conducted to investigate the corrosion behaviour of crystalline fillers and Cu/Cu foam/Cu with Cu foam A (hereinafter as Cu/Cu foam A/Cu) brazed joint interface. Crystalline filler A, B and C were evaluated using electrochemical corrosion analysis and compared with the microstructures of Cu/Cu foam A/Cu brazed joint interface after the immersion test.

#### 4.8.1 Crystalline Cu-Sn-Ni-P Filler

During brazing, as the temperature rises above 450 °C, the internal lattice structure of amorphous filler alloys start to transform by reconstructing its structures that lead to the morphology changes. When the temperature hit the liquidus temperature of the amorphous filler alloys, the grain of the liquid atom was furthered growth. Followed by slow solidification process of the molten amorphous filler alloys leads to a crystalline filler alloys. The crystalline structure comprises of the Cu solid solution, and other compounds of  $\text{Cu}_3\text{P}$ ,  $\text{Ni}_3\text{P}$  and  $\text{Cu}_6\text{Sn}_5$  as discussed in section 4.6. The slow solidification process is contradict with the rapid solidification which produced the amorphous filler alloys explained in section 2.4.1.

Table 4.10 shows elemental composition (at. %) of the crystalline fillers (filler A, filler B and filler C) from the EDX point analysis, labelled in the Figure 4.37. Figure 4.37 shows BSE images of crystalline fillers which consist both large (coarse) and small (fine) grain microstructures. The BSE images exhibit small dark grey island-shaped like features indicate Ni and P-enriched (points 5 and 11) were dominated by  $\text{Ni}_3\text{P}$  phase. While large grey island-shaped like features was found to be P-enriched (points 2, 6 and 10) which present  $\text{Cu}_3\text{P}$  phase. Small grains shows Sn-enriched at points 1, 8 and 12 as a  $\text{Cu}_6\text{Sn}_5$  phase. Light grey and bright regions are Cu-enriched at points 3, 4, 7 and 9.

From the BSE images, filler A (highest P wt.%- 7.8%) shows a lesser mixture of coarse and fine grain microstructure as compared to filler B (lower P wt.%- 7.0%) and filler C (lowest P wt.%- 6.0%). This is due to the good solubility property of P (Hasap et al., 2014) that has enhanced the solubility of filler A. This results in finer grain microstructure formation of the crystalline form after heating of the amorphous form of filler A. Decreasing the wt.% of P (for amorphous filler B and C) resulted in a higher

mixture of coarse and fine-grain microstructure of the crystalline filler, as shown in Figure 4.37.

However, there was no observable correlation between the wt.% of Ni and Sn in the amorphous filler A, B and C to the resultant Ni and Sn enrichments locations of crystalline filler tabulated in Table 4.10. Ni-enriched and Sn-enriched are represented in Figure 4.38 as dark grey phase and small grain, respectively.

The mapping analysis (Figure 4.38) of crystalline filler A shows the highest wt.% of P (8.08%), due to amorphous filler A having the highest wt. % of P. The highest P wt.% in crystalline filler A is also proof of the solubility P had contributed to the solidification of a fine microstructure. The mapping analysis shows that P was distributed in the dark grey phase (BSE images) unlike the irregular distribution of Ni. The distribution of Sn was also uneven in the light grey and bright phase for all the fillers.

**Table 4.10:** EDX point analysis for elemental composition (at.%) of crystalline filler A, crystalline filler B and crystalline filler C based on Figure 4.37

Crystalline filler	Points	Elemental composition (atomic-at. %)			
		Cu	Sn	P	Ni
A	1	79.81	15.16	2.59	2.44
	2	76.86	-	23.14	-
	3	95.51	1.72	2.77	-
	4	90.15	8.06	1.79	-
B	5	8.12	-	28.70	63.18
	6	77.28	-	22.72	-
	7	91.08	7.37	1.55	-
	8	77.86	20.47	1.67	-
C	9	87.85	6.77	3.86	1.52
	10	77.17	-	22.83	-
	11	7.65	-	30.57	61.78
	12	78.36	19.52	2.13	-

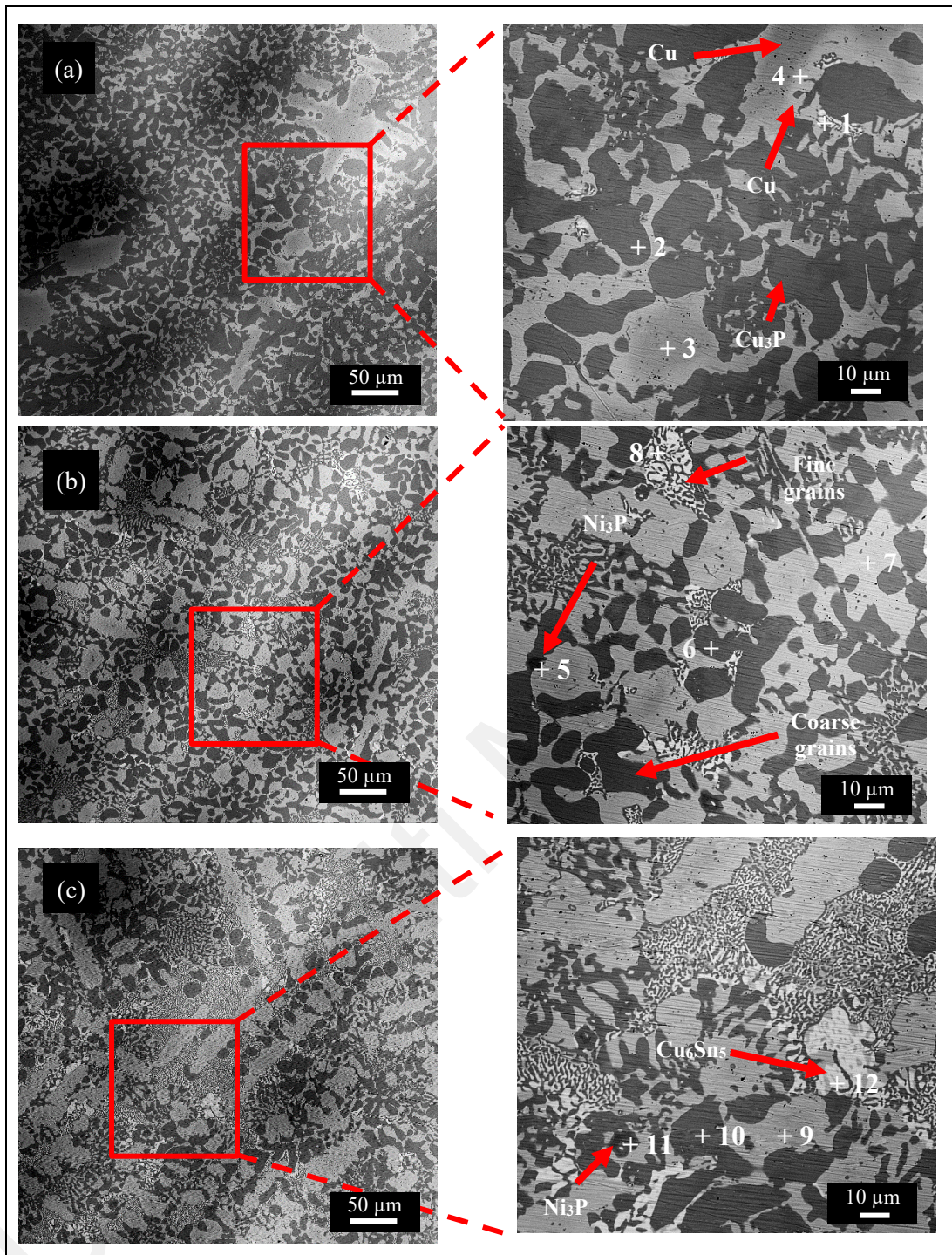


**Figure 4.37:** Microstructure of crystalline (a) filler A (b) filler B (c) filler C with inset of EDX point analysis for elemental composition in Table 4.10 at 2000 magnification

The Cu and Sn elements show dissimilar trend of wt.% content between the composition of amorphous filler and elemental composition analysis of crystalline filler (Figure 4.38). The different in brazing temperature and liquidus temperature of the fillers may affect the wt.% composition analysis result of Cu and Sn elements. The liquidus temperature of amorphous filler A, B, and C are at 610 °C, 591 °C, and 600 °C,

respectively. While the brazing was conducted at temperature of 660 °C (filler A and filler C) and 680 °C (filler B). Noted that the details explanation on brazing temperature selection of the filler is in section 4.5.3. The low melting temperature properties of Sn may contributes to the different trend of wt.% content in the filler and crystalline filler.

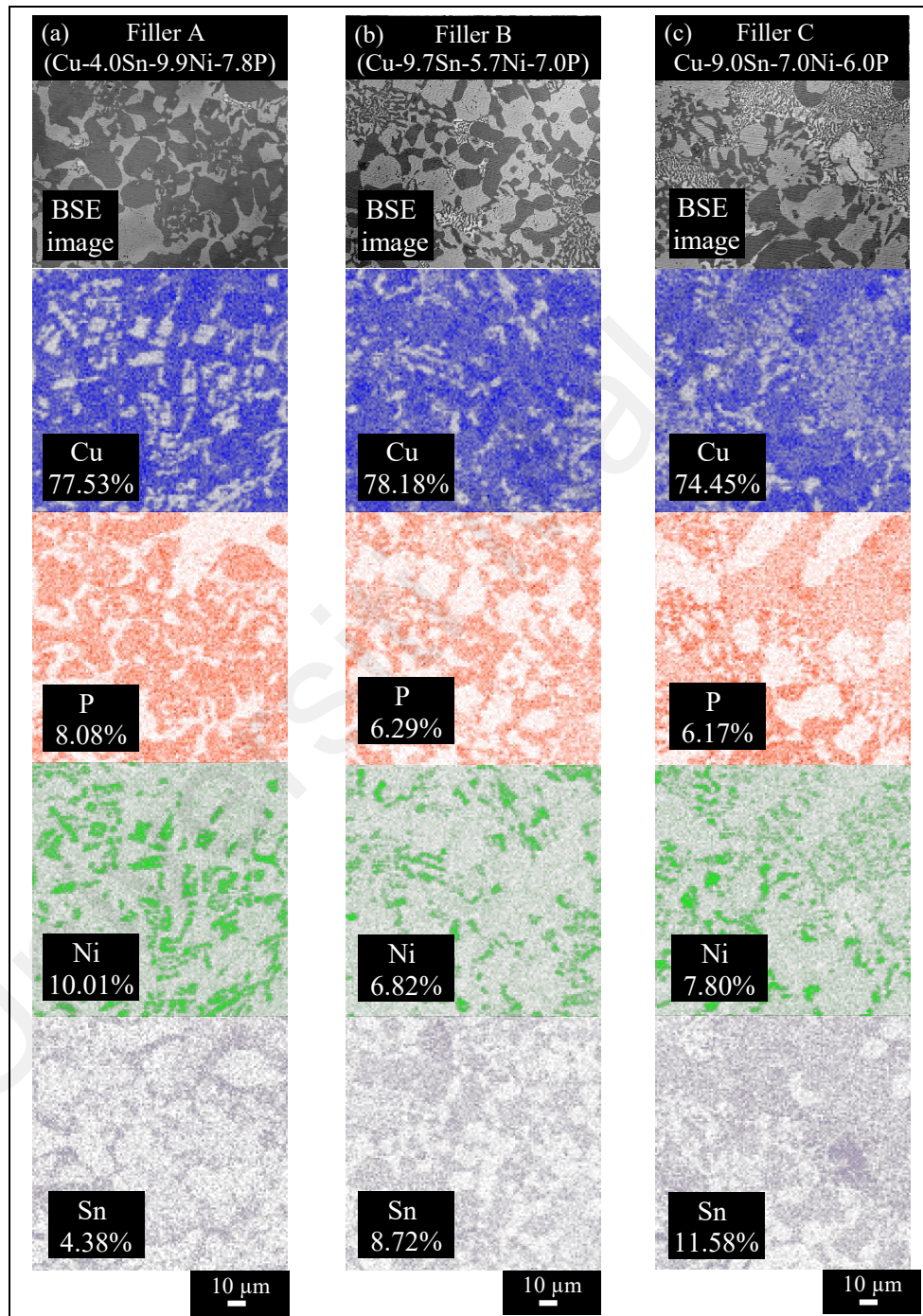


**Figure 4.38:** Mapping analysis and area elemental composition (wt.%) analysis for crystalline (a) filler A (b) filler B (c) filler C

## 4.8.2 Electrochemical Characteristics of Crystalline Cu-Sn-Ni-P Filler

The crystalline filler A, B and C were examined through a short-term corrosion test *via* electrochemical potentiodynamic polarization technique. The corrosion susceptibility and corrosion resistance of the filler alloys from the electrochemical test were compared with the macrostructure of the brazed sample after the immersion test.

### 4.8.2.1 Open Circuit Potential

Open circuit potential (OCP) also known as equilibrium potential or corrosion potential (no current supplied). As crystalline filler alloys being submerged in a 3.5% NaCl electrolyte, they tried to adjust in a new environment before being into equilibrium state. The distributions of metal ions and electrolyte ions on the electrode's surface, take a certain time before the OCP is established.

From Figure 4.39, it was found that the OCP increases for filler A (from 0s to 200s), filler B (from 0s to 300s) and filler C (from 0s to 400s). The increasing OCP reflects the spontaneous formation of passive films on the surface of the fillers after exposure to NaCl solution (Padmavathi et al., 2006; Oladijo et al., 2016).

Upon reaching peak values, the OCP reading would decline and finally plateaued to stable values. The OCP of filler A was observed to be more noble as compared to filler B and filler C. The OCP values shifted from noble to less noble in the following order; filler A, filler C and filler B. The time taken to stabilise the passive film was also found to increase with increasing Sn content in the fillers.

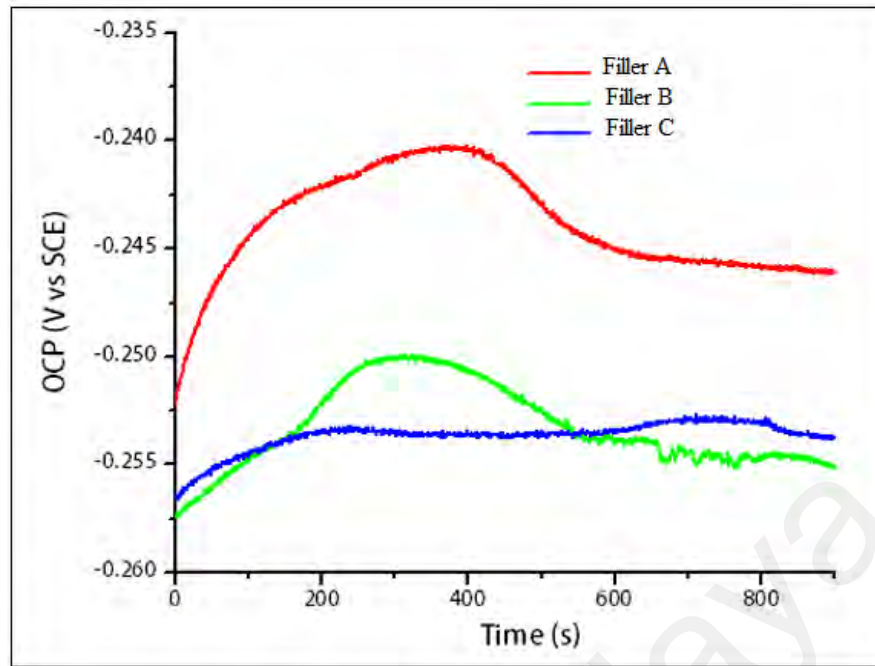
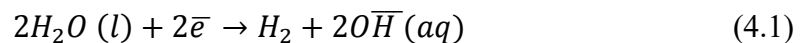


**Figure 4.39:** Open circuit potential for crystalline Cu-Sn-Ni-P filler

#### 4.8.2.2 Potentiodynamic Polarisation

Figure 4.40 shows the anodic and cathodic polarisation curves for filler A, filler B and filler C. The cathodic polarisation curve represents the cathodic reduction reactions happening in the environment. The possible cathodic reactions that could occur in the 3.5% NaCl solution (natural pH: 6.9) (Zhang et al., 2004) are outlined in reactions 2.4; page 43 (Lilja, 2013), 4.1 and 4.2 (Cramer & Covino, 2003).



The anodic polarisation curve reflects the metallic phase dissolution. Sn dissolution can either take place according to reaction 4.3 and 4.4 (Ahmido et al., 2011) while Cu dissolution can be expressed in reaction 2.2 and 2.3 (Lilja, 2013); page 43.

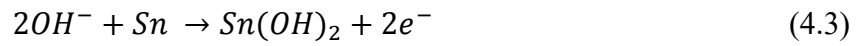
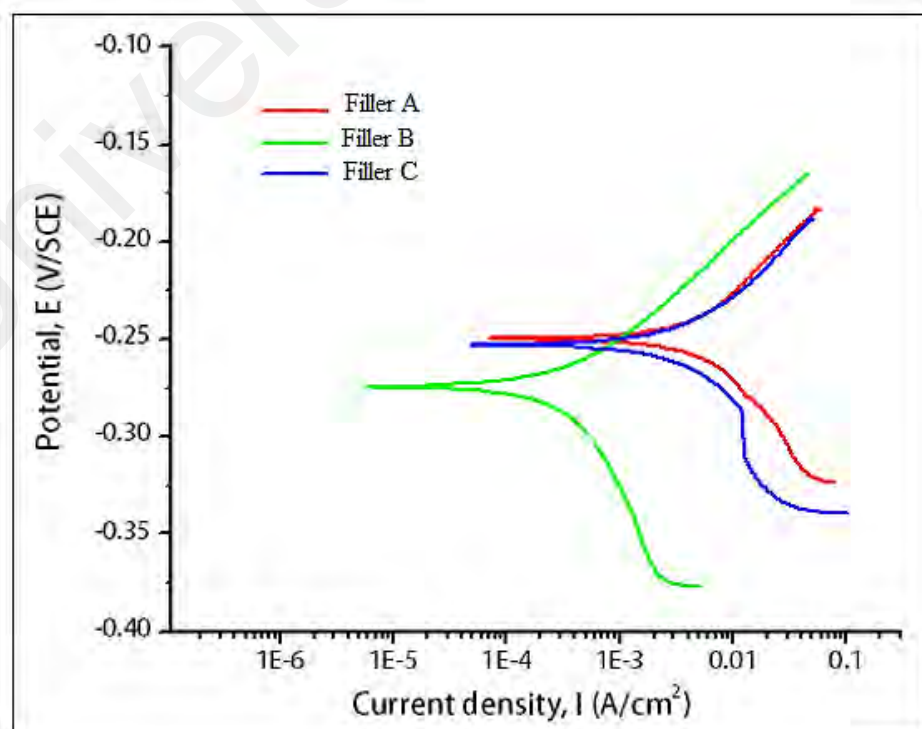


Figure 4.40 shows that the anodic current densities of filler A and filler C were slightly lower than their cathodic current density. In contrast, the anodic current density for filler B was higher than its cathodic current density, which was due to the high Cu and Sn contents of filler B (Cu-9.7Sn-5.7Ni-7.0P wt.%). The high content of these two elements (78.2 wt.% of Cu and 8.7 wt.% of Sn), confirmed by mapping analysis, would enhance the anodic reaction. On the other hand, both filler A and filler C displayed higher cathodic current densities than their anodic current densities. This observation could be credited to the increased hydroxyl ions ( $OH^-$ ) in the cathodic reaction due to low Cu and Sn ions in both fillers. Furthermore, the scarcity of Cu and Sn ions would inhibit the retardation of anodic reaction, causing the shrinking of the anodic polarisation curve (Song & Liu, 2013). This observation has proven that fillers would exhibit unique corrosion performance based on the wt.% elements in the filler.

Tafel fit was investigated by fitting with a linear line using EC-Lab software for quantitative analysis of polarisation curves, as detailed in **Appendix B.3**. Figure 4.41 shows a correlation between corrosion potential ( $E_{corr}$ ) and corrosion current density ( $I_{corr}$ ). A more noble (more positive)  $E_{corr}$  value reflects a lesser tendency for corrosion on the filler. In other words, the value of  $E_{corr}$  can be interpreted as the possibility for the filler to corrode (Shi, 2016). Figure 4.41 shows that the  $E_{corr}$  for filler A ( $-248.22 \text{ mV} \pm 1.67$ ) was more noble than those of filler C ( $-252 \text{ mV} \pm 1.00$ ) and filler B ( $-273.72 \text{ mV} \pm 0.93$ ).

Furthermore, the results also show that  $E_{\text{corr}}$  would shift to a more noble value as the Ni wt.% in the filler increases (Ni wt.% of filler B, filler C and filler A are 5.7%, 7.0% and 9.9%, respectively). This result is in line with area mapping analysis in Figure 4.38 that revealed Ni elemental composition (wt. %) of 6.8%, 7.8% and 10.1% for filler B, filler C, and filler A, respectively. The finer microstructures of filler A relative to the other fillers was also a factor in minimising corrosion. The OCP trend in Figure 4.39 also confirms with the increasing  $E_{\text{corr}}$  from filler B to filler C, and finally to filler A.

On the contrary, a higher  $I_{\text{corr}}$  would result in a higher corrosion rate (Shi, 2016). Filler B ( $0.685 \mu\text{A} \pm 0.13$ ) gave the lowest  $I_{\text{corr}}$  value, followed by filler C ( $1.904 \mu\text{A} \pm 0.10$ ) and filler A ( $2.210 \mu\text{A} \pm 0.3$ ). Davis (2001) has reported a high corrosion resistance in seawater for phosphorus bronze (Cu-Sn-P) with 8% to 10% Sn. This corrosion resistance characteristic was reflected from the low  $I_{\text{corr}}$  values of filler B and filler C since these fillers had more than 8 wt.% of Sn in their compositions. A higher  $I_{\text{corr}}$  and higher corrosion rate were observed for filler A, which contained less than 8% Sn.



**Figure 4.40:** Anodic and cathodic polarisation curve of crystalline Cu-Sn-P-Ni filler

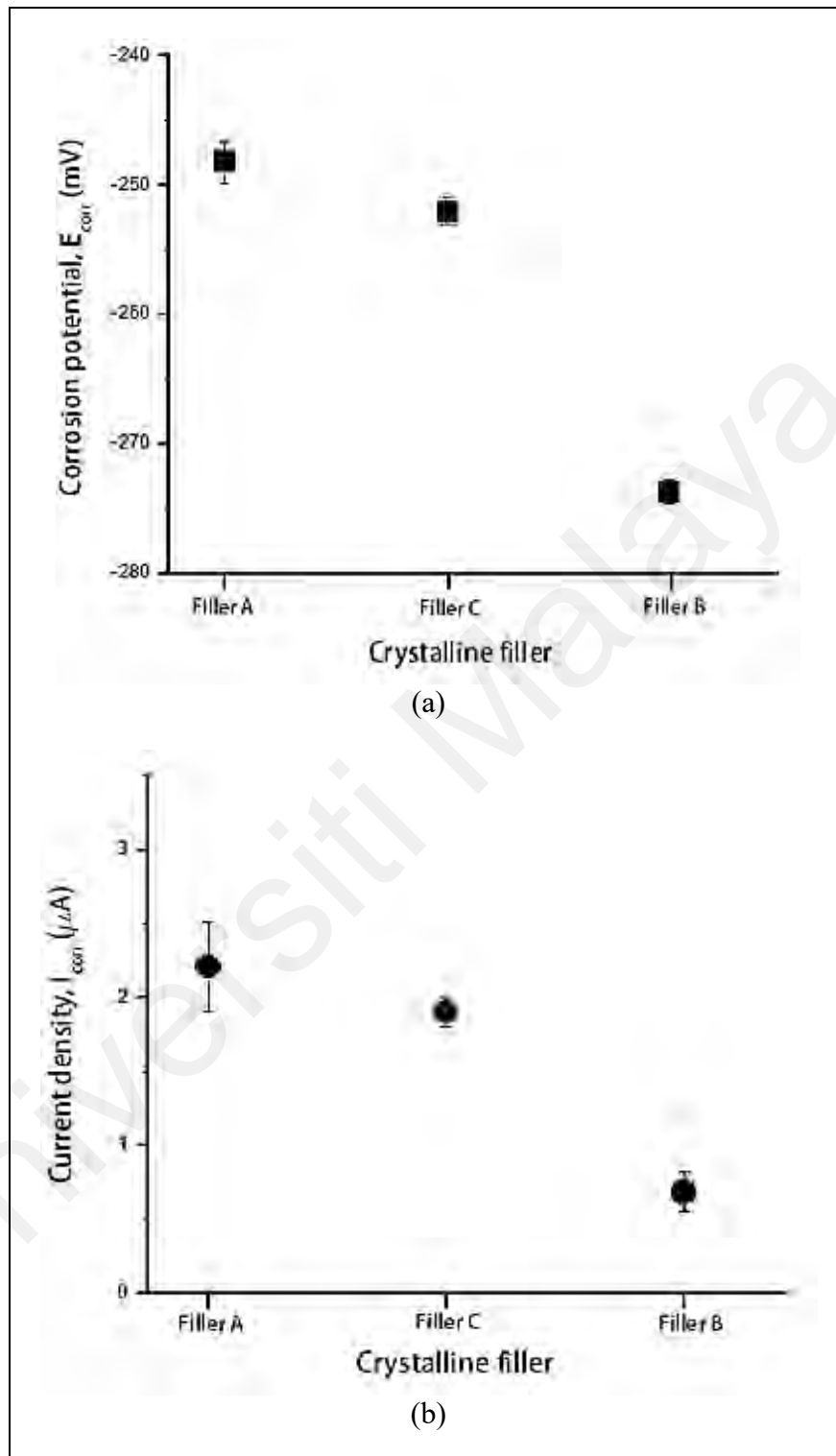


**Figure 4.41:** Polarisation parameters of (a)  $E_{\text{corr}}$  and (b)  $I_{\text{corr}}$  by Tafel fit for filler A, filler B and filler C

Shi (2016) stated that the relationship between  $I_{\text{corr}}$  and corrosion rate is described in several guidelines. If the value of  $I_{\text{corr}}$  is beyond 1.0, a high corrosion rate will ensue,

while an  $I_{\text{corr}}$  value in the range of 0.5-1.0 will display a moderate corrosion rate. Based on the results of this study, filler B has a moderate corrosion rate as compared to filler A and filler C.

Figure 4.42 shows the cyclic polarisation curves of filler A, filler C and filler B in 3.5% NaCl solution, from which local corrosion could be observed (Xiuming, Yanliang, Yadav, Wenjuan & Marco, 2015). The solid and dashed curves in Figure 4.42 represent the forward scan and reverse scan, respectively. Generally, upon the cathodic curve dissolution, the passive region would develop as shown by the anodic curve. The passive region could be used to predict pitting susceptibility if the reverse anodic scan shifted to either lower (negative hysteresis) or higher (positive hysteresis) current densities. Ralph, Debold and Johnson (1987) stated that the type of hysteresis from the reverse scan could determine the pitting resistance of the material.

Figure 4.42 shows that the current densities of the reverse anodic scan have shifted to lower current density values. This shift confirmed a negative hysteresis curve for all fillers. Thus, the possibility of pitting corrosion on the filler A, filler C, and filler B would be very low. The formation of an oxide layer on the fillers' surface may have protected the fillers against pitting corrosion. Previous studies have shown similar trends of cyclic polarisation curves. Zohdy, Sadawy and Ghanem (2014) have found no pitting on Cu-5Sn-5Zn-5Pb, Cu-8Sn-8Zn-8Pb, and Cu-10Sn-10Zn-10Pb that were exposed to saltwater. This observation was supported by the cyclic polarisation curves that showed a lower current density of the reverse anodic curve. Darabara, Bourithis, Zinelis and Papadimitriou (2004) have concluded that stainless steel and nickel-titanium have high pitting resistance in irrigating solutions of R-EDTA reagent and NaOCl due to the presence of negative hysteresis in the cyclic polarisation curves.

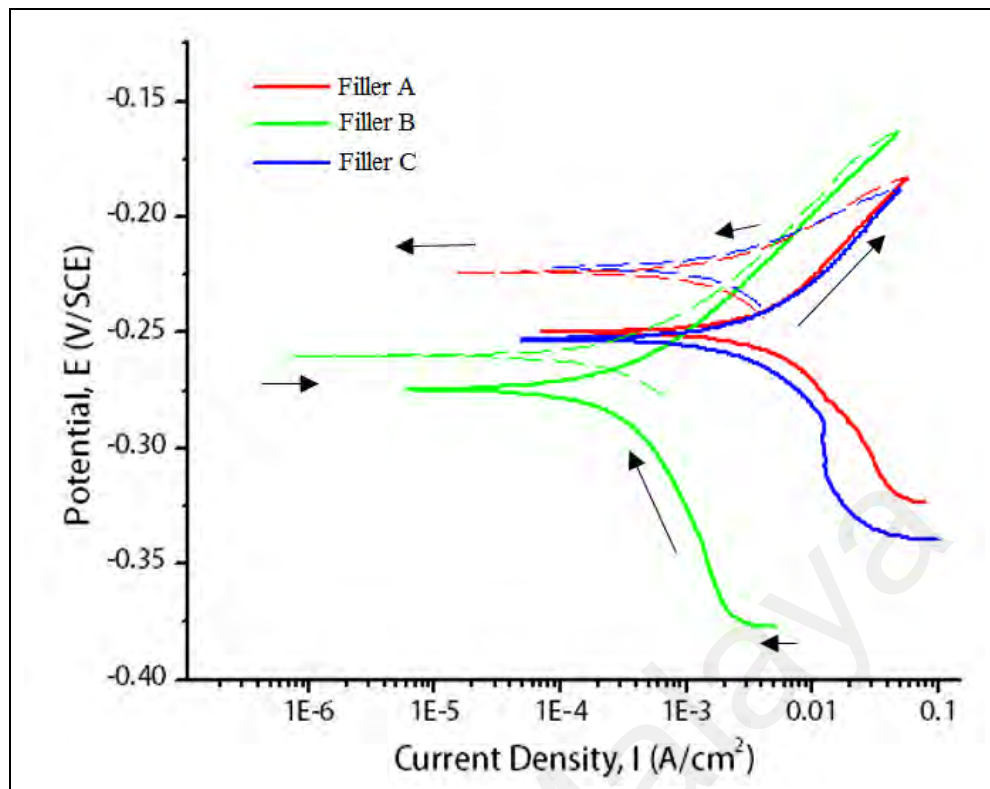


**Figure 4.42:** Cyclic polarisation curve of crystalline Cu-Sn-Ni-P fillers

### 4.8.3 Corrosion Behaviour of Cu/Cu foam A/Cu Brazed Joint Interface

The corrosion behaviour of Cu/Cu foam A/Cu brazed joint interface using different fillers of filler A, filler B and filler C were investigated. The work was conducted to evaluate the correlations between corrosion behaviour and electrochemical characteristics of the Cu-Sn-Ni-P fillers. The immersion test was carried out to observe the surface microstructure of the Cu/Cu foam A brazed joint interface after corrosion. Noted that, the amorphous filler used for brazing of Cu/Cu foam A/Cu become a crystalline filler after the brazing process due to slow cooling.

#### 4.8.3.1 Pre-Immersed Microstructure of Cu/Cu foam A Brazed Joint Interface

Figure 4.43 shows the microstructures of the pre-immersion (before immersion test without etched the brazed sample) of the Cu/Cu foam A brazed joint interface.

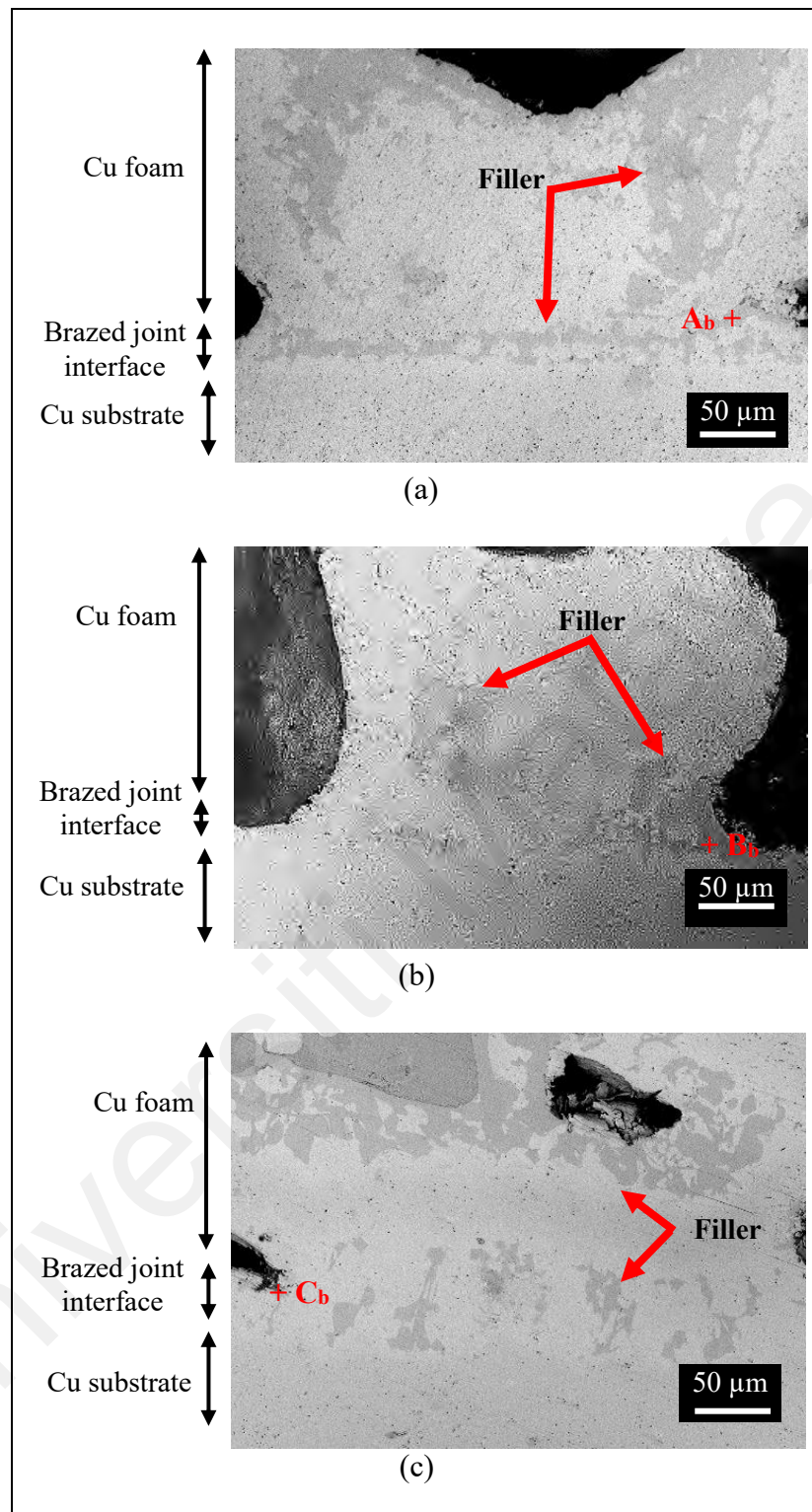


**Figure 4.43:** Pre-immersed microstructure of Cu/Cu foam A brazed joint interface using (a) filler A (b) filler B and (c) filler C

The grey island-shaped like regions indicate filler locations, which are concentrated in the middle of the joint interface and around several areas of the Cu foam. As analysed from the EDX point analysis (section 4.5.3), the filler region is made up of IMC  $\text{Cu}_3\text{P}$  phase (possess P-enriched) and  $\text{Ni}_3\text{P}$  phase (Ni and P-enriched). Similar phases

of IMCs have been reported in past studies (Miettinen, 2003; Hasap et al., 2014; Lutfi et al., 2016; Zhang et al., 2016).

#### **4.8.3.2 Post-Immersed Corrosion Product of Uncleaned Cu/Cu foam A Brazed Joint Interface**

Figure 4.44 reveals an accumulation of blueish-green layer (patina) on the Cu/Cu foam A brazed joint interface after seven days of immersion in 3.5% NaCl solution. The salt electrolyte had attacked the specimen's surface and formed a corrosion product of a patina layer on the brazed joint interface. This patina layer may have inevitably functioned as a protective oxide layer that would minimise further oxidation. However, the substrate surface of Cu was not covered with the patina layer. This show that the presence of the filler on the brazed joint interface may has enhanced the patina layer formation.

The brazed Cu/Cu foam A with filler B was found to have a thickest protective oxide (patina) layer compared to filler A or filler C. This could be due to the filler B having the lowest composition of Ni (5.7 wt.%), exposing the joint to an initial aggressive corrosion attack to cause the formation of corrosion product. This observation is supported by the filler B being less noble  $E_{\text{corr}}$  that relates to a high tendency for corrosion, as described in Figure 4.40. However, this thicker patina layer form would protect the brazed joint from further oxidation. Subsequently, a high corrosion resistance would be obtained, and a more negative  $I_{\text{corr}}$  is recorded, as in Figure 4.40, which results in lower corrosion rate.

Post-immersed specimens of uncleaned Cu/Cu foam A brazed joint interface using different fillers were analyzed using SEM and EDX. Figure 4.45 illustrates the corrosion products of the specimen's surface. EDX point analysis, summarized in Table 4.11, has identified the dots on the microstructure surface as corrosion products of Na and

Cl. The corrosion product was concentrated in the brazed joint interface area and the filler region. Thus, the presence of the filler play a crucial role in suppressing corrosion through the formation of corrosion products on the brazed joint surface.

Compounds that may formed would be copper(II) chloride (CuCl) from the reduction-oxidation reaction. Cramer & Covino (2003) have stated that the Cu would dissolve in the NaCl solution to form a CuCl compound. The possible reactions that may have taken place is described by (Warraky et al., 2004):-

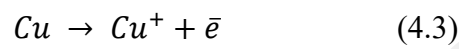


**Table 4.11:** EDX point analysis for elemental composition of post-immersed uncleaned Cu/Cu foam A brazed joint interface in Figure 4.45

Point	Element	Atomic Concentration (%)					
	Cl	Na	Cu	P	O	Sn	
1	56.32	43.68	-	-	-	-	
2	16.78	23.31	41.16	-	18.75	-	
3	15.75	41.53	42.72	-	-	-	
4	41.33	58.67	-	-	-	-	
5	55.00	45.00	-	-	-	-	
6	25.33	31.09	-	11.10	-	32.49	

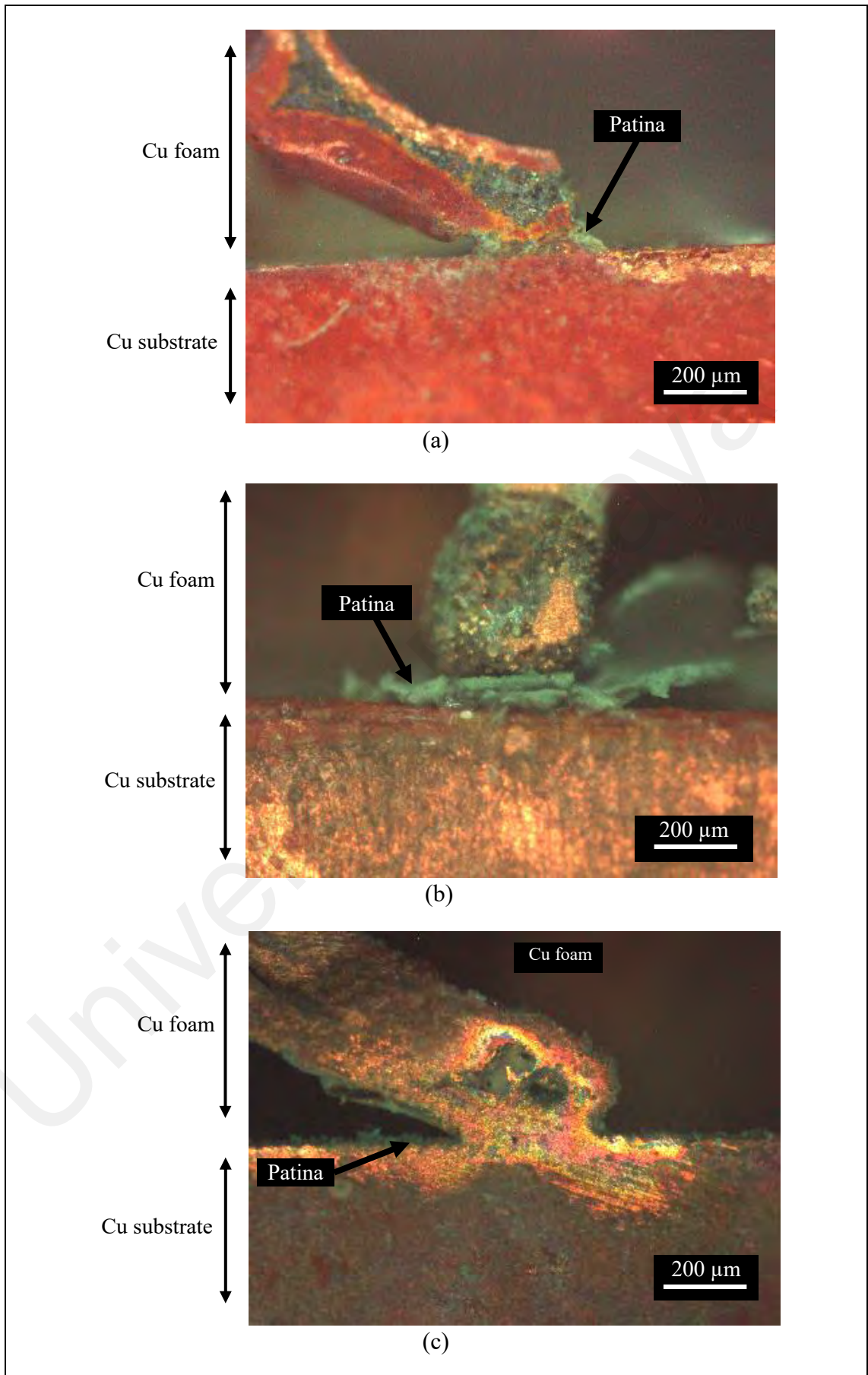


**Figure 4.44:** Post-immersed optical images of uncleaned Cu/Cu foam A using (a) filler A (b) filler B and (c) filler C

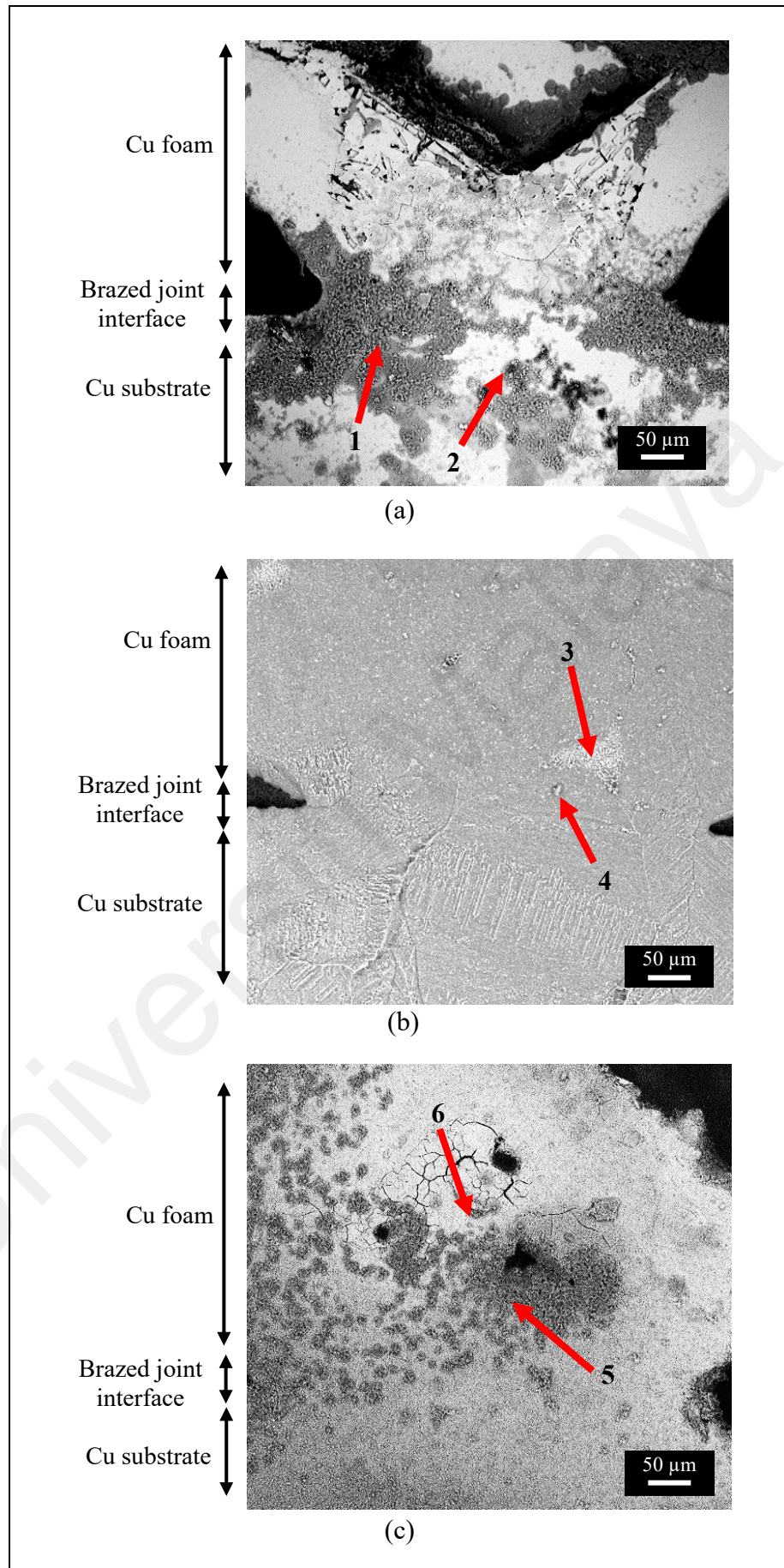


**Figure 4.45:** Post-immersed microstructure of uncleaned Cu/Cu foam A using (a) filler A (b) filler B and (c) filler C

### 4.8.3.3 Post-Immersed Microstructure Characterisation of Cleaned Cu/Cu Foam A Brazed Joint Interface

Figure 4.46 shows the microstructure of the post-immersed for cleaned Cu/Cu foam A brazed joint interface. The corrosion attack on the specimens' surface was confirmed by EDX point analysis, as tabulated in Table 4.12.

Figure 4.46 shows the presence of black spots on the microstructure of the post-immersed for cleaned Cu/Cu foam A, which contrasted the microstructure of pre-immersed Cu/Cu foam A. Pre-immersed Cu/Cu foam A contained Ni, P and Sn elements in the brazed joint interface. However, post-immersed cleaned Cu/Cu foam A showed the presence of the O element, probably belonging to copper(II) oxide (Cu<sub>2</sub>O) compound. Cu<sub>2</sub>O could be formed by the hydrolysis of CuCl which gave off precipitation on the specimen's surface. The hydrolysis reaction can be expressed as (Revie, 2011):

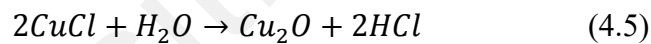


**Table 4.12:** EDX point analysis for elemental composition of pre-immersed Cu/Cu foam A (Figure 4.43) and post-immersed for cleaned Cu/Cu foam A brazed joint interface (Figure 4.46)

Point	Element	Atomic Concentration (%)					
		Cu	Ni	P	Sn	O	C
Pre-immersed Cu/Cu foam A	A <sub>b</sub>	12.17	42.83	44.78	0.22	-	-
	B <sub>b</sub>	50.30	3.72	45.76	0.22	-	-
	C <sub>b</sub>	93.10	6.72	0.19	-	-	-
Post-immersed for cleaned Cu/Cu foam A	A <sub>a</sub>	7.51	-	-	-	11.84	80.65
	B <sub>a</sub>	73.91	-	-	-	26.09	-
	C <sub>a</sub>	58.77	-	9.68	-	31.55	-

In addition, the sample's surface was corroded (darkened regions) along the boundaries of filler region formation in the brazed joint interface area. From the EDX point analysis, the filler region in the brazed joint interface area consisted of  $\text{Cu}_3\text{P}$ , which is more noble than Cu. Outside the filler regions were dominated by Cu, cause the chloride ions to selectively attack the Cu along the filler region boundaries (AWS, 2011).

Figure 4.46 shows severe corrosion for microstructures of Cu/Cu foam A using filler A and filler C as compared to the microstructure of Cu/Cu foam A using filler B. This was due to the filler A having the highest  $I_{\text{corr}}$  value, followed by filler C and then filler B. Thus, the corrosion behaviours (corrosion products and microstructure) of Cu/Cu foam A using filler A, filler B and filler C are supported by the analysis of electrochemical characteristics of  $E_{\text{corr}}$  and  $I_{\text{corr}}$  on filler A, filler B and filler C.

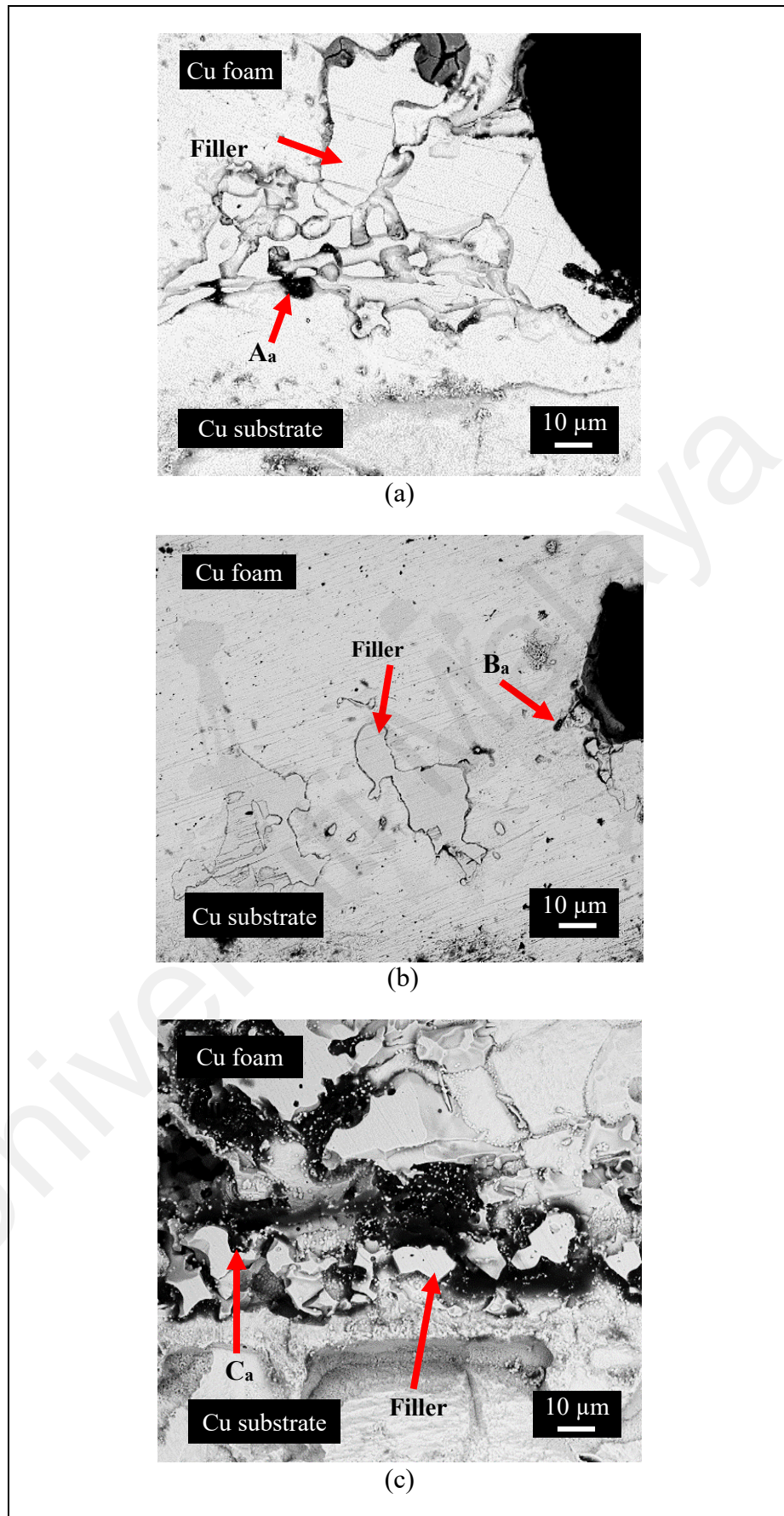


**Figure 4.46:** Post-immersed microstructure of cleaned Cu/Cu foam A brazed joint interface using (a) filler A (b) filler B and (c) filler C

## CHAPTER 5 : CONCLUSION

### 5.1 Introduction

This chapter presents general conclusions on the assessment of the mechanical properties, microstructure analysis and corrosion behaviour of copper foam brazing using amorphous copper-tin-nickel-phosphorus filler.

### 5.1 Conclusion

The mechanical properties of compressive strength and shear strength were evaluated to determine the Cu/Cu foam/Cu brazed joint strengths. Low compressive strength values were found for the nonbrazed Cu/Cu foam/Cu as compared to brazed Cu/Cu foam, due to the presence of filler that has strengthened the Cu foam branches. Cu foam C has the highest compressive strength value since it had an abundance of Cu foam branches as compared to foam B and foam A. However, Cu/Cu foam A has the highest shear strength value as it has larger intact surface area within the Cu foam branches as compared to foam C and B. To achieve the highest compressive strength value required the brazing at high temperature while to obtain the highest shear strength required the brazing to be conducted at lower temperature.

In-depth evaluations of Cu/Cu foam/Cu at selected brazing temperatures of 660 °C (filler A), 680 °C (filler B) and 660 °C (filler C) were conducted. These brazing temperatures are selected based on the highest shear strength values obtained for each filler. The cleavage formation on the Cu substrate surface from Cu/Cu foam shear-fracture indicates a brittle fracture occurrence due to the presence of P and Ni. But, several tear regions present a ductile fracture which agreed with enlarge area under the shear stress-strain curve. The hardness values (HV) in the filler region increase as the number of Cu

foam branches increases (from foam A to foam B, and finally foam C), which was inversely proportional to the shear strength results.

Diffusion of filler is important for the formation of brazed joint interface and filler wettability onto the Cu foam. The behaviour of filler diffusion would influence the mechanical properties of the joint. It was found that a high number of cavities was formed in the brazed joint interface of Cu/Cu foam C as compared to Cu/Cu foam B and Cu/Cu foam A. These cavities were formed due to gas entrapment in the void spaces in the Cu foam. The high number cavities in Cu/Cu foam C brazed joint interface would result in the lower shear strength of the brazed joint interface as compared to the brazed joint of foam A and foam B. A thicker brazed joint interface was observed for Cu/Cu foam using filler A than using filler B and filler C due to high content of P wt.% that has enhanced the solubility of the filler. The brittle fracture on the Cu fractured surface can be attributed to the presence of  $\text{Cu}_3\text{P}$  and  $\text{Ni}_3\text{P}$  brittle phases in the filler regions. The Cu-Sn-Ni-P amorphous alloys was found to have good wettability for the formation of the brazed joint and has diffused into the Cu foam. The migration of P and Ni across the Cu foam is associated with the increase in the compressive strength of brazed Cu/Cu foam/Cu as compared to nonbrazed Cu/Cu foam/Cu. Higher penetration of filler was observed for Cu foam A (low pore density of 15 PPI), which was further investigated for corrosion behaviour.

The operating environment of a heat exchanger is exposed to moisture, corrosive and aggressive compounds that would lead to corrosion. Corrosion on brazed joint interfaces would reduce joint strengths and ultimately the performance of the heat exchanger. In this study, it was initially expected that filler B would experience a high corrosion attack due to it having less noble corrosion potential ( $E_{\text{corr}}$ ), measured in the electrochemical potentiodynamic polarisation (PDP) analysis. However, upon measuring

the corrosion current density ( $I_{\text{corr}}$ ), it was found that filler B had lower corrosion rate with high corrosion resistance. Micrograph analysis of post-immersed uncleaned Cu/Cu foam has revealed a thicker patina layer in filler B joint as compared to Cu/Cu foam A/Cu using filler A or filler C. It can be deduced that for filler B, the joint would have experienced an initial aggressive corrosion (as expected from the PDP analysis), but the resultant thicker patina layer has inadvertently protected the surface, preventing it from further dissolution.

The findings from this work have evaluated the behaviour and performance of Cu/Cu foam/Cu brazing using Cu-Sn-Ni-P (wt.%) amorphous filler alloys, which can be used in heat exchangers. Based on the result and analysis, the Cu/Cu foam A/Cu using filler B at brazing temperature of 680 °C was found to be the most suitable configuration for heat exchanger applications.

## 5.2 Recommendations

This study has explored the experimental evaluation of Cu/Cu foam/Cu joining *via* brazing technique through analysis on Cu foam compressive strength, shear strength of brazed joint interface, wettability and diffusion of filler and corrosion performance. Continuation from this work can be made in several areas. Thus, the recommendations for future work are:

1. The diffusion of Cu-Sn-Ni-P amorphous filler alloys across the Cu foam have shown that the amount filler foil used can be reduced. In this work, the filler foil was placed on both sides to joint Cu/Cu foam/Cu. Instead, the filler could be placed on one-sided of the substrate only. The strength and diffusion behaviour can be evaluated to observe the ability of the filler to spread on the substrate and diffuse in the foam.

2. Detail measurement and characterisation of the intact surface area of Cu foam to substrate would be very useful to determine the relationship between the foam branches and pore densities with the mechanical properties obtained.
3. Applicability of the brazed joint in heat exchanger applications would depend on its ability to withstand fluid velocities, temperatures and service time. Thus a continuation of the work could explore on the dynamic forces exerted on the brazed joint interface and Cu foam.
4. Studies of Cu to Cu foam brazing could utilised others design of experiment for optimization of brazing parameter. The experiment design including orthogonal, taguchi or using software of Response surface methodology *via* different technique of box-behnken or central composite design.

## REFERENCES

- Abadi, G. B., Kim, D. Y., Yoon, S. Y., & Kim, K. C. (2016). Thermal performance of a 10-kW phase-change plate heat exchanger with metal foam filled channels. *Applied Thermal Engineering*, 99, 790–801. doi: 10.1016/j.applthermaleng.2016.01.156
- Ahmido, A., Sabbar, A., Zouihri, H., Dakhsi, K., Guedira, F., Serghini-Idrissi, M., El Hajjaji, S. (2011). Effect of bismuth and silver on the corrosion behaviour of Sn-9Zn alloy in NaCl 3 wt.% solution. *Materials Science and Engineering B*, 176, 1032-1036. doi: 10.1016/j.mseb.2011.05.034
- Air Radiators. (n.d.). *Power generation radiators*. Retrieved from <https://www.airradiators.com/industries/power-energy-generation/>
- Al-Abdallah, M. M., Maayta, A. K., Al-Qudah, M. A., & Al-Rawashdeh, N. A. F. (2009). Corrosion Behavior of Copper in Chloride Media. *The Open Corrosion Journal*, 2(4), 71–76. doi: 10.2174/1876503300902010071
- Alavi, R., Trenggono, A., Champagne, S., & Hermawan, H. (2017). Investigation on Mechanical Behavior of Biodegradable Iron Foams under Different Compression Test Conditions. *Metals*, 7(6), 202-220. doi: 10.3390/met7060202
- Alias, M. A. M. (2011). *Study of Adhesive Strength in Polymer Plate Heat and Mass Exchanger* (Degree's Thesis, University Technology Petronas). Retrieved from <http://utpedia.utp.edu.my/8598/1/2011%20-%20Study%20of%20adhesive%20strength%20in%20polymer%20plate%20heat%20and%20mass%20exchanger.pdf>
- American Welding Society (AWS) C3 Committee. (2011). *Brazing Handbook* (5th Edition). Miami, FL: American Welding Society.
- Aminazad, A. M., Hadian, A. M., & Ghasimakbari, F. (2015). Investigation on Corrosion Behaviour of Copper Brazed Joints. *Procedia Materials Science*, 11, 672–678. <http://dx.doi.org/10.1016/j.mspro.2015.11.024>
- Arentoft, M., Eriksen, R. S., & Hansen, H. N. (2010). *Chapter 7 - Micro-Bulk-Forming*. In Yi Qin (Ed). *Micro manufacturing Engineering and Technology*. (pp. 114-129). Waltham, MA: Elsevier Inc. <http://dx.doi.org/10.1016/B978-0-8155-1545-6.00007-7>.
- ASTM Standard C273. (2000). *Standard Test Method for Shear Properties of Sandwich Core Materials, Annual Book of the ASTM Standards*. West Conshohocken: ASTM International. <http://file.yizimg.com/86194/2009081802421443.PDF>
- ASTM Standard E384. (2011). *Standard Test Method for Microindentation Hardness of Materials, Annual Book of ASTM Standards*. West Conshohocken: ASTM International. <https://www.koopaco.com/Content/file/ASTM-E384.pdf>
- ASTM Standard G1-90. (1999). *Standard Practice for Preparing, Cleaning, and Evaluating Corrosion Test Specimens, Annual Book of ASTM Standards*. West

Conshohocken: ASTM International. [http://www.cosasco.com/documents/ASTM G1 Standard\\_Practice.pdf](http://www.cosasco.com/documents/ASTM G1 Standard_Practice.pdf)

ASTM Standard G-31. (1999). *Standard Practice for Laboratory Immersion Corrosion Testing of Metals, Annual Book of ASTM Standards*. West Conshohocken: ASTM International. Retrieved from [https://www.researchgate.net/profile/Mohammed\\_Hussein\\_J\\_H.Alatia/post/What\\_are\\_the\\_proper\\_book\\_and\\_time\\_period\\_or\\_intervals\\_for\\_weight\\_loss\\_measurements\\_for\\_mild\\_steel\\_corrosion\\_test/attachment/5ada-ca994cde260d15da0e1f/AS%3A617723440660480%401524288153812/download/G31.pdf](https://www.researchgate.net/profile/Mohammed_Hussein_J_H.Alatia/post/What_are_the_proper_book_and_time_period_or_intervals_for_weight_loss_measurements_for_mild_steel_corrosion_test/attachment/5ada-ca994cde260d15da0e1f/AS%3A617723440660480%401524288153812/download/G31.pdf)

AWS Standard C3.6M. (2008). *Specification for Furnace Brazing*. Miami: American Welding Society. Retrieved from [https://pubs.aws.org/Download\\_PDFS/C3.6M-C3.6-2008PV.pdf](https://pubs.aws.org/Download_PDFS/C3.6M-C3.6-2008PV.pdf)

Bernasko, P. K. (2012). *Study of Intermetallic Compound Layer Formation, Growth and Evaluation of Shear Strength of Lead-Free Solder Joints* (Doctor's Dissertation, University of Greenwich, UK). Retrieved from [gala.gre.ac.uk/9452/1/Peter\\_Kojo\\_Bernasko\\_2012.pdf](http://gala.gre.ac.uk/9452/1/Peter_Kojo_Bernasko_2012.pdf)

Bhattacharya, A., Calmidi, V. V., & Mahajan, R. L. (2002). Thermophysical properties of high porosity metal foams. *International Journal of Heat and Mass Transfer*, 45, 1017-1031. doi: 10.1016/S0017-9310(01)00220-4

Boomsma, K., Poulikakos, D., & Zwick, F. (2003). Metal foams as compact high performance heat exchangers. *Mechanics of Materials*, 35, 1161–1176. doi: 10.1016/j.mechmat.2003.02.001

Cao, J., Song, X. G., Li, C., Zhao, L. Y., & Feng, J. C. (2013). Brazing ZrO<sub>2</sub> ceramic to Ti-6Al-4V alloy using NiCrSiB amorphous filler foil: Interfacial microstructure and joint properties. *Materials Characterization*, 81: 85–91. doi: 10.1016/j.matchar.2013.04.009

Chen, J., Li, X., Li, W., He, J., Li, C., Dai, S., Ren, Y. (2017). Study on the Compression Properties and Deformation Failure Mechanism of Open-Cell Copper Foam. *Advanced Engineering Materials*, 19(11). doi: 10.1002/adem.201600861

Chein, R., Yang, H., Tsai, T., & Lu, C. (2009). Experimental Study of Heat Sink Performances Using Copper Foams Fabricated by Electroforming. *Microsystem Technologies*, 16(7), 1157-1164. doi: 10.1007/s00542-009-0950-y

Clarelli, F., Filippo, B. D. E., & Natalini, R. (2014). A Mathematical Model of Copper Corrosion. *Applied Mathematical Modelling*, 38(19–20): 4804–4816. doi: 10.1016/j.apm.2014.03.040

Copper Development Association. (n.d.). The copper advantages. A guide to working with copper and copper alloy. [https://www.copper.org/publications/pub\\_list/pdf/a1360.pdf](https://www.copper.org/publications/pub_list/pdf/a1360.pdf)

Cramer S. D. & Covino Jr. B. S. (Eds.). (2003) *ASM Handbook, Vol 13A Corrosion: Fundamentals, Testing, and Protection*. Materials Park, Ohio: ASM International.

- Craymer, K. (2011). *Development and Evaluation of Brazed Joints for a Plate Microchannel Heat Exchanger* (Master's Thesis, Case Western Reserve University). Retrieved from: [https://etd.ohiolink.edu/rws\\_etd/document/get/case1299695241/inline](https://etd.ohiolink.edu/rws_etd/document/get/case1299695241/inline)
- Cullity, B. D. (1956). *Elements of X-Ray diffraction*. Massachusetts: Addison-Wesley Publishing Company, Inc. doi: 10.1017/CBO9781107415324.004
- Davis, J. R. (2001). *Copper and Copper Alloys*. Materials Park, Ohio: ASM International. doi: 10.1016/B978-0-08-052351-4.50044-3.
- Darabara, M., Bourithis, L., Zinelis, S., & Papadimitriou, G. D. (2004). Susceptibility to localized corrosion of stainless steel and NiTi endodontic instruments in irrigating solutions. *International Endodontic Journal*, 35, 705–710. doi: 10.1111/j.1365-2591.2004.00866.x.
- Dewatwal, J. (2009). *Design of compact plate fin heat exchanger*. (Degree's thesis, National Institute of Technology, India). Retrieved from <https://pdfs.semanticscholar.org/7fdd/a53db11f62efc26503e96ca24829e8244f26.pdf>
- Dubey A. K. (2015). Investigation on suitability of aluminium to copper in a radiator. *Manufacturing Science and Technology*, 3(1), 16-23. doi: 10.13189/mst.2015.030103.
- Elmaaty A., T. M., Kabeel, A. E., & Mahgoub, M. (2017). Corrugated plate heat exchanger review. *Renewable and Sustainable Energy Reviews*, 70, 852–860. doi: 10.1016/j.rser.2016.11.266
- Ejlali, A., Ejlali, A., Hooman, K., and Gurgenci, H. (2009). Application of high porosity metal foams as air-cooled heat exchangers to high heat load removal systems, *International Communication Heat Transfer*, 36, 674-679. doi: 10.1016/j.icheatmasstransfer.2009.03.001
- El-Hadek, M. A., & Kaytbay, S. (2008). Mechanical and physical characterization of copper foam. *International Journal of Mechanics and Materials in Design*, 4(1), 63–69. doi: 10.1007/s10999-008-9058-2.
- Elrefaey, A., & Tillmann, W. (2008). Solid state diffusion bonding of titanium to steel using a copper base alloy as interlayer. *Journal of Materials Processing Technology*, 9: 2746–2752. doi: 10.1016/j.jmatprotec.2008.06.014.
- Elrefaey, A., Wojarski, L., & Tillmann, W. (2010). Investigation on corrosion of titanium/steel brazed joint. *Materialwissenschaft und Werkstofftechnik*, 41(11), 908–913. doi: 10.1002/mawe.201000684
- Feng, S., Li, F., Zhang, F., & Lu, T. J. Natural convection in metal foam heat sinks with open slots, *Experimental Thermal Fluid Science*, 91 (2018) 354–362. doi: 10.1016/j.expthermflusci.2017.07.010.
- Fernandes, C. S., Dias, R. P., & Maia, J. (2010). New Plates for Different Types of Plate Heat Exchangers, *Recent Patents on Mechanical Engineering*, 1(3), 198-205. doi: 10.2174/1874477X10801030198

- Fernández-Seara, J., Diz, R., & Uhía, F. J. (2013). Pressure drop and heat transfer characteristics of a titanium brazed plate-fin heat exchanger with offset strip fins. *Applied Thermal Engineering*, 51(1–2), 502–511. doi: 10.1016/j.applthermaleng.2012.08.066
- Francis, A. (2012). Brazed Aluminium Heat Exchangers – (BAHX) Surveillance – Analysis – Mitigation. *Proceedings of the 3<sup>rd</sup> International Gas Processing Symposium*. (pp. 170-182). Qatar: Elsevier B.V. doi: 10.1016/B978-0-444-59496-9.50026-6.
- Gejdoš, P., Klakurková, L., Juliš, M., Horynová, M., Páleníková, L., & Švejcar, J. (2017). Analysis of Damage of Solder Joint of Heat Exchanger. *Solid State Phenomena*, 270, 63–67. doi: 10.4028/www.scientific.net/SSP.270.63.
- Ghayad, I. M., Hamid, Z. A., & Gomaa, N. (2015). A Case Study: Corrosion Failure of Tube Heat Exchanger. *Journal of Metallurgical Engineering*, 4, 57–61. doi: 10.14355/me.2015.04.007
- Ghosh, I. (2009). How Good Is Open-Cell Metal Foam as Heat Transfer Surface? *Journal of Heat Transfer*, 131: 1–8. doi: 10.1115/1.3160537
- Ghovanlou, M. K., Jahed, H., & Khajepour, A. (2013). Cohesive zone modeling of ductile tearing process in brazed joints. *Engineering Fracture Mechanics*, 102, 156–170. doi: 10.1016/j.engfracmech.2012.11.018
- Gnyloskurenko, S., Nakamura, T., Byakova, A., Podrezov, Y., Ishikawa, R. & Maeda, M. (2005). Development of lightweight Al alloy and technique. *Canadian Metallurgical Quarterly*, 44(1), 7-12. doi: 10.1179/000844305794409742
- Gregory, E.J. (2011, February 2). Plate fin heat exchanger. Retrieved from 10.1615/AtoZ.p.plate\_fin\_heat\_exchangers
- Gunnarsson, J., Sinclair, I. J.C., & Alanis F. (2009, February 7). Compact Heat Exchangers: Improving heat recovery. *Chemical Engineering*, 116(2) pp. 44–47. Retrieved from: [https://issuu.com/androsov.info/docs/che\\_2009\\_02](https://issuu.com/androsov.info/docs/che_2009_02)
- Haack, D. P., Butcher, K. R., Kim, T., & Lu, T. J. (2001). Novel Lightweight Metal Foam Heat Exchangers. *ASME Congress Proceedings*. (pp. 1–7). New York: ASME. [https://pdfs.semanticscholar.org/53c2/0060dfe89d5035f14c7c8cd445ad381dfddb.pdf?\\_ga=2.154566704.906842658.1596999190-1480421229.1573968746](https://pdfs.semanticscholar.org/53c2/0060dfe89d5035f14c7c8cd445ad381dfddb.pdf?_ga=2.154566704.906842658.1596999190-1480421229.1573968746)
- Hafeez, P., Chandra, S. & Mostaghimi, J. (2017). Heat Transfer during High Temperature Gas Flow through Metal Foam Heat Exchangers. *Journal of Heat Transfer*, 139, 1–11. doi: 10.1115/1.4037082
- Haidar, S., & Sekh, M. (2018) Effects of Production Parameters on Density and Tensile Properties of Aluminium MMC Foam. *International Journal of Advanced in Management, Technology and Engineering Sciences*, 8(III), 924-933. Retrieved from [https://www.researchgate.net/publication/326624037\\_Effects\\_of\\_Production\\_Parameters\\_on\\_Density\\_and\\_Tensile\\_Properties\\_of\\_Aluminium\\_MMC\\_Foam](https://www.researchgate.net/publication/326624037_Effects_of_Production_Parameters_on_Density_and_Tensile_Properties_of_Aluminium_MMC_Foam)

- Han, X., Wang, Q. I. N., Park, Y., Joen, C. T., Sommers, A., & Jacobi, A. (2012). A review of metal foam and metal matrix composites for heat exchangers and heat sinks. *Heat Transfer Engineering*, 33(12), 1–75. doi: 10.1080/01457632.2012.659613
- Hangai, Y., Utsunomiya, T., Kuwazuru, O., & Kitahara, S. (2015). Deformation and Plateau Region of Functionally Graded Aluminum Foam by Amount Combinations of Added Blowing Agent. *Materials*, 8, 7161–7168. <http://doi.org/10.3390/ma8105366>
- Hartmann, T., & Nuetzel, D. (2010, June 15-17). Nickel-Chromium-Based Amorphous Brazing Foils for Continuous Furnace Brazing of Stainless Steel [Conference session]. Proceedings of the 9<sup>th</sup> International Conference of Brazing, High Temperature Brazing and Diffusion Bonding, Aachen, Germany. Retrieved from: <https://pdfs.semanticscholar.org/4624/9ff07561491741273658f94c50d65c111a48.pdf>
- Hasap, A., Noraphaiphaksa, N., & Kanchanomai, C. (2014). The Microstructure and Strength of Copper Alloy Brazing Joints. *Welding Journal*, 93: 116–123. Retrieved from [https://www.researchgate.net/publication/269411918\\_The\\_Microstructure\\_and\\_Strength\\_of\\_Copper\\_Alloy\\_Brazing\\_Joints](https://www.researchgate.net/publication/269411918_The_Microstructure_and_Strength_of_Copper_Alloy_Brazing_Joints)
- Hasap, A., Noraphaiphaksa, N., & Kanchanomai, C. (2015). Torsional strength and failure of copper alloy brazing joint. *Engineering Failure Analysis*, 48: 174–184. doi: 10.1016/j.engfailanal.2014.11.008
- Heimann, R. B. (2008). *Plasma Spray Coating*. New York, USA: VCH Publishers, Inc. doi: 10.1002/9783527614851
- Heo, H., Kim, G., Yeon, D., Moon, C., & Chun, K. (2019). Microstructure and mechanical properties of Ni foam / stainless steel joint brazed using Ni-based alloy. *Materials Science & Engineering A*, 740–741, 63–70. doi: 10.1016/j.msea.2018.10.022
- Hu, H., Weng, X., Zhuang, D., Ding, G., Lai, Z., & Xu, X. (2016). Heat transfer and pressure drop characteristics of wet air flow in metal foam under dehumidifying conditions. *Applied Thermal Engineering*, 93, 1124–1134. doi: 10.1016/j.applthermaleng.2015.09.019.
- Hudson Products Corporation. (2007). *The Basic of Air-cooled Heat Exchangers*. Retrieved from <https://files.chartindustries.com/hudson/BasicsofACHEBrochure-Web.pdf>.
- ISO 13314. (2011). *Mechanical testing of metals - Ductility testing - Compression test for porous and cellular metals, ISO (Vol. 2011)*. Geneva: International Standard.
- Jacobi, A. M., Han, X., Park, Y., Sommers, A., Joen, C. T., & Wang, Q. (2008). Novel Materials for Heat Exchanger (ARTI Report No. 06030-01). Air-Conditioning and Refrigeration Technology Institute. Retrieved from [http://ahrinet.org/App\\_Content/ahri/files/RESEARCH/Technical%20Results/ARTI-Rpt-06030-01.pdf](http://ahrinet.org/App_Content/ahri/files/RESEARCH/Technical%20Results/ARTI-Rpt-06030-01.pdf).

- Jacobson, D. M., & Humpston, G. (2005). *Principles of Brazing*. Materials Park, Ohio: ASM International.
- Jaeger, P. De, Joen, C. T., Huisseune, H., Ameel, B., Schampheleire, S. De, & Paepe, M. De. (2012). International Journal of Heat and Mass Transfer Assessing the influence of four bonding methods on the thermal contact resistance of open-cell aluminum foam. *International Journal of Heat and Mass Transfer*, 55(21–22), 6200–6210. doi: 10.1016/j.ijheatmasstransfer.2012.06.043
- Jamadon, N. H., Tan, A. W., Yusof, F., Ariga, T., Miyashita, Y., & Hamdi, M. (2016). Utilization of a Porous Cu Interlayer for the Enhancement of Pb-Free Sn-3.0Ag-0.5Cu Solder Joint. *Metals*, 6(220), 1–15. doi: 10.3390/met6090220
- Jangid, S. (2018). Plate Type Heat Exchanger – A Review Study. *IOSR Journal of Engineering*, 08(10), 11–18. Retrieved from [https://www.iosrjen.org/Papers/vol8\\_issue10/Version-3/C0810031118.pdf](https://www.iosrjen.org/Papers/vol8_issue10/Version-3/C0810031118.pdf).
- Jarvis, T., Voice, W., & Goodall, R. (2011). The bonding of nickel foam to Ti-6Al-4V using Ti-Cu-Ni braze alloy. *Materials Science and Engineering A*, 528(6), 2592–2601. doi: org/10.1016/j.msea.2010.11.077
- Jingxin, S., Minyu, M., Tianjing, W., Xiaomei, G., Ligu, H., & Zhiping, W. (2015). Fouling corrosion in aluminum heat exchangers. *Chinese Journal of Aeronautics*, 28(3), 954–960. doi: 10.1016/j.cja.2015.02.015
- Joen, C. T., Jaeger, P. De, Huisseune, H., Herzele, S. Van, Vorst, N., & Paepe, M. De. (2010). Thermo-hydraulic study of a single row heat exchanger consisting of metal foam covered round tubes. *International Journal of Heat and Mass Transfer*, 53:3262-3274. doi: 10.1016/j.ijheatmasstransfer.2010.02.055
- Kalin, B. A., Suchkov, A. N., Fedotov, V. T., Sevryukov, O. N., Ivannikov, A. A., & Gervash, A. A. (2016). Brazing of Be with CuCrZr-bronze using copper-based filler metal STEMET. *Nuclear Materials and Energy*, 9, 388–393. doi: 10.1016/j.nme.2016.07.004
- Kaya, A. C. (2020). *In situ* shear behavior of open-cell austenitic 316L steel foams. *Materials Chemistry and Physics*, 252, 123303. doi: 10.1016/j.matchemphys.2020.123303.
- Kennedy, A. (2012). Porous Metals and Metal Foams made from Powders In K. Kondoh (Ed.). *Powder Metallurgy* (pp. 31-46). London, UK: IntechOpen.
- Khot, A. R., Thombare, D. G., Gaikwad, S. P. & Adandande, A. S. (2013) Overview of radiator performance evaluation and testing. *IOSR Journal of Mechanical and Civil Engineering*, 7-14. Retrieved from <https://www.semanticscholar.org/paper/An-Overview-of-Radiator-Performance-Evaluation-and-Khot-Thombare/f6bf17246bd760561f27f58770bca5f0777e3526>
- Kim, S. Y., Paek, J. W., & Kang, B. H. (2000). Flow and Heat Transfer Correlations for Porous Fin in a Plate-Fin Heat Exchanger. *Journal of Heat Transfer*, 122: 572–578. Retrieved from <http://asmedigitalcollection.asme.org/>

- Kim, S.-H., Heo, H.-J., Yoon, T.-J., & Kang, C.-Y. (2016). Effect of Bonding Pressure and Bonding Time on the Tensile Properties of Cu-Foam/Cu-Plate Diffusion Bonded Joint. *Korean Journal Metal Material*, 54(12): 899–907. doi: 10.3365/KJMM. 2016.54.12.899
- Kolb, G. (2018). Innovative Design of Microstructured Plate-and-Frame Heat Exchangers. In H.-J. Bart & S. Scholl (Eds.). *Innovative Heat Exchangers* (pp. 117-134). Springer International Publishing. doi: 10.1007/978-3-319-71641-1\_3.
- Komolafe, B. (2014). *A Study on the Wetting Behaviour of Ti-20Zr-20Cu-20Ni Brazing Filler on Ti-6Al-4V* (Master's Thesis, Concordia University, Canada). Retrieved from [https://spectrum.library.concordia.ca/979192/1/Komolafe\\_MASc\\_S2015.pdf](https://spectrum.library.concordia.ca/979192/1/Komolafe_MASc_S2015.pdf)
- Landolt, D. (2007). *Corrosion and surface chemistry of metals*. Boca Raton, FL: CRC Press.
- Leeuw, B. M. d. (1999). *Corrosion of Aluminium Alloys used in Automotive Radiators* (Master's Thesis, University of Natal, South Africa). Retrieve from <https://pdfs.semanticscholar.org/2812/0db918213b4124615ac00500f844bca15fde.pdf>
- Lewinsohn, C., Fellows, J., & Wilson, M. (2014). Compact Ceramic Heat Exchangers and Microchannel Devices. *Joining and Integration*, 88, 148–155. <http://doi.org/10.4028/www.scientific.net/AST.88.148>
- Li, Q., Flamant, G., Yuan, X., Neveu, P., & Luo, L. (2011). Compact heat exchangers: A review and future applications for a new generation of high temperature solar receivers. *Renewable and Sustainable Energy Reviews*, 15, 4855–4875. <http://doi.org/10.1016/j.rser.2011.07.066>
- Li, X., Wang, H., Wang, T., Zhang, B., Yu, T., & Li, R. (2017). Microstructural evolution mechanisms of Ti600 and Ni-25%Si joint brazed with Ti-Zr-Ni-Cu amorphous filler foil. *Journal of Materials Processing Technology*, 240: 414–419. doi: 10.1016/j.jmatprotec.2016.10.021
- Lilja, C. (2013). Influence of high chloride concentration on copper corrosion. *Swedish Nuclear Fuel and Waste Management*, 1–6. Retrieved from [http://www.skb.se/wp-content/uploads/2015/05/Bilaga-till-1398013\\_1398014-Influence-of-high-chloride-concentration-on-copper-corrosion.pdf](http://www.skb.se/wp-content/uploads/2015/05/Bilaga-till-1398013_1398014-Influence-of-high-chloride-concentration-on-copper-corrosion.pdf)
- Lin, C. C., Shu, C. H., Chen, C., Shiue, R. K., & Shy, H. J. (2012). Brazing porous tungsten and molybdenum using palladium and titanium foils. *International Journal of Refractory Metals and Hard Materials*, 31: 284–287. doi: 10.1016/j.ijrmhm.2011.10.007
- Liu, P., Tan, Q., Wu, L., & He, G. (2010). Compressive and pseudo-elastic hysteresis behavior of entangled titanium wire materials. *Materials Science and Engineering A*, 527(15): 3301–3309. doi: 10.1016/j.msea.2010.02.071
- Liu, X. H., Huang, H. Y., & Xie, J. X. (2014). Effect of strain rate on the compressive deformation behaviors of lotus-type porous copper. *International Journal of*

*Minerals, Metallurgy and Materials*, 21(7): 687–695. doi: 10.1007/s12613-014-0959-9

- Liu, W., & Gao, S. L. X. L. X. (1990). Crystallization of amorphous Cu-6Ni-10Sn-7P alloy ribbons. *Journal of Materials Science Letters*, 9: 904–905. doi: 10.1007/BF00722165
- Loh, C., Chou, B., & Nelson, D. (2000). Study of thermal characteristics on solder and adhesive bonded folded fin heat sink. *Thermal and Thermomechanical Phenomena in Electronic Systems*, 1–7. doi: 10.1109/ITHERM.2000.866162
- Lu, C., Sun, L., Zhang, J., Qi, Q., & Hug, G. (2017). Brazing mechanisms of the Ti<sub>2</sub>AlC joints using a pure Al filler metal. *Ceramics International*, 43: 8579–8584. doi: 10.1016/j.ceramint.2017.03.113
- Lu, W., Zhao, C. Y., & Tassou, S. A. (2006). Thermal analysis on metal-foam filled heat exchangers. Part I : Metal-foam filled pipes. *International Journal of Heat and Mass Transfer*, 49, 2751–2761. doi: 10.1016/j.ijheatmasstransfer.2005.12.012
- Lunsford, K. M. (2006). *Advantages of Brazed Heat Exchangers in the Gas Processing Industry*. Bryan, Texas: Bryan Research and Engineering Inc. Retrieved from <https://www.bre.com/PDF/Advantages-of-Brazed-Heat-Exchangers-in-the-Gas-Processing-Industry.pdf>
- Luo, Y., Zhang, Q., Jiang, W., Zhang, Y., Hao, M., & Tu, S. T. (2017). The microstructure, mechanical properties and fracture behavior of hastelloy C276-BNi2 brazed joint. *Materials and Design*, 115: 458–466. doi: 10.1016/j.matdes.2016.11.069
- Lutfi, M., Yusof, F., Ariga, T., Singh, R., & Hamdi, A. S. M. (2016). Interfacial Reaction Analysis of Cu-Sn-Ni-P/Cu Joint Using Microwave Hybrid Heating. *Key Engineering Materials*, 701: 148–153. doi: 10.4028/www.scientific.net/KEM.701.148
- Lutfi, M., Yusof, F., Singh, R., Ariga, T., & Hamdi, A. S. M. (2017). A novel method of brazing Cu/Cu-7.0Ni-9.3Sn-6.3P/Cu using microwave hybrid heating. *Materialwissenschaft Und Werkstofftechnik*, 48(3–4): 299–305. doi: 10.1002/mawe.201600780
- Lv, F. & Fu, G. (2014). Weld failure analysis of air radiator. *Journal of Failure Analysis and Prevention*, 14: 95–101. doi: 10.1007/s11668-013-9768-0
- Mancin, S., Zilio, C., Diani, A., & Rossetto, L. (2012). Experimental air heat transfer and pressure drop through copper foams. *Experimental Thermal and Fluid Science*, 36: 224–232. doi: 10.1016/j.expthermflusci.2011.09.016
- Metal foam market analysis by material (Aluminium, Nickel, Magnesium, Copper) by application (heat exchanger, energy absorbers, side impact bars), by end use and segment forecast, 2018-2025. (2017, October). Grand View Research. Retrieved from <http://grandviewresearch.com>.

- Miettinen, J. (2003). Thermodynamic description of the Cu-Ni-Sn system at the Cu-Ni side. *Computer Coupling of Phase Diagrams and Thermochemistry*, 27(3), 309–318. doi: 10.1016/j.calphad.2003.10.001
- Mirzaei, M., & Paydar, M. H. (2017). A novel process for manufacturing porous 316 L stainless steel with uniform pore distribution. *Materials & Design*, 121, 442–449. <http://doi.org/10.1016/j.matdes.2017.02.069>
- Montemor, M. F. (2016). Corrosion issues in joining lightweight materials : A review of the latest achievements. *Physical Science Reviews*, 1(2): 53–71. doi: 10.1515/psr-2015-0011
- Muley, A., Kiser, C., Sunden, B., & Shah, R. K. (2012). Foam Heat Exchangers: A Technology Assessment. *Heat Transfer Engineering*, 33(1), 42–51. doi: 10.1080/01457632.2011.584817
- Nannan, C., Jie, C., Bin, L., & Fanyan, C. (2013). Vacuum Brazing Processes of Aluminum Foam. *Rare Metal Materials and Engineering*, 42(6), 1118–1122. doi: 10.1016/S1875-5372(13)60072-7
- Nawaz, K., Bock, J., & Jacobi, A. M. (2012, July 16-19). *Thermal-Hydraulic Performance of Metal Foam Heat Exchangers* [Paper presentation]. 14<sup>th</sup> International Refrigeration and Air Conditioning Conference, Purdue University, Indiana, US. Retrieved from <https://docs.lib.purdue.edu/iracc/1283/>
- Nawaz, K., Bock, J., Dai, Z., & Jacobi, A. M. (2010). Experimental Studies to Evaluate the Use of Metal Foams in Highly Compact Air-Cooling Heat Exchangers. *International Refrigeration and Air Conditioning Conference*, 2502, 1–10. doi: 10.1016/j.applthermaleng.2017.03.056.
- Nowacki, J., Grabian, J. & Krajewski, S. (2014). Problems of aluminium foam soldering. *Welding Technology Review*, 1(1), 7-12. doi: 10.26628/ps.v86i1.114
- Ochiai, S., Nakano, S., Fukazawa, Y., Aly, M. S., Okuda, H., Kato, K. & Honma, K. (2010). Tensile Deformation and Failure Behavior of Open Cell Nickel and Copper Foams. *Materials Transactions*, 51(4), 699–706. doi:10.2320/matertrans.M2009383
- Oladijo, O. P., Obadele, B. A., Venter, A. M. & Cornish, L. A. (2016). Investigation the effect of porosity on corrosion resistance and hardness of WC-Co coatings on metal substrates. *African Corrosion Journal*, 2(1), 37-44. Retrieved from <https://www.mendeley.com/catalogue/3387e8a2-1852-3245-a172-9c8e4f5399e1/>
- Ohadi, M. M. (2000). Heat Exchangers. In R. C. Dorf, (Ed.). *The Engineering Handbook*. Boca Raton, Florida: CRC Press LLC.
- Odabae M. & Hooman, K. (2012) Metal foam heat exchangers for heat transfer augmentation from a tube bank, *Applied Thermal Engineering*, 36, 456–463. doi: 10.1016/j.applthermaleng.2011.10.063
- Padmavathi, C., Panda, S. S., Agarwal, D., & Upadhyaya, A. (2006). Effect of microstructural characteristics on corrosion behaviour of microwave sintered

stainless steel composites. *Materials Science and Technology*, 517–528. Retrieved from: [https://www.mri.psu.edu/sites/default/files/file\\_attach/137.pdf](https://www.mri.psu.edu/sites/default/files/file_attach/137.pdf)

- Patil, A. G., Gosavi, A. S., Deshpande, M. S., Pahilwan, P. V., & Rathod, R. M. (2019). A review paper on analysis of vortex tube cold outlet for radiator cooling. *International Research Journal of Engineering and Technology (IRJET)*, 6(4), 4091-4098. Retrieved from <https://www.irjet.net/archives/V6/i4/IRJET-V6I4899.pdf>
- Peltola, H., & Lindgren, M. (2015). Failure analysis of a copper tube in a finned heat exchanger. *Engineering Failure Analysis*, 51, 83–97. doi: [org/10.1016/j.engfailanal.2015.02.016](https://doi.org/10.1016/j.engfailanal.2015.02.016)
- Qasem, N. A. A., & Zubair, S. M. (2018). Compact and microchannel heat exchangers : A comprehensive review of air- side friction factor and heat transfer correlations. *Energy Conversion and Management*, 173, 555–601. doi: [10.1016/j.enconman.2018.06.104](https://doi.org/10.1016/j.enconman.2018.06.104)
- Rabinkin, A. (2001). Brazing with amorphous foil preforms. *Advanced Materials & Process*, 159(6), 65-67. Retrieved from: <https://metglas.com/wp-content/uploads/2016/12/Brazing-with-Amorphous-Foil-Preforms.pdf>
- Rahmani, H., & Meletis, E. I. (2019). Corrosion study of brazing Cu-Ag alloy in the presence of benzotriazole inhibitor Applied Surface Science Corrosion study of brazing Cu-Ag alloy in the presence of benzotriazole inhibitor. *Applied Surface Science*, 497(August), 143759. doi: [10.1016/j.apsusc.2019.143759](https://doi.org/10.1016/j.apsusc.2019.143759)
- Rai, S. K., & Dubey, P. (2017). A review on heat exchanger. *International Journal of Advance Research and Innovative Ideas in Education*, 3(1), 322–329. doi: [16.0415/IJARIE-3678](https://doi.org/10.160415/IJARIE-3678)
- Ralph, M.D., DeBold, T. & Johnson, M.J. (1987). *Corrosion of stainless steel*. In: Davis JR ed. *Corrosion*. Materials Park, Ohio: ASM International.
- Ramos, A. I. C., & Dunand, D. C. (2012). Preparation and Characterization of Directionally Freeze-cast Copper Foams. *Metals*, 2(4), 265–273. doi: [10.3390/met2030265](https://doi.org/10.3390/met2030265)
- Reay, D. A. (1994). Compact heat exchangers: A review of current equipment and R&D in the field. *Heat Recovery System & CHP*, 14(5), 459-474. doi: [10.1016/0890-4332\(94\)90050-7](https://doi.org/10.1016/0890-4332(94)90050-7)
- Ribeiro G. B., Barbosa J. R, & Prata A. T. (2012). Performance of microchannel condensers with metal foams on the air-side: Application in small-scale refrigeration systems. *Applied Thermal Engineering*, 36, 152-160. <http://doi.org/10.1016/j.applthermaleng.2011.12.032>
- Renault, V., Villemiane, I. A-G., Philippe, M., Dubois, A., Casenave, C. & Delaux, D. (2018, September 9-13). Reliable corrosion test development for heat exchanger fin debonding evaluation [Paper presentation]. European Federation of Corrosion Event No. 429, ICE, Krakow, Poland. Retrieved from: <http://eurocorr.efcweb.org/2018/abstracts/17/120385.pdf>

- Revie, R. W. (2011). *Uhlig's Corrosion Handbook The Electrochemical Society Series*. USA: John Wiley & Sons, Inc.
- Rybar, R. Beer, M., Kudelas, D. & Pandula, B. (2016). Copper metal foam as an essential construction element of innovative heat exchanger. *Metallurgija*, 55(3), 489-492. Retrieved from: <https://hrcak.srce.hr/file/226427>
- Saberi, M. A. M. W. M. (2010). *Comparison between method of one-factor-at-a-time (OFAT) & design of experiment (DOE) in screening of immunoglobulin production stimulating factors*. (Degree's thesis, University Malaysia Pahang, Malaysia). Retrieved from <http://umpir.ump.edu.my/id/eprint/2509/>
- Santos, H., Morgado, J., Martinho, N., Pereira, J., & Moita, A. (2017). Selecting and Optimizing a Heat Exchanger for Automotive Vehicle Rankine Cycle Waste Heat Recovery Systems. *Energy Procedia*, 107, 390–397. doi: 10.1016/j.egypro.2016.12.181
- Saw, L. H., Ye, Y., Yew, M. C., Chong, W. T., Yew, M. K., & Ng, T. C. (2017). Computational fluid dynamics simulation on open cell aluminium foams for Li-ion battery cooling system. *Applied Energy*, 204, 1489–1499. doi: 10.1016/j.apenergy.2017.04.022
- Schamphelreire, S. De., Jaeger, P. De., Kerpel, K. De., Ameal, B., Huisseune, H., Paepe, M. De. (2014). Experimental study of free convection in open-cell aluminum foam. *Procedia Material Science*, 4, 359–364. doi: 10.3390/ma9020094
- Scheel, J., & Gustafsson, B. (2000). CuproBrazed Mobile Heat Exchanger Technology. *SAE Technical Paper Series*. doi: 10.4271/2000-01-3456
- Schwartz, M. M. (2003). *Brazing* (2<sup>nd</sup> Ed.). Materials Park, Ohio: ASM International.
- Șerban, V. A, Codrean, C., Uțu, D., & Opreș, C. (2009). Amorphous alloys for brazing copper based alloys. *Journal of Physics: Conference Series*, 144, 1-4. <http://doi.org/10.1088/1742-6596/144/1/012098>
- Sevryukov, O. N., Fedotov, V. T., & Polyansky, A. A. (2016). Neutron-absorbing amorphous alloys for cladding coatings. *IOP conference series: Materials Science and Engineering*, 130, 012028. doi: 10.1088/1757-899X/130/1/012028
- Shabtay, Y. L., Ainali, M., & Lea, A. (2004). New brazing processes using anneal-resistant copper and brass alloys. *Materials and Design*, 25, 83–89. doi: 10.1016/S0261-3069(03)00162-6
- Shah, R. K. (1981). Classification of heat exchangers. In S. Kakac, A. E. Bergles & F. Mayinger (Eds.). *Heat Exchangers: Thermal-Hydraulic Fundamentals and Design*, Eds. (pp. 9–46). Washington, DC: Hemisphere Publishing.
- Shah, R. K., & Sekulić, D. P. (2003). *Fundamentals of heat exchanger design*. Hoboken, New Jersey: John Wiley & Sons.
- Shi, D., Dong, C., Yang, X., Zhang, L., Hou, J., & Liu, Y. (2012). Experimental investigations on creep rupture strength and failure mechanism of vacuum brazed

- joints of a DS superalloy at elevated temperature. *Materials Science & Engineering A*, 545, 162–167. doi: 10.1016/j.msea.2012.02.099
- Shi, K. (2016). Study on Fe-Cr-based brazing filler metals as substitutes for Ni-based brazing filler metals [Master's thesis Gunma University, Japan] Retrieved from <https://gair.media.gunma-u.ac.jp/dspace/bitstream/10087/10388/1/e-k0511-3.pdf>.
- Shirzadi, A. A., Zhu, Y., & Bhadeshia, H. K. D. H. (2008). Joining Ceramics to Metals using Metallic Foam. *Materials Science and Engineering A*, 496, 501–506. doi: 10.1016/j.msea.2008.06.007.
- Song, G., & Liu, M. (2013). Corrosion and electrochemical evaluation of an Al – Si – Cu aluminum alloy in ethanol solutions. *Corrosion Science*, 72, 73–81. doi: 10.1016/j.corsci.2013.03.009.
- Song, Y. F., Xiao, L. R., Zhao, X. J., Zhou, H., Zhang, W., Guo, L., & Wang, Y. H. (2015). Fabrication, Microstructure and Shear Properties of Al Foam Sandwich. *Materials and Manufacturing Processes*, 31(8), 1046–1051. doi: 10.1080/10426914.2015.1037900.
- Srinath, M. S., Sharma, A. K., & Kumar, P. (2011). A new approach to joining of bulk copper using microwave energy. *Materials and Design*, 32(5), 2685–2694. doi: 10.1016/j.matdes.2011.01.023.
- Subramaniam, K., Mazuki, T. A. T., Shukor, M. Y., & Ahmad, S. A. (2019). Isolation and optimisation of phenol degradation by Antarctic isolate using one factor at time. *Malaysian Journal of Biochemistry & Molecular Biology*. 1, 79-86.
- Sun, R., Zhu, Y., Guo, W., Peng, P., Li, L., Zhang, Y., & Fu, J. (2018). Microstructural evolution and thermal stress relaxation of Al<sub>2</sub>O<sub>3</sub> / 1Cr18Ni9Ti brazed joints with nickel foam. *Vacuum*, 148, 18–26. doi: 10.1016/j.vacuum.2017.10.030.
- Tajfar, M., Ganjeh, E., & Mirbagheri, M. H. (2016). Evaluation of copper brazed joint failure by thermal-fatigue test applicable in heat exchangers. *Journal of Alloys and Compounds*, 656, 347–356. doi: 10.1016/j.jallcom.2015.09.276
- Tan, W.-C., & Chong, K.-K. (2016). Simplification of heat transfer modelling for 3-D open cell copper foam by using single-direction aligned cylinder-bank geometry. *Applied Thermal Engineering*, 107, 1192–1200. doi: 10.1016/j.applthermaleng.2016.07.035.
- Tapper L., Sundberg R. & Miner D. K. (1993). New joining method for copper/brass heat exchangers. doi: 10.4271/931076
- Thonon, B. & Breuil E. (2001). Compact heat exchangers technologies for HTRs recuperator application. (Report No. IAEA-TECDOC-1238). International Atomic Energy Agency. [https://inis.iaea.org/collection/NCLCollectionStore/\\_Public/32/047/32047838.pdf?r=1](https://inis.iaea.org/collection/NCLCollectionStore/_Public/32/047/32047838.pdf?r=1)
- Tioual-demange, S., Bergin, G., & Mazet, T. (2019, September 19-20). Highly efficient plate-fin heat exchanger (PFHE) technical development for S-CO<sub>2</sub> power cycles [Conference session]. 3<sup>rd</sup> European CO<sub>2</sub> Conference, Paris, France. Retrieved from:

[https://duepublico2.uni-due.de/servlets/MCRFileNodeServlet/duepublico\\_derivate\\_00070569/Tioual-Demange\\_et\\_al\\_Highly\\_efficient\\_Plate-Fin.pdf](https://duepublico2.uni-due.de/servlets/MCRFileNodeServlet/duepublico_derivate_00070569/Tioual-Demange_et_al_Highly_efficient_Plate-Fin.pdf)

- Tuzovskaya, I., Pacheco B., S., Chinthaginjala, J. K., Reed, C., Lefferts, L., & Van Der Meer, T. (2012). Heat exchange performance of stainless steel and carbon foams modified with carbon nano fibers. *International Journal of Heat and Mass Transfer*, 55(21–22), 5769–5776. doi: 10.1016/j.ijheatmasstransfer.2012.05.073
- Ubertalli, G., Ferraris, M., & Bangash, M. K. (2017). Joining of AL-6016 to Al-foam using Zn-based joining materials. *Composites Part A*, 96, 122-128. doi: 10.1016/j.compositesa.2017.02.019
- Utsunomiya, T., Yamaguchi, R., Hangai, Y., Kuwazuru, O., & Yoshikawa, N. (2013). Estimation of Plateau Stress of Porous Aluminum Based on Mean Stress on Maximum-Porosity Cross Section. *Materials Transaction*, 54(7), 1182–1186. doi: 10.2320/matertrans.M2013069
- Vekariyamukesh, V., Selokar, G. R., & Paul, A. (2012). Optimization and Design of Heat Exchanger with Different Materials. *International Journal of Mathematical, Engineering and Management Sciences*, 5(1), 37–42. Retrieved from: [http://www.darshan.ac.in/Upload/DIET/Publications/ME/7-Vekariyamukesh%20V\\_17092014\\_124321PM.pdf](http://www.darshan.ac.in/Upload/DIET/Publications/ME/7-Vekariyamukesh%20V_17092014_124321PM.pdf)
- Vesenjak, M., Hokamoto, K., Sakamoto, M., Nishi, T., Krstulović-Opara, L., & Ren, Z. (2016). Mechanical and microstructural analysis of unidirectional porous (UniPore) copper. *Materials and Design*, 90, 867–880. doi: 10.1016/j.matdes.2015.11.038
- Vohra, I. A., Aijaj, A., & Saxena, B. B. (2013). Modern heat exchanger- A review. *International Journal of Engineering Research & Technology*, 2(2), 1-6. Retrieved from: <https://www.ijert.org/modern-heat-exchanger-a-review>
- Wan, Z., Liu, B., Zhou, W., Tang, Y., Hui, K. S., & Hui, K. N. (2012). Experimental study on shear properties of porous metal fiber sintered sheet. *Materials Science and Engineering A*, 544, 33–37. doi: 10.1016/j.msea.2012.02.070
- Wang, H., & Guo, L. (2016). Experimental investigation on pressure drop and heat transfer in metal foam filled tubes under convective boundary condition. *Chemical Engineering Science*, 155, 438–448. doi: 10.1016/j.ces.2016.08.031
- Wang, Z., Wang, G., Li, M., Lin, J., Ma, Q., Zhang, A., & Feng, J. (2017). Three-dimensional graphene-reinforced Cu foam interlayer for brazing C/C composites and Nb. *Carbon*, 118, 723–730. doi: 10.1016/j.carbon.2017.03.099
- Warraky, A. El., Shayeb, H. A. El., & Sherif, E. M. (2004). Pitting corrosion of copper in chloride solutions. *Anti-Corrosion Methods and Materials*, 51(1), 52–61. doi: 10.1108/00035590410512735
- Weishaupt, E. R., Stevenson M. E., Mc Dougall J. L & Turnquist D. A. (2012). Case study: corrosion failure of yellow brass tubing in radiator application. *Journal Failure and Prevention*, 12, 242–7. doi: 10.1007/s11668-012-9561-5

- Weiyuan, Y., Wenjiang, L., & Tiandong, X. (2013). Formation Process of Joints Brazing with Amorphous Filler Metal. *Rare Metal Materials and Engineering*, 42(4): 688–691. doi: 10.1016/S1875-5372(13)60057-0
- Wu, N., Li, Y., & Wang, J. (2012). Microstructure of Ni-NiCr laminated composite and Cr18-Ni8 steel joint by vacuum brazing. *Vacuum*, 86(12), 2059–2063. doi: 10.1016/j.vacuum.2012.05.027
- Xie, S., & Evans, J. R. G. (2004). High porosity copper foam. *Journal of Materials Science*, 39, 5877–5880. doi: 10.1023/B:JMSC.0000040107.04387.b7
- Xihui, D., Xiaoqiang, L., Min'ai, Z., Shengguan, Q., & Zhongli, D. (2016). Study on Vacuum Brazed MGH956 Alloy with Cu-P-Sn-Ni Filler Research of brazing MGH956 alloy with Cu-Ni-Sn-Ni filler metal in vacuum. *Materials Science & Technology*, 24(5), 14–19. doi: 10.11951/j.issn.1005-0299.20160503
- Xiuming, Y., Yanliang, H., Yadav, A. P., Wenjuan, Q., & Marco R. D. (2015). Study on the temperature dependence of pitting behaviour of AISI 4135 Steel in marine splash zone. *Electrochemistry*, 83(7), 541-548. doi: 10.5796/electrochemistry.83.541
- Xu, X., Ma, Q. & Xia, C. (2019). Micromorphology change and microstructure of Cu-P based amorphous filler during heating process. *High Temperature Material Process*, 38, 651–661. doi: 10.1515/htmp-2019-0013
- Yang, D.-N., Shao, Y., & Yao, K.-F. (2019). Understanding the fracture behaviors of metallic glasses- An overview. *Applied Science*, 9(20), 4277. doi: 10.3390/app9204277
- Zaharinie, T., Moshwan, R., Yusof, F., Hamdi, M., & Ariga, T. (2014). Vacuum brazing of sapphire with Inconel 600 using Cu / Ni porous composite interlayer for gas pressure sensor application. *Materials and Design*, 54, 375–381. doi: 10.1016/j.matdes.2013.08.046
- Zaharinie, T., Huda, Z., Izuan, M. F., & Hamdi, M. (2015). Development of optimum process parameters and a study of the effects of surface roughness on brazing of copper. *Applied Surface Science*, 331, 127–131. doi: 10.1016/j.apsusc.2015.01.078
- Zhang, X., Bohm, S., Bosch, A. J., van Westing, E. P. M., & de Wit, J. H. W. (2004). Influence of drying temperature on the corrosion performance of chromate coatings on galvanized steel. *Materials and Corrosion*, 55(7), 501-510. doi: 10.1002/maco.200303769
- Zhang, P. L., Yao, S., Ding, M., Lu, F. G., & Lou, S. N. (2010). Microstructural analysis in the vacuum brazing of copper to copper using a phosphor – copper brazing filler metal. *International Journal of Materials Research*, 101, 1436–1440. doi: 10.3139/146.110376
- Zhang, H., Chen, L., Liu, Y., & Li, Y. (2013). International Journal of Heat and Mass Transfer Experimental study on heat transfer performance of lotus-type porous copper heat sink. *International Journal of Heat and Mass Transfer*, 56(1–2), 172–180. doi: 10.1016/j.ijheatmasstransfer.2012.08.047

- Zhang, J., Wang, T., Liu, C., & He, Y. (2014). Effect of brazing temperature on microstructure and mechanical properties of graphite/copper joints. *Materials Science and Engineering A*, 594, 26–31. doi: 10.1016/j.msea.2013.11.059
- Zhang, J., Yu, W., & Lu, W. (2016). Mechanical Properties and Microstructure of Pure Copper Joints Brazed with Amorphous Cu<sub>68.5</sub>Ni<sub>15.7</sub>Sn<sub>9.3</sub>P<sub>6.5</sub> Filler Metal. *International Journal of Simulation System, Science and Technology*, 17(24), 15–19. doi: 10.5013/IJSSST.a.17.24.19
- Zhang, Y., Long, E., & Zhang, M. (2018). Experimental study on heat sink with porous copper as conductive material for CPU cooling. *Materials Today: Proceedings*, 5(7), 15004–15009. doi: 10.1016/j.matpr.2018.04.046
- Zhao, C. Y., Lu, W., & Tassou, S. A. (2006). Thermal analysis on metal-foam filled heat exchangers. Part II : Tube heat exchangers. *International Journal of Heat and Mass Transfer*, 49, 2762–2770. doi: 10.1016/j.ijheatmasstransfer.2005.12.014
- Zhao, C. Y. (2012). Review on thermal transport in high porosity cellular metal foams with open cells. *International Journal of Heat and Mass Transfer*, 55(13–14), 3618–3632. doi: 10.1016/j.ijheatmasstransfer.2012.03.017
- Zhong, Z., Zhou, J., Shen, X., & Ling, X. (2012). Study on Vacuum Brazing of Glass to Kovar ® Alloy with Cu-Ni-Sn-P. *Welding Journal*, 91, 237–240. Retrieved from: [http://files.aws.org/wj/supplement/WJ\\_2012\\_09\\_s237.pdf](http://files.aws.org/wj/supplement/WJ_2012_09_s237.pdf)
- Zhou, J., Mercer, C., & Soboyejo, W. O. (2002). An Investigation of the Microstructure and Strength of Open-Cell 6101 Aluminum Foams. *Metallurgical and Materials Transactions A*, 33, 1413–1427. doi: 10.1007/s11661-002-0065-x
- Zhou, Z., Su, B., Wang, Z., Shu, X., & Zhao, L. (2016). Impact response of aluminium alloy foams under complex stress states. *Latin American Journal of Solids and Structures*, 13(4), 665–689. doi: 10.1590/1679-78252344
- Zhuang, Y. L., Lin, T. S., Wang, S. J., He, P., Sekulic, D. P., & Jia, D. C. (2016). Microstructural and mechanical properties of porous Si<sub>3</sub>N<sub>4</sub> carbon coated ceramic brazed with a cobalt-silicon filler. *Journal of the European Ceramic Society*, 37, 3293–3301. doi: 10.1016/j.jeurceramsoc.2017.03.031
- Zohdy, K. M., Sadawy, M. M., & Ghanem, M. (2014). Corrosion behavior of leaded-bronze alloys in sea water. *Materials Chemistry and Physics*, 147(3), 878–883. doi: 10.1016/j.matchemphys.2014.06.033
- Zou, J., Jiang, Z., Zhao, Q., & Chen, Z. (2009). Brazing of Si<sub>3</sub>N<sub>4</sub> with amorphous Ti<sub>40</sub>Zr<sub>25</sub>Ni<sub>15</sub>Cu<sub>20</sub> filler. *Materials Science and Engineering A*, 507(1–2), 155–160. doi: 10.1016/j.msea.2008.11.056
- Zupancic, R., Legat, A. & Funduk, N. (2006). Tensile strength and corrosion resistance of brazed and laser-welded cobalt-chromium alloy joints. *The Journal of Prosthetic Dentistry*, 96(4), 273–282. doi: 10.1016/j.prosdent.2006.08.006

## LIST OF PUBLICATIONS AND PAPERS PRESENTED

### Academic Journals

Zahri, N. A. M., Yusof, F., Ariga T., Haseeb, A. S. M. A., Mansoor, M. A., Sukiman, N. L. (2019) Open cell copper foam joining: Joint strength and interfacial behaviour. *Materials Science & technology*. 35(16), 2004-2012. doi: 10.1080/02670836.2019.1661649.

Zahri, N. A. M., Yusof, F., Miyashita, Y., Ariga T., Haseeb, A. S. M. A., Jamadon, N. H., Sukiman, N. L. (2020) Brazing of porous copper foam/copper with amorphous Cu-9.7Sn-5.7Ni-7.0P (wt.%) filler metal: Interfacial microstructure and diffusion behavior. *Welding in The World*. 64, 209-217. doi: 10.1007/s40194-019-00804-2.

Zahri, N. A. M., Yusof, F., Miyashita, Y., Ariga T., Haseeb, A. S. M. A., Sukiman, N. L. (2021). Effect of porous copper pore density on joint interface. *Journal of Harbin Institute of Technology (New Series)*. doi: 10.11916/j.ssn.1005-9113.2020056.

Zahri, N. A. M., Shafee, N. E. S., Yusof, F., Musa, S. N., Sukiman, N. L., Haseeb, A. S. M. A., Ariga T. (2019) Brazing of porous copper foam using Cu-Sn-Ni-P foil for heat sink application. *Materials Science & Engineering Technology (Materialwissenschaft und Werkstofftechnik)*. Status: Accepted on 7th April 2021. doi: 10.1002/mawe.202000059.

Zahri, N.A.M, Yusof, F., Miyashita, Y., Ariga, T., Haseeb, A.S.M.A., Sukiman, N.L. Deformation and fracture behaviour of sandwiched copper foam brazed joint interface using amorphous copper-tin-nickel-phosphorus filler. *Frontiers in Materials*. Status: Accepted on 4th May 2021.

Zahri, N. A. M., Yusof, F., Miyashita, Y., Ariga T., Haseeb, A. S. M. A., Sukiman, N. L. Brazing of copper foam using Cu-4.0Sn-9.9Ni-7.8P filler foil (MBF 2002): Effect of brazing temperature and copper foam pore density. *Indian Journal of Engineering & Materials Sciences*. **Status: In progress (25 May 2021)**

Zahri, N. A. M., Yusof, F., Miyashita, Y., Ariga T., Haseeb, A. S. M. A., Sukiman, N. L. Corrosion behavior of copper/porous copper foam brazed interface. *Journal of Materials Engineering and Performance*. **Status: In progress (25 May 2021)**

### Conferences

Oral presentation in 4<sup>th</sup> *International Conference on the Science and Engineering of Materials 2019 (ICoSEM2019)* on 26<sup>th</sup>-28<sup>th</sup> August 2019, Petaling Jaya, Malaysia.

Oral presentation in 4<sup>th</sup> *International Conference on the Science and Engineering of Advances in Manufacturing & Laser Processing Technology Conference*, Kuala Lumpur, Malaysia.